

May 2016

Characterizing the Earliest Stages of Partial Melting: A Study of the Pyrometamorphic Aureole of Miocene Mt. Perkins Pluton, Northwest Arizona

Mathew Beshears
University of Nevada, Las Vegas

Follow this and additional works at: <https://digitalscholarship.unlv.edu/thesesdissertations>



Part of the [Geochemistry Commons](#), and the [Geology Commons](#)

Repository Citation

Beshears, Mathew, "Characterizing the Earliest Stages of Partial Melting: A Study of the Pyrometamorphic Aureole of Miocene Mt. Perkins Pluton, Northwest Arizona" (2016). *UNLV Theses, Dissertations, Professional Papers, and Capstones*. 2639.
<http://dx.doi.org/10.34917/9112031>

This Thesis is protected by copyright and/or related rights. It has been brought to you by Digital Scholarship@UNLV with permission from the rights-holder(s). You are free to use this Thesis in any way that is permitted by the copyright and related rights legislation that applies to your use. For other uses you need to obtain permission from the rights-holder(s) directly, unless additional rights are indicated by a Creative Commons license in the record and/or on the work itself.

This Thesis has been accepted for inclusion in UNLV Theses, Dissertations, Professional Papers, and Capstones by an authorized administrator of Digital Scholarship@UNLV. For more information, please contact digitalscholarship@unlv.edu.

CHARACTERIZING THE EARLIEST STAGES OF PARTIAL MELTING: A STUDY OF
THE PYROMETAMORPHIC AUREOLE OF MIOCENE MT. PERKINS PLUTON,
NORTHWEST ARIZONA

By

Mathew Beshears

Bachelor of Science in Geosciences

Indiana University – Purdue University Indianapolis

December 2011

A thesis submitted in partial fulfillment
of the requirements for the

Master of Science – Geoscience

Department of Geoscience

College of Sciences

The Graduate College

University of Nevada, Las Vegas

May 2016

Thesis Approval

The Graduate College
The University of Nevada, Las Vegas

April 13, 2016

This thesis prepared by

Mathew Beshears

entitled

Characterizing the Earliest Stages of Partial Melting: A Study of the Pyrometamorphic
Aureole of Miocene Mt. Perkins Pluton, Northwest Arizona

is approved in partial fulfillment of the requirements for the degree of

Master of Science – Geoscience
Department of Geoscience

Rodney V. Metcalf, Ph.D.
Examination Committee Chair

Kathryn Hausbeck Korgan, Ph.D.
Graduate College Interim Dean

Terry Spell, Ph.D.
Examination Committee Member

Jean Cline, Ph.D.
Examination Committee Member

George Rhee, Ph.D.
Graduate College Faculty Representative

Abstract

Partial melting is an important process in the evolution of continental crust. Due to its progressive nature, evidence of the early stages of partial melting is often overprinted by later, advanced stages of partial melting. Experimental work has provided a model for the early stages of partial melting, but is limited to timescales of hours to weeks. Pyrometamorphic environments within the contact aureole of mafic intrusions provide natural laboratories for the study of the earliest stages of partial melt production on geologic time scales of 10^2 to 10^4 years. Samples collected along two traverses of the tilted pyrometamorphic aureole of the Mt. Perkins pluton provide an opportunity to quantify partial melt volume percent and chemistry at 2 kbar. Using titanium-in-quartz geothermometry, EPMA techniques to obtain mineral chemistry, and a point-counting method using imaging software, melt volume percent, whole-rock, melt, and residual chemistry and percent minerals in each category were quantified. Melt volume percent and temperature decrease with distance from the pluton. Melt geochemistries plot near the cotectic in the quartz-(Ab+Or)-An system. Plagioclase anorthite components were quantified and compared with each other based on textures. The earliest stages of partial melting are recorded in samples that experienced a lower heat budget distal to the pluton. These data confirm hypotheses that earliest melts are silica rich and become progressively enriched in other cations as melting continues.

Table of Contents

Abstract	iii
Table of Contents	iv
List of Tables	vii
List of Figures	xiii
1. Introduction	1
2. Background	3
<i>2.1 Recognizing Pseudomelt Pockets</i>	<i>3</i>
<i>2.2 Current Model for Early Stages of Partial Melt (Low Melt Percent)</i>	<i>4</i>
<i>2.3 The Plagioclase Problem</i>	<i>5</i>
<i>2.4 Melt mobility</i>	<i>7</i>
3. Geologic Setting – Mt. Perkins pluton	9
4. Study Design	12
<i>4.1 Hypotheses</i>	<i>12</i>
<i>4.2 Predictions</i>	<i>13</i>
5. Methods	16
<i>5.1 Sample Collection</i>	<i>16</i>

<i>5.2 Point counting method</i>	18
<i>5.3 Analytical Methods</i>	21
<i>5.4 Geothermometry</i>	22
6. Results	25
<i>6.1 Mineralogy and Textures</i>	25
<i>6.2 Point Count Results</i>	26
<i>6.3 Melt connectivity</i>	27
<i>6.4 Plagioclase chemistry with respect to textures.</i>	28
<i>6.5 A and B traverse plagioclase.</i>	30
<i>6.6 Calculated whole-rock, melt, and residual geochemistry</i>	31
<i>6.7 Melt, residual, and whole rock geochemistry in the Q-An-(Ab+Or)-H₂O system</i>	33
<i>6.8 Melt volume percent</i>	34
<i>6.9 TitaniQ geothermometry</i>	34
7.1 Discussion	36
<i>7.1 Melt Textures</i>	36
<i>7.2 Melt Reaction</i>	36
<i>7.3 Melt Volume</i>	38
<i>7.4 Geochemical evolution</i>	39
<i>7.5 Plagioclase geochemistry</i>	40

8. Conclusions	42
Appendix A	81
Appendix B	101
Appendix C	167
References	218
Cirriculum Vitae	222

List of Tables

Table 1	List of minerals found in various textures.....	76
Table 2	Modal mineral abundances for each sample divided into three types: melt, residual and whole rock, and distance from pluton.....	77
Table 3	Average EPMA analysis of plagioclase within each sample.....	78
Table 4	Whole rock geochemistry for each sample separated into melt, residual, and whole rock as well as distance from pluton and titanium-in-quartz geothermometry.....	79
Table 5	CIPW norm results from point counting divided into three types: melt, residual and whole rock	80
Table A1	Point count results from the pilot study on sample 925-1.....	81
Table A2	Whole rock, melt and residual geochemistries.....	82
Table A3	Average mineral composition used to calculate residual geochemistry for sample 136-1A.....	83
Table A4	Average mineral composition used to calculate melt geochemistry for sample 136-1A.....	84
Table A5	Average mineral composition used to calculate whole rock geochemistry for sample 136-1A.....	85
Table A6	Average mineral composition used to calculate residual geochemistry for sample 136-6A.....	86
Table A7	Average mineral composition used to calculate melt geochemistry for sample 136-6A.....	87

Table A8	Average mineral composition used to calculate whole rock geochemistry for sample 136-6A.....	88
Table A9	Average mineral composition used to calculate residual geochemistry for sample 136-11A.....	89
Table A10	Average mineral composition used to calculate melt geochemistry for sample 136-11A.....	90
Table A11	Average mineral composition used to calculate whole rock geochemistry for sample 136-11A.....	91
Table A12	Average mineral composition used to calculate residual geochemistry for sample 136-2B.....	92
Table A13	Average mineral composition used to calculate melt geochemistry for sample 136-2B.....	93
Table A14	Average mineral composition used to calculate whole rock geochemistry for sample 136-2B.....	94
Table A15	Average mineral composition used to calculate residual geochemistry for sample 136-8B.....	95
Table A16	Average mineral composition used to calculate melt geochemistry for sample 136-8B.....	96
Table A17	Average mineral composition used to calculate whole rock geochemistry for sample 136-8B.....	97
Table A18	Average mineral composition used to calculate residual geochemistry for sample 136-14B.....	98

Table A19	Average mineral composition used to calculate melt geochemistry for sample 136-14B.....	99
Table A20	Average mineral composition used to calculate whole rock geochemistry for sample 136-14B.....	100
Table A21	EPMA results showing residual plagioclase chemistry for sample 111-2.....	102
Table A22	EPMA results showing euhedral and rounded plagioclase chemistry for sample 111-2.....	103
Table A23	EPMA results showing rounded plagioclase chemistry for sample 111-2.....	105
Table A24	EPMA results showing residual plagioclase chemistry for sample 111-2.....	106
Table A25	EPMA results showing K-feldspar chemistry for sample 111-2.....	107
Table A26	EPMA results showing rounded plagioclase chemistry for sample 111-2.....	109
Table A27	EPMA results showing top residual plagioclase chemistry for sample 111-2.....	110
Table A28	EPMA results showing left residual plagioclase chemistry for sample 111-2....	111
Table A29	EPMA results showing middle LPP plagioclase chemistry for sample 111-2....	113
Table A30	EPMA results showing top LPP plagioclase chemistry for sample 111-2.....	114
Table A31	EPMA results showing right LPP plagioclase chemistry for sample 111-2.....	115
Table A32	EPMA results showing left residual plagioclase chemistry for sample 111-2....	116
Table A33	EPMA results showing melt film plagioclase chemistry for sample 111-4a.....	118
Table A34	EPMA results showing melt film plagioclase chemistry for sample 111-4a.....	120
Table A35	EPMA results showing overgrowth plagioclase chemistry for sample 111-4a...121	
Table A36	EPMA results showing residual plagioclase chemistry for sample 111-4a.....	122
Table A37	EPMA results showing melt film plagioclase chemistry for sample 111-4a.....	124
Table A38	EPMA results showing residual plagioclase chemistry for sample 111-4a.....	125

Table A39	EPMA results showing melt film plagioclase chemistry for sample 111-4a.....	127
Table A40	EPMA results showing string of beads plagioclase chemistry for sample 111-4a.....	128
Table A41	EPMA results showing melt film plagioclase chemistry for sample 111-4a.....	130
Table A42	EPMA results showing line 1 plagioclase chemistry for sample 925-1.....	132
Table A43	EPMA results showing line 2 plagioclase chemistry for sample 925-1.....	133
Table A44	EPMA results showing line 3 plagioclase chemistry for sample 925-1.....	134
Table A45	EPMA results showing line 4 plagioclase chemistry for sample 925-1.....	135
Table A46	EPMA results showing string of beads plagioclase chemistry for sample 925-1.....	136
Table A47	EPMA results showing LPP plagioclase chemistry for sample 925-1.....	138
Table A48	EPMA results showing residual line 2 plagioclase chemistry for sample 925-1.....	139
Table A49	EPMA results showing residual line 1 plagioclase chemistry for sample 925-1.....	140
Table A50	EPMA results showing K-feldspar chemistry for sample 925-1.....	141
Table A51	EPMA results showing LPP plagioclase chemistry for sample 925-1.....	143
Table A52	EPMA results showing line 1 residual plagioclase chemistry for sample 925-1.....	144
Table A53	EPMA results showing line 2 residual plagioclase chemistry for sample 925-1.....	145
Table A54	EPMA results residual LPP plagioclase chemistry for sample 925-1.....	147

Table A55	EPMA results line 1 residual LPP plagioclase chemistry for sample 925-1.....	149
Table A56	EPMA results residual LPP plagioclase chemistry for sample 925-1.....	150
Table A57	EPMA results of various minerals for sample 136-1A.....	152
Table A58	EPMA results of various minerals for sample 136-6A.....	154
Table A59	EPMA results of various minerals for sample 136-11A.....	156
Table A60	EPMA results of plagioclase line A for sample 136-11A.....	157
Table A61	EPMA results of plagioclase line B for sample 136-11A.....	158
Table A62	EPMA results of various minerals for sample 136-2B.....	160
Table A63	EPMA results of various minerals for sample 136-8B.....	162
Table A64	EPMA results of plagioclase line A minerals for sample 136-8B.....	163
Table A65	EPMA results of various minerals for sample 136-14B.....	165
Table A66	EPMA results of plagioclase line A for sample 136-14B.....	166
Table A67	EPMA titanium analysis and TitaniQ temperatures for Figure A21.....	168
Table A68	EPMA titanium analysis and TitaniQ temperatures for Figure A22.....	170
Table A69	EPMA titanium analysis and TitaniQ temperatures for Figure A23.....	172
Table A70	EPMA titanium analysis and TitaniQ temperatures for Figure A24.....	174
Table A71	EPMA titanium analysis and TitaniQ temperatures for Figure A25.....	176
Table A72	EPMA titanium analysis and TitaniQ temperatures for Figure A26.....	178
Table A73	EPMA titanium analysis and TitaniQ temperatures for Figure A27.....	180
Table A74	EPMA titanium analysis and TitaniQ temperatures for Figure A28.....	182
Table A75	EPMA titanium analysis and TitaniQ temperatures for Figure A29.....	184
Table A76	EPMA titanium analysis and TitaniQ temperatures for Figure A30.....	186
Table A77	EPMA titanium analysis and TitaniQ temperatures for Figure A31.....	188

Table A78	EPMA titanium analysis and TitaniQ temperatures for Figure A32.....	190
Table A79	EPMA titanium analysis and TitaniQ temperatures for Figure A33.....	192
Table A80	EPMA titanium analysis and TitaniQ temperatures for Figure A34.....	194
Table A81	EPMA titanium analysis and TitaniQ temperatures for Figure A35.....	196
Table A82	EPMA titanium analysis and TitaniQ temperatures for Figure A36.....	198
Table A83	EPMA titanium analysis and TitaniQ temperatures for Figure A37.....	200
Table A84	EPMA titanium analysis and TitaniQ temperatures for Figure A38.....	202
Table A85	EPMA titanium analysis and TitaniQ temperatures for Figure A39.....	204
Table A86	EPMA titanium analysis and TitaniQ temperatures for Figure A40.....	206
Table A87	EPMA titanium analysis and TitaniQ temperatures for Figure A41.....	208
Table A88	EPMA titanium analysis and TitaniQ temperatures for Figure A42.....	210
Table A89	EPMA titanium analysis and TitaniQ temperatures for Figure A43.....	212
Table A90	EPMA titanium analysis and TitaniQ temperatures for Figure A44.....	214
Table A91	EPMA titanium analysis and TitaniQ temperatures for Figure A45.....	216
Table A92	Summary of TitaniQ temperatures divided by core and rim analysis.....	217

List of Figures

Figure 1	Examples of partial melt textures from various sources.....	44
Figure 2	3-D sketch of initial melting along crystal boundaries.....	45
Figure 3	Images from Johanness (1989) illustrating the effects of “meta-stable” melting.....	46
Figure 4	Experimental results of Johannes (1989).....	47
Figure 5	Cartoon of progressive melting away from the heat source and sampling strategy.....	48
Figure 6	Photomicrographs of melt textures from samples collected within the contact aureole of the Mt. Perkins pluton from a previous study.....	49
Figure 7	Geologic map of the Mt. Perkins pluton.....	50
Figure 8	Photomicrographs of melt textures from samples collected within the contact aureole of the Mt. Perkins pluton from this study.....	51
Figure 9	Screenshot of point counting method.....	52
Figure 10	Whole slide scan showing the area of the thin section that was point counted.....	53
Figure 11	Results of pilot study on point counting.....	54
Figure 12	SEM-CL image showing dark cores and bright rims.....	55
Figure 13	Photomicrograph of sample 136-2B showing the relationship between mafic minerals.....	56
Figure 14	Photomicrograph of sample 111-2 showing examples of melt connectivity.....	57
Figure 15	Analysis of plagioclase composition based on texture.....	58

Figure 16	An-Ab-Or ternary diagram of plagioclase based on textures from sample 111-2.....	59
Figure 17	An-Ab-Or ternary diagrams of plagioclase based on textures from sample 111-4a.....	60
Figure 18	An-Ab-Or ternary diagrams of plagioclase based on textures from sample 925-1.....	61
Figure 19	An-Ab-Or ternary diagram of plagioclase based on textures from sample 111-8.....	62
Figure 20	An-Ab-Or ternary diagrams of plagioclase based on textures from samples 136-1A, -6A, -11A, -2B, -8B, -14B.....	63
Figure 21	Graph showing the change in melt oxides over the A-traverse.....	64
Figure 22	Graph showing the change in melt oxides over the B-traverse.....	65
Figure 23	Graph showing the cation change between melt, residual and whole rock geochemistries for sample 136-1A.....	66
Figure 24	Graph showing the cation change between melt, residual and whole rock geochemistries for sample 136-6A.....	67
Figure 25	Graph showing the cation change between melt, residual and whole rock geochemistries for sample 136-11A.....	68
Figure 26	Graph showing the cation change between melt, residual and whole rock geochemistries for sample 136-2B.....	69
Figure 27	Graph showing the cation change between melt, residual and whole rock geochemistries for sample 136-8B.....	70

Figure 28	Graph showing the cation change between melt, residual and whole rock geochemistries for sample 136-14B.....	71
Figure 29	Ternary diagrams showing melt, residual, whole rock geochemistry for samples 136-1A, -6A, -11A, -2B, -8B, -14B.....	72
Figure 30	Ternary diagram showing melt geochemistry for samples 136-1A, 6A, -11A, 2B, -8B, -14B.....	73
Figure 31	Graph comparing distance with melt %.....	74
Figure 32	Graph comparing distance with titanium-in-quartz temperatures.....	75
Figure A1	SEM-BSE image showing EPMA targets and plagioclase chemistries for sample 111-2.....	101
Figure A2	SEM-BSE image with photomicrograph overlay showing EPMA targets and plagioclase chemistries for sample 111-2.....	104
Figure A3	SEM-BSE image showing EPMA targets and plagioclase chemistries for sample 111-2.....	108
Figure A4	SEM-BSE image with photomicrograph overlay showing EPMA targets and plagioclase chemistries for sample 111-2.....	112
Figure A5	SEM-BSE image showing EPMA targets and plagioclase chemistries for sample 111-4a.....	117
Figure A6	SEM-BSE image showing EPMA targets and plagioclase chemistries for sample 111-4a.....	119
Figure A7	SEM-BSE image showing EPMA targets and plagioclase chemistries for sample 111-4a.....	123

Figure A8	SEM-BSE image showing EPMA targets and plagioclase chemistries for sample 111-4a.....	126
Figure A9	SEM-BSE image showing EPMA targets and plagioclase chemistries for sample 111-4a.....	129
Figure A10	SEM-BSE image showing EPMA targets and plagioclase chemistries for sample 925-1.....	131
Figure A11	SEM-BSE image showing EPMA targets and plagioclase chemistries for sample 925-1.....	137
Figure A12	SEM-BSE image showing EPMA targets and plagioclase chemistries for sample 925-1.....	142
Figure A13	SEM-BSE image showing EPMA targets and plagioclase chemistries for sample 925-1.....	146
Figure A14	SEM-BSE image showing EPMA targets and plagioclase chemistries for sample 925-1.....	148
Figure A15	SEM-BSE image showing EPMA targets of various minerals for sample 136-1A.....	151
Figure A16	SEM-BSE image showing EPMA targets of various minerals for sample 136-6A.....	153
Figure A17	SEM-BSE image showing EPMA targets of various minerals for sample 136-11A.....	155
Figure A18	SEM-BSE image showing EPMA targets of various minerals for sample 136-2B.....	159

Figure A19	SEM-BSE image showing EPMA targets of various minerals for sample 136-8B.....	161
Figure A20	SEM-BSE image showing EPMA targets of various minerals for sample 136-14B.....	164
Figure A21	EPMA capture of site 1A showing TitaniQ temperatures for sample 136-1A....	167
Figure A22	EPMA capture of site 5A showing TitaniQ temperatures for sample 136-1A....	169
Figure A23	EPMA capture of site 10A showing TitaniQ temperatures for sample 136-1A..	171
Figure A24	EPMA capture of site 1B showing TitaniQ temperatures for sample 136-1A....	173
Figure A25	EPMA capture of site 8B showing TitaniQ temperatures for sample 136-1A....	175
Figure A26	EPMA capture of site 9B showing TitaniQ temperatures for sample 136-1A....	177
Figure A27	EPMA capture of site 3 showing TitaniQ temperatures for sample 136-6A.....	179
Figure A28	EPMA capture of site 4 showing TitaniQ temperatures for sample 136-6A.....	181
Figure A29	EPMA capture of site 8 showing TitaniQ temperatures for sample 136-6A.....	183
Figure A30	EPMA capture of site 9 showing TitaniQ temperatures for sample 136-6A.....	185
Figure A31	EPMA capture of site 10 showing TitaniQ temperatures for sample 136-6A.....	187
Figure A32	EPMA capture of site 5 showing TitaniQ temperatures for sample 136-11A.....	189
Figure A33	EPMA capture of site 7 showing TitaniQ temperatures for sample 136-11A.....	191
Figure A34	EPMA capture of site 9 showing TitaniQ temperatures for sample 136-11A.....	193
Figure A35	EPMA capture of site 1 showing TitaniQ temperatures for sample 136-2B.....	195
Figure A36	EPMA capture of site 5 showing TitaniQ temperatures for sample 136-2B.....	197
Figure A37	EPMA capture of site 9 showing TitaniQ temperatures for sample 136-2B.....	199
Figure A38	EPMA capture of site 2 showing TitaniQ temperatures for sample 136-8B.....	201
Figure A39	EPMA capture of site 6 showing TitaniQ temperatures for sample 136-8B.....	203

Figure A40	EPMA capture of site 7 showing TitaniQ temperatures for sample 136-8B.....	205
Figure A41	EPMA capture of site 9 showing TitaniQ temperatures for sample 136-8B.....	207
Figure A42	EPMA capture of site 1 showing TitaniQ temperatures for sample 136-14B.....	209
Figure A43	EPMA capture of site 4 showing TitaniQ temperatures for sample 136-14B.....	211
Figure A44	EPMA capture of site 6 showing TitaniQ temperatures for sample 136-14B.....	213
Figure A45	EPMA capture of site 8 showing TitaniQ temperatures for sample 136-14B.....	215

1. Introduction

Partial melting is an important process in the evolution and chemical differentiation of the continental crust. Partial melt is a progressive process that begins at grain boundaries, but as melt percent increases melt pockets become more interconnected to form a network of melt that may or may not promote melt migration on the meso-scale. Small degrees of partial melting can have profound effects on rheology of the crust and can play a role in contamination of mafic mantle-derived magma. More advanced stages of partial melting form migmatite zones where melts may segregate and ascend as granitic magmas transferring silicic chemical (lithophile) components to the upper crust (Sawyer, 2001; Brown *et al.*, 2011).

Feldspars are omnipresent within the crust and are commonly involved in crustal anatexis. Laboratory experiments observing plagioclase melting (Bowen, 1913, Mehnert and Busch, 1973; Johannes, 1983, 1984, 1985, 1989) are restricted to geologically extremely short timescales (10 – 10³ hours) or field studies on regional metamorphic terrains whereas plagioclase has undergone melting in timescales of millions of years and subsequent solid-state equilibration (Gupta and Johannes, 1982).

Typically, the record of the earliest stages of partial melting is overprinted or obliterated by processes operating during more advanced stages of partial melting. Current models for the initial stages of partial melting (low percent partial melt) comes from two sources, (1) experimental work using rock cores (Mehnert *et al.*, 1973; Busch *et al.*, 1974; Acosta-Vigil *et al.*, 2006; Figure 1a-b) and (2) pyrometamorphic contact aureole of mafic intrusions (Holness and Clemons, 1999; Rosenberg and Riller, 2000; Sawyer, 2001; Holness and Watt, 2002; Holness *et al.*, 2005; Holness and Sawyer, 2008; Figure 1c). Experimental studies, equilibrium thermodynamics, and kinetics of melting should predict the characteristics of the initial stages of

partial melting (Sawyer, 2001). Studying the initial stages of partial melting via pyrometamorphic contact aureoles is a new approach with few studies available, and because of the new approach interest in investigating the initial stages of partial melting is rising.

Preliminary work (Metcalf and Kopeitz, 2011) has documented partial melt microstructures (pseudomelt pockets) within Precambrian tonalitic gneiss intruded by mafic magmas of the Miocene Mt Perkins pluton, Mohave County, Arizona. The pyrometamorphic contact aureole of the Mt. Perkins pluton provides a natural laboratory to test the current models of partial melting, and this study will focus on plagioclase melting behavior as it relates to a spatially decreasing heat budget on an intermediate time scale ($10^2 - 10^4$ years) (Metcalf *et al.*, 1995). This study focuses on plagioclase chemistry in relation to texture using electron probe microanalyzer (EPMA) techniques on samples from Metcalf and Kopeitz (2011). Samples that were systematically collected from two traverses orthogonal to the Mt. Perkins pluton – quartzofeldspathic tonalitic orthogneiss contact were analyzed using a point-counting method that identifies modal mineral portions and melt volume percent. electron probe microanalyser (EPMA) and scanning electron microscope (SEM) – backscatter electron (-BSE) and cathodoluminescence (-CL) techniques were used to obtain mineral chemistry to calculate whole, melt, and residual chemistry. Titanium-in-quartz (TitaniQ; Wark and Watson, 2006) methods were applied to obtain geothermometry. These data show that (1) plagioclase experiences “meta-stable” melting and not equilibrium melting, (2) heat budget (maximum temperature) and melt volume percent does not progressively diminish from the heat source, (3) Partial melt within samples distal to the heat source contain only felsic minerals whereas samples proximal to the heat source are more likely to involve ferromagnesian minerals, and (4) zoned plagioclase records the local history of plagioclase growth.

2. Background

2.1 Recognizing Pseudomelt Pockets

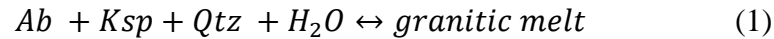
Pseudomelt pockets are defined as the pore space between crystals that were occupied with melt, but have since crystallized as minerals or frozen into glass (Sawyer, 2001; Holness, 2008; Holness and Sawyer, 2008; Holness *et al.*, 2011). Melt films refer to single-phase pseudomelt pockets which exist between two rounded crystals where the melt-solid-solid dihedral angle is typically less than 30° (dark areas in Figure 1B; Holness 2008; Holness *et al.*, 2011) Large multi-phase pseudomelt pockets along grain boundaries have multiple euhedral crystals between two unmelted crystals, a texture termed “string of beads” (Figure 1C; Holness and Isherwood, 2003). Larger pseudomelt pockets are characterized by euhedral crystals with euhedral, “igneous-like” zoning (Figure 1A) and overgrowth on quartz grains made visible by SEM cathodoluminescence imaging (Holness and Sawyer, 2008). Melt pockets can also be recognized by the presence of minerals produced from incongruent melt reactions, such as orthopyroxene formed from biotite breakdown (Holness, 2008; Holness *et al.*, 2011). Small single-phase pseudomelt pockets reflect nucleation difficulties and represent late melt crystallization. For example, Holness and Sawyer (2008) show low Anorthite (An) content in plagioclase within narrow films between restitic grains, but relatively high An in plagioclase content in large spaces. This is explained by preferential An fractional crystallization in a space large enough for plagioclase to nucleate causing the melt to be enriched in albite, which crystallizes in relatively small space after the drop in temperature has “overstepped” nucleation difficulties associated with crystallizing within very small spaces.

2.2 Current Model for Early Stages of Partial Melt (Low Melt Percent)

The earliest stages of partial melting are controlled by the lowest temperature melt reactions for a given pre-melt phase assemblage (minerals + fluids). Based on experimental work (Mehnert *et al.*, 1973; Busch *et al.*, 1974; Acosta-Vigil *et al.*, 2006) and studies of pyrometamorphic contact aureoles (Holness and Clemons, 1999; Rosenberg and Riller, 2000; Sawyer, 2001; Holness and Watt, 2002; Holness *et al.*, 2005; Holness and Sawyer, 2008; Bufe *et al.*, 2014), melting begins at grain boundaries where reactant phases are in contact. Partial melt typically begins within triple-grain boundaries and grows outward to form films of melt around the reactant grains as melt volume increases (Figure 2). In low temperature melting, e.g. quartz-feldspar minimum melts and fluid availability likely controls the location of melt production. For minimum melt (fluid present) generation, pre-existing pathways for fluid transport are critical in the early stages of partial melting. Water-saturated melting of muscovite granite at $P_{H_2O} = 2$ kbar begins at ~ 650 °C and water-saturated melting of tonalite begins at ~ 720 °C (Wyllie, 1976). At higher temperatures dehydration and incongruent melting is driven by possible release of fluids from hydrous phases; such melting causes new fluid pathways to be formed due to positive volume change and increased hydrostatic pressure (Acosta-Vigil *et al.*, 2006). For example, at $P_{H_2O} = 2$ kbar and $T \approx 975$ °C, peritectic clinopyroxene crystallizes from dehydration melting of amphiboles (Wyllie, 1978), and at $P = 3$ kbar and $T = 875$ °C clinopyroxene and orthopyroxene crystallize at the expense of hornblende and magnetite during dehydration melting (Patiño Douce and Beard, 1995). Fluid-absent congruent melting is possible at even higher temperatures.

Melt production can be limited by two factors: heat budget and reactant availability. The heat budget needs to be sufficient to reach melt reaction temperature and to drive endothermic melt reactions for some finite period of time. Melt production is essentially a chemical reaction as

described using the example of haplogranitic systems by Equation 1, where albite (Ab), K-feldspar (Ksp), quartz (Qtz), and water are required components to produce congruent melting at the lowest possible temperature assuming no other volatiles (e.g. B, F) are present in the system (Manning and Pichavant, 1983).



In the tonalitic system where Ksp is a minor component and An is involved, initial melts will be granitic in composition until Ksp is exhausted. If conditions favor melting after Ksp is exhausted, then tonalitic melt will be produced (Wyllie, 1976). This reaction is described by Equation 2:



Melting may be limited by availability of one reactant, for example grain boundary water in Equations 1 and 2. Identifying melt reactions and compositions in natural environments is further complicated by multiple melt reactions occurring as heat budget changes over time, melting of solid-solution minerals (i.e. plagioclase), or any combination of the aforementioned complications.

2.3 The Plagioclase Problem

Slow intracrystalline diffusion of albite (Ab)-anorthite components is responsible for the preservation of zoning in plagioclase and can complicate plagioclase melting behavior.

Compositional zoning is commonly observed in igneous plagioclase, both optically and in SEM images, and is particularly common in volcanic rocks of intermediate composition (Shcherbakov *et al.*, 2011). Zoning in plagioclase often preserves euhedral crystal shapes that provide a history of plagioclase growth. This “crystal stratigraphy” record found in chemically and isotopically zoned plagioclase has been used as a monitor for changing melt compositions and related petrogenetic processes such as fractional crystallization or magma mixing (Davidson *et al.*, 2007). Such zoning is preserved because of the slow intracrystalline diffusion linked to the $(\text{CaAl})_1(\text{NaSi})_{-1}$ coupled substitution in plagioclase solid solution (Johannes, 1983, 1985).

Plagioclase compositional differences between melted (leucosome) and unmelted (mesosome) portions of regional migmatite terranes are often smaller than that predicted from equilibrium melting experiments (Johannes and Gupta, 1982; Gupta and Johannes, 1982; Ashworth, 1985), a situation referred to in the migmatite literature as the “plagioclase problem” (Ashworth, 1985; Grapes 2006). Slow intracrystal diffusion in plagioclase has a significant effect on partial melting behavior, particularly at lower temperatures (Johannes, 1983, 1985, 1989). Kinetic barriers hinder Equilibration of plagioclase crystals are a function of temperature and time, but may require up to 10^5 years’ duration at temperatures of $\sim 730^\circ\text{C}$ (Johannes, 1978, 1985).

The melting behavior of plagioclase has been investigated in two ways: experimental studies (Bowen, 1913; Tuttle and Bowen, 1958; Johannes, 1983, 1985, 1989) and natural studies (Gupta and Johannes, 1982, Johannes and Gupta, 1982; Johannes, 1985). Models from experimental studies suggest the minimum temperature of plagioclase melting depends on pressure, composition (An-Ab) and presence of other phases (i.e. water, quartz, orthoclase etc.) which generally reduces the melting temperature (Busch *et al.*, 1974). Experimental studies suggest that

plagioclase melting may be limited by kinematics rather than thermodynamic constraints (Johannes, 1985, 1989). For example, Johannes (1989) observed an An-rich film encapsulating a plagioclase (An_{60}) crystal shortly after plagioclase-quartz- H_2O melting conditions were achieved (Figure 3). The An-rich film shielded the plagioclase core from interacting with the melt, thus preventing complete breakdown. As plagioclase crystallizes from melt, $(CaAl)_1(NaSi)_{-1}$ coupled substitution retards intracrystalline diffusion, thus causing older rims and/or cores of plagioclase crystals to be isolated from the melt (Johannes, 1989; Figure 3), although increasing temperature exponentially increases diffusion rates (Johannes, 1985). Johannes (1989) discovered the solidus and liquidus in the system Qtz – Ab (+Or) – An, P = 2 kbar (Figure 4). Johannes (1985) has termed this melting phenomenon “meta-stable” melting. However, experimental studies can only produce results based on limited time frames of 10^1 - 10^3 hours, whereas natural studies examine plagioclase under regional metamorphic events on geologic time scales.

2.4 Melt mobility

After melt has been produced along grain boundaries, there is a potential for melt to migrate away from the initial site of formation. Melt can mobilize during or post melt generation. In static environments, studies have concluded that partial melt migration is minimal or non-existent (Mehnert *et al.*, 1973; Holness and Clemons, 1999; Holness and Watt, 2002; Holness *et al.*, 2005). However, in dynamic environments (deformation), melt preferentially pools along pre-existing fabric or at sites of syn-melting fabric development (Rosenberg and Riller, 2000; Sawyer, 2001). Sawyer (2001) has proposed a model for melt migration in a dynamic environment based on thin section to outcrop scale observations (Figure 5). Sawyer (2001) predicts a dynamic environment at least on the grain scale because of two factors: (1)

heterogeneous mineral distribution in natural rocks creates pressure gradients around grain boundaries, driving melt segregation and eventual migration, and (2) a regional and/or local tectonic stress is often present in high temperature environments. . As partial melts become progressively more abundant, pockets of melt become interconnected creating a network of melt. During syn-kinematic melting, a single channel, suborthogonal-to-foliation, may form allowing melt to escape its initial position. If the heat budget is not large enough later stages may not be observed, such that rocks furthest away from a pyrometamorphic or regional heat source may partially melt in relatively small, disconnected melt pockets, but rocks closer to the heat source may progress to form large interconnected networks of melt that may have drained out of the original site of generation through a single channel.

3. Geologic Setting – Mt. Perkins pluton

In order to observe the product of partial melt in its earliest stages rocks must achieve melting conditions during a geologically short thermal pulse. This scenario has high probability to preserve early melt textures before continued heating obliterates then early textures. Based on previous examples, this natural laboratory can be found within the contact aureole of a rapid heat source, such as a mafic sill (Holness and Watt, 2002) or pluton (Holness *et al.*, 2005). Metcalf and Kopyetz (2011) have documented pseudomelt textures (Figure 6) within 2 meters of the contact aureole of the gabbro of the Miocene Mt. Perkins pluton in the central Black Mountains of northwest Arizona (Figure 7). Other pseudomelt textures are documented on Figure 8.

Within the Northern Colorado River Extensional Corridor (NCREC) synchronous magmatism and tilting has generated and exposed several plutons. The Mt. Perkins pluton is located at Mt. Perkins within the Black mountains in the northern section of the NCREC, about 20 km west of Dolan Springs, AZ and 90 km southeast of Las Vegas, NV. The Miocene Mt. Perkins pluton is a composite magma conduit (Metcalf *et al.*, 1995) linking surface volcanoes with deeper intrusive bodies (Faulds *et al.*, 1995). The Mt. Perkins pluton was emplaced into Proterozoic gneiss as four distinct phases (Figure 7); gabbro and diorite (phase 1) were emplaced first, followed by intermediate rocks (phase 2), enclave-rich and enclave poor granodiorite (phase 3), and aphanitic dikes (phase 4). Excluding phase 4 dikes, each phase solidified as an oblate spheroid before emplacement of the next sequential phase. Phase emplacement history was determined by cross-cutting and xenolith relationships. Metcalf *et al.*, (2013) reported ion probe zircon ages for phase 1 gabbro (15.7 ± 0.2 Ma), phase 3 granodiorite (15.8 ± 0.2 Ma), and a phase 4 dike (15.4 ± 0.2 Ma) and concluded that phase 1 through 4 emplacement spanned approximately 2×10^5 years. Al-in-hornblende geobarometry suggests emplacement of phases 2

and 3 at 7.5 ± 2.2 km (Metcalf and Smith, 1991), and geometric relationships and tilt history suggest the paleodepth of the Mt. Perkins pluton is 5.5 ± 1.0 km (Faulds *et al.*, 1995). Field evidence suggests extension preceded or was synchronous with pluton emplacement, tilting the Mt. Perkins block 90° to the west where it is bounded to the west by the east-dipping Mt. Davis fault and to the east by the east-dipping Mockingbird Mine fault (Faulds *et al.*, 1995). To the north, the Mt. Perkins block is sharply terminated by an accommodation zone and the southern margin gradually tapers away along the Mockingbird Mine fault (Faulds *et al.*, 1995). The Precambrian hornblende-biotite quartzofeldspathic orthogneiss is a meta-igneous rock with Mojave-Yavapai boundary zone affinity (Duebendorfer *et al.*, 2001). These rocks within the pyrometamorphic contact aureole of the Mt. Perkins pluton provides an excellent natural laboratory to test the current models on partial melting because of the pluton's temporally segmented, yet brief emplacement time (2×10^5 years) and *in situ* crystallization of partial melt within the contact aureole.

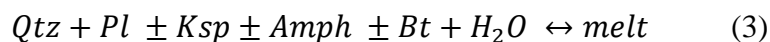
The pyrometamorphic contact aureole exposed on the eastern margin of the Mt. Perkins pluton is described as foliated Proterozoic biotite-amphibole tonalitic orthogneiss (Metcalf and Kopeitz, 2011). On the outcrop scale, the only evidence of deformation is exposed within a few meters of the contact along the northern exposure, but not observed in the southern exposure, and is described as an open fold. Deformation is not observed anywhere else within the contact aureole. The compositional bands are composed of alternating mafic and felsic layers. For this study, the mafic layer is ignored for reasons described in the sample collection section (Section 5.1). In collected hand samples the felsic band is composed of approximately 50% feldspar, 30% quartz, 15% amphibole and/or biotite, and 5% oxide. In general, the felsic layer is composed of approximately 80% feldspar and quartz, and their proportions relative to each other may vary

about 15%. In the northern exposure, biotite is the dominant mafic mineral until about 60 m east of the contact, where amphibole, like the entire southern exposure, is the dominant mafic mineral. Biotite and amphibole form a compositional layer that separates felsic layers.

4. Study Design

4.1 Hypotheses

The high temperature gabbroic intrusion (Figure 7, Phase 1) drove partial melting in the adjacent tonalitic gneiss which is represented as the grey area to the east of the phase 1 gabbro on Figure 7. Drawing on photomicrographs described by Metcalf and Kopeitz (2011) and observations from this study, the following six hypotheses are made: (1) partial melting was in a static (no deformation) environment where the heat budget diminished with increasing distance from the pluton, (2) there were no dehydration, incongruent melt reactions, (3) melting was dominated by Quartz (Qtz) + Plagioclase (Pl) + H₂O and at higher temperatures biotite (Bt) and amphibole (Amph) were dissolved into the melt. (4) K-feldspar melted with Qtz and Pl, but is a minor component, (5) melting was water saturated, and (6) the primary melt reaction is depicted in Equation 3.



These observations suggest congruent, hydrous melting (Equation 3). The shallow (paleodepth = ~7 km, Metcalf and Smith, 1991) Mt. Perkins pluton resides within a highly faulted and structurally complex extensional environment (Faulds *et al.* 1995), which allows for speculation of a meteoric water source. Alternatively, fractional crystallization of the hydrous, hornblende-bearing Mt. Perkins mafic magmas may have released water similar to the pyrometamorphic aureole of the western margin of the Ballachulish Igneous Complex (Holness and Clemons, 1999).

4.2 Predictions

Previous work on partial melting (experimental and natural) and the aforementioned hypotheses allow for the following predictions about rocks proximal to the Mt. Perkins pluton as compared to distal rocks: (1) larger heat budget such that proximal rocks undergo higher temperatures for a longer duration, (2) larger melt networks (i.e. melt pathways have higher connectivity), (3) higher melt volume, (4) higher probability of additional phases participating in the melt in higher temperature water-saturated melting (e.g. amphibole and biotite), (5) plagioclase composition should be more homogenized within crystals because of the higher heat allowing for more successful $(\text{CaAl})_1(\text{NaSi})_{-1}$ coupled substitution. Additionally, (6) Large melt pockets with euhedral plagioclase crystals should show “igneous-like” zoning and be anorthite-rich whereas small melt pockets should be anorthite-poor, and (7) conditions for dehydration melting of biotite and amphibole (i.e. $P = 3\text{kbar}$ and $T = 875\text{ }^\circ\text{C}$, Patiño Douce, and Beard, 1995; $P_{\text{H}_2\text{O}} = 2\text{kbar}$ and $T \approx 975\text{ }^\circ\text{C}$, Wyllie, 1978) were not met. The model presented by Sawyer (2001) on melt connectivity (Figure 5) suggests that rocks with a higher heat budget should progressively produce more melt, larger networks of melt pockets, and higher maximum temperatures for longer durations in comparison to rocks with a lower heat budget; a trend observed in many pyrometamorphic aureoles (Holness and Clemons, 1999; Rosenberg and Riller, 2000; Sawyer, 2001; Holness and Watt, 2002; Holness *et al.*, 2005; Holness and Sawyer, 2008; Bufe *et al.*, 2014) and can be predicted for the pyrometamorphic aureole of the Mt. Perkins pluton.

First melts typically begin where two or three phases are in contact; limiting Equation 1 and 2 to two or three reactants. The minimum melting temperature for plagioclase-dominant systems

is a range of temperatures. For example, for Qtz-Pl (Ab + An)-H₂O system at P = 2 kbar, melting begins at ~740 °C (Ab-rich) to ~920°C (An-rich; Johannes, 1989). The first reactants participating in the melt will have the lowest eutectic melting temperature assuming water saturated conditions within the system, indicating higher temperatures are required to involve other phases (Wyllie, 1978). Based on experimental work of Piwinski and Wyllie (1968), Wyllie (1977), Mehnert *et al.* (1973), and Busch *et al.* (1974), and microtextural considerations of thin sections from rocks within the Mt Perkins pyrometamorphic aureole, melting is predicted to begin at feldspar-quartz boundaries (Equation 1), until K-feldspar is exhausted (Equation 2) and include biotite and amphibole with progressively rising temperatures (Equation 3). Weinberg and Hasalova (2015) present a review of studies involving experimental and field studies which focus on hydrous melting reactions. They conclude that water saturated melting could produce melt with or without peritectic minerals (e.g. garnet, cordierite, amphibole, etc). Previous experimental work on tonalites suggests that melt reactions depend on P-T-x conditions. In experimental studies amphibole is reported replacing biotite or new amphibole crystallizes out of melt (Gardien *et al.*, 1999; Singh and Johannes, 1996; Busch *et al.*, 1974). However, Sawyer (2010) investigated leucogranodiorite, leucotonalites, and orthogneisses within the Opatca Subprovince in the Canadian Shield and observed a melt reaction described by Equation (2). Ferromagnesian phases were not involved in the reaction based on petrographic observations of biotite, however rocks investigated in this study rarely have biotite and/or amphibole within melt textures. Drawing from experimental and natural work on tonalities and observations in this study, the melt reaction rarely involved hydrous breakdown of biotite and/or amphibole, and Equation (2) best describes the most prevalent melt reaction.

The kinetics of plagioclase melting presents a complicating factor that must be accommodated. Plagioclase equilibrium within a given system is dependent on the $(\text{CaAl})_1(\text{NaSi})_{-1}$ coupled substitution via diffusion, which has been determined experimentally to be very slow at magmatic temperatures (Johannes, 1983, 1985, 1989). Plagioclase crystals proximal to the heat source should show evidence of more advanced stages of equilibrium compared to distal plagioclase given fast diffusion rates at higher temperature and with longer duration of heat infiltration.

5. Methods

5.1 Sample Collection

In order to test the aforementioned hypotheses samples were collected in two traverses orthogonal to the pluton-country rock contact, and point counted using a method modified from Holness & Clemons (1999) for distinguishing melt and residual (unmelted) minerals, which quantifies melt volume percent, and residual, melt, and whole rock chemistry. TitaniQ geothermometry (Wark and Watson, 2006) was applied to quartz crystals to quantify the cooling temperature of quartz crystals and confirm decreasing temperature with distance. Plagioclase chemistry was obtained to identify melt chemistry changes in zoned plagioclase crystals. Photomicrographs, SEM-CL and –BSE imagery were used to guide EMPA analysis of melt-derived plagioclase and quartz overgrowths.

Samples were collected along two traverses orthogonal to the pluton-country rock contact with the space between each sample progressively further apart with distance from the pluton in order to capture chemical and textural changes closest to the pluton (Figure 5). Distance from the pluton was measured using a field tape measure. Samples 111-2, 111-4a, 111-8, and 925-1 were provided by R. Metcalf and briefly discussed in Metcalf and Kopeitz (2011). Samples across two traverses on the eastern margin were collected in an effort to replicate results. Because of the abundant quartz and feldspar present in the felsic layers and the low probability that ferromagnesian phases are involved in partial melting, the felsic layers of the tonalitic orthogneiss were targeted, while the mafic layer portions were not collected, hence not analyzed.

Samples were cut into thin sections orthogonal to foliation, such that the long axis of the slide is parallel with foliation. Samples were evaluated for further analysis and point counting

based on three criteria: (1) geographic location of the sample, (2) abundance of alteration on a thin section scale (i.e. samples with significant visible alteration were not selected for further evaluation), and (3) samples that exhibited compositional and textural homogeneity on a thin sectional scale were favored over samples with heterogeneous textures and mineralogy (e.g. samples with large veins or quartz-rich subdomains were not selected). Samples were collected progressively further apart, which means that outcrops proximal to the pluton was preferentially sampled relative to distal outcrops. Additionally, samples, collected within 2 meters of a mapped dike were avoided or discarded because heat from the intruding dike could create secondary pseudomelt textures that may be misinterpreted as primary melt textures. However subsurface dikes that are not exposed at the surface cannot be ruled out as a complicated factor. Secondary alteration would overprint original mineral chemistry and may alter pseudomelt textures. Ideal samples selected for point counting exhibited homogenous compositional layering as well as homogeneous modal mineralogy within each compositional layer, such that a slide did not preferentially capture significantly more felsic or mafic layers than another sample collected within the same traverse. Select samples were analyzed using SEM and EPMA techniques and point counting.

Samples 136-1A through -11A were collected along the A-traverse (northern), while Samples 136-1B through -14B were collected along the B-traverse (southern). Samples with low numbers are proximal to the pluton whereas samples with higher numbers are distal. In the northern A-traverse, sample 136-1A was collected 0.15 m from the pluton-host rock contact, sample 136-6A was collected 8.84 m, and sample 136-11A was collected 91.44 m. Along the B-traverse, sample 136-2B was collected 0.46 m from the pluton-host rock contact, sample 136-8B was collected 7.01 m, and 136-14B was collected 60.96 m from the contact.

5.2 Point counting method

Point counting was used to quantify melt and residual volume percent, and melt, residual, and whole rock compositions. Holness and Clemons (1999) point counted their samples using a 1000 count grid density that encompasses the whole slide, and divided mineral identification into two categories based on texture: melt and residual (unmelted; Figure 9). In this study, points that were selected as melt had three criteria: (1) the point must be on a pseudomelt texture described in this study (e.g. melt film, string of beads, or large pseudomelt pocket), (2) melt textures surrounded by quartz and/or plagioclase residual crystals, and (3) plagioclase rims were counted as pseudomelt if they were observed within a melt texture and the point was clearly on a rim that was discernable from the core. Ambiguous points were counted as residual. Melt textures observed within the scale of one slide are too small for a whole-slide 1000 point grid density. The grid spacing must be tight enough to accommodate small melt film, but cover enough of the slide to reduce bias toward non-melt textures. Thin sections were scanned into a PC using a flat-bed scanner in order to visually analyze scanned slides to observe mineralogical and textural heterogeneities, and avoid hydrothermally altered samples. Selected samples exhibited visual textural and composition homogeneity; therefore a strip approximately 5mm wide orthogonal to the long axis of the slide was point counted (Figure 10). The goal was to find a grid spacing that encompasses enough of the “strip” while ensuring that small (<0.5mm) melt textures are counted. Determining the grid spacing was an iterative process where distance between points, or grid spacing, was manipulated using a guide tool in Adobe Photoshop© to ensure melt textures are being counted and reduce bias toward non-melt minerals. Points were set at a ~0.38 mm spacing creating a grid that has 1090 points on the vertical stripe of the slide.

Determining the minimum number of counts is required to produce consistent results and to evaluate the effect of sample heterogeneity on counting. Sample 925-1 was counted with 1090 points (See *Appendix A*, Tables A1-A2 for results) and subdomains within the counted area were analyzed to test the homogeneity of the slide (Figure 11). Individually subtracting the upper, lower, left, and right halves, and removing some of the points by random selection, points of each count revealed melt volume percent. To randomly select points, each layer or point is numbered from 1-1090. A random number generator provided 100s of numbers which are tied to a label (or point) and then discarded. The remaining points are selected to be analyzed for melt and residual volume percent. Random selection has an average melt volume percent of $38 \pm 0.88\%$ and the selection portions average melt volume percent is $38 \pm 4.3\%$. While the random selection has the narrowest error, the standard deviation for all point counting strategies is within range of each other, confirming homogeneity within the strip. Random selection requires significantly more time to count, and counting only the top 521 points has a melt volume percent that is within range of the random selection mean and the total pilot count (Figure 11). For further counts a 1090 point grid was overlain the stitched photomicrograph image, then only the top 650 points of the composite image were counted to reduce counting time and maintain efficient grid spacing. A total 650 points were used instead of the 521 points to add more data to each count.

Pseudomelt textures are often too small to be observed at low power magnification (e.g. 40x) and require high magnification ($\geq 200x$), and quartz overgrowth textures require SEM-CL imaging. One photomicrograph is insufficient to point count because not all textures or mineralogy could be observed in a small image relative to the whole slide, nor could additional information (e.g. SEM-CL images) necessary to identify melt textures. Thus a composite image

consisting of photomicrographs, SEM-CL, and SEM-BSE images was created. The method used to create the composite image is to take multiple photomicrographs, and SEM –CL and –BSE images and stitch them together in Adobe Photoshop© to create one image with many overlays. Overlays were toggled on or off using the Layers window in Adobe Photoshop© (Figure 9). Optical microscopy reveals melt textures, but identifying minerals, particularly distinguishing feldspars and quartz, can be difficult and quartz overgrowths are not observable. To alleviate these problems, SEM-EDS was used as a second order mineral identification tool, and following Holness and Watt (2001) SEM-CL was utilized to observe CL-bright quartz overgrowths on dark, residual quartz grains (Figures 6a, 9, and 12). Backscatter electron and CL images are stitched together and overlain in Adobe Photoshop CS6© on the selected area to be point counted (Figures 9, 10). The guide tool in Adobe Photoshop© is not robust enough to create such a precise spacing; hence GuideGuide by Cameron Mcefee (<http://cameronmcefee.com/>) was necessary (light blue grid lines in Figure 9). To track the counts each point (or guide intersection) is represented by a layer containing a circle. Each point is then categorized by moving the layer from the generic points group into the respective melt or residual mineral category (Figure 9). After all the points have been categorized, a script designed to rename selected layers developed by Trever Morris (<http://morris-photographics.com/>) was used on each group to rename each layer in numerical order, essentially counting the points. The end result is a numerical value for each melt and residual mineral and a graphic representation of where each mineral and/or melt is located.

Point counting with Adobe Photoshop© requires knowledge of manipulating layers in Adobe Photoshop© and some additional add-ons, but has added benefits over traditional point counting. Points can be color-coded for easy identification of mineral populations within the

sample. For example, melt vs. non-melt minerals can be color-coded to visually display melt-rich vs. melt-poor domains. Because of the subjective nature of identifying minerals (or other criteria such as textures) optically, interpretations may be changed and counts can be edited afterwards to reflect such changes. Minerals can be counted and categorized using any criteria. However, the preparation requires high-resolution photomicrographs and a petrographic microscope is required during counting to ensure proper mineral identification. Depending on how minerals are categorized this method may be more time consuming than traditional point counting because of the preparation involved and criteria used to categorize minerals.

5.3 Analytical Methods

Selected samples were prepared as polished thin sections, carbon-coated and analyzed using SEM-BSE, -CL, and -EDS techniques using a JEOL JSM 5610. For BSE and EDS analysis the accelerating voltage was 15 KeV, spot size was 40 microns, and the working distance was 20 microns. SEM-CL images were obtained using an accelerating voltage of 15 KeV, spot size 50 microns, and a working distance of 20 microns. Some samples had plagioclase grains with CL-bright rims that proved to be problematic when attempting to observe CL-bright quartz rims. Two methods were used to alleviate this: (1) the spot size and working distance was decreased in effort to capture less CL signal, but reduce the plagioclase signal, or (2) the spot size was increased to capture more, but less focused CL signal. Both methods were used to capture CL-bright rims on quartz crystals where possible, but relatively reduce the CL signal being received from plagioclase crystals.

Mineral chemistry was obtained by electron probe microanalysis (EPMA) at UNLV on a JEOL JXA-8900 superprobe. The EPMA lab has a comprehensive set of oxide, carbonate,

sulfide, sulfate, and native element standards that cover the majority of the periodic table for quantitative analysis. Mineral analyses were performed under the condition of 15 kV accelerating voltage, 10 nA beam current, 20 μm beam size, and 30 seconds peak counting time. The beam size was reduced to a range of 2 μm to 10 μm to capture small scale chemical variations on plagioclase (i.e. An content variation along a 2D transect on a plagioclase crystal). Calibration standards include Gellar pure Si and Mg standards, Ca, Cr, Fe, Ti, Na, and P from Smithsonian standards, plagioclase for CaO, chromite for Cr_2O_3 , ilmenite for TiO_2 , MnO and FeO, albite for Na_2O , apatite for P_2O_5 ; Al, K, F and Cl from MAC standards, orthoclase for Al and K, fluorite for F, and AgCl for Cl. Several standards from Smithsonian were analyzed as internal standards to monitor the accuracy and precision of the analyses. Average values and percent differences of these standards for the period of the study can be provided. Mineral analysis of quartz for trace titanium were performed under the condition of 20 kV accelerating voltage, 150 nA beam current, 2 μm beam diameter. Counting time was 300 seconds on peak and 100 seconds on both background. SiO_2 was fixed as 100 percent.

5.4 Geothermometry

Titanium-in-Quartz (TitaniQ; Wark and Watson, 2006) was applied due to the prevalence of quartz crystals with CL-bright rims. Such CL-bright rims have been interpreted as melt overgrowths in other pyrometamorphic aureoles (Holness and Watt, 2001; Holness and Sawyer, 2008; Holness, 2008; Bufe *et al.*, 2014). In the samples collected in this study rounded quartz crystals associated with pseudomelt textures typically have CL-bright rims with CL-dark cores interpreted as melt overgrowths on residual quartz. Spatial association with Ti-saturating phases (oxide minerals and CL-bright overgrowths suggest chemical communication. Geothermometers

using oxides (e.g. ilmenite-magnetite, Powell and Powell, 1977) or hornblende-plagioclase (Hollond and Blundy, 1994) could not be applied with confidence due to the difficulty identifying minerals involved with the melt and/or the scarcity of these temperature-sensitive minerals. The cause of CL signal in minerals is not well constrained, but studies show it can be related to either by trace element impurities or lattice defects (Gotze *et al.*, 2000). Titanium concentrations within quartz have been shown to correlate with CL-brightness (Holness and Watt, 2003; Figure 12). Using CL images as a guide, titanium concentrations were collected along transects across quartz grains (Figure 6a, 12).

Titanium activity must be constrained to apply the TitaniQ geothermometer. Ti-bearing phases can reveal information about titanium activity. Samples collected for this study have trace amounts of ilmenite, rarely sphene, and more rarely rutile. Because rutile is not the dominant titanium-bearing phase and ilmenite is present, titanium activity must be less than 1.0. Comparing the tonalitic orthogneiss of Mt. Perkins with other studies of common rock types should delimit a_{TiO_2} for rocks in this study. Wark and Watson (2006) report that the Bishop Canyon Tuff has trace ilmenite and $a_{\text{TiO}_2} = 0.6$ implying rutile is absent. Ghent and Stout (1984) have analyzed metabasites and metapelites in the southeast Canadian Cordillera, and concluded that metapelites have $a_{\text{TiO}_2} > 0.8$, and metabasites have $a_{\text{TiO}_2} > 0.6$. In this study we estimate $a_{\text{TiO}_2} = 0.6$ for the following reasons: (1) Rutile is nearly absent and the tonalitic orthogneiss has a magmatic origin as opposed to metapelites studied in Ghent and Stout (1984), thus $a_{\text{TiO}_2} \neq 1$. (2) The highest temperature recorded by geothermometry results is 818 – 918 °C (sample 136-6A; Section 6.9). Experimental work on tonalities from Wyllie (1978) shows that at $P_{\text{H}_2\text{O}} = 2\text{kbar}$, temperatures must be above 975 °C to induce dehydration melting. While geothermometry suggests this sample may have undergone dehydration melting, peritectic

minerals (e.g. orthopyroxene) were not observed and other samples in this study have TitaniQ temperatures below 975 °C. Wark and Watson (2006) show that underestimating $a\text{TiO}_2$ results in artificially high temperatures, and $a\text{TiO}_2$ is most likely less than 0.6 for rocks in this study. Thus, our TitaniQ temperatures are most likely minimum values and actual temperatures are likely underestimated by 25-50 °C for an overestimation of $a\text{TiO}_2$ by 0.1-0.2 over the temperature interval of 700-1000 °C (Wark and Watson, 2006). Although the temperatures reported do not record absolute temperatures, the change in temperature (Figure 12) over transects from dark cores to light rims is significant and show systematic change from low temperature cores to high temperature rims on quartz crystals.

6. Results

6.1 Mineralogy and Textures

Table 1 shows which minerals are found in each texture, and Table 2 is comprised of modal mineral volume percent, distance from the pluton, and melt percent obtained from point counting. All samples are dominated by quartz (21.5 % - 51.9 %), plagioclase (36.3% - 64.2%) and a mafic phase (5.2% - 13.1%); the latter is typically amphibole or biotite (Table 2). Orthopyroxene, a common product of dehydration melting of biotite or amphibole (Patiño Douce and Beard, 1995), was not observed. The modal mineralogy of each sample is catalogued into three types: melt, residual, and whole rock. The mineralogy of the melt is quartz, plagioclase and K-feldspar, while the residual has quartz, plagioclase, and mafic minerals. In the A-traverse, samples 136-1A and -6A are biotite rich with respect to 136-11A, -2B, -6B, and -14B, which have amphibole instead of biotite. All samples have minor amounts of K-feldspar, magnetite and ilmenite (listed in Table 2 as “Opaque”), and trace amounts of apatite and zircon. Zircon was observed in thin sections, but is too small to be counted via point count, therefore not listed in Table 2. Sample 136-14B has trace amounts of spinel, and samples 136-2B and 136-8B have trace amounts of clinopyroxene.

Three specific textures were recognized as “mappable units” used as a guide for identifying pseudomelt pockets: (1) melt films, (2) string of beads, and (3) large pseudomelt pockets. Two prominent textures observed at the Mt. Perkins pluton aureole are similar to those reported by Holness (2008) and Holness and Isherwood (2003): melt films and string of beads (Holness and Isherwood, 2003), and examples of pseudomelt textures observed within the pyrometamorphic aureole of the Mt. Perkins pluton are shown in Figures 6 and 8. Major minerals found in

pseudomelt textures are quartz, plagioclase and K-feldspar. Most melt films observed in this study are anhedral plagioclase inserts between rounded quartz crystals, although rarely, biotite and K-feldspar are present in melt films (Figure 2a, b, d; Figure 8a-f). Melt film sizes range from 0.1-0.5 mm at their largest axis. String of beads textures are described as euhedral plagioclase crystals between residual quartz and/or plagioclase crystals (Figure 6c, 6e; Figure 8g-i). The string of beads plagioclase crystals are often 0.5-1.0 mm in diameter at their largest axis, and the neighboring residual quartz and/or plagioclase commonly measures ≥ 1 mm.

In the rocks examined in this study an additional melt texture was identified, designated as large pseudomelt pocket (Figure 6c, f, g; Figure 8j-l). These textures range in size from 0.25 to > 1 mm, and consist of sub-euhedral plagioclase crystals are enveloped by K-feldspar and rarely quartz, and are commonly outlined by large (>1 mm) residual quartz and/or feldspar crystals. Plagioclase crystals within the large pseudomelt pocket commonly have rounded cores with optically zoned rims (Figure 6f-g, Figure 8j).

All melt films were associated with quartz-feldspar contacts, and residual quartz crystals commonly have CL-bright rims in contact with the melt film (Figures 6a, 12), CL-bright rims are in contrast to darker rims seen in CL.

6.2 Point Count Results

The mineralogy and modal volume percent of the pseudomelt and residual textures for samples collected for this study are presented in Tables 1 and 2. The mineralogy of pseudomelt and residual textures observed in this study are dominated by quartz and plagioclase with minor K-feldspar. Only rarely were ferromagnesian minerals (biotite or amphibole) observed within the pseudomelt textures. Qualitative results are available via point counting. Samples 136-1A, -6A, -

2B have trace biotite (Figure 8e) or amphibole in pseudomelt pockets, while samples 136-11A, -8B, -14B lack biotite and amphibole in pseudomelt pockets. Trace amounts (<1%) of apatite are observed in pseudomelt pockets. In samples 136-1A and 136-6A biotite is enriched in residual textures compared to pseudomelt textures. In sample 136-11A, biotite is not observed in either pseudomelt nor residual textures. Amphibole and biotite are observed in residual textures in sample 136-2B. Amphibole is rarely observed in pseudomelt textures, and amphibole is more abundant than biotite in residual textures. However, amphibole is present as a volumetrically minor component in pseudomelt textures, and amphibole is enriched compared to biotite in residual textures, similar to sample 136-8B. In sample 136-14B, amphibole is observed in residual textures only. Clinopyroxene is only present in samples 136-2B and 136-8B as a residual texture (Figure 13). The clinopyroxenes have similar size to amphiboles, are subhedral, and have biotite inclusions, all of which suggest clinopyroxene is an original constituent to the protolith, and is not a product of dehydration melting (i.e. compare to peritectic clinopyroxene observed by Singh and Johannes, 1996). K-feldspar is observed in all pseudomelt textures, however, in sample 136-1A K-feldspar is observed in residual textures as well.

6.3 Melt connectivity

Analyzing melt connectivity can reveal qualitative information about melt volume percent. At the onset of partial melting, melt pockets may be isolated, while late-stage partial melting can link melt pockets, and allow partial melts to chemically communicate (Sawyer, 2001). By highlighting textures interpreted as pseudomelt within a photomicrograph, the 2D connectivity of melts can be observed (Figure 14). Sample 111-2 has excellent pseudomelt textures (Metcalf and Kopeitz, 2011), and a representative photomicrograph from sample 111-2 (Figure 14) illustrates

the connectivity of melts within the pyrometamorphic aureole of the Mt. Perkins pluton. Figure 14 illustrates pseudomelt pockets that are connected locally around quartz-feldspar contacts. Areas highlighted in purple are areas interpreted as pseudomelt pockets. Pseudomelt pockets are generally disjointed, although connectivity may be underestimated due to the 2D nature of thin sections. Ergo, connected pseudomelt pockets may not be observed in 2D, but exist in 3D. For example, distinct large pseudomelt pockets are generally observed within close proximity of each other with melt films extending toward neighboring pseudomelt textures. Ferromagnesian minerals and monomineralic (e.g. quartz or plagioclase dominated) domains generally disrupt connectivity as well as quartz or plagioclase dominated domains. However, quartz-plagioclase contacts may be void of interlocks, suggesting melt has not migrated, nor formed within plagioclase-quartz contacts (Figure 14). In general for the contact aureole of the Mt. Perkins pluton, pseudomelt textures observed in thin sections are weakly or not connected and variability between samples was not observed.

6.4 Plagioclase chemistry with respect to textures.

Plagioclase chemistry was investigated to observe variation in An content with respect to residual textures and three pseudomelt textures described in this study using samples 925-1, 111-2, 111-4a, and 111-8, which were collected in Metcalf and Kopeitz (2011) and have a diverse set of easy to interpret pseudomelt textures. In large pseudomelt pockets euhedral plagioclase with optically zoned rims and rounded cores were targeted. Cores and rims were targeted for euhedral plagioclase in string of beads pseudomelt textures. Variations in plagioclase composition in melt film pseudomelt textures were investigated by targeting points on the texture proximal and distal to surrounding residual minerals. Sample 111-8 lacks clear pseudomelt textures compared to the

other samples, and only residual plagioclase was investigated using EPMA analysis. See *Appendix B*, Figures A1-A14, Tables A21-A56 for texture and EPMA results.

Figure 15 is a histogram showing the average An% content based on sample and texture. Numbers are reported as mean plus or minus standard deviation to show variability. Figures 16-19 show the same information on An-Ab-Or ternary diagrams. In sample 111-2 (Figure 16) large pseudomelt plagioclase (LPP) has a mean An% of $44 \pm 4\%$ ($n = 68$), which is similar to that of residual plagioclase which has An% of $40 \pm 2\%$ ($n = 106$). Sample 111-4a (Figure 17) melt film, string of beads, and overgrowth plagioclase crystals have an average An% of $37 \pm 7\%$ ($n = 70$), $42 \pm 3\%$ ($n = 33$), and $43 \pm 6\%$ ($n = 10$), respectively, which is similar to that of residual plagioclase crystals which has an An% of $40 \pm 2\%$ ($n = 34$). Sample 925-1 (Figure 18) LPP and string of beads textures have an average An% of $36 \pm 2\%$ ($n = 109$) and $35 \pm 2\%$ ($n = 13$), respectively, and are similar to the average An% of residual plagioclase crystals, which is $36 \pm 1\%$ ($n = 39$). The low An% (8-12%) for melt films in 111-4a are from analysis of points on plagioclase crystals that are very close ($<10 \mu\text{m}$) of neighboring residual crystals. Sample 111-8 (Figure 19) has no petrographically visible melt textures, but seven residual plagioclase crystals were analyzed, and their average An% is $41 \pm 1\%$ ($n = 145$). The range of average residual plagioclase crystals are more restricted (1-2% standard deviation) compared to melt texture plagioclase crystals (2-7% standard deviation). Melt films and SOB plagioclase have a lower, but less restricted mean An% (Figure 15).

The analysis of plagioclase crystals based on texture found that residual and pseudomelt plagioclase An% show little difference in their mean An%, with the exception of pseudomelt plagioclase crystals in very small spaces (Figure A9). The wider range of An% in all melt textures for samples 111-2, 111-4a and 925-1 could be caused by fractional crystallization where

plagioclase grains nucleate in relatively larger pore space (Figure 17), preferentially incorporating more Ca in their crystal structure compared to Na. Plagioclase crystals that have formed in this way have low An% components in small spaces where temperature has decreased enough to overcome nucleation difficulties in small spaces (i.e. Holness and Sawyer, 2008). Figure A9 illustrates this by showing An% ~45 plagioclase in larger space, but An 8-12% in relatively small space. Another possibility is that plagioclase melting was retarded due to kinematic factors (Ashworth, 1985), a problem known as the “plagioclase problem”. Residual plagioclase crystals probably never approached equilibrium with the melt, and new plagioclase overgrowths or crystals have similar An% components compared to unmelted, residual plagioclase crystals (e.g. Johannes and Gupta, 1982; Gupta and Johannes, 1982). Because the mean An% for different plagioclase textures is within error of each other textures, plagioclase chemistries were not separated for further analysis based on texture. Instead, representative plagioclase chemistries for samples 136-1A, -6A, -11A, -2B, -8B, -14B, were calculated using the mean An% for each sample.

6.5 A and B traverse plagioclase.

Given the plagioclase problem discussed above (Section 6.4), plagioclase composition from the samples from traverses A and B were used without regard to texture. The results of EMPA analysis of plagioclase for A and B traverse plagioclase are shown in Table 3 and plotted on the Ab-An-Or ternary diagram (Figure 20). Plagioclase crystals were chosen for geochemistry at random within a representative site, having a range of common minerals that compose the rock, as well as plagioclase crystals in multiple melt and residual textures. Most plagioclase crystals were large enough for at least one core and rim spot to be analyzed. The average An% of

plagioclase in the 136-1A, 136-6A, and 136-11A is $37 \pm 2\%$ ($n = 20$), $37 \pm 3\%$ ($n = 25$), and $45 \pm 3\%$ ($n = 66$), respectively. Sample 136-1A and 136-6A plagioclases have An% that are within the standard deviation of each other, while 136-11A is ~ 8 An% higher. This difference is likely due to differences in inherited protolith compositions as the lower samples with lower An% plagioclase are biotite-bearing (136-1A, -6A), while the higher An% is amphibole bearing (136-11A). The standard deviation is narrow (2-3 An%) which indicates little change in plagioclase chemistry in residual and melt geochemistry, similar to that observed in samples 111-2, 111-4a, and 925-1 discussed above.

Plagioclases in samples 136-2B, 136-8B, and 136-14B (B-traverse) have an average An% of 57 ± 4 ($n = 29$), 48 ± 5 ($n = 60$), and 41 ± 2 ($n = 78$), respectively (Figure 20; Table 3). The rocks within the B-traverse lack a lithology change and amphibole is the dominant ferromagnesian phase, similar to 136-11A.

6.6 Calculated whole-rock, melt, and residual geochemistry

Because there is no evidence of melt migration the whole rock geochemistry is derived from the total point count for each sample, while melt and residual are calculated from dividing the total into two categories based on texture while counting: melt and residual. Table 4 shows the distance from the pluton, melt volume percent, rim and core TitaniQ temperatures and the calculated whole-rock, melt, and residual geochemistries obtained from point counting (see *Appendix* Tables A3-A20). Point counts and mineral chemistries were used to calculate whole-rock, melt and residual geochemistry. EPMA analysis of minerals for samples 136-1A, -6A, -11A, -2B, -8B, -14B are available in *Appendix* (Figures A15-A20, Tables A57-A66). Table 5 shows the CIPW normative mineralogies calculated using whole, melt, and residual

compositions reported in Table 4. Plagioclases interpreted as pseudomelt and residual (i.e. cores and rims) were not separated because plagioclase compositions do not vary significantly between interpreted pseudomelt textures and residual textures (Figures 15-20). Plagioclase chemistries were calculated regardless of texture and a mean plagioclase chemistry was used to calculate melt and residual composition. Figure 21 represents melt chemistries the A-traverse, while Figure 22 represents the B-traverse. Values listed in vertical, bold text represent sample number, and the x-axis is distance from the pluton. For the A-traverse, the maximum and minimum MgO weight percent value for melt is 0.5 (-1A) and 0.02 (-11A), respectively. The maximum and minimum value for FeO weight percent for melt is 0.85 (-1A) and 0.06 (-11A), respectively. FeO and MgO for melts decrease with distance from the pluton. The maximum and minimum K₂O weight percent value for melt is 2.68 (-11A) and 1.93 (-6A), respectively, and the maximum and minimum value Na₂O weight percent value for melt is 4.24 (-11A) and 3.21 (-1A), respectively. K₂O and Na₂O show an increasing trend with distance. The maximum and minimum CaO weight percent value for melt is 4.51 (-11A) and 3.11 (-6A), respectively. CaO shows a weak increasing trend with distance.

The B-traverse (Figure 22) the maximum and minimum MgO weight percent value for melt is 0.36 (-2B) and 0.01 (-14B), respectively. The maximum and minimum FeO weight percent value for melt is 0.70 (-2B) and 0.10 (-14B), respectively. FeO and MgO show a decreasing trend with distance. The maximum and minimum K₂O weight percent value for melt is 1.92 (-14B) and 1.07 (-8B), respectively, and the maximum and minimum Na₂O weight percent value for melt is 2.52 (-8B) and 1.95 (-2B), respectively. K₂O and Na₂O show an increasing trend with distance. The maximum and minimum CaO weight percent value for melt is 5.10 (-2B) and 3.03 (-14B), respectively. CaO shows a decreasing trend with distance.

Figures 23-28 illustrate the change in total, melt and residual MgO and FeO weight percent values with respect to SiO₂. Weight percent values for MgO and FeO increase and SiO₂ decrease in the residual compared to the total chemistries. The opposite is true for melt chemistries as melt chemistries have enriched SiO₂ weight percent values compared to the whole rock melt chemistry, ~10-20 percent increase. Residual SiO₂ weight percent values are depleted by ~ 4-8 percent. The change between whole rock and melt or residual for SiO₂ weight percent is lesser for samples 136-11A and 136-14B when compared to their proximal counter parts (-1A, -6A, -2B, and -8B). A similar trend is true for FeO and MgO weight percent.

6.7 Melt, residual, and whole rock geochemistry in the Q-An-(Ab+Or)-H₂O system

Johannes (1989) experimentally determined the cotectic liquidus relationships for the Quartz (Q), Anorthite (An) and Albite (Ab) + Orthoclase (Or) system at P_{H₂O} = 2 kbar; this pressure is similar to pressure suggested by the paleodepth of the Mt. Perkins pluton. Melt, residual and whole rock (whole-rock) geochemistries for each sample from this study were plotted on the Q-An-(Ab + Or) ternary diagram and compared to the results of Johannes (1989) (Figure 29). whole rock bulk compositions plot within the plagioclase + liquid field for all samples, which suggests that under water saturated conditions quartz would be the first reactant to be exhausted. Melt compositions (Figure 30) for four samples (136-1A, -6A, 11A, 136-14B) plot near or on the cotectic, and samples 136-2B and -8B plot slightly off the cotectic within the plagioclase + liquid field. The melt composition for the most distal sample for each traverse plots as the lowest temperature for that traverse, while the closer sample plot at higher temperature compositions. Residual compositions are depleted in quartz relative to the whole rock composition, with the exception of sample 136-11A.

6.8 Melt volume percent

Melt volume percent results are presented in Table 2 and are plotted against distance in Figure 31, in general melt volumes are large in samples proximal to the pluton heat source. The B-Traverse has the highest melt percent with 136-2B, -8B, and -14B having melt volume percent of 26%, 30%, and 11%, respectively. Samples 136-1A, -6A, and -11A have melt volume percent of 18%, 23%, and 6%, respectively. The difference in melt volume percent between samples 136-1A and -6A may be negligible due to point counting uncertainties, and a similar argument exists for samples 136-2B and -8B. The B-traverse is adjacent to the olivine-clinopyroxene-plagioclase cumulate, most likely the highest temperature section of the gabbro unit (Rodney Metcalf, written commun., 2016), while the A-traverse is adjacent to hornblende gabbro area, a lower temperature section of the gabbro unit. Melt volume percent values may be underestimated due to the small sample size of the point count, and the homogeneity of quartz and plagioclase rich layers. In addition to, melt volume percent may be underestimated due to the sub-microscopic melt textures that were under point counted within the point count grid developed for each sample. Melt volume percent data taken from point counting mimics the up-then-down trend in temperature (Figures 31 and 32).

6.9 TitaniQ geothermometry

TitaniQ temperatures measured on each sample are compared with distance from the pluton (Figure 32); within each traverse calculated temperatures are large in samples proximal to the pluton heat source. Values were calculated using rim values only, and the error bars represent the

standard deviation of the mean rim temperature from multiple rim analyses. Because Ti concentrations are erroneously high as recommended by Wark and Watson, (2006), points that were within 100 μm of an oxide were discarded. The samples collected closest to the pluton have the highest range of temperatures (136-1A, 762 – 884 °C; 136-2B, n = 45; 663 – 833° C, n = 33). Sample 136-6A has the highest upper range of temperatures and spans the values 818 – 918 °C (n = 28). Sample 136-8B has a temperature range of 704 – 804 °C (n = 32), and 136-14B has a temperature range of 711 – 817 °C (n = 26). Sample 136-11A has no data because points were too close to an oxide and/or were below detection limit, which suggests temperatures were below 561 °C. Temperature rim averages increase with distance for the B-traverse, however all temperatures are within error. The A-traverse average rim temperatures increase, then decrease with distance.

These data show strong evidence for partial melting within the pyrometamorphic contact aureole in contact with the base of the Mt. Perkins pluton. The next section will describe the systematic nature of partial melting and distance as a proxy for time to demonstrate the chemical evolution of melt produced by anatexis of a tonalite protolith.

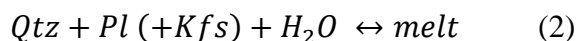
7.1 Discussion

7.1 Melt Textures

Melt textures (Figure 6, 8) are similar to those described by Holness *et al.* (2011) and Holness (2008; Figure 1c), and similar to experimental results of Jurewicz and Watson (1984; Figure 1a, b). The string of beads and melt film textures described by Holness (2008) were observed in this study (Figure 6c, e; Figure 8g-i). Photomicrographs show a pseudomelt pocket described in this paper as a “large pseudomelt pocket” where melt pools have recrystallized around residual “unmelted” plagioclase crystals, a texture not reported by others. (Figure 6f, g; Figure 8j-l).

7.2 Melt Reaction

As indicated by the point count data (See *Appendix A*, Tables A3-A20) plagioclase and quartz dominate the mineralogy of melt and non-melt textures, and other minerals (biotite, hornblende, oxides) were only very rarely identified as melt texture, but commonly identified in non-melt textures. The primary melt reaction was:



Similar to Opatca Subprovince investigated by Sawyer (2010), melting did not involve biotite or amphibole, and was generated along quartz-feldspar grain boundaries. The initial stages of melt are in agreement with Mehnert *et al.* (1973), and Busch *et al.* (1974) experimental studies that suggest that the initial stages of partial melting involve felsic minerals first and begin around grain boundaries of reactant minerals. The rocks in this study have biotite and amphibole with textures inherited from a prior metamorphic event, and/or show late-stage hydrothermal

alteration (e.g. biotite to chlorite). Additionally, biotite has straight contacts as opposed to wavy, embayed contacts with surrounding minerals implying biotite was not involved in melting (Busch et al, 1974). These lines of evidence suggest that ferromagnesian phases were not, or rarely, involved with melting, but may have dissolved in melt similar to tonalite melting experiments of Wyllie (1976). As mentioned in section 6.2 peritectic minerals such as pyroxenes and cordierite were not observed in association with pseudomelt textures, and clinopyroxene that is observed in samples 136-2B and 136-8B has textures that suggest it was inherited from the protolith. These lines of evidence preclude dehydration melting as described in Patiño Douce and Beard (1995).

Geothermometry and the lack of peritectic minerals (e.g. orthopyroxene, Patiño Douce and Beard, 1995) suggests the temperature was too low to facilitate water-absent quartz-feldspar melt generation ($T > \sim 925$ °C, $P = 2$ kbar; Wyllie, 1977), but high enough for water present quartz-amphibole and biotite gneiss melt generation ($T > \sim 700$ °C, $P_{H_2O} = 2$ kbar; Wyllie, 1977). Anhydrous incongruent melt products (e.g. pyroxenes, cordierite) were not observed within pseudomelt pockets, yet hydrous phases (biotite and amphibole) are present in pseudomelt textures (Figure 2, 3a, 3e). These lines of evidence from experimental studies suggest water-present melting (i.e. Bufe *et al.*, 2014; Sawyer, 2010; Holness *et al.*, 2005; Holness and Watt, 2002; Holness and Isherwood, 2003; Holness and Clemons, 1999; Pattison and Harte, 1988). There is evidence that suggests that the phase 1 gabbro (dominantly amphibole) was a wet melt which could have expelled water into the surrounding rocks during crystallization (Metcalf et al, 1995, Danielson, 1998). Because the Mt. Perkins pluton was emplaced at a shallow level (~ 2.5 kbar, ~ 7 km; Metcalf and Smith, 1991) a meteoric water source can also be surmised. TitaniQ geothermometry yields the highest possible temperature on sample 136-6A at 918 °C (Figure 32)

and the other samples have temperature values below the onset of dehydration melting in an anhydrous system which is 925 to 850 °C (Wyllie, 1976). Assuming $a\text{TiO}_2 \approx 0.6$ (section 5.4), all TitaniQ temperatures (Figure 32) are in agreement with the experimentally obtained P-T range for partial melt generation in tonalities (Wyllie, 1976). In addition, the P-T conditions of the contact aureole of the Mt. Perkins pluton were insufficient for dehydration melting as described in Patiño Douce and Beard (1995). These temperatures suggest the addition of water is necessary to induce partial, congruent melting as described by equation (2) within the contact aureole of the Mt. Perkins pluton.

7.3 Melt Volume

Melt volume percent and TitaniQ temperatures for each sample do not show systematic decrease when compared with the distance from the pluton (Figures 31 and 32). Some reasons for this are: (1) the contact between the phase 1 gabbro and the host rock is possibly irregular, such that the 2D distance measured from the contact does not reflect the 3D subsurface distance, (2) TitaniQ temperatures may not be accurate due to the estimated $a\text{TiO}_2$ and unknown growth rate for recrystallized quartz (Haung and Audétat, 2012), (3) water distribution may not be heterogeneous causing “pockets” of high melt production, and (4) convective heat transfer. Convective heat transfer may have influenced water to flow systematically in convection cell(s) causing “spikes” of high melt production. Melt volume percent and TitaniQ temperatures are most elevated in samples 136-6A and -8B (Figure 27-28), which are 8.84 and 7.01 meters away from the mapped contact. This suggests the contact between the country rock and the phase 1 gabbro is closer to these samples than 136-1A and -2B, which were collected within 0.61 meters of the mapped contact. Assuming the contact is closer to the intermediate samples or heat

transfer through convection in addition to conduction, these samples would show the most evolved melt chemistries and textures.

Given the lack of petrographic evidence of dehydration melting, water must be involved to generate high melt volume, the heterogeneous distribution of melt at thin section scale, the limited melt volumes, water was probably the limiting factor. Water most likely infiltrated fractures within the rock or was transferred with heat convection, then drove congruent melting where water was in contact with quartz-plagioclase boundaries. The driver for fluid mobility within the host rock could be caused by convective and/or conductive heat transfer.

7.4 Geochemical evolution

Limiting factors for the generation of melt are reactant availability, temperature, and time. Using distance as a proxy for time and TitaniQ geothermometry as a proxy for temperature (Figure 32) the chemical evolution of the melt and residual can be investigated. Melt chemistry from distal samples (136-11A and 136-14B) represent the least chemically evolved melt because these samples experienced melt-inducing conditions for the least amount of time compared to other samples. In the both traverses FeO and MgO are strongly depleted in the melt with respect to the residual. FeO and MgO decrease in the melt with increasing distance from the heat source or decreasing temperature (Figures 22 and 23). In addition, point count data (Table 2) shows that samples 136-1A (0.3 meters from contact) and 136-6A (15.24 meters from the contact) have biotite in melt textures, and sample 136-2B has amphibole in melt textures. This is in agreement with experimental work of Busch (1974) and Wyllie (1977) which suggest that FeO and MgO require elevated temperatures to migrate to the melt. Na₂O and K₂O decrease with increasing distance from the heat source and decreasing temperature, suggesting that first melts are

relatively enriched in Na_2O and K_2O relative to more evolved melts where higher temperatures dissolve Fe- and Mg-bearing minerals into the melt. Trends for Na_2O and K_2O are in alignment with conclusions presented in Johannes (1989), but may be reflective of the local geochemistry. However, CaO weight percent and An percent show opposite trends between the two traverses (Figures 21 and 22). Experimental work (Piwinski and Wyllie, 1968; Wyllie, 1977) suggest that restitic material should be elevated in CaO with respect to melt, and these data are in agreement (Table 2; Figure 21-22). This is most likely a function of the initial (protolith) whole rock chemistry as plagioclase chemistry shows no significant difference between crystals interpreted as melt or overgrowths compared to restitic, unmelted plagioclase crystals (Figures 15-19). The reason CaO does not show significant difference between melt and residual crystals are attributed to the “plagioclase problem” (Ashworth, 1985) where CaO experiences difficult intracrystal diffusion melting conditions due to kinetic barriers involved with $(\text{CaAl})_1(\text{NaSi})_{-1}$ coupled substitution. As melting continues more cations (e.g. CaO, FeO, MgO etc.) enter the melt and reduce the relative abundance of alkali metals (Figure 21-22).

7.5 Plagioclase geochemistry

Because the country rock is predominately quartz and plagioclase, the mobility of Ca, Na, and K can be investigated in further detail. In both traverses plagioclase crystals interpreted as melt and residual have negligible compositional differences (Figure 15-20), thus plagioclase geochemistry was compared within individual samples ignoring textures. In all samples plagioclase crystals near new quartz overgrowths (interpreted as overgrowth from melt) exhibit altered, rounded cores with optically zoned, euhedral overgrowths, however the An% of the cores and rims are too similar and should be ~20 An% different according to experimental work

(Ashford, 1985; Johannes, 1989). Johannes and Holtz (1992) suggested the cause of imperfect partitioning of Ca to environments with slow cooling and high H₂O where An% can be re-established. The rocks within the Mt. Perkins pluton contact aureole underwent fast heating and fast cooling with inhomogeneous “pockets” of high fluid. These data (evidence of water-saturated melting, disconnected melt pockets, Mt. Perkins pluton temporal history) suggest that high fluid content and fast heating followed by fast cooling temperatures can cause incomplete partitioning of Ca between melt and restitic plagioclase. Proximal rocks probably underwent melt conditions (i.e. longer duration at higher temperature) compared to distal rocks, which invoked the “plagioclase problem”, which caused incomplete melting of plagioclase crystals observed as unmelted, altered cores.

As predicted by Holness *et al.* (2011), as the contact cooled from peak temperature, fractional crystallization can cause plagioclase to be normally zoned such that cores are rich in Ca compared to rims. Textures and corresponding mineral chemistry confirm the hypothesis presented by Holness *et al.* (2011). Figure A9 shows a plagioclase crystal with no altered core and occupies space between rounded crystals (e.g. melt film). The crystal has no optical zoning; however, the core is An-rich compared to the smaller melt films that occupy the space between two residual crystals. Here there is a marked difference between core and rim An% content. This is most likely caused from fractional crystallization as the system cooled where Ca-rich plagioclase crystallizes first in large spaces, depleting the local melt in Ca. In small spaces, cooling must understep the thermodynamic barrier in order to crystallize. In small spaces the melt is “undercooled” and depleted in Ca, causing Na(+K) rich plagioclase to crystallize.

8. Conclusions

Experimental and natural studies have provided descriptions of pseudomelt microtextures that match those observed within the pyrometamorphic contact aureole of the Mt. Perkins pluton (Figures 1, 6, 8), which suggest these rocks were partially melted. Plagioclase involved with melt experienced the “plagioclase problem” as evidenced by the lack of significant change in An content between pseudomelt plagioclase and local residual plagioclase (Figures 15-20), although pseudomelt plagioclase in melt films show low An content (An₈₋₁₂) in very small spaces which record the crystallization history of plagioclase. Melt volume and peak metamorphic temperature are highest about nine meters from the contact and diminish further from the contact (Figures 31-32), which suggest the 3D contact is not reflective of the 2D map surface, and convective heat cells may influence heat transfer within the contact aureole. Melt geochemistries plot within error range of the cotectic (Figure 30) discovered experimentally by Johannes (1989), which is in agreement with petrological observations (i.e. residual plagioclase and quartz are observed). Samples proximal to the heat source have ferromagnesian minerals in pseudomelt pockets, while distal samples do not, illustrating that higher temperatures and a longer duration at melt-inducing conditions are required to breakdown ferromagnesian phases.

Characterizing the pyrometamorphic aureole of the Mt. Perkins pluton could benefit from applying the same methodology to an expanded suite of samples. This information could reveal a higher resolution of melt volume %, melt geochemistry, and *T_{itainQ}* temperatures. Such information could further reveal the nature of heat flow in pyrometamorphic aureoles. While water-saturated melting is implied here, investigating oxygen isotopes in fluid inclusions could reveal information about the water source, such that was the water from the crystallizing phase 1 gabbro or meteoric. Thermodynamic modelling could predict melting temperatures, melt volume

%, and $a\text{TiO}_2$, all of which would reinforce information obtained from the methods used in this study.

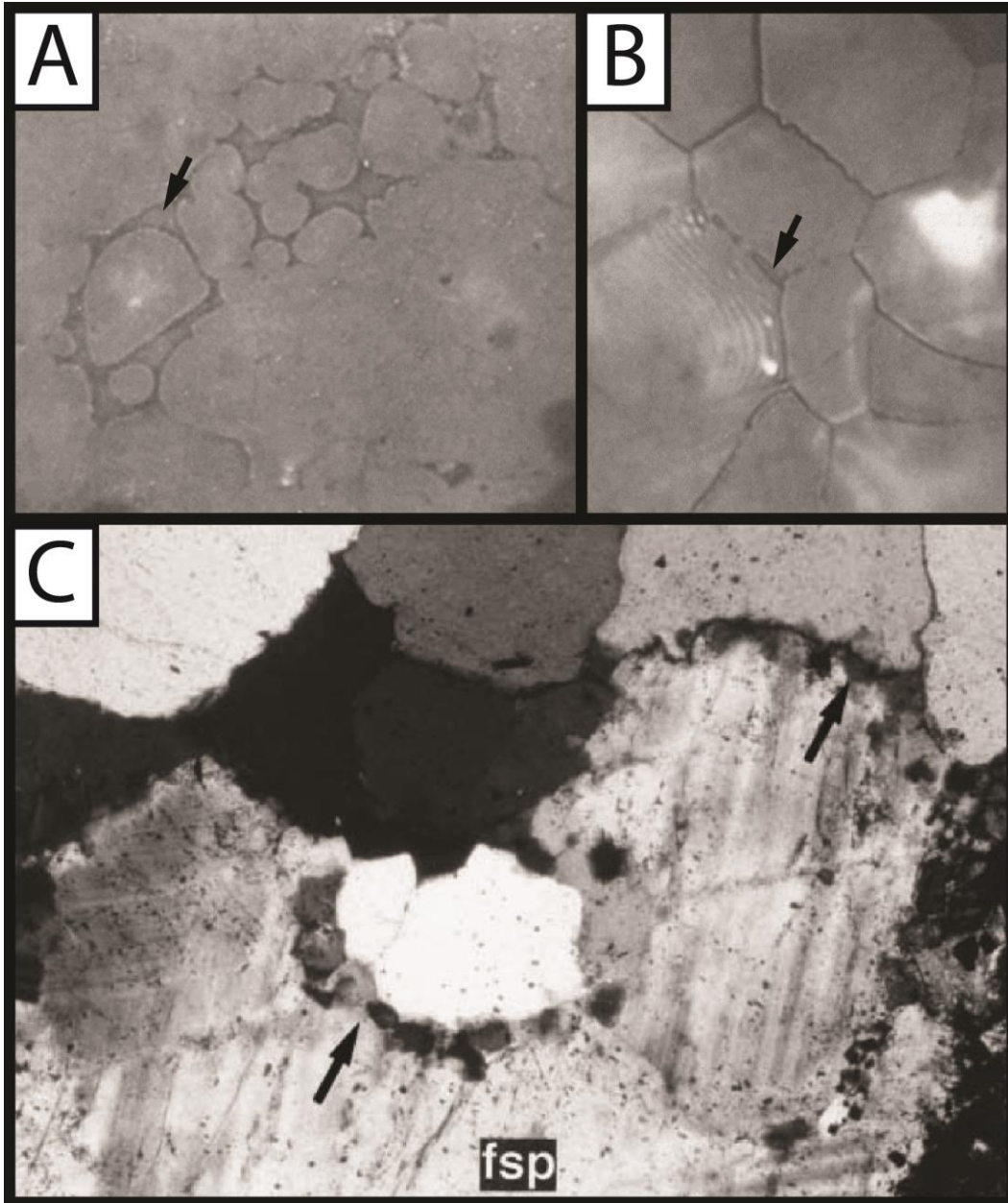


Figure 1. (A) SEM-BSE image of a large pseudomelt pocket within partially melted synthetic quartzite. The arrow indicates melt (darker material), while the rounded grains are quartz. No scale given (Jurewicz and Watson, 1984). (B) SEM-BSE image of a melt film within partially melted quartzite. The arrow indicates a melt film. The average grain size is 20 μm (Jurewicz and Watson, 1984). (C) Photomicrograph of “string of beads” pseudomelt texture within partially melted gneiss. The arrows indicate equant quartz and feldspar (fsp) grains of varying orientation between residual quartz and feldspar grains. The field of view is 1.25 mm across (Holness and Isherwood, 2003).

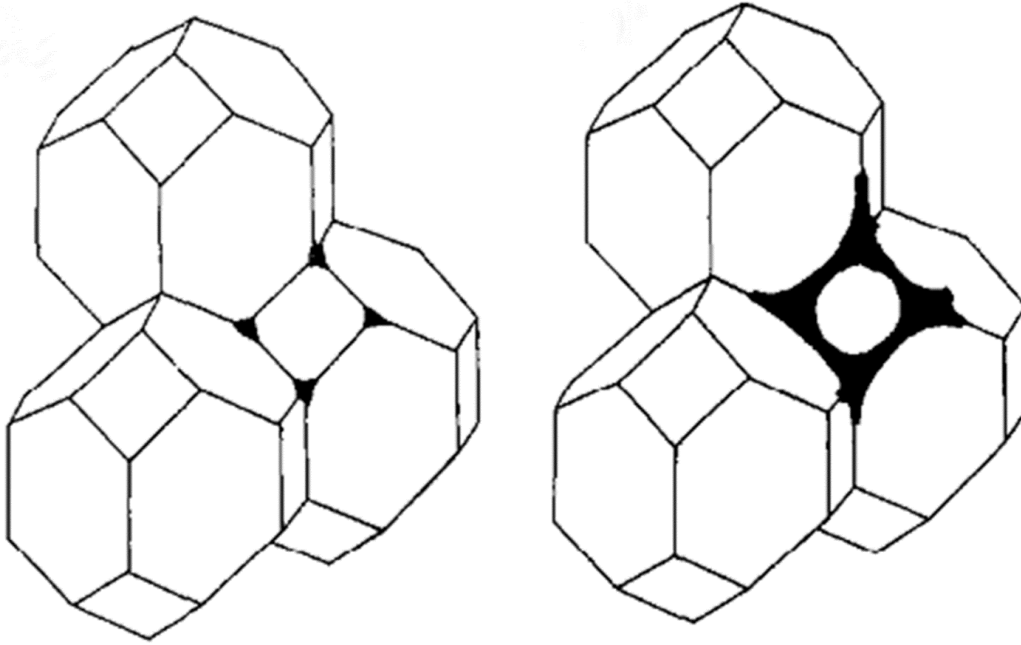


Figure 2. 3-D sketch of initial melting along crystal boundaries beginning with the left image and progressing to the right image (Sawyer, 2001).

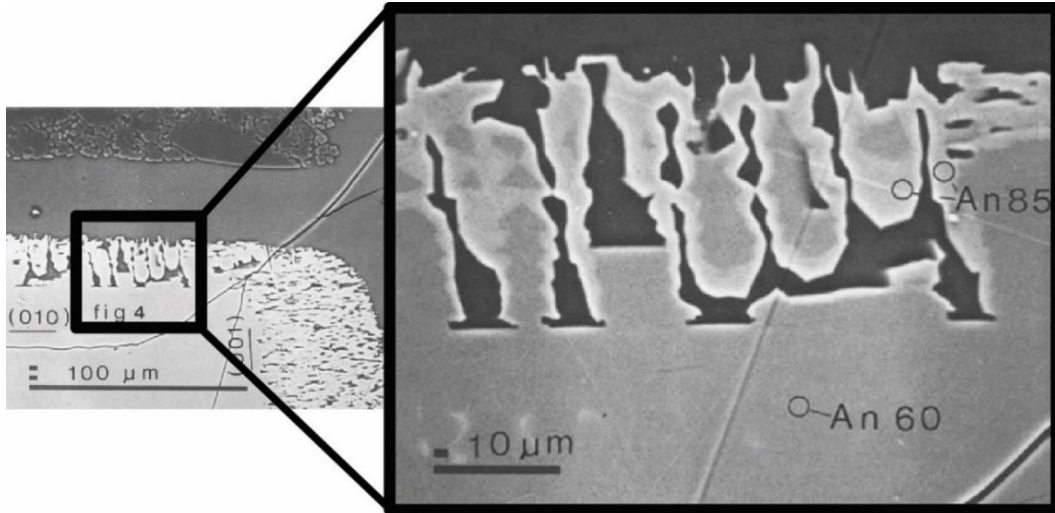


Figure 3. Images from Johannes (1989) showing the effects of "meta-stable" melting. The AN% 60 plagioclase crystal developed an AN % 85 core, which shielded the core of the original plagioclase causing incomplete melting (modified from Johannes, 1989).

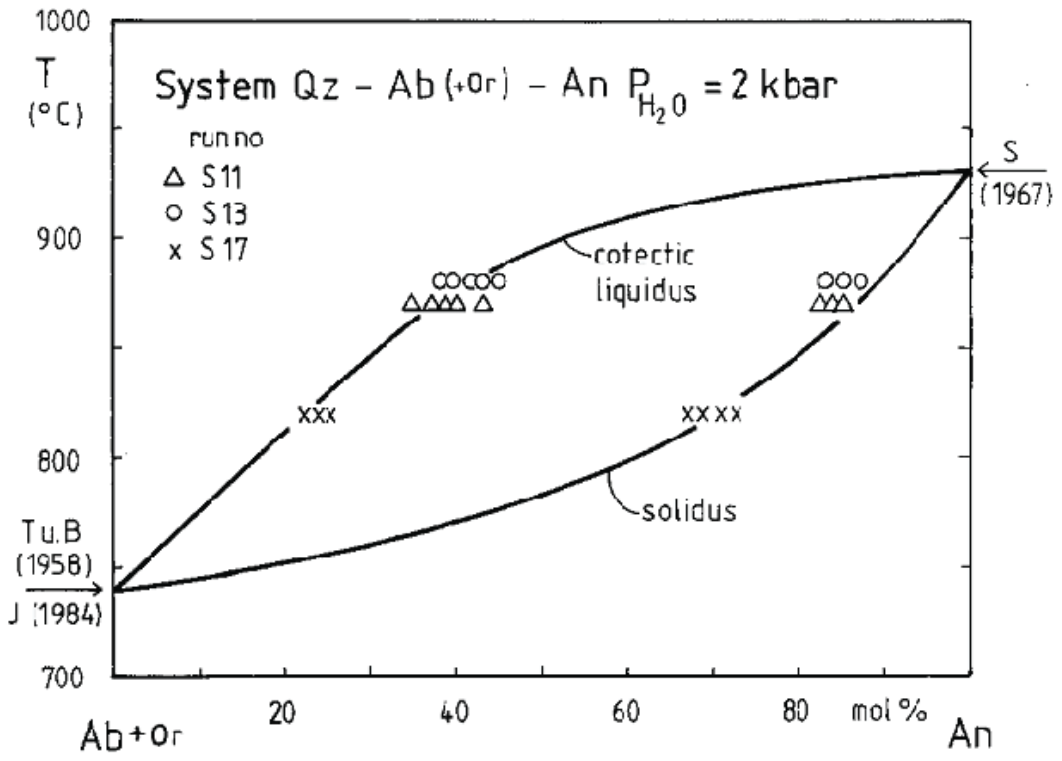


Figure 4. Experimental results of Johannes (1989). The solidus and cotectic liquidus are from Tuttle and Bowen (1958), Johannes (1984), and Stewart *et al.* (1967).

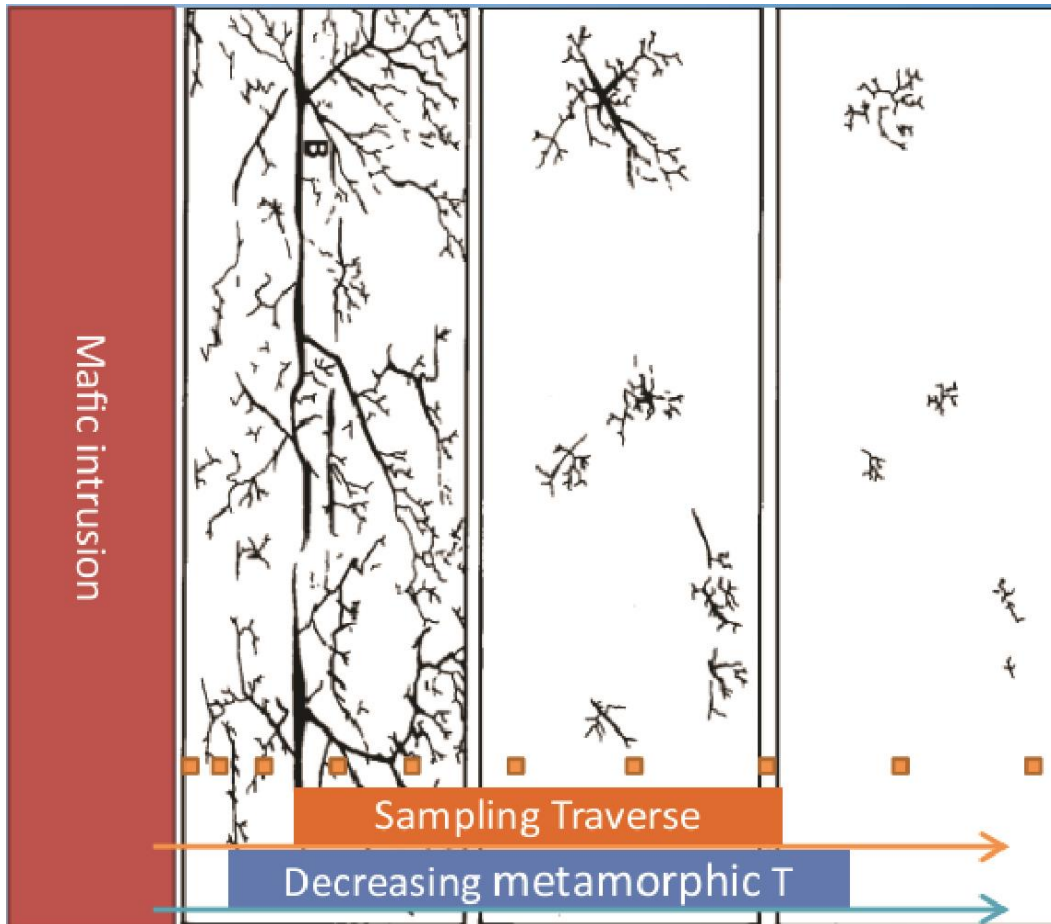


Figure 5. Cartoon of progressive melting away from the heat source. Black lines or veins represent melt. Note that melt pockets are disjointed and become progressively connected and larger for rocks closer to the heat source. The orange boxes represent the sampling strategy for this study. The distance between samples will progressively increase with distance from the heat source (mafic intrusion). Blue box and arrow represents decreasing metamorphic T (modified from Sawyer, 2001).

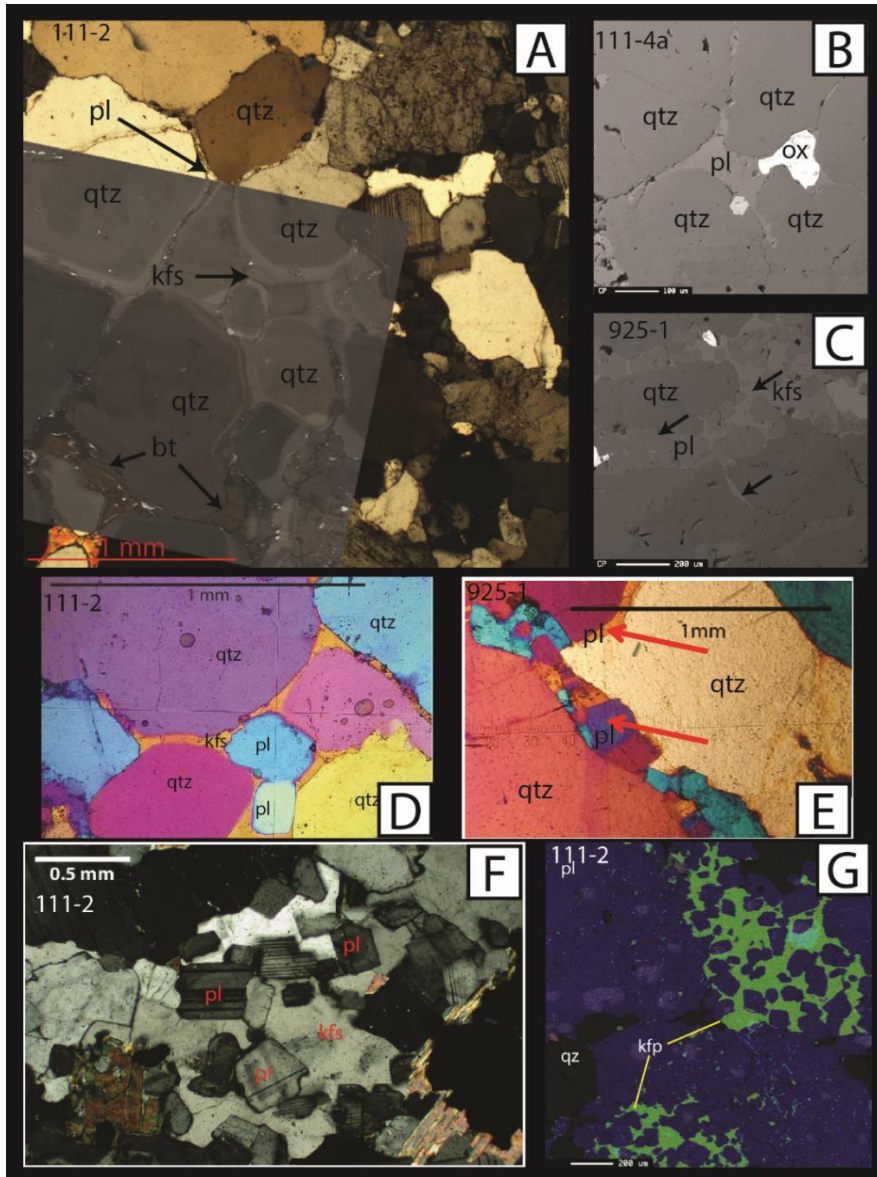


Figure 6. Photomicrographs or SEM images of melt films, string of beads, and large pseudomelt pockets from samples collected by Metcalf and Kopeitz (2011). **(A)** Sample 111-2. Photomicrograph with transparent SEM-CL overlay. Note the rounded quartz crystals with interstitial pseudomelt pockets. The melt film consists of plagioclase (top arrow), K-feldspar (middle arrow), and biotite (bottom arrow). The SEM-CL overlay shows quartz crystals with CL-bright rims and mottled cores similar to those observed in Holness and Watt (2001). CL-bright rims are interpreted to be quartz overgrowths from melt. **(B)** Sample 111-4a. SEM-BSE image of plagioclase melt film between rounded residual quartz grains. **(C)** Sample 925-1. SEM-BSE image of melt film (bottom arrow), string of beads (middle arrow) and large pseudomelt pocket (top arrow) melt textures. **(D)** Sample 111-2. Photomicrograph with the cross-polars and gypsum plate inserted illustrating K-feldspar melt film around rounded quartz and plagioclase grains (photo credit: Dr. Rodney Metcalf). **(E)** Sample 925-1. Photomicrograph with the cross-polars and gypsum plate inserted illustrating plagioclase melt film (top arrow) and plagioclase string of beads pseudomelt textures (photo credit: Dr. Rodney Metcalf). **(F)** Sample 111-2. Photomicrograph with the cross-polars inserted illustrating a large pseudomelt pocket. Plagioclase grains have optically visible rims with rounded cores and are encapsulated by K-feldspar (photo credit: Dr. Rodney Metcalf). **(G)** Sample 111-2. SEM BSE image with chemical scan overlay. Green areas indicate K-feldspar and blue areas indicate plagioclase. Qtz, qz = quartz; pl = plagioclase; ksp, kfp = K-feldspar; bt = biotite.

Geologic Setting

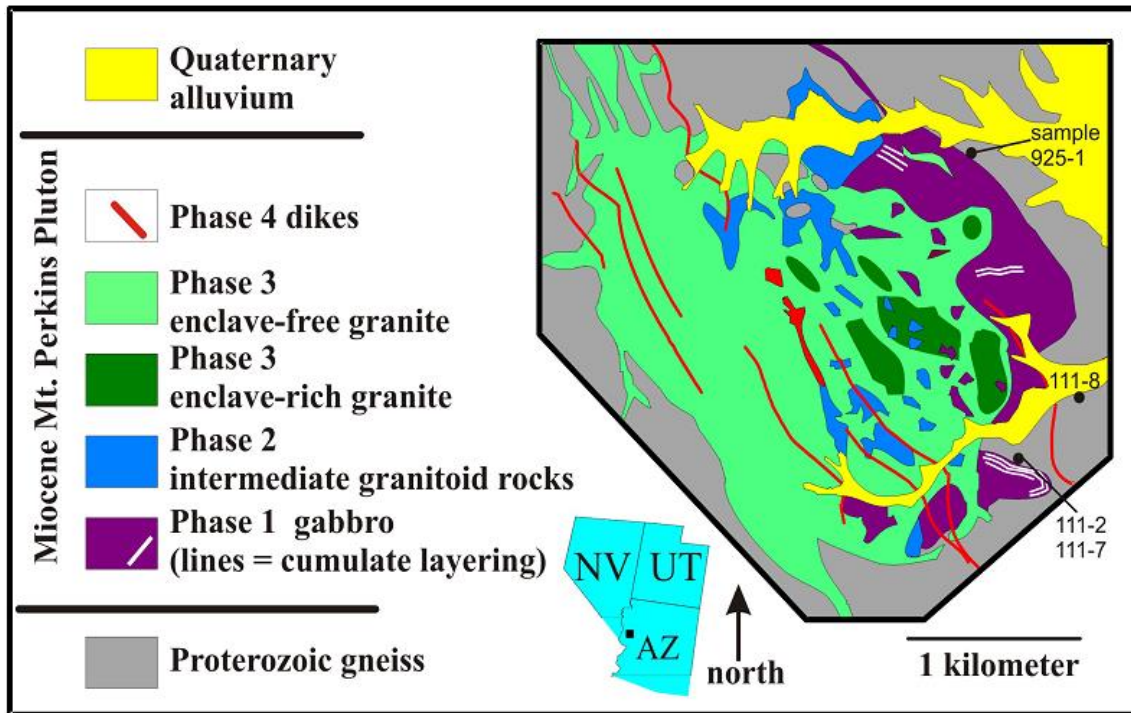


Figure 7. Geologic map of Mt. Perkins pluton (Metcalf, 1995).

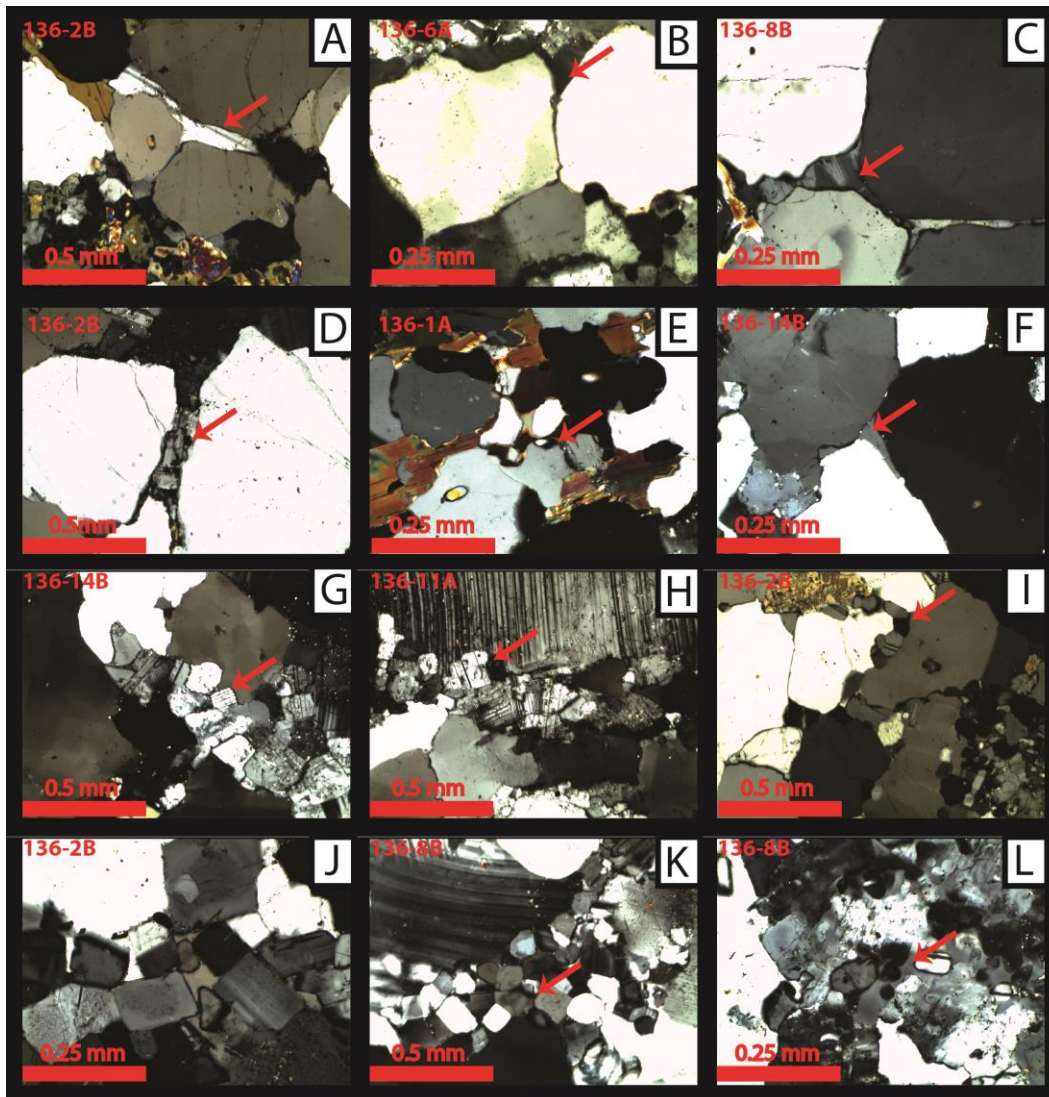


Figure 8. Photomicrographs with the cross polars inserted melt films (A, B, C, D, E, F), string of beads (G, H, I), and large pseudomelt pockets (J, K, L) from samples collected by Metcalf and Kopeitz (2011). (A) Sample 136-2B. The red arrow indicates a plagioclase melt film between rounded quartz grains. (B) Sample 136-6A. The red arrow indicates a plagioclase melt film between rounded quartz grains. (C) Sample 136-8B. The red arrow indicates a plagioclase melt film between rounded quartz grains. (D) Sample 136-2B. The red arrow indicates a plagioclase melt film between rounded quartz grains. (E) Sample 136-1A. The red arrow indicates a biotite melt film between rounded quartz grains. (F) Sample 136-14B. The red arrow indicates a plagioclase melt film between rounded quartz grains. (G) Sample 136-14B. The arrow indicates plagioclase string of beads pseudomelt texture between quartz grains. (H) Sample 136-11A. The arrow indicates plagioclase string of beads pseudomelt texture between residual plagioclase (top) and quartz grains (bottom). (I) Sample 136-2B. The arrow indicates plagioclase string of beads pseudomelt texture between quartz grains. (J) Sample 136-2B. Euhedral plagioclase grains with optically visible rims encapsulated by K-feldspar interserts. (K) Sample 136-8B. Euhedral plagioclase grains with optically visible rims encapsulated by K-feldspar interserts indicated by the red arrow (L) Sample 136-8B. Rounded plagioclase grains with optically visible rims encapsulated by K-feldspar interserts indicated by the red arrow.

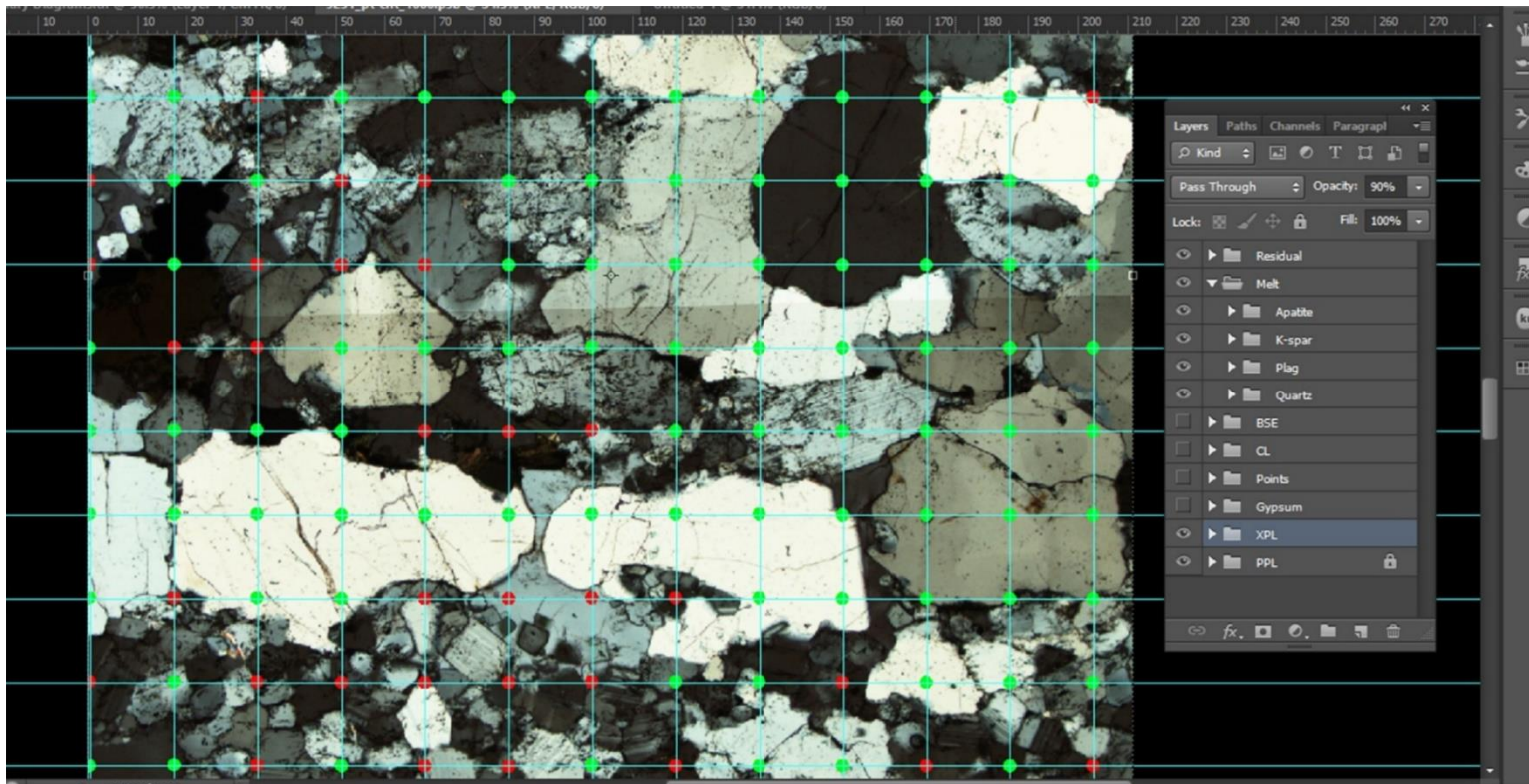


Figure 9. Screenshot of point counting using Adobe Photoshop©. The Layers window to the right acts as the point counting mechanism with options to overlay in plane polarized, cross polarized light, gypsum plate, SEM-CL and SEM-BSE.



Figure 10. Example of how slides were visually inspected for homogeneity. The slide was scanned using a flat-bed scanner. To show the sample size for the sample, a composite photomicrograph was overlain onto the slide, and the area within the red box was point counted.

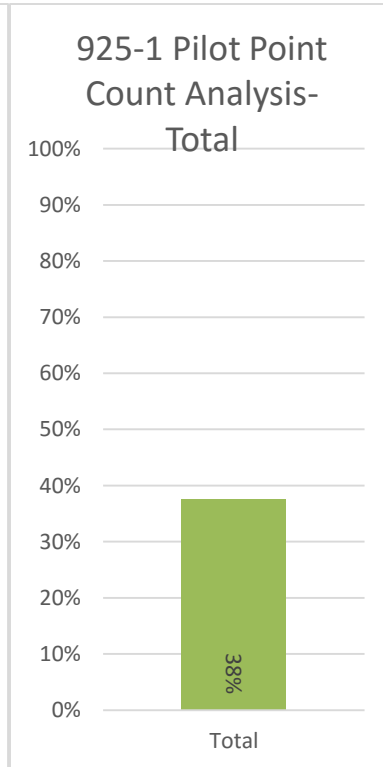
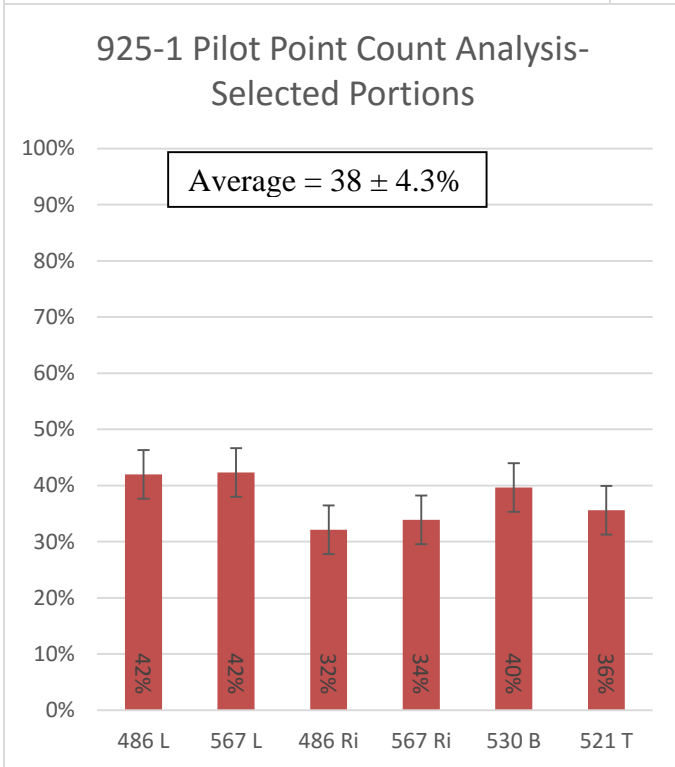
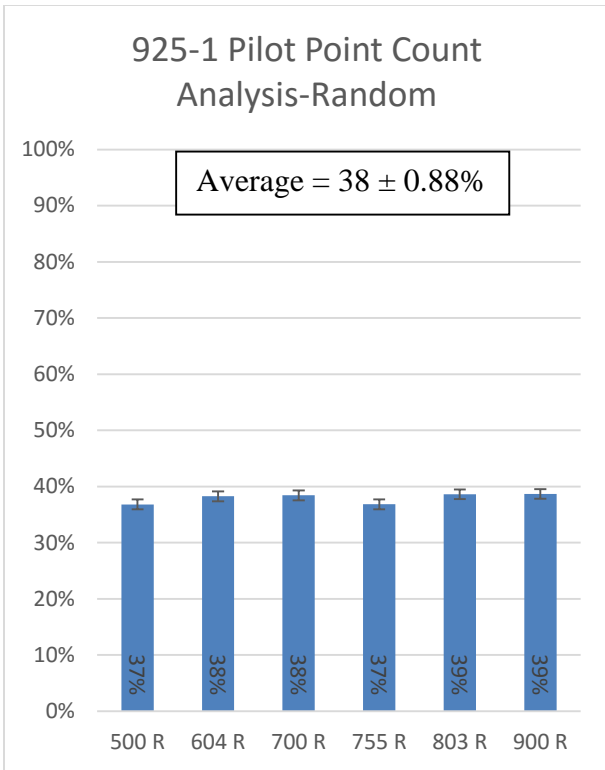


Figure 11. Melt volume % based on point counting method. The average melt volume percent based on all point counting arrangements is 38%. Letters on the X-axis indicate which portion was counted. L = Left side, Ri = Right side, T = Top, B = Bottom, R = Random.

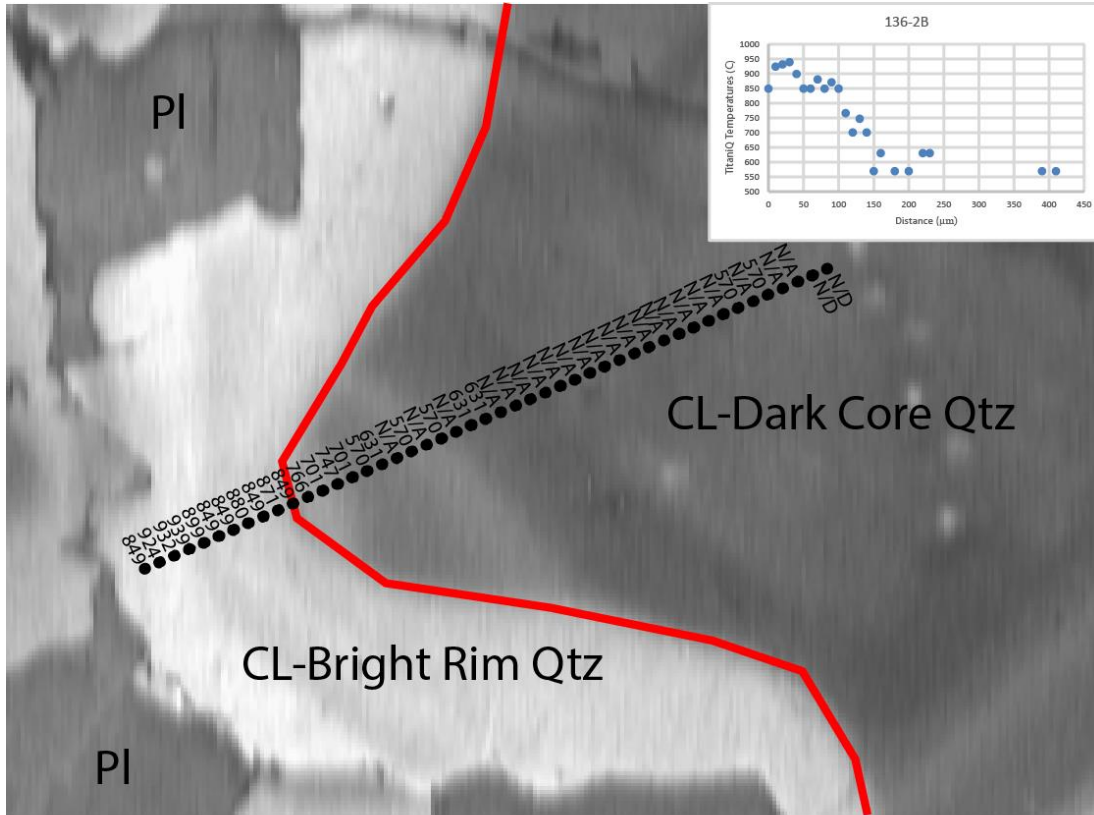


Figure 12. SEM-CL image with TitaniQ temperature overlay and enclosed graph showing Distance (μm) vs. TitaniQ Temperatures ($^{\circ}\text{C}$). Dark cores record low TitaniQ temperatures, while Bright rims have relatively higher TitaniQ temperatures. Temperatures in the CL-bright rim range from ~ 850 to 940 $^{\circ}\text{C}$, while the CL-dark core temperatures range from ~ 760 to <561 $^{\circ}\text{C}$. Omitted are values with Ti concentrations below detection limit. N/A = Ti Concentration below detection limit. N/D = No data, Pl = plagioclase, Qtz = quartz.

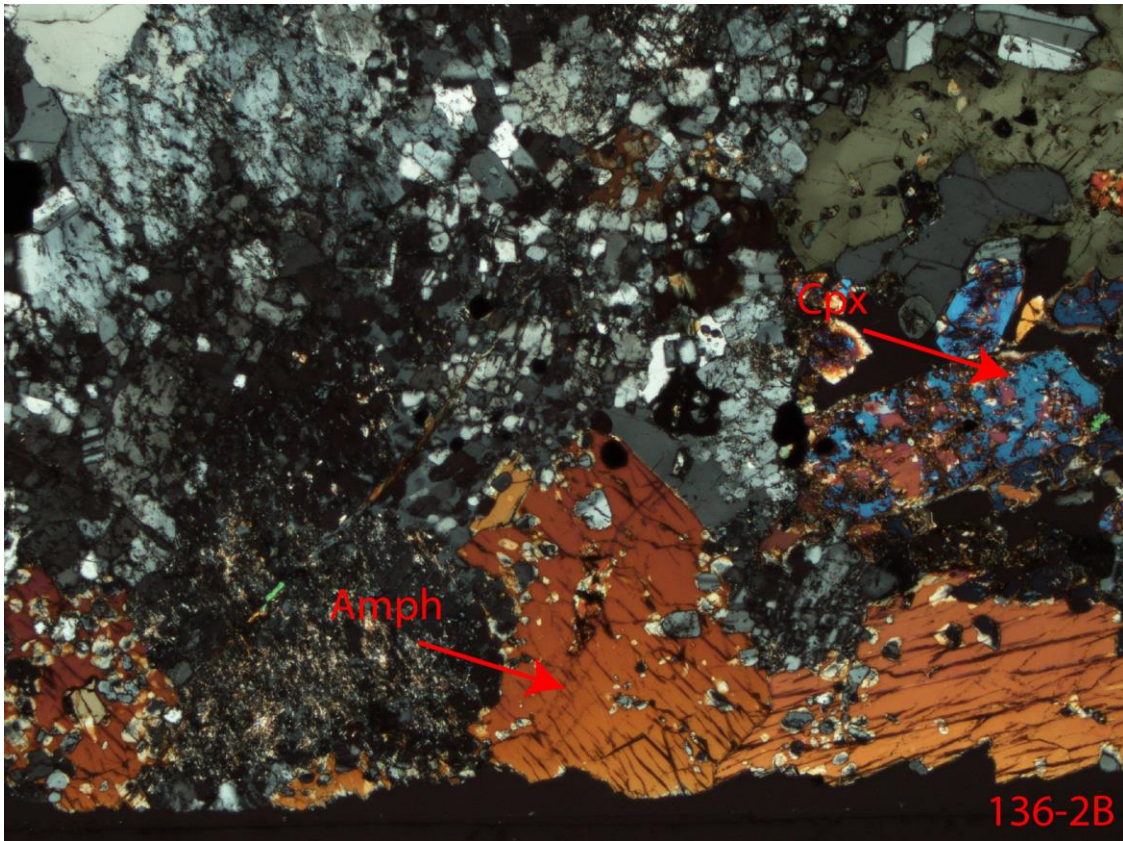


Figure 13. Photomicrograph of sample 136-2B taken with the cross plolars in illustrating the association of clinopyroxene (cpx) and amphibole (Amph). The base of the photomicrograph is approximately 5mm wide.

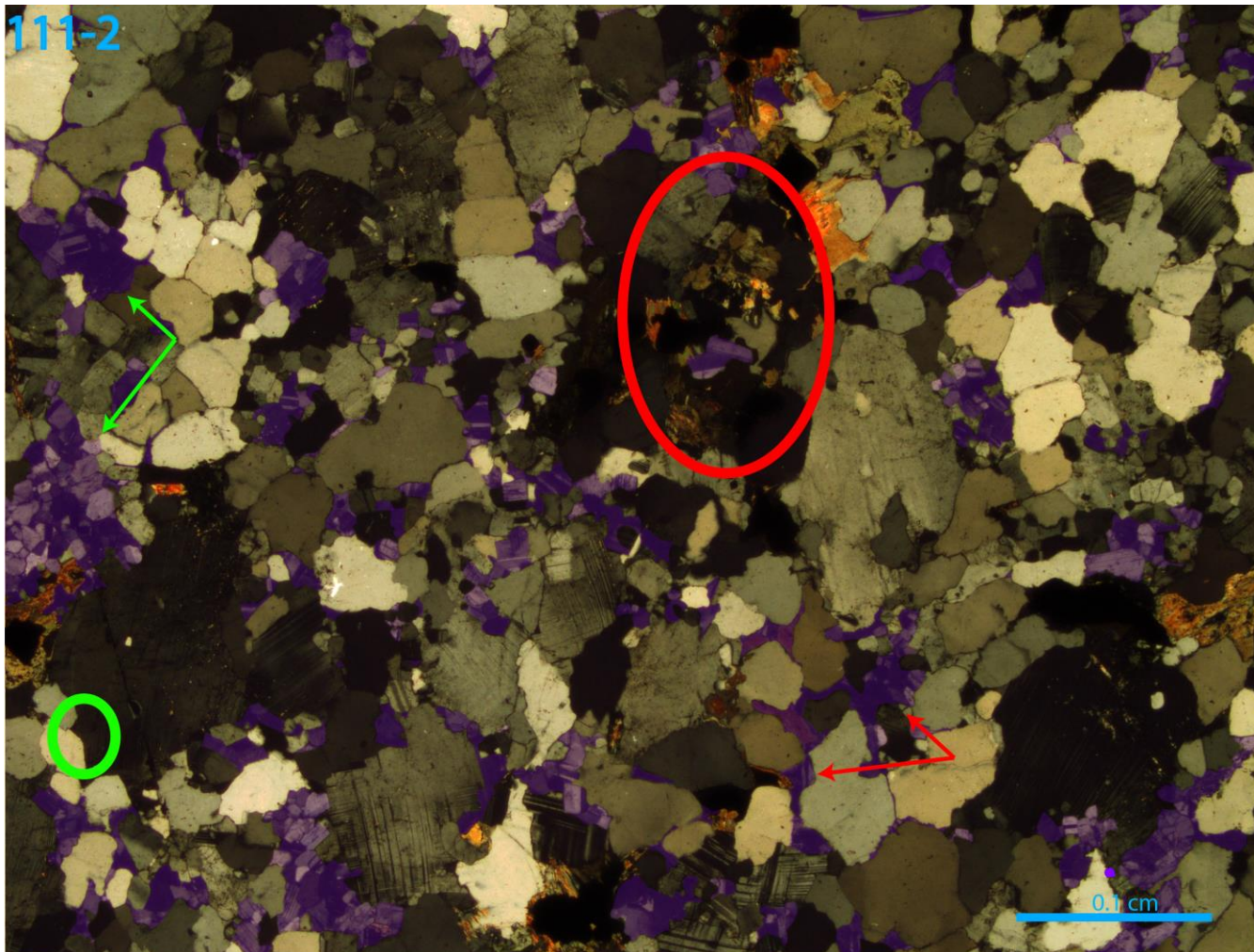


Figure 14. Photomicrograph of sample 111-2 taken with the crossed polars in. The purple transparent overlay highlights pseudomelt textures. The within the red circle are mafic minerals and oxides that hinder melt production and connectivity. The green circle illustrates an area where melt was not generated between quartz-feldspar grain boundaries. The red arrows points to a string of beads and a large pseudomelt pocket that connected via melt film, while the green arrows point to two large pseudomelt pockets that are not connected.

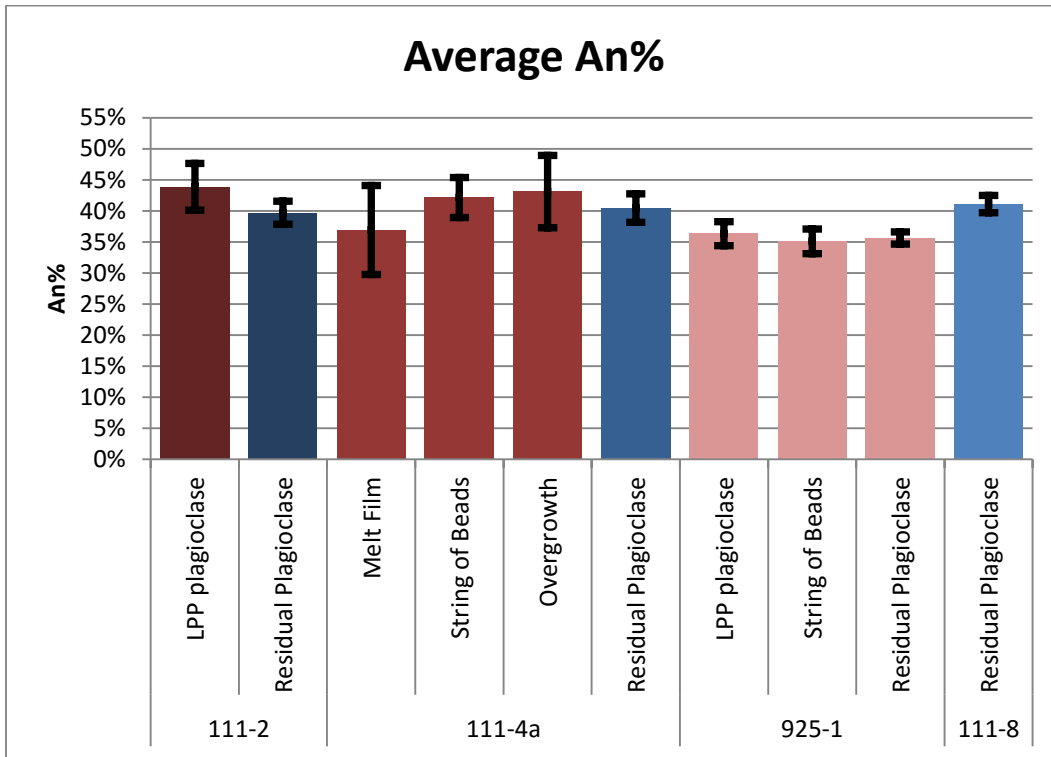


Figure 15. Analysis of plagioclase crystals based on texture for each sample. Black error bars show the variability of An% based on texture. The top of the error bar is the upper limit of the error. Plagioclase crystals have similar An % regardless of texture for each sample. LPP = Large Pseudomelt Pocket.

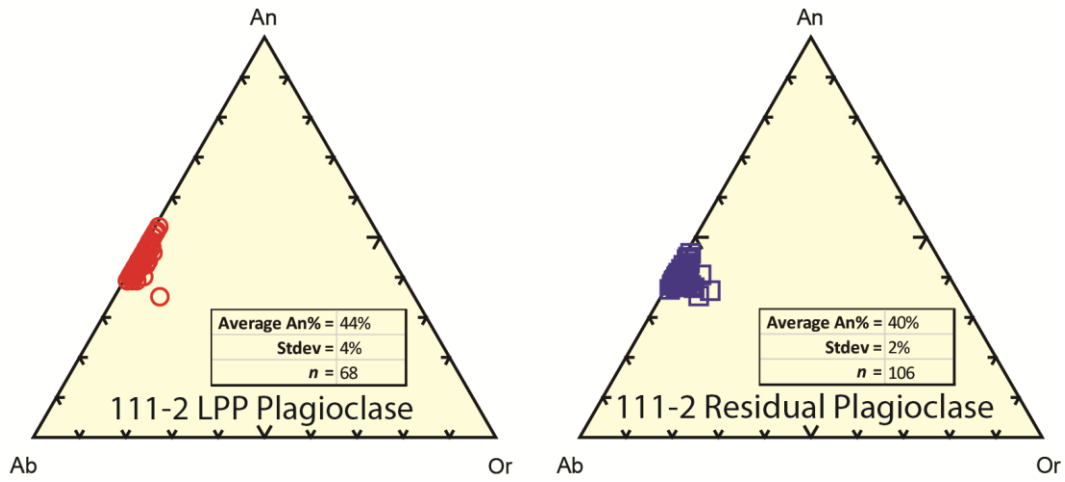


Figure 16. An-Ab-Or ternary diagram of large pseudomelt plagioclase (LPP) plagioclase and residual plagioclase for sample 111-2.

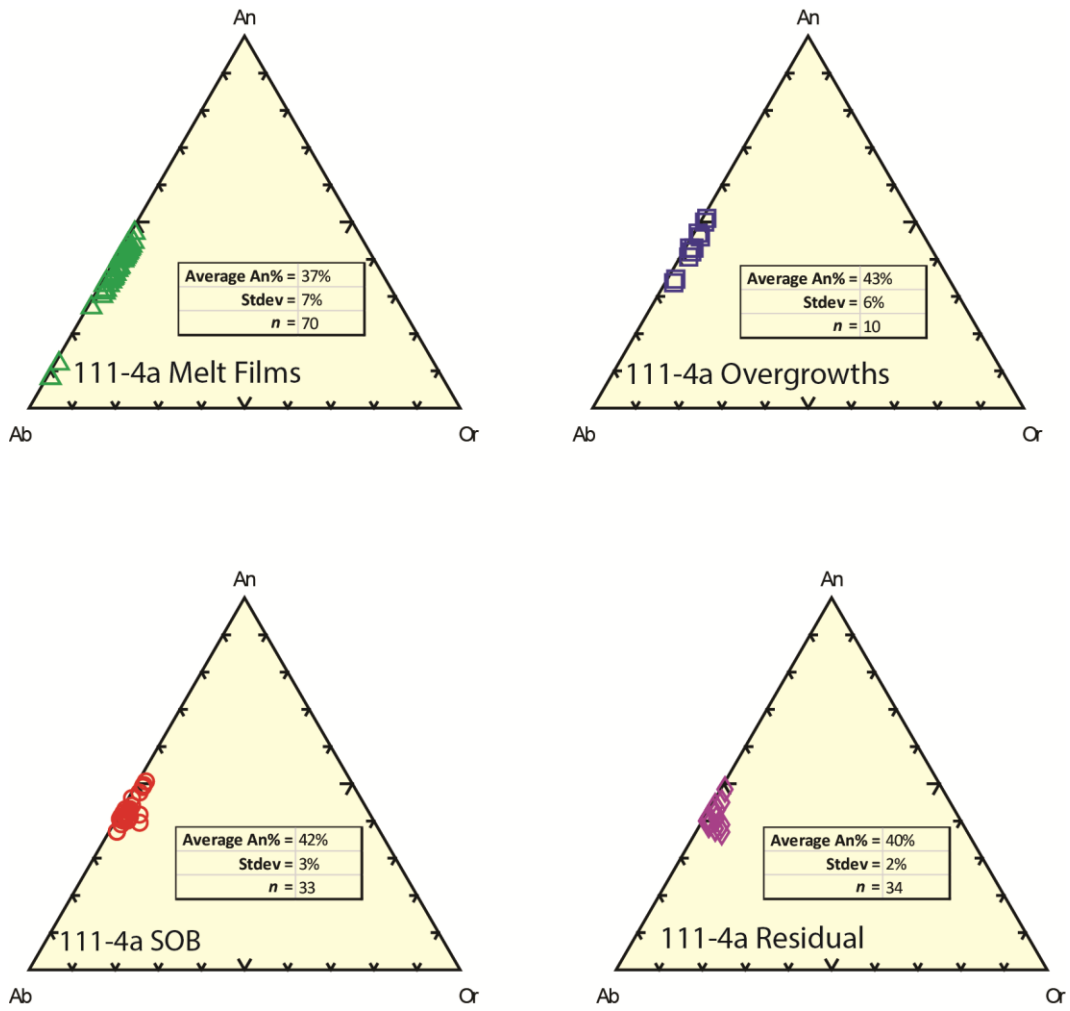


Figure 17. Ab-An-Or ternary diagrams of plagioclases based on pseudomelt texture for sample 111-4a. Overgrowths refer to plagioclase grains that have optically different rims and are in close proximity to other melt textures. SOB = string of beads.

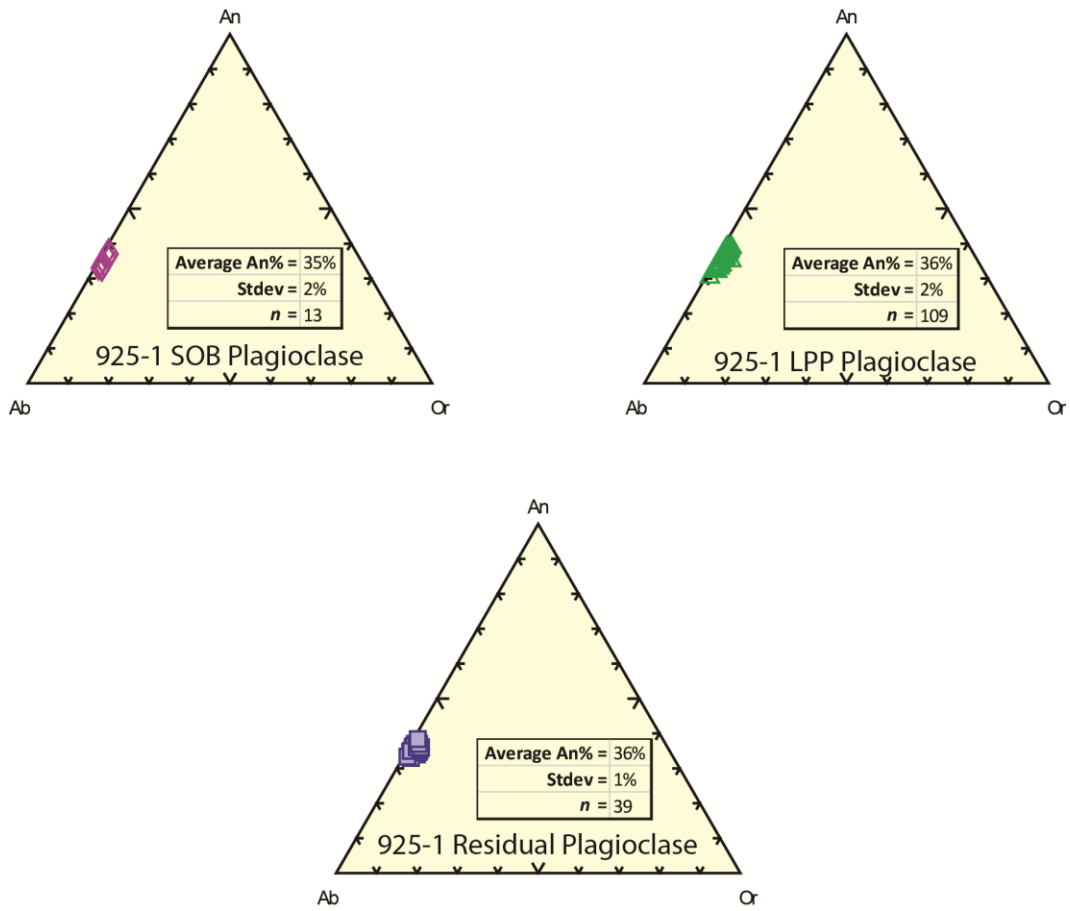


Figure 18. Ab-An-Or ternary diagrams of plagioclases based on pseudomelt texture for sample 925-1. SOB = string of beads, LPP = large pseudomelt pocket.

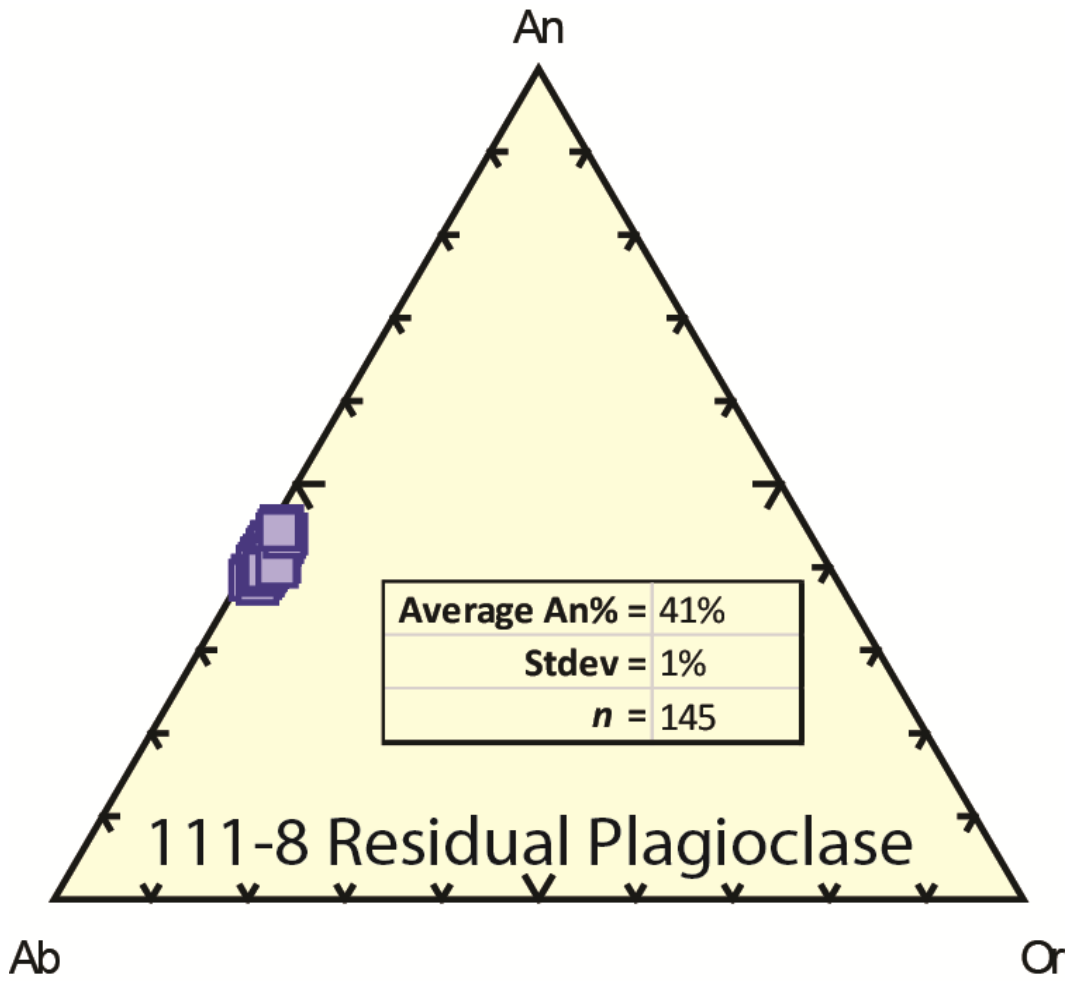


Figure 19. Ab-An-Or ternary diagrams of plagioclases for sample 111-8. Sample 111-8 has no discernable melt textures observed via optical microscopy.

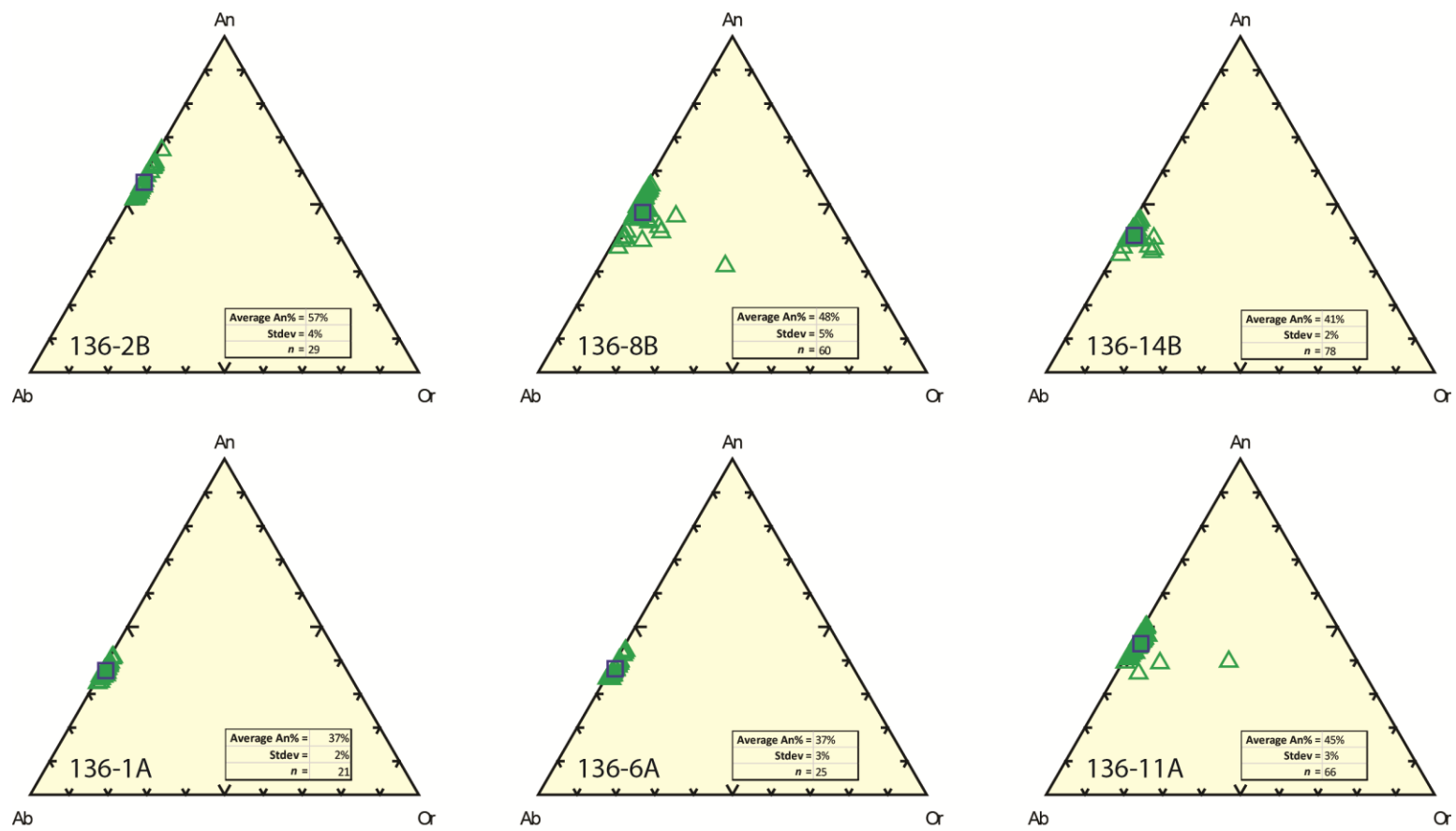


Figure 20. Ab-An-Or ternary diagrams for plagioclases analyzed in the B (top row) and A (bottom row) traverses

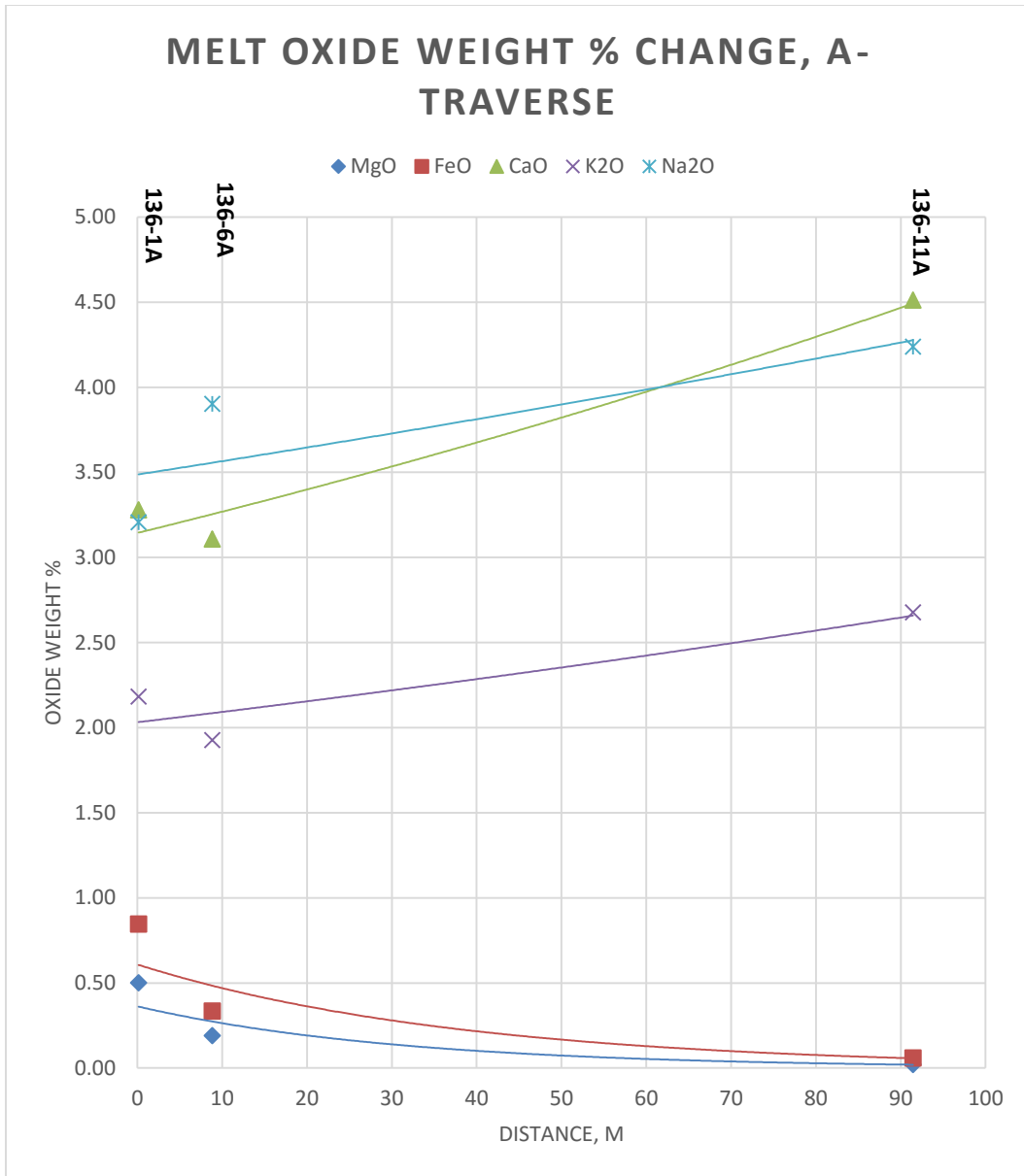


Figure 21. Melt geochemistry comparing distance with various cations for rocks within the A-traverse. Sample 136-11A shows the least evolved melt with low MgO and FeO, compared to 136-1A which shows the most evolved melts. CaO, Na₂O and K₂O show a weak increasing trend with distance, but is most likely reflective of the local geochemistry.

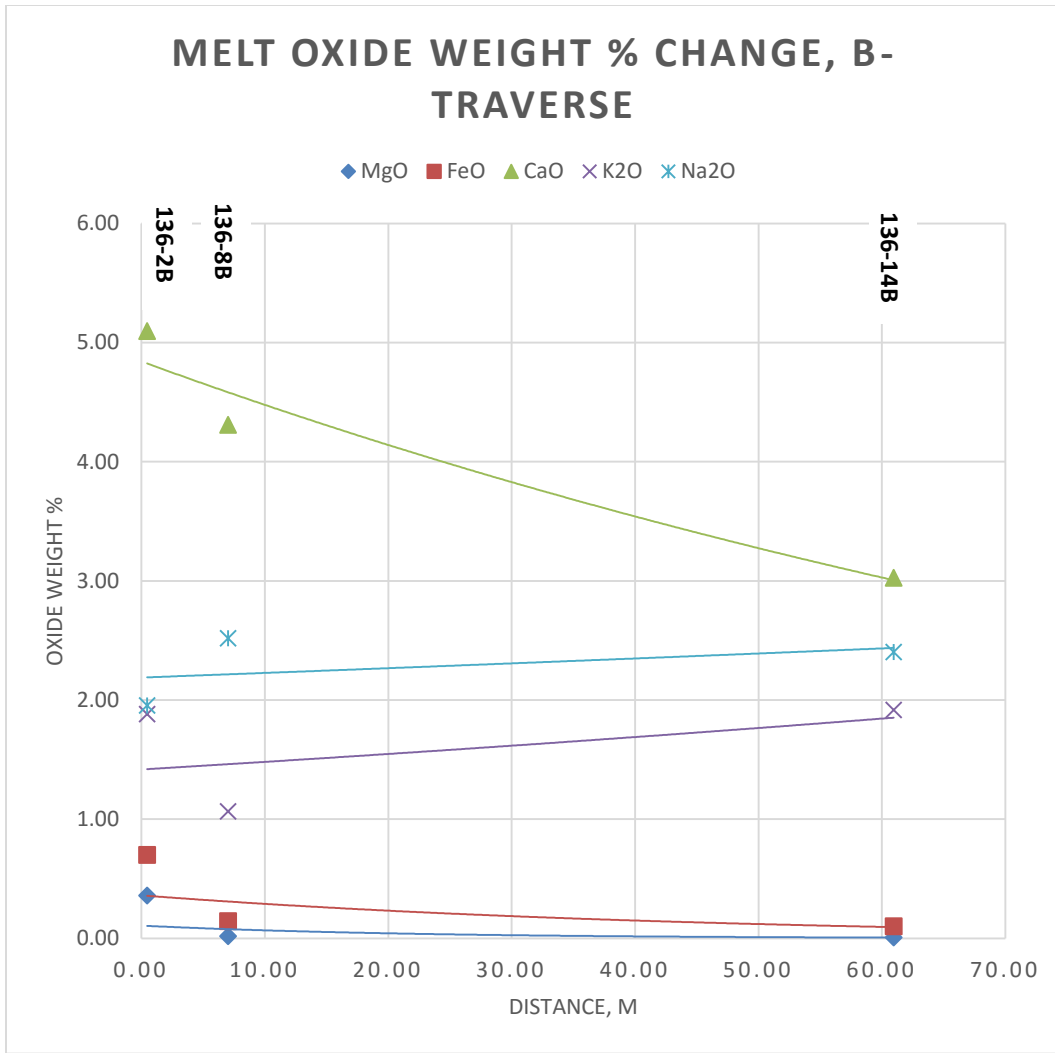


Figure 22. Melt geochemistry comparing distance with various cations for rocks within the B-traverse. Sample 136-14B shows the least evolved melt with low MgO and FeO, compared to 136-2B which shows the most evolved melts. CaO, Na₂O and K₂O shows no clear trends because these values are likely reflective of the local geochemistry.

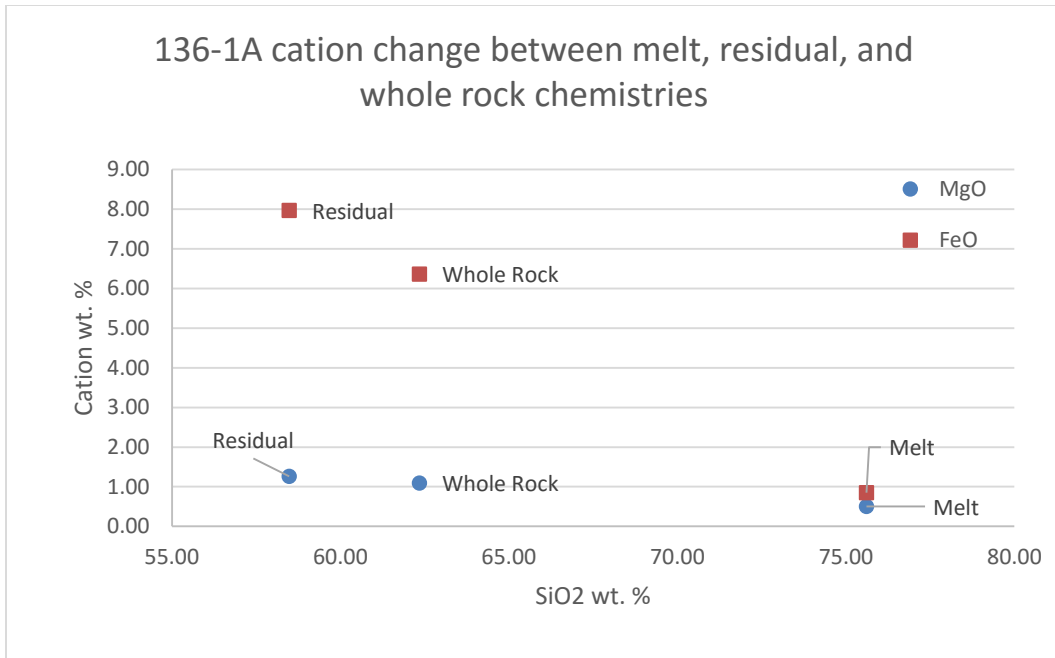


Figure 23. FeO, MgO, and SiO₂ change between residual, whole rock, and melt chemistries. Note that residual chemistries are enriched in MgO and FeO, and depleted in SiO₂ compared to the whole rock, while melt chemistries show the opposite trend.

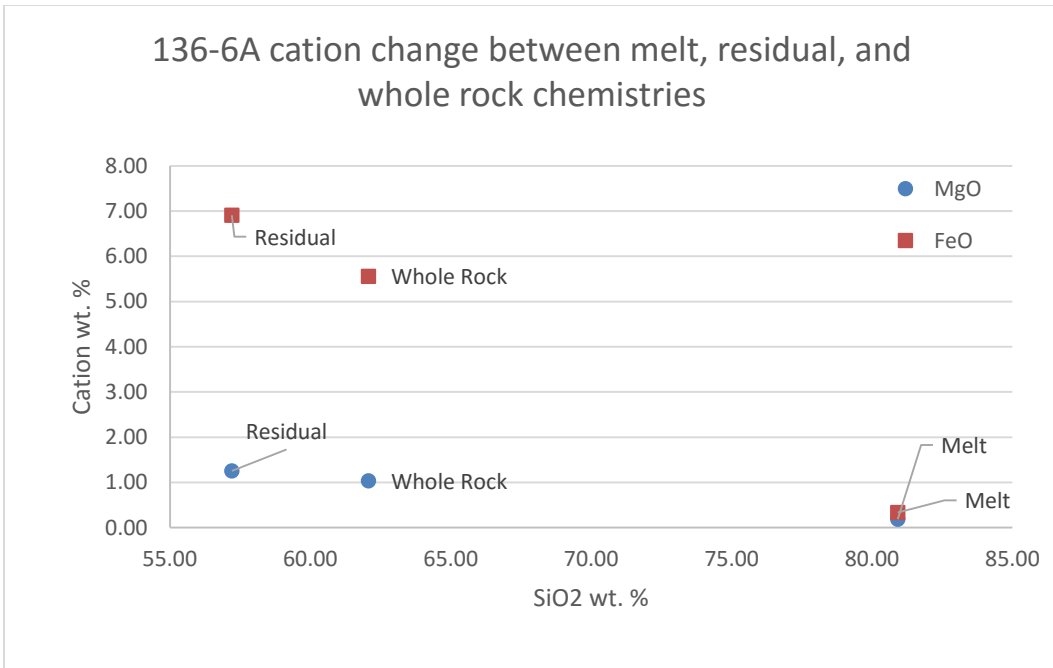


Figure 24. FeO, MgO, and SiO₂ change between residual, whole rock, and melt chemistries. Note that residual chemistries are enriched in MgO and FeO, and depleted in SiO₂ compared to the whole rock, while melt chemistries show the opposite trend.

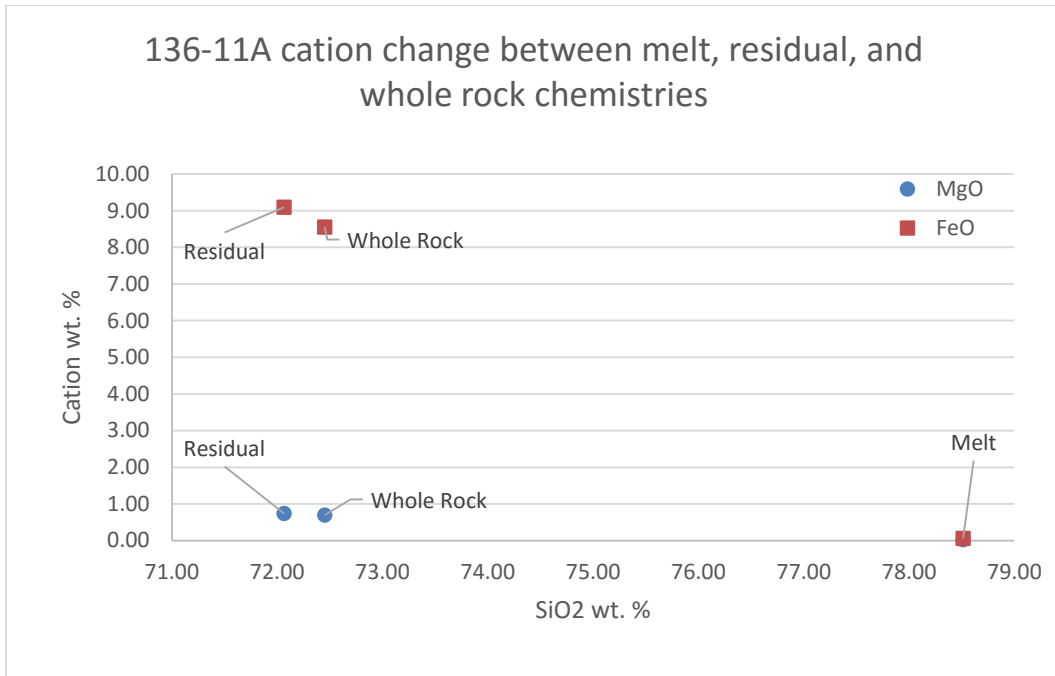


Figure 25. FeO, MgO, and SiO₂ change between residual, whole rock, and melt chemistries. Note that residual chemistries are enriched in MgO and FeO, and depleted in SiO₂ compared to the whole rock, while melt chemistries show the opposite trend.

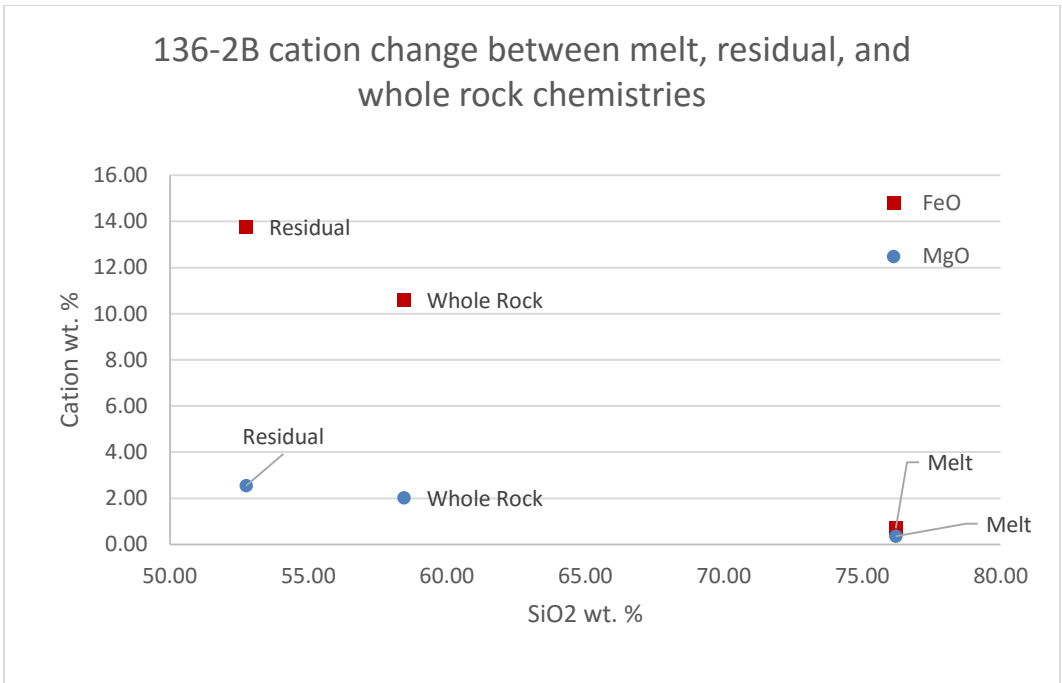


Figure 26. FeO, MgO, and SiO₂ change between residual, whole rock, and melt chemistries. Note that residual chemistries are enriched in MgO and FeO, and depleted in SiO₂ compared to the whole rock, while melt chemistries show the opposite trend.

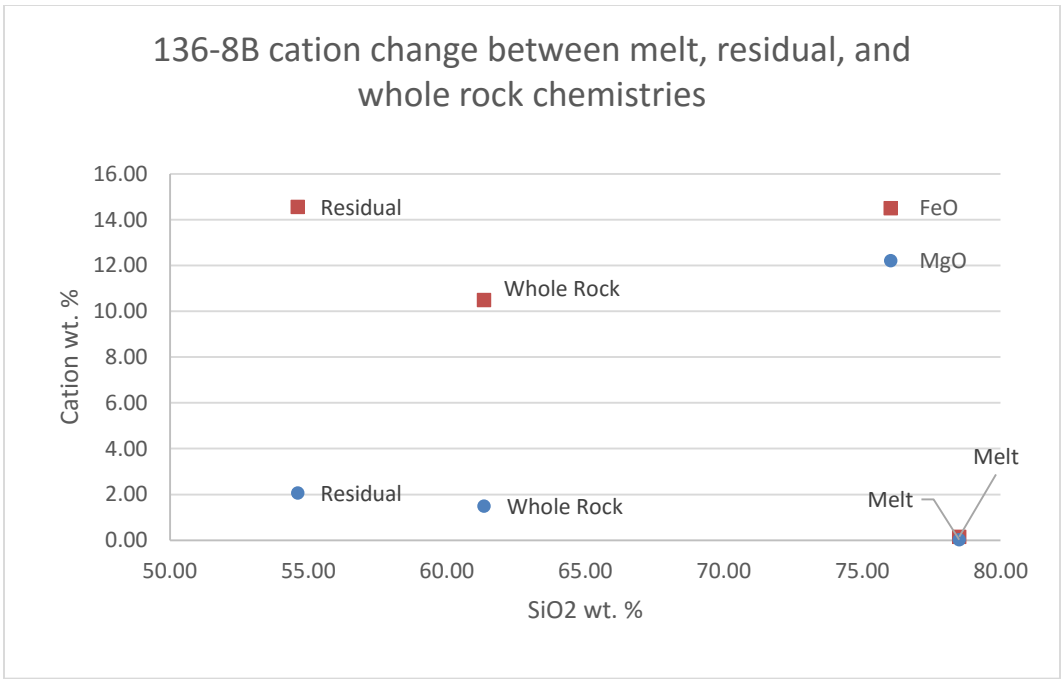


Figure 27. FeO, MgO, and SiO₂ change between residual, whole rock, and melt chemistries. Note that residual chemistries are enriched in MgO and FeO, and depleted in SiO₂ compared to the whole rock, while melt chemistries show the opposite trend.

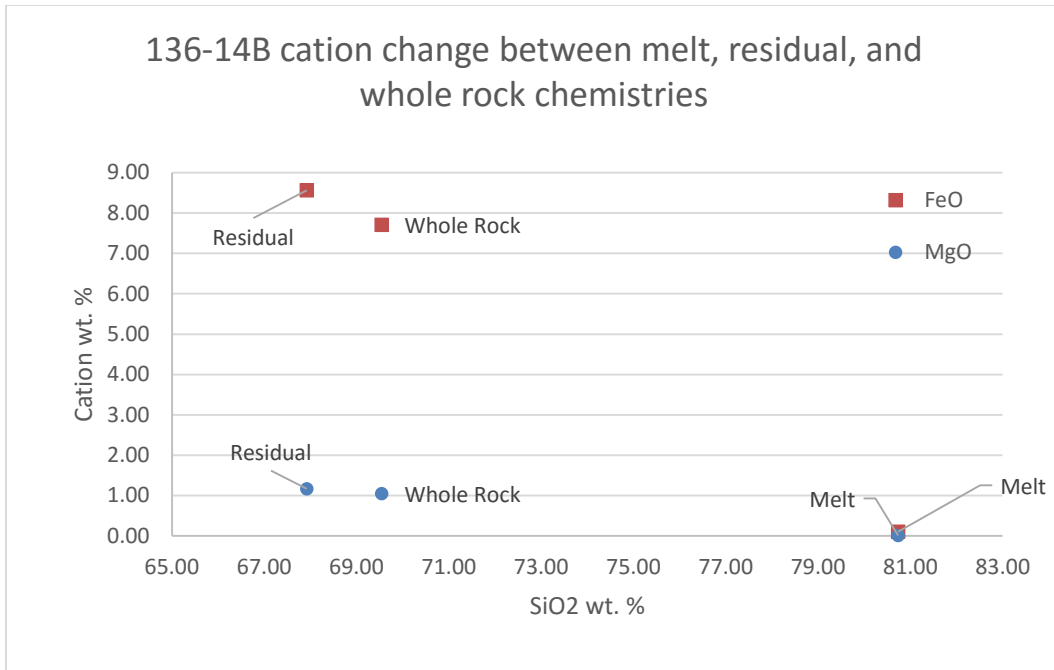


Figure 28. FeO, MgO, and SiO₂ change between residual, whole rock, and melt chemistries. Note that residual chemistries are enriched in MgO and FeO, and depleted in SiO₂ compared to the whole rock, while melt chemistries show the opposite trend.

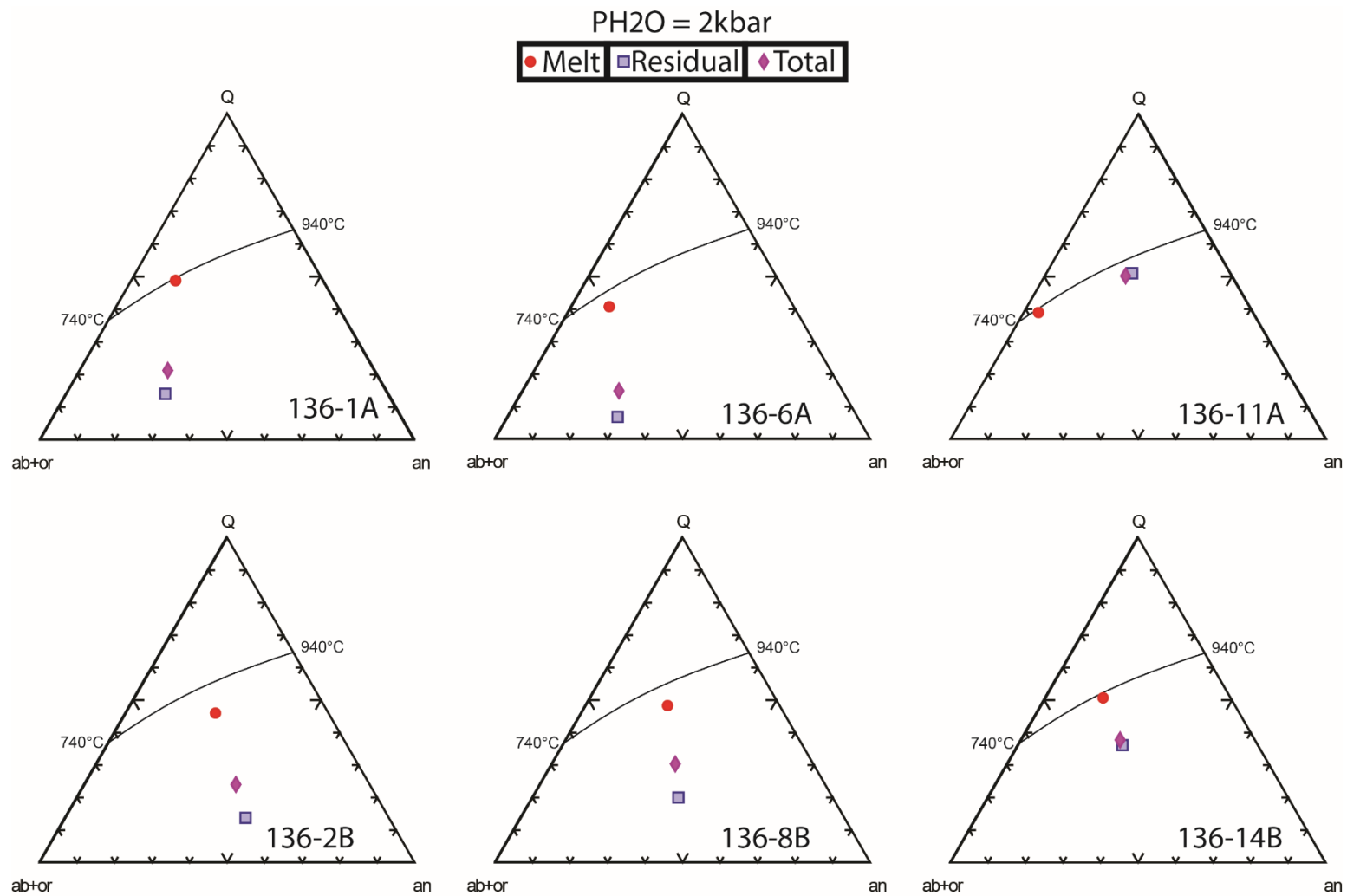


Figure 29 Ternary diagrams showing plagioclase-quartz assemblage for A-traverse (top) and the B-traverse (bottom). Temperatures and the cotectic are from Johannes (1989). Melt chemistries generally plot closer to the Q-ab+or axis compared to their residual counterparts, which plot closer to the ab+or – an axis.

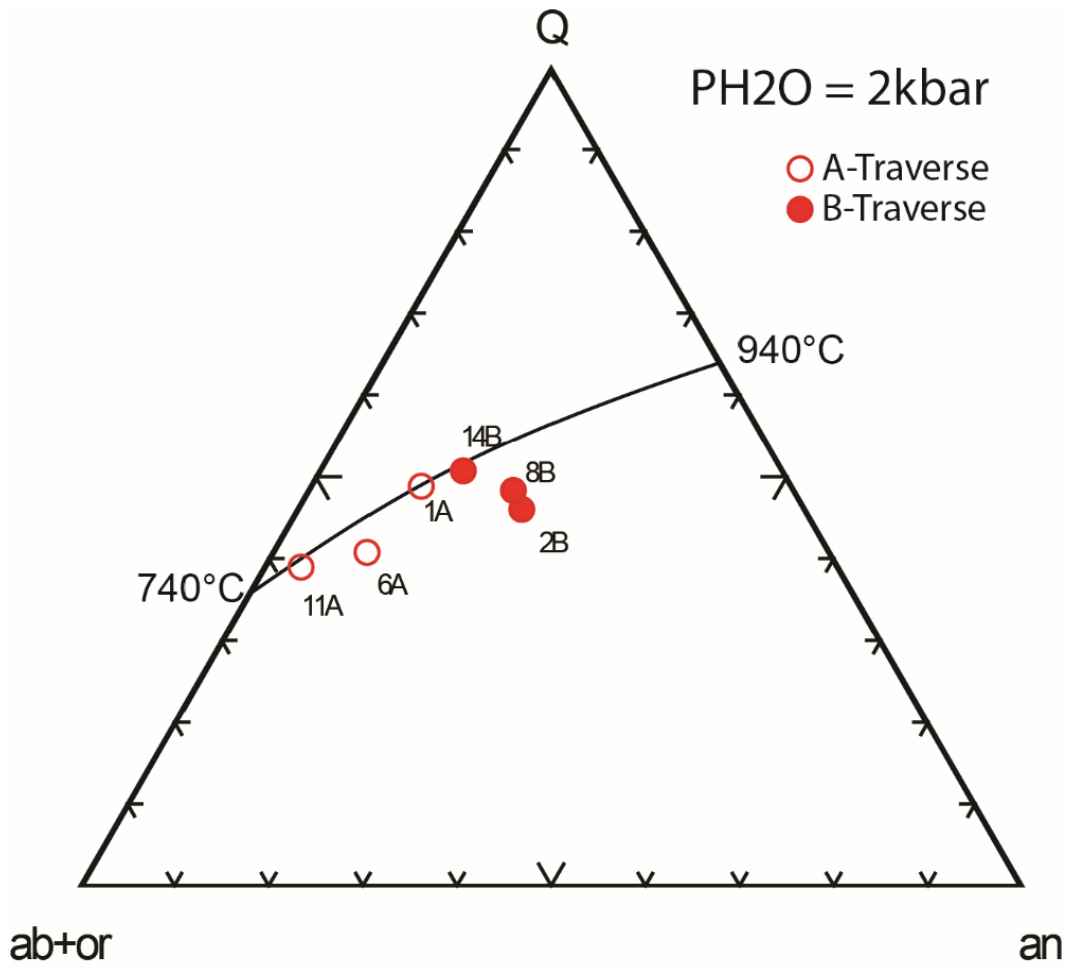


Figure 30. Q-Ab(+or)-an ternary diagram with melt geochemistries. Cotectic and temperatures from Johannes (1989).

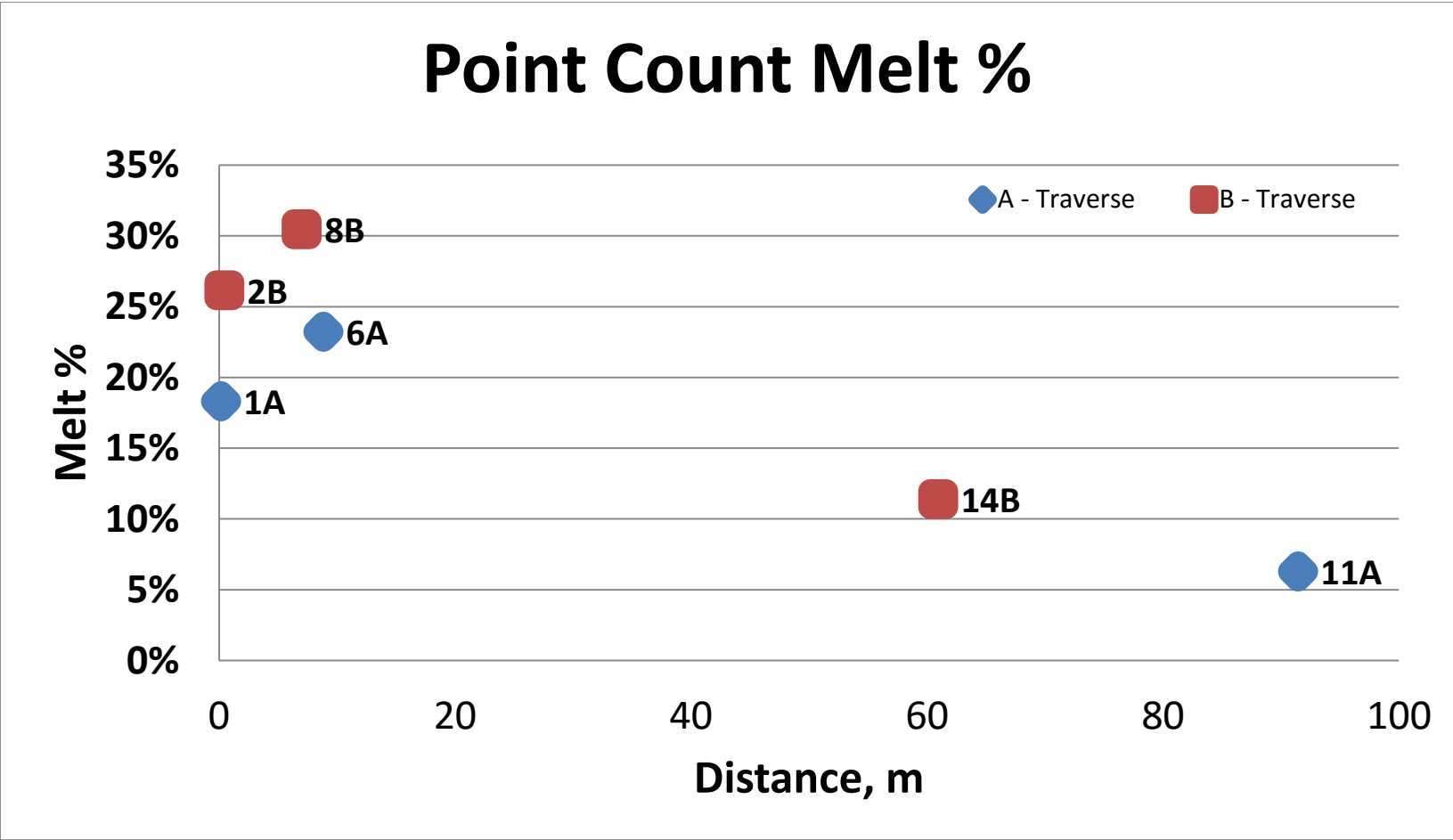


Figure 31. Point count melt volume percent.

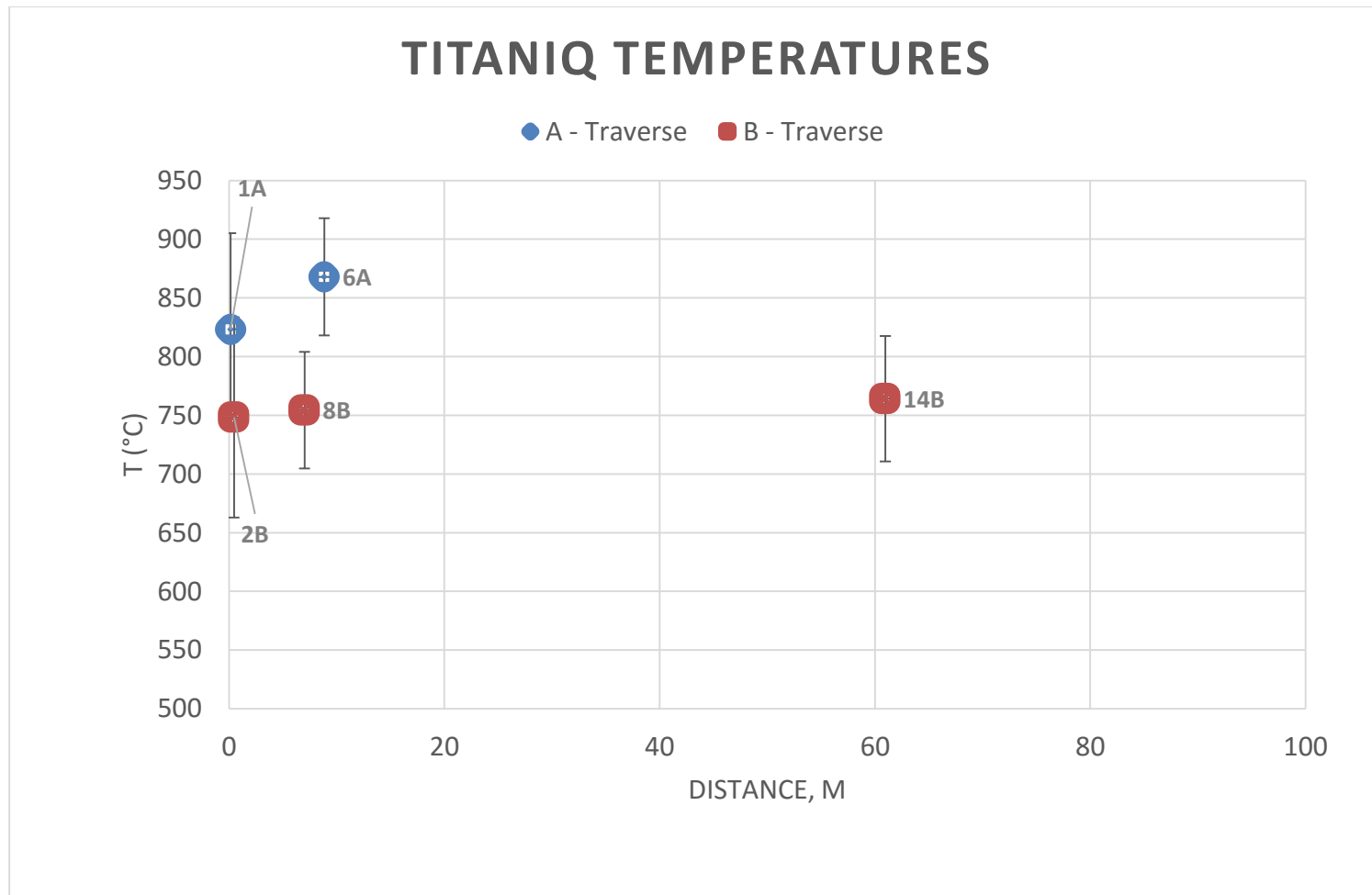


Figure 32. TitaniQ temperatures (Wark and Watson, 2006) for each traverse. There is no decreasing trend with distance.

Table 1. Table illustrates what minerals are found in what texture. Biotite, amphibole, clinopyroxene, apatite, and oxides are rarely found.

Texture	Minerals
Melt film	Quartz, plagioclase, K-feldspar, biotite, oxide, amphibole
String of beads	Plagioclase
Large pseudomelt pocket	Quartz, plagioclase, K-feldspar
Residual	Quartz, plagioclase, K-feldspar, biotite, amphibole, apatite, clinopyroxene, oxide

Table 2. Point count results showing distance from the pluton and modal mineral abundances divided into three types: melt, residual, and whole rock.

Sample	Distance (m)	Melt %	Type	Volume Percent										
				Quartz	Plagioclase	K-feldspar	Amphibole	Biotite	Opaque	Apatite	Clinopyroxene	Chlorite	Spinel	Calcite
136-1A	0.15	18	Melt	41.8	41.8	12.4	0.0	3.9	0.0	0.0	0.0	0.0	0.0	0.0
			Residual	17.5	67.6	0.0	0.0	10.5	4.2	0.2	0.0	0.0	0.0	0.0
			Whole Rock	23.2	61.5	2.9	0.0	8.9	3.2	0.2	0.0	0.0	0.0	0.0
136-6A	8.84	23	Melt	54.7	30.2	12.9	0.0	1.4	0.0	0.7	0.0	0.0	0.0	0.0
			Residual	12.5	73.4	0.0	0.0	10.6	3.5	0.0	0.0	0.0	0.0	0.0
			Whole Rock	21.5	64.2	2.8	0.0	8.6	2.8	0.2	0.0	0.0	0.0	0.0
136-11A	91.44	6	Melt	51.2	26.8	19.5	0.0	0.0	0.0	2.4	0.0	0.0	0.0	0.0
			Residual	52.0	36.9	0.0	5.6	0.0	4.6	0.0	0.0	1.0	0.0	0.0
			Whole Rock	51.9	36.3	1.2	5.2	0.0	4.3	0.2	0.0	0.9	0.0	0.0
136-2B	0.46	26	Melt	47.6	35.9	12.9	2.9	0.0	0.0	0.6	0.0	0.0	0.0	0.0
			Residual	18.1	53.8	0.0	16.7	1.3	7.3	0.3	2.7	0.0	0.0	0.0
			Whole Rock	25.8	49.1	3.4	13.1	0.9	5.4	0.3	2.0	0.0	0.0	0.0
136-8B	7.01	30	Melt	50.5	43.4	6.1	0.0	0.0	0.0	0.0	0.0	0.0	0.0	0.0
			Residual	22.1	54.2	0.0	10.2	0.4	9.3	0.0	3.8	0.0	0.0	0.0
			Whole Rock	30.8	50.9	1.8	7.1	0.3	6.5	0.0	2.6	0.0	0.0	0.0
136-14B	60.96	11	Melt	52.7	35.1	12.2	0.0	0.0	0.0	0.0	0.0	0.0	0.0	0.0
			Residual	39.9	48.8	0.0	6.1	0.0	4.3	0.2	0.0	0.0	0.5	0.2
			Whole Rock	41.4	47.2	1.4	5.4	0.0	3.8	0.2	0.0	0.0	0.5	0.2

Table 3. Average EPMA analysis of randomly selected plagioclase crystals from each sample. Where possible, core and rim analysis was taken to reduce bias toward melt or non-melt plagioclase. Stdev. = Standard deviation. AN% = percent anorthite component. Distance refers to distance from the pluton.

A-traverse Plagioclase Chemistry			Average Plagioclase composition (wt. %)													
	Average AN%	Stdev. AN%	Distance (m)	SiO ₂	TiO ₂	Al ₂ O ₃	Cr ₂ O ₃	FeO	MnO	MgO	CaO	Na ₂ O	K ₂ O	P ₂ O ₅	F	Cl
136-1A	37%	2%	0.15	58.89	0.02	26.96	0.01	0.08	0.01	0	7.76	7.2	0.17	0.02	0.03	0
136-6A	37%	3%	8.83	58.55	0.01	27.26	0.01	0.1	0.01	0.01	7.89	7.14	0.19	0.02	0.03	0.01
136-11A	45%	3%	91.44	56.78	0.01	28.12	0.01	0.16	0.01	0.02	9.3	6.07	0.33	0	0.02	0.01
B-traverse Plagioclase Chemistry																
136-2B	57%	4%	0.45	53.9	0.01	30.18	0.01	0.31	0.01	0.01	11.84	4.91	0.19	0.01	0.03	0.01
136-8B	48%	5%	7.01	55.99	0.01	28.15	0	0.3	0.01	0.04	9.81	5.62	0.54	0	0.03	0.01
136-14B	41%	2%	60.96	57.87	0.01	27.2	0.01	0.27	0.01	0.02	8.49	6.56	0.4	0	0.04	0

Table 4. Whole rock geochemistry for each sample separated into melt(M), residual(R), and Total(T) or whole rock. Distance to pluton, melt percent, Rim, Core TitaniQ temperatures are also displayed. Melt generated furthest from the pluton is the earliest stage and has higher silica and alkali earth metals compared to proximal samples.

Sample	Distance (m)	Melt %	Rim Temp (°C)	Core Temp (°C)	SiO2	TiO2	Al2O3	Cr2O3	FeO	MnO	MgO	CaO	Na2O	K2O	P2O5	F	Cl	Total
1A - Melt	0.15	18	899 ± 70	751 ± 110	75.61	0.18	14.38	0.00	0.85	0.01	0.50	3.28	3.21	2.18	0.01	0.05	0.02	100.29
6A - Melt	8.84	23	950 ± 57	656 ± 77	80.92	0.07	11.03	0.00	0.33	0.01	0.19	3.11	3.90	1.93	0.36	0.05	0.01	101.93
11A - Melt	91.44	6	<561	538 ± 37	78.51	0.01	11.31	0.00	0.06	0.01	0.02	4.51	4.24	2.68	1.21	0.13	0.02	102.71
1A - Residual					58.49	1.92	19.21	0.01	7.97	0.13	1.26	5.13	4.66	1.16	0.11	0.11	0.04	100.20
6A - Residual					57.20	1.80	21.07	0.01	6.91	0.10	1.26	5.56	5.05	1.19	0.01	0.07	0.04	100.26
11A - Residual					72.06	0.05	10.41	0.00	9.09	0.05	0.74	4.01	2.20	0.15	0.00	0.01	0.01	98.80
1A - Total					62.35	1.52	18.12	0.01	6.36	0.10	1.09	4.72	4.33	1.39	0.09	0.10	0.04	100.22
6A - Total					62.07	1.44	19.01	0.01	5.56	0.08	1.04	5.06	4.81	1.34	0.09	0.07	0.04	100.61
11A - Total					72.45	0.04	10.47	0.00	8.55	0.05	0.70	4.04	2.32	0.30	0.07	0.02	0.01	99.03
2B - Melt	0.46	26	805 ± 104	625 ± 79	76.21	0.04	13.63	0.01	0.70	0.02	0.36	5.10	1.95	1.88	0.28	0.04	0.02	100.25
8B - Melt	7.01	30	813 ± 70	605 ± 53	78.50	0.01	13.47	0.00	0.15	0.00	0.02	4.31	2.52	1.07	0.00	0.02	0.00	100.07
14B - Melt	60.96	11	832 ± 60	640 ± 54	80.74	0.01	11.93	0.00	0.10	0.01	0.01	3.03	2.40	1.92	0.00	0.02	0.00	100.17
2B - Residual					52.75	2.12	16.54	0.01	13.76	0.33	2.55	8.75	2.60	0.40	0.10	0.06	0.07	100.06
8B - Residual					54.61	2.73	14.73	0.01	14.56	0.47	2.06	7.02	2.85	0.38	0.00	0.03	0.03	99.47
14B - Residual					67.92	0.08	13.67	0.01	8.56	0.04	1.17	4.94	3.13	0.22	0.08	0.04	0.01	99.88
2B - Total					58.46	1.62	15.83	0.01	10.58	0.26	2.02	7.86	2.45	0.76	0.14	0.06	0.06	100.10
8B - Total					61.34	1.96	14.37	0.01	10.50	0.34	1.49	6.26	2.76	0.57	0.00	0.03	0.02	99.64
14B - Total					69.55	0.07	13.59	0.01	7.71	0.04	1.05	4.77	3.08	0.41	0.08	0.04	0.01	100.39

Table 5. CIPW norm results from melt (M), residual (R), and whole rock (T) or whole-rock geochemistries. All samples have the suffix 136 (e.g. 136-1A is represented on this table as 1A).

CIPW Norm Results																							
Sample	%An	quartz	orthoclase	albite	anorthite	leucite	nepheline	kaliophilite	corundum	diopside	hypersthene	wollastonite	olivine	acmite	magnetite	ilmenite	hematite	titanite	apatite	chalcocite	perovskite	wuestite	rutile
1A - M	34.94	47.31	16.50	21.69	11.65	0.00	0.00	0.00	0.83	0.00	1.28	0.00	0.00	0.00	0.00	0.02	0.60	0.00	0.02	0.00	0.00	0.00	0.10
1A - R	36.70	12.18	11.96	39.51	22.91	0.00	0.00	0.00	1.38	0.00	5.80	0.00	0.00	0.00	3.48	2.54	0.00	0.00	0.23	0.00	0.00	0.00	0.00
1A - T	36.50	18.83	12.66	36.29	20.86	0.00	0.00	0.00	1.27	0.00	4.57	0.00	0.00	0.00	3.19	2.14	0.00	0.00	0.19	0.00	0.00	0.00	0.00
6A - M	20.78	39.39	9.68	37.97	9.96	0.00	0.00	0.00	0.00	0.05	0.00	2.20	0.00	0.00	0.02	0.00	0.02	0.00	0.71	0.00	0.00	0.00	0.00
6A - R	35.86	5.96	10.13	46.12	25.78	0.00	0.00	0.00	0.68	0.00	5.26	0.00	0.00	0.00	3.48	2.57	0.00	0.00	0.00	0.00	0.00	0.00	0.00
6A - T	34.52	13.52	10.02	44.35	23.38	0.00	0.00	0.00	0.07	0.00	3.44	0.00	0.00	0.00	3.05	1.99	0.00	0.00	0.19	0.00	0.00	0.00	0.00
11A - M	9.32	36.18	15.62	37.56	3.86	0.00	0.00	0.00	0.00	0.11	0.00	4.11	0.00	0.00	0.02	0.00	0.03	0.00	2.50	0.00	0.00	0.00	0.00
11A - R	47.80	42.73	0.94	20.94	19.17	0.00	0.00	0.00	0.00	1.53	12.90	0.00	0.00	0.00	1.72	0.07	0.00	0.00	0.00	0.00	0.00	0.00	0.00
11A - T	45.33	42.39	1.87	21.98	18.22	0.00	0.00	0.00	0.00	1.96	11.66	0.00	0.00	0.00	1.70	0.06	0.00	0.00	0.15	0.00	0.00	0.00	0.00
2B - M	56.66	44.74	11.39	17.95	23.46	0.00	0.00	0.00	0.00	0.42	0.81	0.00	0.00	0.00	0.00	0.02	0.56	0.05	0.60	0.00	0.00	0.00	0.00
2B - R	58.03	9.56	2.44	24.14	33.38	0.00	0.00	0.00	0.00	8.67	14.63	0.00	0.00	0.00	3.91	3.05	0.00	0.00	0.22	0.00	0.00	0.00	0.00
2B - T	57.66	18.41	4.63	22.69	30.90	0.00	0.00	0.00	0.00	6.71	10.66	0.00	0.00	0.00	3.36	2.33	0.00	0.00	0.30	0.00	0.00	0.00	0.00
8B - M	48.59	47.90	6.48	23.18	21.91	0.00	0.00	0.00	0.37	0.00	0.06	0.00	0.00	0.00	0.00	0.00	0.12	0.00	0.00	0.00	0.00	0.00	0.00
8B - R	50.67	14.12	2.35	26.77	27.50	0.00	0.00	0.00	0.00	7.16	13.50	0.00	0.00	0.00	4.63	3.98	0.00	0.00	0.00	0.00	0.00	0.00	0.00
8B - T	50.36	24.14	3.50	25.77	26.15	0.00	0.00	0.00	0.00	4.92	8.92	0.00	0.00	0.00	3.76	2.84	0.00	0.00	0.00	0.00	0.00	0.00	0.00
14B - M	41.10	50.28	11.63	22.10	15.42	0.00	0.00	0.00	0.44	0.00	0.03	0.00	0.00	0.00	0.02	0.00	0.06	0.00	0.00	0.00	0.00	0.00	0.00
14B - R	44.58	30.29	1.34	28.97	23.30	0.00	0.00	0.00	0.00	1.14	12.97	0.00	0.00	0.00	1.70	0.11	0.00	0.00	0.17	0.00	0.00	0.00	0.00
14B - T	44.36	32.36	2.48	28.35	22.60	0.00	0.00	0.00	0.00	0.90	11.36	0.00	0.00	0.00	1.68	0.10	0.00	0.00	0.17	0.00	0.00	0.00	0.00

Appendix A

Table A1 Point count results from the pilot study on sample 925-1.

650 Point Count		Sample: 925-1															
Count	Melt %	mQtz	mPlag	mKfs	mBt	mChl	mAmph	mOpaque	mAp	Total	%mQtz	%mPlag	%mKfs	%mBt	mAmph	%mOpaque	%mAp
1090	39.72%	116	244	72	0	0	0	0	1	433	26.8%	56.4%	16.6%	0.0%	0.0%	0.0%	0.2%
	Res %	Qtz	Plag	Kfs	Bt	Chl	Amph	Opaque	Ap	Total	%Qtz	%Plag	%Kfs	%Bt	Amph	%Opaque	%Ap
1090	60.28%	333	244	0	38	0	19	21	2	657	50.7%	37.1%	0.0%	5.8%	0.0%	3.2%	0.3%
										Total	41.2%	44.8%	6.6%	3.5%	0.0%	1.9%	0.3%

Table A2 Whole rock (total), melt and residual geochemistries obtained via point count.

Sample 925-1			
Oxides	Residual (wt. %)	Melt (wt. %)	Total (wt. %)
SiO ₂	73.45	69.40	73.96
TiO ₂	0.19	0.00	0.12
Al ₂ O ₃	11.07	18.53	14.45
FeO	7.31	0.11	1.34
MgO	0.85	0.00	0.95
CaO	3.73	5.57	4.63
Na ₂ O	1.95	3.04	2.41
K ₂ O	0.61	2.37	1.32
P ₂ O ₅	0.15	0.12	0.00
Total	99.31	99.14	99.19

Table A3 Average mineral composition used to calculate residual geochemistry.

136-1A		Average mineral composition							
Residual	Qtz	Plag	Kfs	Bt	Amph	Opaque	Ap	Total	
Specific G	2.65	2.69	2.57	3.00	3.00	5.15	3.20		
Volume x	0.46	1.82	0.00	0.31	0.00	0.22	0.01		
Wt%	0.16	0.64	0.00	0.11	0.00	0.08	0.00	1.00	
SiO2	100.00	58.89	64.26	36.47	0.00	0.07	0.00	58.49	
TiO2		0.02	0.02	3.84	0.00	19.12	0.00	1.92	
Al2O3		26.96	19.26	16.34	0.00	0.11	0.00	19.21	
Cr2O3		0.01	0.00	0.01	0.00	0.02	0.00	0.01	
FeO		0.08	0.04	18.35	0.00	76.15	0.00	7.97	
MnO		0.01	0.00	0.24	0.00	1.29	0.00	0.13	
MgO		0.00	0.00	11.33	0.00	0.02	0.00	1.26	
CaO		7.76	0.08	0.03	0.00	0.01	56.00	5.13	
Na2O		7.20	1.39	0.13	0.00	0.02	0.00	4.66	
K2O		0.17	14.19	9.44	0.00	0.00	0.00	1.16	
P2O5		0.02	0.03	0.00	0.00	0.00	42.00	0.11	
F		0.03	0.04	0.86	0.00	0.00	0.00	0.11	
Cl		0.00	0.02	0.35	0.00	0.00	0.00	0.04	
							Total	100.201	

Table A4 Average mineral composition used to calculate melt geochemistry.

136-1A		Average mineral composition							
Melt	Qtz	Plag	Kfs	Bt	Amph	Opaque	Ap	Total	
Specific G	2.65	2.69	2.57	3.00	3.00	5.15	3.20		
Volume x	1.11	1.13	0.32	0.12	0.00	0.00	0.00		
Wt%	0.42	0.42	0.12	0.04	0.00	0.00	0.00	1.00	
SiO2	100.00	58.89	64.26	36.47	0.00	0.07	0.00	75.61	
TiO2		0.02	0.02	3.84	0.00	19.12	0.00	0.18	
Al2O3		26.96	19.26	16.34	0.00	0.11	0.00	14.38	
Cr2O3		0.01	0.00	0.01	0.00	0.02	0.00	0.00	
FeO		0.08	0.04	18.35	0.00	76.15	0.00	0.85	
MnO		0.01	0.00	0.24	0.00	1.29	0.00	0.01	
MgO		0.00	0.00	11.33	0.00	0.02	0.00	0.50	
CaO		7.76	0.08	0.03	0.00	0.01	56.00	3.28	
Na2O		7.20	1.39	0.13	0.00	0.02	0.00	3.21	
K2O		0.17	14.19	9.44	0.00	0.00	0.00	2.18	
P2O5		0.02	0.03	0.00	0.00	0.00	42.00	0.01	
F		0.03	0.04	0.86	0.00	0.00	0.00	0.05	
Cl		0.00	0.02	0.35	0.00	0.00	0.00	0.02	
							Total	100.2918	

Table A5 Average mineral composition used to calculate whole rock (total) geochemistry.

136-1A		Average mineral composition							
Total	Qtz	Plag	Kfs	Bt	Amph	Opaque	Ap	Total	
Specific G	2.65	2.69	2.57	3.00	3.00	5.15	3.20		
Volume x	0.62	1.66	0.08	0.27	0.00	0.17	0.00		
Wt%	0.22	0.59	0.03	0.10	0.00	0.06	0.00	1.00	
SiO2	100.00	58.89	64.26	36.47	0.00	0.07	0.00	62.35	
TiO2	0.00	0.02	0.02	3.84	0.00	19.12	0.00	1.52	
Al2O3	0.00	26.96	19.26	16.34	0.00	0.11	0.00	18.12	
Cr2O3	0.00	0.01	0.00	0.01	0.00	0.02	0.00	0.01	
FeO	0.00	0.08	0.04	18.35	0.00	76.15	0.00	6.36	
MnO	0.00	0.01	0.00	0.24	0.00	1.29	0.00	0.10	
MgO	0.00	0.00	0.00	11.33	0.00	0.02	0.00	1.09	
CaO	0.00	7.76	0.08	0.03	0.00	0.01	56.00	4.72	
Na2O	0.00	7.20	1.39	0.13	0.00	0.02	0.00	4.33	
K2O	0.00	0.17	14.19	9.44	0.00	0.00	0.00	1.39	
P2O5	0.00	0.02	0.03	0.00	0.00	0.00	42.00	0.09	
F	0.00	0.03	0.04	0.86	0.00	0.00	0.00	0.10	
Cl	0.00	0.00	0.02	0.35	0.00	0.00	0.00	0.04	
							Total	100.2215	

Table A6 Average mineral composition used to calculate residual geochemistry.

136-6A	Average mineral composition							
Residual	Qtz	Plag	Kfs	Bt	Amph	Opaque	Ap	Total
Specific G	2.65	2.69	2.57	3.00	3.00	5.15	3.20	
Volume x	0.33	1.97	0.00	0.32	0.00	0.18	0.00	
Wt%	0.12	0.70	0.00	0.11	0.00	0.06	0.00	1.00
SiO2	100.00	58.55	63.85	36.66	0.00	0.08	0.10	57.20
TiO2	0.00	0.01	0.03	3.89	0.00	20.84	0.03	1.80
Al2O3	0.00	27.26	19.49	16.56	0.00	0.14	0.01	21.07
Cr2O3	0.00	0.01	0.01	0.01	0.00	0.02	0.00	0.01
FeO	0.00	0.10	0.07	18.02	0.00	74.16	0.20	6.91
MnO	0.00	0.01	0.00	0.22	0.00	1.03	0.37	0.10
MgO	0.00	0.01	0.07	11.06	0.00	0.04	0.05	1.26
CaO	0.00	7.89	1.68	0.04	0.00	0.03	56.28	5.56
Na2O	0.00	7.14	13.73	0.15	0.00	0.04	0.00	5.05
K2O	0.00	0.19	13.73	9.32	0.00	0.00	0.01	1.19
P2O5	0.00	0.02	0.03	0.01	0.00	0.00	41.13	0.01
F	0.00	0.03	0.01	0.48	0.00	0.00	4.26	0.07
Cl	0.00	0.01	0.01	0.36	0.00	0.00	0.36	0.04
							Total	100.262

Table A7 Average mineral composition used to calculate melt geochemistry.

136-6A	Average mineral composition							
Melt	Qtz	Plag	Kfs	Bt	Amph	Opaque	Ap	Total
Specific G	2.65	2.69	2.57	3.00	3.00	5.15	3.20	
Volume x	1.45	0.81	0.33	0.04	0.00	0.00	0.02	
Wt%	0.54	0.31	0.13	0.02	0.00	0.00	0.01	1.00
SiO2	100.00	58.55	63.85	36.66	0.00	0.08	0.10	80.92
TiO2	0.00	0.01	0.03	3.89	0.00	20.84	0.03	0.07
Al2O3	0.00	27.26	19.49	16.56	0.00	0.14	0.01	11.03
Cr2O3	0.00	0.01	0.01	0.01	0.00	0.02	0.00	0.00
FeO	0.00	0.10	0.07	18.02	0.00	74.16	0.20	0.33
MnO	0.00	0.01	0.00	0.22	0.00	1.03	0.37	0.01
MgO	0.00	0.01	0.07	11.06	0.00	0.04	0.05	0.19
CaO	0.00	7.89	1.68	0.04	0.00	0.03	56.28	3.11
Na2O	0.00	7.14	13.73	0.15	0.00	0.04	0.00	3.90
K2O	0.00	0.19	13.73	9.32	0.00	0.00	0.01	1.93
P2O5	0.00	0.02	0.03	0.01	0.00	0.00	41.13	0.36
F	0.00	0.03	0.01	0.48	0.00	0.00	4.26	0.05
Cl	0.00	0.01	0.01	0.36	0.00	0.00	0.36	0.01
							Total	101.9346

Table A8 Average mineral composition used to calculate whole rock (total) geochemistry.

136-6A	Average mineral composition							
Total	Qtz	Plag	Kfs	Bt	Amph	Opaque	Ap	Total
Specific G	2.65	2.69	2.57	3.00	3.00	5.15	3.20	
Volume x	0.57	1.73	0.07	0.26	0.00	0.14	0.00	
Wt%	0.21	0.62	0.03	0.09	0.00	0.05	0.00	1.00
SiO2	100.00	58.55	63.85	36.66	0.00	0.08	0.10	62.07
TiO2	0.00	0.01	0.03	3.89	0.00	20.84	0.03	1.44
Al2O3	0.00	27.26	19.49	16.56	0.00	0.14	0.01	19.01
Cr2O3	0.00	0.01	0.01	0.01	0.00	0.02	0.00	0.01
FeO	0.00	0.10	0.07	18.02	0.00	74.16	0.20	5.56
MnO	0.00	0.01	0.00	0.22	0.00	1.03	0.37	0.08
MgO	0.00	0.01	0.07	11.06	0.00	0.04	0.05	1.04
CaO	0.00	7.89	1.68	0.04	0.00	0.03	56.28	5.06
Na2O	0.00	7.14	13.73	0.15	0.00	0.04	0.00	4.81
K2O	0.00	0.19	13.73	9.32	0.00	0.00	0.01	1.34
P2O5	0.00	0.02	0.03	0.01	0.00	0.00	41.13	0.09
F	0.00	0.03	0.01	0.48	0.00	0.00	4.26	0.07
Cl	0.00	0.01	0.01	0.36	0.00	0.00	0.36	0.04
							Total	100.6051

Table A9 Average mineral composition used to calculate residual geochemistry. *Chlorite taken from Clinocllore species via webmineral.com No EPMA data was collected. **K-feldspar data taken from sample 136-6A (Table A6-A8)

136-11A	Average mineral composition								
Residual	Qtz	Plag	Kfs**	Bt	Chl*	Amph	Opaque	Ap	Total
Specific G	2.65	2.69	2.57	3.00	3.00	3.00	5.15	3.20	
Volume x	1.38	0.99	0.00	0.00	0.03	0.17	0.24	0.00	
Wt%	0.49	0.35	0.00	0.00	0.01	0.06	0.08	0.00	1.00
SiO2	100.00	56.78	63.85	36.28		47.20	0.07	0.09	72.06
TiO2	0.00	0.01	0.03	3.74		0.58	0.11	0.00	0.05
Al2O3	0.00	28.12	19.49	15.11		7.45	0.15	0.02	10.41
Cr2O3	0.00	0.01	0.01	0.01		0.01	0.02	0.00	0.00
FeO	0.00	0.16	0.07	19.51		16.17	95.67	0.11	9.09
MnO	0.00	0.01	0.00	0.30		0.74	0.04	0.12	0.05
MgO	0.00	0.02	0.07	11.12		12.28	0.01	0.03	0.74
CaO	0.00	9.30	1.68	0.25		11.99	0.00	56.90	4.01
Na2O	0.00	6.07	13.73	0.09		0.87	0.00	0.00	2.20
K2O	0.00	0.33	13.73	9.01		0.60	0.00	0.00	0.15
P2O5	0.00	0.00	0.03	0.00		0.00	0.00	41.16	0.00
F	0.00	0.02	0.01	0.20		0.10	0.00	4.05	0.01
Cl	0.00	0.01	0.01	0.28		0.12	0.00	0.56	0.01
								Total	98.79805

Table A10 Average mineral composition used to calculate melt geochemistry. *Chlorite taken from Clinocllore species via webmineral.com No EPMA data was collected. **K-feldspar data taken from sample 136-6A (Table A6-A8)

136-11A	Average mineral composition								
Melt	Qtz	Plag	Kfs**	Bt	Chl*	Amph	Opaque	Ap	Total
Specific G	2.65	2.69	2.57	3.00	3.00	3.00	5.15	3.20	
Volume x	1.36	0.72	0.50	0.00	0.00	0.00	0.00	0.08	
Wt%	0.51	0.27	0.19	0.00	0.00	0.00	0.00	0.03	1.00
SiO2	100.00	56.78	63.85	36.28	0.00	47.20	0.07	0.09	78.51
TiO2	0.00	0.01	0.03	3.74	0.00	0.58	0.11	0.00	0.01
Al2O3	0.00	28.12	19.49	15.11	0.00	7.45	0.15	0.02	11.31
Cr2O3	0.00	0.01	0.01	0.01	0.00	0.01	0.02	0.00	0.00
FeO	0.00	0.16	0.07	19.51	0.00	16.17	95.67	0.11	0.06
MnO	0.00	0.01	0.00	0.30	0.00	0.74	0.04	0.12	0.01
MgO	0.00	0.02	0.07	11.12	0.00	12.28	0.01	0.03	0.02
CaO	0.00	9.30	1.68	0.25	0.00	11.99	0.00	56.90	4.51
Na2O	0.00	6.07	13.73	0.09	0.00	0.87	0.00	0.00	4.24
K2O	0.00	0.33	13.73	9.01	0.00	0.60	0.00	0.00	2.68
P2O5	0.00	0.00	0.03	0.00	0.00	0.00	0.00	41.16	1.21
F	0.00	0.02	0.01	0.20	0.00	0.10	0.00	4.05	0.13
Cl	0.00	0.01	0.01	0.28	0.00	0.12	0.00	0.56	0.02
	100.00	100.83	112.70	95.89	0.00	98.12	96.07	103.03	
							Total		102.71

Table A11 Average mineral composition used to calculate whole rock (total) geochemistry.
 *Chlorite taken from Clinocllore species via webmineral.com No EPMA data was collected.
 **K-feldspar data taken from sample 136-6A (Table A6-A8)

136-11A	Average mineral composition								
Total	Qtz	Plag	Kfs**	Bt	Chl*	Amph	Opaque	Ap	Total
Specific G	2.65	2.69	2.57	3.00	3.00	3.00	5.15	3.20	
Volume x	1.38	0.98	0.03	0.00	0.03	0.16	0.22	0.00	
Wt%	0.49	0.35	0.01	0.00	0.01	0.06	0.08	0.00	1.00
SiO2	100.00	56.78	63.85	36.28	0.00	47.20	0.07	0.09	72.45
TiO2	0.00	0.01	0.03	3.74	0.00	0.58	0.11	0.00	0.04
Al2O3	0.00	28.12	19.49	15.11	0.00	7.45	0.15	0.02	10.47
Cr2O3	0.00	0.01	0.01	0.01	0.00	0.01	0.02	0.00	0.00
FeO	0.00	0.16	0.07	19.51	0.00	16.17	95.67	0.11	8.55
MnO	0.00	0.01	0.00	0.30	0.00	0.74	0.04	0.12	0.05
MgO	0.00	0.02	0.07	11.12	0.00	12.28	0.01	0.03	0.70
CaO	0.00	9.30	1.68	0.25	0.00	11.99	0.00	56.90	4.04
Na2O	0.00	6.07	13.73	0.09	0.00	0.87	0.00	0.00	2.32
K2O	0.00	0.33	13.73	9.01	0.00	0.60	0.00	0.00	0.30
P2O5	0.00	0.00	0.03	0.00	0.00	0.00	0.00	41.16	0.07
F	0.00	0.02	0.01	0.20	0.00	0.10	0.00	4.05	0.02
Cl	0.00	0.01	0.01	0.28	0.00	0.12	0.00	0.56	0.01
								Total	99.03

Table A12 Average mineral composition used to calculate residual geochemistry. *Biotite data taken from webmineral.com

136-2B	Average mineral composition									
Residual	Qtz	Plag	Kfs	Amph	Bt*	Cpx	Opagues	Ap	Total	
Specific G	2.65	2.69	2.57	3.00	3.00	3.50	5.15	3.20		
Volume x	0.48	1.45	0.00	0.50	0.04	0.09	0.38	0.01		
Wt%	0.16	0.49	0.00	0.17	0.01	0.03	0.13	0.00	1.00	
SiO2	100.00	53.90	63.14	45.23	41.58	51.88	0.18	0.70	52.75	
TiO2	0.00	0.01	0.00	1.11	0.00	0.14	15.10	0.00	2.12	
Al2O3	0.00	30.18	19.41	8.68	11.76	1.19	0.31	0.00	16.54	
Cr2O3	0.00	0.01	0.01	0.01	0.00	0.01	0.03	0.02	0.01	
FeO	0.00	0.31	0.12	17.37	8.29	10.76	79.87	0.10	13.76	
MnO	0.00	0.01	0.01	0.45	0.00	0.76	1.79	0.06	0.33	
MgO	0.00	0.01	0.00	10.78	23.24	12.59	0.08	0.02	2.55	
CaO	0.00	11.84	0.10	12.20	0.00	22.24	0.09	56.20	8.75	
Na2O	0.00	4.91	1.15	1.05	0.00	0.31	0.02	0.02	2.60	
K2O	0.00	0.19	14.27	1.02	10.86	0.01	0.01	0.01	0.40	
P2O5	0.00	0.01	0.00	0.01	0.00	0.01	0.00	39.99	0.10	
F	0.00	0.03	0.02	0.14	1.10	0.02	0.00	3.27	0.06	
Cl	0.00	0.01	0.00	0.36	0.00	0.01	0.00	1.20	0.07	
Total	100.00	101.41	98.24	98.40	96.83	99.93	97.47	101.58		
								Total	100.06	

Table A13 Average mineral composition used to calculate melt geochemistry. *Biotite data taken from webmineral.com

136-2B	Average mineral composition									
Melt	Qtz	Plag	Kfs	Amph	Bt*	Cpx	Opaques	Ap	Total	
Specific G	2.65	2.69	2.57	3.00	3.00	3.50	5.15	3.20		
Volume x	1.26	0.97	0.33	0.09	0.00	0.00	0.00	0.02		
Wt%	0.47	0.36	0.12	0.03	0.00	0.00	0.00	0.01		1.00
SiO2	100.00	53.90	63.14	45.23	41.58	51.88	0.18	0.70		76.21
TiO2	0.00	0.01	0.00	1.11	0.00	0.14	15.10	0.00		0.04
Al2O3	0.00	30.18	19.41	8.68	11.76	1.19	0.31	0.00		13.63
Cr2O3	0.00	0.01	0.01	0.01	0.00	0.01	0.03	0.02		0.01
FeO	0.00	0.31	0.12	17.37	8.29	10.76	79.87	0.10		0.70
MnO	0.00	0.01	0.01	0.45	0.00	0.76	1.79	0.06		0.02
MgO	0.00	0.01	0.00	10.78	23.24	12.59	0.08	0.02		0.36
CaO	0.00	11.84	0.10	12.20	0.00	22.24	0.09	56.20		5.10
Na2O	0.00	4.91	1.15	1.05	0.00	0.31	0.02	0.02		1.95
K2O	0.00	0.19	14.27	1.02	10.86	0.01	0.01	0.01		1.88
P2O5	0.00	0.01	0.00	0.01	0.00	0.01	0.00	39.99		0.28
F	0.00	0.03	0.02	0.14	1.10	0.02	0.00	3.27		0.04
Cl	0.00	0.01	0.00	0.36	0.00	0.01	0.00	1.20		0.02
Total	100.00	101.41	98.24	98.40	96.83	99.93	97.47	101.58		
								Total		100.25

Table A14 Average mineral composition used to calculate whole rock (total) geochemistry.
 *Biotite data taken from webmineral.com

136-2B		Average mineral composition								
Total	Qtz	Plag	Kfs	Amph	Bt*	Cpx	Opaques	Ap	Total	
Specific G	2.65	2.69	2.57	3.00	3.00	3.50	5.15	3.20		
Volume x	0.68	1.32	0.09	0.39	0.03	0.07	0.28	0.01		
Wt%	0.24	0.46	0.03	0.14	0.01	0.02	0.10	0.00	1.00	
SiO2	100.00	53.90	63.14	45.23	41.58	51.88	0.18	0.70	58.46	
TiO2	0.00	0.01	0.00	1.11	0.00	0.14	15.10	0.00	1.62	
Al2O3	0.00	30.18	19.41	8.68	11.76	1.19	0.31	0.00	15.83	
Cr2O3	0.00	0.01	0.01	0.01	0.00	0.01	0.03	0.02	0.01	
FeO	0.00	0.31	0.12	17.37	8.29	10.76	79.87	0.10	10.58	
MnO	0.00	0.01	0.01	0.45	0.00	0.76	1.79	0.06	0.26	
MgO	0.00	0.01	0.00	10.78	23.24	12.59	0.08	0.02	2.02	
CaO	0.00	11.84	0.10	12.20	0.00	22.24	0.09	56.20	7.86	
Na2O	0.00	4.91	1.15	1.05	0.00	0.31	0.02	0.02	2.45	
K2O	0.00	0.19	14.27	1.02	10.86	0.01	0.01	0.01	0.76	
P2O5	0.00	0.01	0.00	0.01	0.00	0.01	0.00	39.99	0.14	
F	0.00	0.03	0.02	0.14	1.10	0.02	0.00	3.27	0.06	
Cl	0.00	0.01	0.00	0.36	0.00	0.01	0.00	1.20	0.06	
Total	100.00	101.41	98.24	98.40	96.83	99.93	97.47	101.58		
							Total		100.10	

Table A15 Average mineral composition used to calculate residual geochemistry. *Biotite data taken from webmineral.com **Apatite data taken from sample 136-2B (Table A12-14)

136-8B		Average Mineral Composition								
Residual	Qtz	Plag	Kfs	Amph	Bt*	Cpx	Opaque	Ap**	Total	
Specific G	2.65	2.69	2.57	3.00	3.00	3.50	5.15	3.20		
Volume x	0.59	1.46	0.00	0.31	0.01	0.13	0.48	0.00		
Wt%	0.20	0.49	0.00	0.10	0.00	0.04	0.16	0.00	1.00	
SiO2	100.00	55.99	62.68	48.07	41.58	52.05	0.06	0.70	54.61	
TiO2	0.00	0.01	0.01	0.30	0.00	0.11	16.68	0.00	2.73	
Al2O3	0.00	28.15	19.08	7.08	11.76	1.31	0.51	0.00	14.73	
Cr2O3	0.00	0.00	0.00	0.01	0.00	0.00	0.04	0.02	0.01	
FeO	0.00	0.30	0.27	14.40	8.29	10.12	77.33	0.10	14.56	
MnO	0.00	0.01	0.02	0.52	0.00	0.81	2.32	0.06	0.47	
MgO	0.00	0.04	0.06	13.20	23.24	13.08	0.03	0.02	2.06	
CaO	0.00	9.81	0.06	11.93	0.00	22.24	0.00	56.20	7.02	
Na2O	0.00	5.62	0.90	0.82	0.00	0.30	0.01	0.02	2.85	
K2O	0.00	0.54	14.20	0.60	10.86	0.01	0.01	0.01	0.38	
P2O5	0.00	0.00	0.00	0.00	0.00	0.00	0.00	39.99	0.00	
F	0.00	0.03	0.07	0.12	1.10	0.02	0.00	3.27	0.03	
Cl	0.00	0.01	0.00	0.21	0.00	0.01	0.01	1.20	0.03	
								Total	99.46866	

Table A16 Average mineral composition used to calculate melt geochemistry. *Biotite data taken from webmineral.com **Apatite data taken from sample 136-2B (Table A12-14)

136-8B		Average Mineral Composition								
Melt	Qtz	Plag	Kfs	Amph	Bt	Cpx	Opaque	Ap	Total	
Specific G	2.65	2.69	2.57	3.00	3.00	3.50	5.15	3.20		
Volume x	1.34	1.17	0.16	0.00	0.00	0.00	0.00	0.00		
Wt%	0.50	0.44	0.06	0.00	0.00	0.00	0.00	0.00	1.00	
SiO2	100.00	55.99	62.68	48.07	41.58	52.05	0.06	0.70	78.50	
TiO2	0.00	0.01	0.01	0.30	0.00	0.11	16.68	0.00	0.01	
Al2O3	0.00	28.15	19.08	7.08	11.76	1.31	0.51	0.00	13.47	
Cr2O3	0.00	0.00	0.00	0.01	0.00	0.00	0.04	0.02	0.00	
FeO	0.00	0.30	0.27	14.40	8.29	10.12	77.33	0.10	0.15	
MnO	0.00	0.01	0.02	0.52	0.00	0.81	2.32	0.06	0.00	
MgO	0.00	0.04	0.06	13.20	23.24	13.08	0.03	0.02	0.02	
CaO	0.00	9.81	0.06	11.93	0.00	22.24	0.00	56.20	4.31	
Na2O	0.00	5.62	0.90	0.82	0.00	0.30	0.01	0.02	2.52	
K2O	0.00	0.54	14.20	0.60	10.86	0.01	0.01	0.01	1.07	
P2O5	0.00	0.00	0.00	0.00	0.00	0.00	0.00	39.99	0.00	
F	0.00	0.03	0.07	0.12	1.10	0.02	0.00	3.27	0.02	
Cl	0.00	0.01	0.00	0.21	0.00	0.01	0.01	1.20	0.00	
								Total	100.07	

Table A17 Average mineral composition used to calculate whole rock (total) geochemistry.
 *Biotite data taken from webmineral.com **Apatite data taken from sample 136-2B (Table A12-14)

136-8B	Average Mineral Composition								
Total	Qtz	Plag	Kfs	Amph	Bt	Cpx	Opaque	Ap	Total
Specific G	2.65	2.69	2.57	3.00	3.00	3.50	5.15	3.20	
Volume x	0.82	1.37	0.05	0.21	0.01	0.09	0.33	0.00	
Wt%	0.28	0.48	0.02	0.07	0.00	0.03	0.12	0.00	1.00
SiO2	100.00	55.99	62.68	48.07	41.58	52.05	0.06	0.70	61.34
TiO2	0.00	0.01	0.01	0.30	0.00	0.11	16.68	0.00	1.96
Al2O3	0.00	28.15	19.08	7.08	11.76	1.31	0.51	0.00	14.37
Cr2O3	0.00	0.00	0.00	0.01	0.00	0.00	0.04	0.02	0.01
FeO	0.00	0.30	0.27	14.40	8.29	10.12	77.33	0.10	10.50
MnO	0.00	0.01	0.02	0.52	0.00	0.81	2.32	0.06	0.34
MgO	0.00	0.04	0.06	13.20	23.24	13.08	0.03	0.02	1.49
CaO	0.00	9.81	0.06	11.93	0.00	22.24	0.00	56.20	6.26
Na2O	0.00	5.62	0.90	0.82	0.00	0.30	0.01	0.02	2.76
K2O	0.00	0.54	14.20	0.60	10.86	0.01	0.01	0.01	0.57
P2O5	0.00	0.00	0.00	0.00	0.00	0.00	0.00	39.99	0.00
F	0.00	0.03	0.07	0.12	1.10	0.02	0.00	3.27	0.03
Cl	0.00	0.01	0.00	0.21	0.00	0.01	0.01	1.20	0.02
								Total	99.64

Table A18 Average mineral composition used to calculate residual geochemistry. *Biotite, calcite, and spinel data taken from webmineral.com **Apatite data taken from sample 136-2B (Table A12-14)

136-14B	Average mineral composition										
Residual	Qtz	Plag	Kfs	Amph	Bt	Cpx	Opaques	Ap**	Calcite*	Spinel*	Total
Specific G	2.65	2.69	2.57	3.00	3.00	3.50	5.15	3.20	2.71	3.80	
Volume x	1.06	1.31	0.00	0.18	0.00	0.00	0.22	0.01	0.00	0.02	
Wt%	0.38	0.47	0.00	0.06	0.00	0.00	0.08	0.00	0.00	0.01	0.99
SiO2	100.00	57.87	63.83	48.51	38.85	0.00	0.05	0.70	0.00	0.00	67.92
TiO2	0.00	0.01	0.04	0.99	0.53		0.08	0.00	0.00	0.00	0.08
Al2O3	0.00	27.20	19.10	6.76	12.74		0.10	0.00	0.00	71.67	13.67
Cr2O3	0.00	0.01	0.00	0.00	0.00		0.03	0.02	0.00	0.00	0.01
FeO	0.00	0.27	0.07	12.95	17.80		95.41	0.10	0.00	0.00	8.56
MnO	0.00	0.01	0.02	0.54	0.72		0.08	0.06	0.00	0.00	0.04
MgO	0.00	0.02	0.00	14.70	14.87		0.00	0.02	0.00	28.33	1.17
CaO	0.00	8.49	0.02	11.82	6.70		0.00	56.20	56.03	0.00	4.94
Na2O	0.00	6.56	0.59	1.04	0.41		0.00	0.02	0.00	0.00	3.13
K2O	0.00	0.40	15.05	0.54	0.34		0.00	0.01	0.00	0.00	0.22
P2O5	0.00	0.00	0.00	0.00	0.00		0.00	39.99	0.00	0.00	0.08
F	0.00	0.04	0.08	0.23	0.08		0.00	3.27	0.00	0.00	0.04
Cl	0.00	0.00	0.01	0.11	0.08		0.01	1.20	0.00	0.00	0.01
								Total			99.88427

Table A19 Average mineral composition used to calculate melt geochemistry. *Biotite, calcite, and spinel data taken from webmineral.com **Apatite data taken from sample 136-2B (Table A12-14)

136-14B	Average mineral composition										
Melt	Qtz	Plag	Kfs	Amph	Bt	Cpx	Opaques	Ap**	Calcite*	Spinel*	Total
Specific G	2.65	2.69	2.57	3.00	3.00	3.50	5.15	3.20	2.70	3.80	
Volume x	1.40	0.95	0.31	0.00	0.00	0.00	0.00	0.00	0.00	0.00	
Wt%	0.53	0.36	0.12	0.00	0.00	0.00	0.00	0.00	0.00	0.00	1.00
SiO2	100.00	57.87	63.83	48.51	38.85	0.00	0.05	0.00	0.00	0.00	80.74
TiO2	0.00	0.01	0.04	0.99	0.53	0.00	0.08	0.00	0.00	0.00	0.01
Al2O3	0.00	27.20	19.10	6.76	12.74	0.00	0.10	0.00	0.00	71.67	11.93
Cr2O3	0.00	0.01	0.00	0.00	0.00	0.00	0.03	0.00	0.00	0.00	0.00
FeO	0.00	0.27	0.07	12.95	17.80	0.00	95.41	0.00	0.00	0.00	0.10
MnO	0.00	0.01	0.02	0.54	0.72	0.00	0.08	0.00	0.00	0.00	0.01
MgO	0.00	0.02	0.00	14.70	14.87	0.00	0.00	0.00	0.00	28.33	0.01
CaO	0.00	8.49	0.02	11.82	6.70	0.00	0.00	55.60	56.03	0.00	3.03
Na2O	0.00	6.56	0.59	1.04	0.41	0.00	0.00	0.00	0.00	0.00	2.40
K2O	0.00	0.40	15.05	0.54	0.34	0.00	0.00	0.00	0.00	0.00	1.92
P2O5	0.00	0.00	0.00	0.00	0.00	0.00	0.00	42.22	0.00	0.00	0.00
F	0.00	0.04	0.08	0.23	0.08	0.00	0.00	3.77	0.00	0.00	0.02
Cl	0.00	0.00	0.01	0.11	0.08	0.00	0.01	0.00	0.00	0.00	0.00
								Total			100.17

Table A20 Average mineral composition used to calculate whole rock (total) geochemistry. *Biotite, calcite, and spinel data taken from webmineral.com **Apatite data taken from sample 136-2B (Table A12-14)

136-14B	Average mineral composition										
Total	Qtz	Plag	Kfs	Amph	Bt	Cpx	Opauques	Ap**	Calcite*	Spinel*	Total
Specific G	2.65	2.69	2.57	3.00	3.00	3.50	5.15	3.20	2.71	3.81	
Volume x	1.10	1.27	0.04	0.16	0.00	0.00	0.20	0.00	0.00	0.02	
Wt%	0.39	0.46	0.01	0.06	0.00	0.00	0.07	0.00	0.00	0.01	1.00
SiO2	100.00	57.87	63.83	48.51	38.85	0.00	0.05	0.00	0.00	0.00	69.55
TiO2	0.00	0.01	0.04	0.99	0.53	0.00	0.08	0.00	0.00	0.00	0.07
Al2O3	0.00	27.20	19.10	6.76	12.74	0.00	0.10	0.00	0.00	71.67	13.59
Cr2O3	0.00	0.01	0.00	0.00	0.00	0.00	0.03	0.00	0.00	0.00	0.01
FeO	0.00	0.27	0.07	12.95	17.80	0.00	95.41	0.00	0.00	0.00	7.71
MnO	0.00	0.01	0.02	0.54	0.72	0.00	0.08	0.00	0.00	0.00	0.04
MgO	0.00	0.02	0.00	14.70	14.87	0.00	0.00	0.00	0.00	28.33	1.05
CaO	0.00	8.49	0.02	11.82	6.70	0.00	0.00	55.60	56.03	0.00	4.77
Na2O	0.00	6.56	0.59	1.04	0.41	0.00	0.00	0.00	0.00	0.00	3.08
K2O	0.00	0.40	15.05	0.54	0.34	0.00	0.00	0.00	0.00	0.00	0.41
P2O5	0.00	0.00	0.00	0.00	0.00	0.00	0.00	42.22	0.00	0.00	0.08
F	0.00	0.04	0.08	0.23	0.08	0.00	0.00	3.77	0.00	0.00	0.04
Cl	0.00	0.00	0.01	0.11	0.08	0.00	0.01	0.00	0.00	0.00	0.01
								Total			100.39

Appendix B

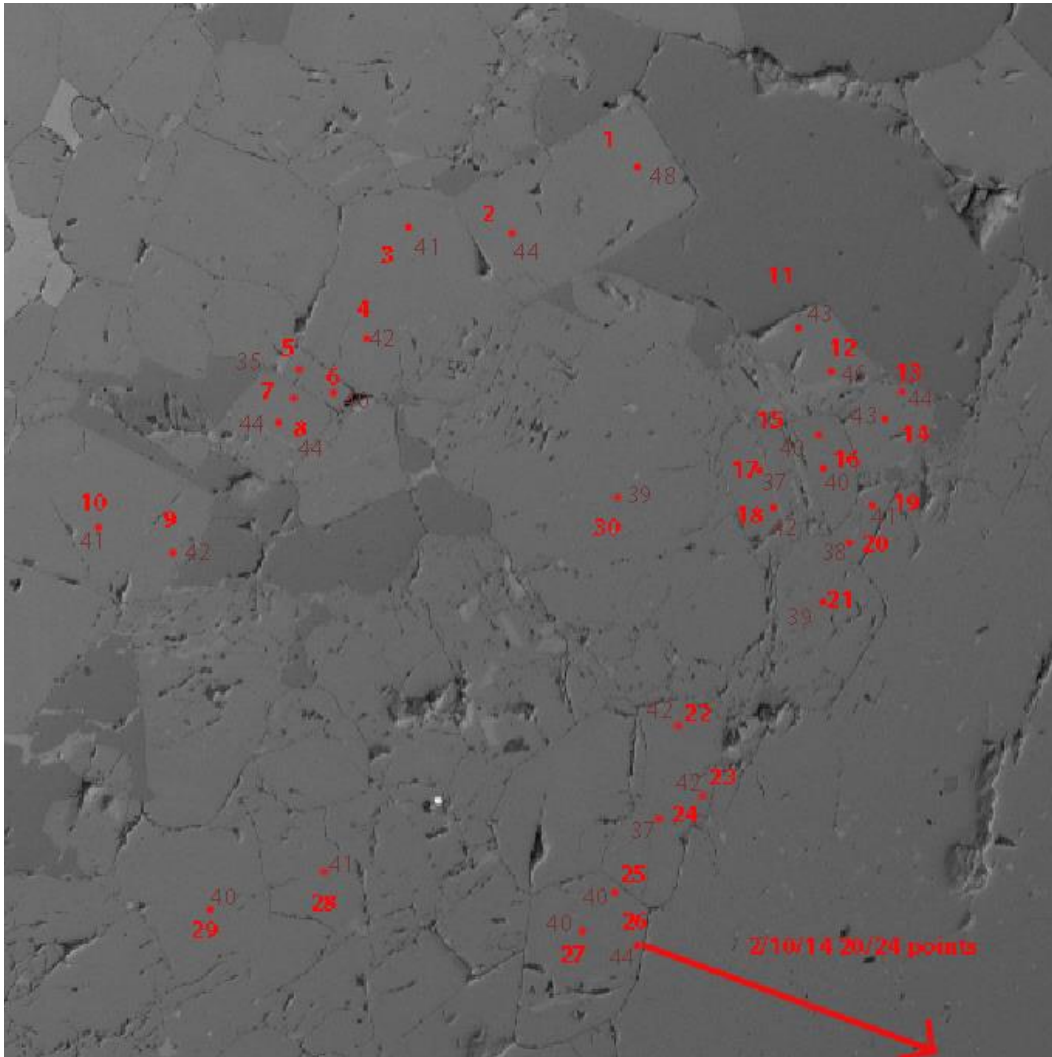


Figure A1 Sample 111-2. SEM-BSE (Scanning electron microscope – backscatter electron) image. Red dots are EPMA targets. Faded red numbers correspond to An % content of plagioclase crystals. Bright red numbers refer to point numbers listed in Tables A21-22. The red arrow is 480 μm .

Table A21 Sample 111-2 EPMA results. Numbers refer to Figure A1 red dots excluding the line analysis (red arrow in Figure A1) which encompasses No. 31-54.

Sample 111-2 Residual Plagioclase EPMA Analysis													
No.	An%	Ab%	Or%	SiO2	TiO2	Al2O3	FeO	MgO	CaO	Na2O	K2O	Total	Comment
31	38%	61%	1%	57.3653	0	26.8248	0.2257	0.0092	8.416	6.754	0.1431	99.7382	Line 1 111-2-s1-line
32	39%	60%	1%	56.906	0.0121	26.877	0.2329	0.0109	8.4667	6.5115	0.1835	99.2007	Line 2 111-2-s1-line
33	39%	59%	1%	57.2663	0	26.5281	0.262	0.0105	8.4225	6.5119	0.2581	99.2595	Line 3 111-2-s1-line
34	40%	59%	2%	56.9946	0.0115	26.7538	0.3004	0	8.4	6.3233	0.3068	99.0904	Line 4 111-2-s1-line
35	39%	59%	2%	56.8592	0	26.4744	0.2645	0.0191	8.471	6.5872	0.3017	98.9771	Line 5 111-2-s1-line
36	38%	59%	2%	57.0657	0.0274	26.6295	0.3088	0.0061	8.2605	6.5262	0.4029	99.2271	Line 6 111-2-s1-line
37	38%	59%	3%	57.2483	0.0061	26.68	0.3043	0.0121	8.1332	6.3838	0.4956	99.2635	Line 7 111-2-s1-line
38	39%	58%	3%	56.3447	0.0357	26.4212	0.2815	0.0159	8.1425	6.2877	0.5376	98.0668	Line 8 111-2-s1-line
39	38%	61%	2%	57.5657	0	26.7545	0.2795	0.0091	7.982	6.4906	0.314	99.3955	Line 9 111-2-s1-line
40	37%	56%	6%	57.4161	0	26.2466	0.2554	0.0155	7.8855	6.0847	1.138	99.0418	Line 10 111-2-s1-line
41	39%	59%	2%	57.1424	0.0035	26.5394	0.282	0.0174	8.2235	6.3987	0.4027	99.0097	Line 11 111-2-s1-line
42	39%	59%	2%	57.3579	0.0006	26.8572	0.2729	0.0081	8.4448	6.3674	0.3631	99.6721	Line 12 111-2-s1-line
43	37%	54%	10%	57.5337	0	26.1978	0.2503	0.0169	7.8016	5.8149	1.7353	99.3505	Line 13 111-2-s1-line
44	38%	57%	5%	57.0174	0	26.6519	0.2648	0.0058	8.1139	6.1672	0.9604	99.1815	Line 14 111-2-s1-line
45	39%	57%	4%	57.1661	0.008	26.7282	0.2532	0.006	8.2487	6.146	0.8	99.3563	Line 15 111-2-s1-line
46	40%	58%	2%	57.5802	0	26.5273	0.2684	0.0341	8.4611	6.1848	0.3168	99.3728	Line 16 111-2-s1-line
47	38%	60%	2%	57.1539	0.0025	26.9614	0.2331	0.001	8.3255	6.5832	0.3351	99.5958	Line 17 111-2-s1-line
48	39%	59%	2%	57.255	0.0013	26.9836	0.2668	0.0191	8.5523	6.4874	0.3309	99.8965	Line 18 111-2-s1-line
49	39%	60%	2%	57.2496	0.0057	26.8218	0.242	0	8.371	6.5537	0.3125	99.5564	Line 19 111-2-s1-line
50	40%	59%	1%	57.1667	0.0156	26.7208	0.2101	0	8.6027	6.4436	0.2569	99.4165	Line 20 111-2-s1-line
51	41%	58%	2%	56.882	0.0003	27.0856	0.2354	0.0095	8.6379	6.2151	0.2993	99.3652	Line 21 111-2-s1-line
52	42%	57%	1%	56.8434	0.0249	27.3119	0.2329	0.007	8.7755	5.9701	0.2029	99.3687	Line 22 111-2-s1-line
53	41%	58%	1%	56.3655	0.0134	27.21	0.2228	0	8.9318	6.3477	0.1765	99.2677	Line 23 111-2-s1-line
54	41%	58%	1%	56.0822	0.0016	27.0067	0.206	0.006	8.6648	6.3975	0.1872	98.5521	Line 24 111-2-s1-line
Average													
Stdev													

Table A22 Sample 111-2 EPMA results. Numbers refer to Figure A1 red dots excluding the line analysis (red arrow in Figure A1) which encompasses No. 31-54.

Sample 111-2 Euhedral and Rounded Plagioclase EPMA Analysis													
No.	An%	Ab%	Or%	SiO2	TiO2	Al2O3	FeO	MgO	CaO	Na2O	K2O	Total	Comment
1	48%	50%	1%	55.1955	0.03	28.4984	0.231	0.0062	10.1661	5.4056	0.2649	99.7978	111-2s1-3-pt1
2	44%	55%	1%	55.8045	0.0252	28.0137	0.1942	0.0183	9.6631	6.0267	0.2375	99.9833	111-2s1-3-pt2
3	41%	58%	2%	56.5632	0.0414	27.1905	0.2242	0.0279	8.905	6.3704	0.3009	99.6236	111-2s1-3-pt3
4	42%	56%	1%	56.1808	0	27.5783	0.2309	0.007	9.1865	6.1685	0.2633	99.6153	111-2s1-3-pt4
5	35%	55%	10%	57.417	0.0319	26.2041	0.1605	0.0141	7.5527	6.058	1.812	99.2504	111-2s1-3-pt5
8	44%	53%	3%	55.7967	0.0548	26.9994	0.1934	0	9.4133	5.8799	0.4687	98.8062	111-2s1-3-pt8
9	42%	56%	1%	56.4867	0.0388	27.2044	0.1892	0.0068	8.6979	5.897	0.2374	98.7582	111-2s1-3-pt9
10	41%	58%	2%	56.7152	0	27.2953	0.1889	0.007	8.7733	6.3122	0.2999	99.5919	111-2s1-3-pt10
11	43%	55%	2%	56.1686	0.0242	27.6269	0.2046	0	9.3914	6.059	0.276	99.7508	111-2s1-3-pt11
12	46%	51%	3%	55.3335	0.0188	28.0557	0.1849	0	9.6987	5.6071	0.5294	99.4282	111-2s1-3-pt12
13	44%	55%	1%	56.0426	0.0188	27.958	0.2048	0.0064	9.5335	6.0677	0.2071	100.0388	111-2s1-3-pt13
14	43%	54%	3%	56.1591	0.0022	27.6311	0.22	0	9.3271	5.9407	0.4792	99.7595	111-2s1-3-pt14
15	40%	59%	1%	56.4722	0.0185	27.138	0.2146	0.0021	8.6011	6.5196	0.1867	99.1529	111-2s1-3-pt15
16	40%	59%	1%	56.8906	0.0032	27.1818	0.2387	0	8.6811	6.382	0.1825	99.56	111-2s1-3-pt16
18	42%	57%	1%	56.7262	0.0131	27.2226	0.2377	0.0188	8.8163	6.044	0.1519	99.2307	111-2s1-3-pt18
21	39%	58%	3%	57.0936	0.0038	26.9735	0.2593	0.0141	8.415	6.3907	0.4852	99.6352	111-2s1-3-pt21
22	42%	57%	1%	56.5425	0.0236	27.2355	0.1927	0.0215	8.815	6.1514	0.1554	99.1377	111-2s1-3-pt22
23	42%	57%	1%	56.1163	0.0159	26.9729	0.1953	0.0098	9.0546	6.2922	0.141	98.798	111-2s1-3-pt23
25	40%	58%	1%	56.7795	0	27.2247	0.2363	0.0092	8.7336	6.3893	0.219	99.5917	111-2s1-3-pt25
26	44%	55%	1%	55.6218	0.0003	27.6636	0.2257	0.0082	9.3776	6.0237	0.1871	99.1081	111-2s1-3-pt26
27	40%	58%	1%	56.8431	0	27.1716	0.2461	0.0046	8.6242	6.3196	0.2522	99.4614	111-2s1-3-pt27
28	41%	58%	1%	56.7989	0.0207	26.9928	0.2117	0.0045	8.6072	6.2572	0.1852	99.0783	111-2s1-3-pt28
29	40%	59%	1%	56.8137	0	27.2696	0.1672	0.001	8.6156	6.4737	0.2004	99.5413	111-2s1-3-pt29
30	39%	60%	1%	57.3052	0.0019	26.8487	0.2322	0.0116	8.4444	6.4894	0.2321	99.5656	111-2s1-3-pt30
Averate	42%	56%	2%										
Stdev	3%	2%	2%										

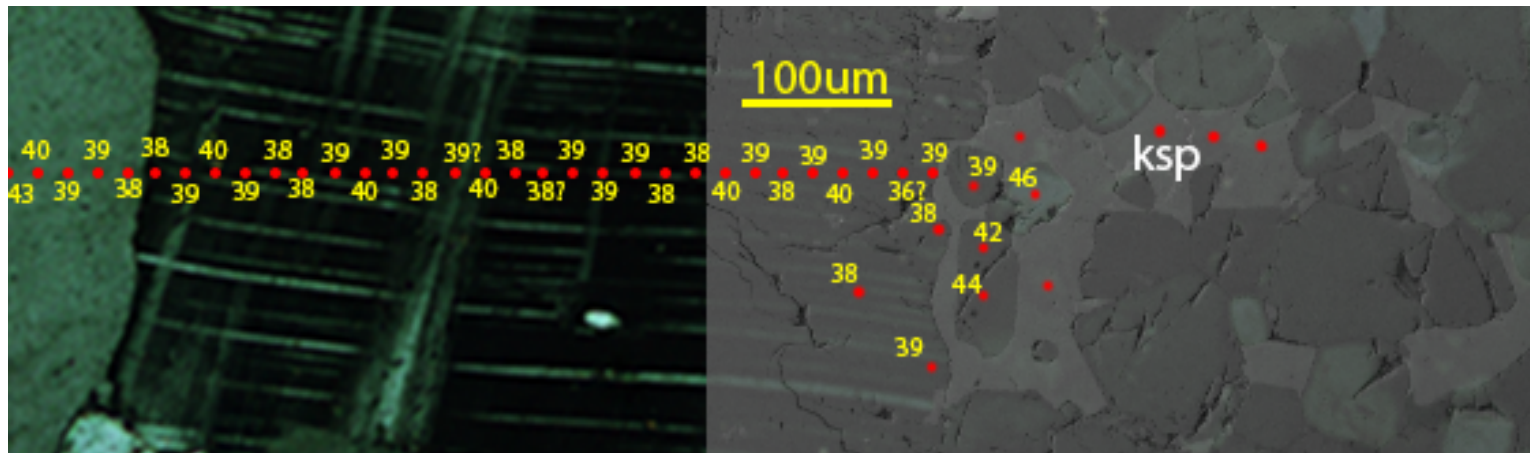


Figure A2 Sample 111-2. SEM-BSE image with photomicrograph underlay. Rod dots indicate EPMA targets. Yellow numbers indicate An % content of plagioclase. Values with a “?” are questionable EPMA analysis. Red dots with no values are not plagioclase. Refer to tables A23-25 for corresponding EPMA analysis. Ksp = K-feldspar

Table A23 EPMA results from rounded plagioclase crystals. Refer to Figure A2 for targets.

Sample 111-2 Rounded Plagioclase Analysis														
No.	An%	Ab%	Or%	SiO2	TiO2	Al2O3	FeO	MgO	CaO	Na2O	K2O	Total	Comment	Comment2
112	39%	59%	2%	56.8994	0.0019	26.9471	0.1773	0.0108	8.4578	6.5097	0.3003	99.3044	111-2s1-3-pt112	Residual 0.5mm Xtal
113	47%	52%	1%	55.2431	0	28.6208	0.193	0	10.2177	5.7181	0.23	100.2226	111-2s1-3-pt113	Residual 0.5mm Xtal
114	43%	56%	2%	56.3374	0.022	27.6552	0.2334	0.0117	9.1282	5.9772	0.2856	99.6507	111-2s1-3-pt114	Residual 0.5mm Xtal
115	44%	55%	1%	55.9723	0.0064	28.1004	0.2013	0.0067	9.7344	6.0466	0.2365	100.3046	111-2s1-3-pt115	Residual 0.5mm Xtal
Average	43%	55%	1%											
Stdev	3%	3%	0%											

Table A24 EPMA results from residual plagioclase crystals. Refer to Figure A2 for targets.

Sample 111-2 Residual Plagioclase EPMA Analysis														
No.	An%	Ab%	Or%	SiO2	TiO2	Al2O3	FeO	MgO	CaO	Na2O	K2O	Total	Comment	Comment2
116	39%	60%	1%	56.7266	0.0003	27.0226	0.1307	0.0049	8.3828	6.6908	0.1798	99.1385	111-2s1-3-pt116	Residual 0.5mm Xtal
117	39%	60%	1%	57.3183	0.0035	26.879	0.1925	0	8.3117	6.5369	0.2484	99.4903	111-2s1-3-pt117	Residual 0.5mm Xtal
124	39%	60%	1%	57.3102	0.001	26.9199	0.1493	0.0269	8.4635	6.5901	0.1696	99.6306	Line 1 111-2s1-4line	Large Residual xtal
126	39%	60%	1%	57.0825	0.0249	26.9687	0.223	0.0189	8.3554	6.5068	0.2457	99.426	Line 3 111-2s1-4line	Large Residual xtal
127	40%	59%	1%	57.093	0.0102	26.9813	0.2328	0.0019	8.5059	6.4327	0.2328	99.4907	Line 4 111-2s1-4line	Large Residual xtal
128	39%	60%	1%	57.0366	0.0188	26.7178	0.2505	0.027	8.3361	6.4778	0.2556	99.1202	Line 5 111-2s1-4line	Large Residual xtal
129	38%	60%	1%	57.1316	0	27.0226	0.2356	0	8.2942	6.5656	0.2631	99.5127	Line 6 111-2s1-4line	Large Residual xtal
131	39%	59%	2%	57.3665	0.0491	26.7713	0.3588	0.0135	8.2955	6.4117	0.3766	99.6431	Line 8 111-2s1-4line	Large Residual xtal
133	40%	58%	2%	57.0974	0.0332	26.7347	0.2566	0.0138	8.3599	6.1296	0.3322	98.9575	Line 10 111-2s1-4line	Large Residual xtal
134	38%	59%	3%	57.0372	0.0319	26.5677	0.2978	0	8.162	6.4293	0.5244	99.0503	Line 11 111-2s1-4line	Large Residual xtal
135	38%	60%	2%	57.3442	0.0217	26.8928	0.2777	0	8.3355	6.6448	0.337	99.8538	Line 12 111-2s1-4line	Large Residual xtal
136	39%	59%	2%	57.7176	0.0093	26.4137	0.2755	0.0102	8.2981	6.3705	0.4016	99.4966	Line 13 111-2s1-4line	Large Residual xtal
137	39%	60%	2%	57.4428	0	26.9553	0.2684	0.0185	8.3772	6.5005	0.3539	99.9166	Line 14 111-2s1-4line	Large Residual xtal
138	39%	59%	2%	57.4635	0.0131	26.867	0.2637	0.0195	8.4236	6.4737	0.3545	99.8787	Line 15 111-2s1-4line	Large Residual xtal
140	38%	60%	2%	57.3482	0.0096	26.5873	0.2296	0.0158	8.2097	6.5243	0.395	99.3196	Line 17 111-2s1-4line	Large Residual xtal
141	40%	58%	2%	57.8662	0.0294	26.4018	0.2365	0.0021	8.3203	6.1629	0.4021	99.4214	Line 18 111-2s1-4line	Large Residual xtal
143	38%	58%	3%	56.8716	0.0278	26.7187	0.2486	0.0052	8.1954	6.3586	0.5655	98.9915	Line 20 111-2s1-4line	Large Residual xtal
144	39%	59%	2%	56.9589	0.0124	26.6964	0.2872	0.0364	8.1143	6.2499	0.4325	98.788	Line 21 111-2s1-4line	Large Residual xtal
146	39%	58%	2%	56.8091	0.0214	26.8404	0.2418	0.0235	8.4864	6.4194	0.3867	99.2288	Line 23 111-2s1-4line	Large Residual xtal
147	38%	58%	4%	57.3024	0.0326	26.6234	0.2591	0.0088	8.2228	6.3711	0.6673	99.4875	Line 24 111-2s1-4line	Large Residual xtal
148	38%	59%	3%	57.4221	0.0003	26.8572	0.2048	0.0089	8.2913	6.4881	0.5239	99.7967	Line 25 111-2s1-4line	Large Residual xtal
149	39%	59%	2%	57.2171	0.022	26.8191	0.2422	0.0135	8.4461	6.4563	0.3409	99.5573	Line 26 111-2s1-4line	Large Residual xtal
151	40%	59%	2%	56.7208	0	27.014	0.2055	0.0024	8.4839	6.4496	0.2772	99.1535	Line 28 111-2s1-4line	Large Residual xtal
Average	39%	59%	2%											
Stdev	1%	1%	1%											

Table A25 EPMA results from K-feldspar crystals. Refer to Figure A2 for targets.

111-2 K-feldspar EPMA Analysis														
No.	An%	Ab%	Or%	SiO2	TiO2	Al2O3	FeO	MgO	CaO	Na2O	K2O	Total	Comment	Comment2
108	0%	6%	94%	61.33	0.00	18.77	0.10	0.00	0.00	0.66	14.95	95.82	111-2s1-3-pt108	Kspar pseudomelt
109	0%	7%	93%	60.62	0.00	18.82	0.09	0.00	0.00	0.74	15.08	95.35	111-2s1-3-pt109	Kspar pseudomelt
110	0%	7%	93%	61.72	0.00	18.91	0.08	0.00	0.00	0.71	15.12	96.54	111-2s1-3-pt110	Kspar pseudomelt
111	0%	7%	93%	60.85	0.00	19.00	0.10	0.01	0.00	0.73	14.72	95.41	111-2s1-3-pt111	Kspar pseudomelt
Average	0%	6%	94%											
Stdev	0%	0%	0%											

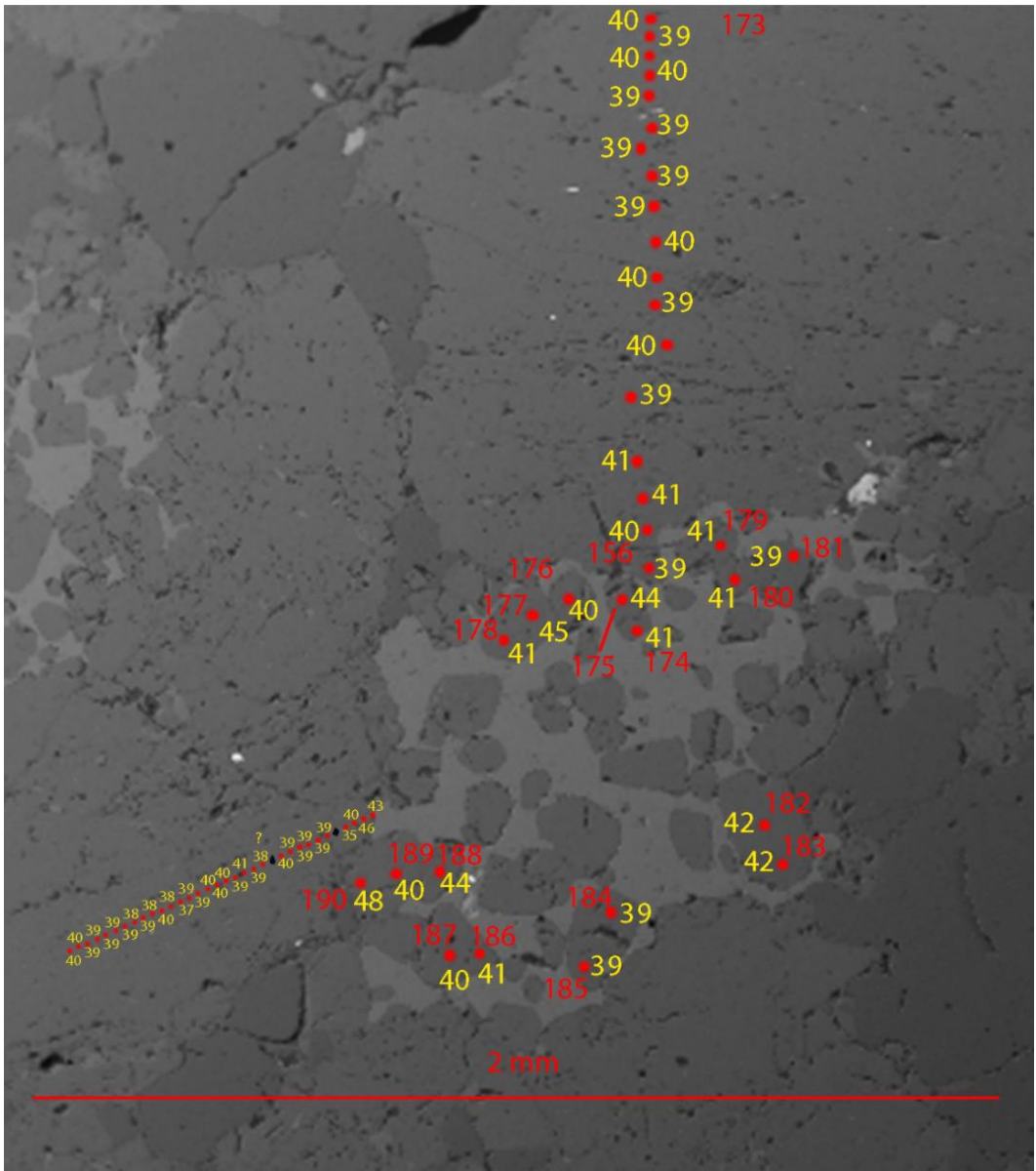


Figure A3 Sample 111-2. SEM-BSE image of Large Pseudomelt Pocket (LPP). Rod dots indicate EPMA targets. Red numbers indicate sample run numbers. Yellow numbers indicate An % content of plagioclase. Values with a “?” are questionable EPMA analysis. Red dots with no values are not plagioclase. Refer to tables A26-28 for corresponding EPMA analysis.

Table A26 EPMA results of rounded plagioclase. Refer to Figure A3 for targets.

Sample 111-2 Rounded Plagioclase														
No.	%An	%Ab	%Or	SiO2	TiO2	Al2O3	FeO	MgO	CaO	Na2O	K2O	Total	Comment	Comment2
174	41%	57%	2%	56.6353	0.0319	27.4597	0.2161	0	8.8899	6.1937	0.3592	99.7859	111-2s2-3-pt174	Small (<0.5 mm) plag
175	44%	55%	1%	55.9271	0	27.9842	0.2311	0.0175	9.4784	6.0395	0.1891	99.867	111-2s2-3-pt175	Small (<0.5 mm) plag
176	40%	58%	2%	57.054	0.0451	27.4856	0.2367	0.0108	8.9603	6.4738	0.352	100.6182	111-2s2-3-pt176	Small (<0.5 mm) plag
177	45%	54%	1%	55.0392	0.0144	27.7768	0.2299	0.0089	9.4131	5.924	0.2086	98.615	111-2s2-3-pt177	Small (<0.5 mm) plag
178	41%	57%	2%	56.6857	0.0006	27.2496	0.2305	0.0231	8.8307	6.2763	0.2792	99.5758	111-2s2-3-pt178	Small (<0.5 mm) plag
179	41%	58%	2%	56.7524	0	27.1475	0.223	0.0205	8.5419	6.2029	0.2716	99.1599	111-2s2-3-pt179	Small (<0.5 mm) plag
180	41%	58%	1%	56.6451	0.016	27.2016	0.2313	0.0208	9.0436	6.3904	0.2304	99.7793	111-2s2-3-pt180	Small (<0.5 mm) plag
182	42%	56%	2%	56.3839	0.0102	27.4849	0.2321	0.0149	9.0933	6.2112	0.317	99.7476	111-2s2-3-pt182	Small (<0.5 mm) plag
183	42%	56%	2%	56.9154	0.0128	27.0975	0.2352	0.0127	8.7957	5.9391	0.2953	99.3038	111-2s2-3-pt183	Small (<0.5 mm) plag
184	39%	60%	1%	57.2889	0.0102	27.2782	0.2006	0.0249	8.6687	6.5367	0.1921	100.2002	111-2s2-3-pt184	Small (<0.5 mm) plag
186	41%	58%	1%	56.491	0.0157	27.4542	0.197	0	8.8858	6.2936	0.2447	99.5821	111-2s2-3-pt186	Small (<0.5 mm) plag
187	40%	58%	2%	56.994	0.0022	27.1102	0.1833	0.0105	8.6714	6.3376	0.2952	99.6044	111-2s2-3-pt187	Small (<0.5 mm) plag
188	44%	54%	2%	56.7289	0.024	27.2791	0.1828	0.003	8.8878	5.522	0.2987	98.9264	111-2s2-3-pt188	Small (<0.5 mm) plag
189	40%	56%	4%	56.904	0.0166	27.0833	0.231	0.0115	8.6501	6.1537	0.6786	99.7289	111-2s2-3-pt189	Small (<0.5 mm) plag
190	48%	51%	1%	54.9322	0.0323	27.9278	0.2216	0.0123	10.0478	5.4872	0.2306	98.8919	111-2s2-3-pt190	Small (<0.5 mm) plag
Average	42%	56%	2%											
Stdev	2%	2%	1%											

Table A27 EPMA results of the top residual plagioclase. Refer to Figure A3 for targets.

Sample 111-2 Residual Plagioclase (top)														
No.	An%	Ab%	Or%	SiO2	TiO2	Al2O3	FeO	MgO	CaO	Na2O	K2O	Total	Comment	Comment2
156	39%	59%	1%	56.9812	0.0086	27.1872	0.2009	0.0225	8.5181	6.4671	0.22	99.6057	111-2s2-3	Large residual plag
157	40%	59%	1%	56.5996	0	26.763	0.2423	0.001	8.396	6.4254	0.228	98.6553	111-2s2-3	Large residual plag
158	41%	58%	1%	57.0236	0.0054	26.9062	0.3176	0.0303	8.4987	6.1697	0.2229	99.1745	111-2s2-3	Large residual plag
159	41%	58%	2%	57.0279	0.0287	26.8149	0.287	0.0185	8.4698	6.1303	0.2966	99.0738	111-2s2-3	Large residual plag
160	39%	59%	1%	56.9378	0.001	26.8146	0.3561	0.0263	8.4544	6.4994	0.2047	99.2943	111-2s2-3	Large residual plag
161	40%	59%	1%	56.7927	0.0144	26.9214	0.3952	0.0253	8.6635	6.5223	0.2418	99.5767	111-2s2-3	Large residual plag
163	40%	58%	2%	56.8259	0	26.9115	0.3637	0.0057	8.6025	6.4012	0.3271	99.4377	111-2s2-3	Large residual plag
164	40%	59%	2%	57.0436	0.0157	26.7681	0.5799	0.0313	8.5938	6.4453	0.326	99.8037	111-2s2-3	Large residual plag
165	39%	59%	2%	57.3455	0.0236	26.86	0.3731	0.0072	8.4494	6.4452	0.3299	99.834	111-2s2-3	Large residual plag
166	39%	60%	1%	57.053	0	26.9505	0.368	0.0095	8.4688	6.5377	0.2401	99.6277	111-2s2-3	Large residual plag
167	39%	59%	1%	57.0934	0.008	26.8057	0.3494	0.0163	8.4556	6.5224	0.2627	99.5136	111-2s2-3	Large residual plag
168	39%	59%	1%	57.0814	0	27.0701	0.3833	0.0164	8.4555	6.4493	0.2414	99.6975	111-2s2-3	Large residual plag
169	39%	60%	1%	56.9984	0	26.9191	0.2929	0.0061	8.3961	6.4976	0.2571	99.3674	111-2s2-3	Large residual plag
170	40%	58%	2%	56.7179	0.0019	26.9771	0.3436	0.0134	8.4477	6.3117	0.3778	99.1912	111-2s2-3	Large residual plag
171	40%	58%	2%	57.1834	0.0137	26.7027	0.3626	0.0217	8.4969	6.1869	0.3607	99.3287	111-2s2-3	Large residual plag
172	39%	59%	2%	57.4849	0.0284	26.7109	0.4458	0	8.4404	6.3995	0.2896	99.7995	111-2s2-3	Large residual plag
173	40%	58%	3%	56.6894	0.014	26.5785	0.3861	0.0193	8.4628	6.3002	0.4582	98.9086	111-2s2-3	Large residual plag
Average	40%	59%	2%											
Stdev	1%	1%	0%											

Table A28 EPMA results of the left residual plagioclase. Refer to Figure A3 for targets.

Sample 111-2 Residual Plagioclase (left)														
No.	XAN	XAB	XOR	SiO2	TiO2	Al2O3	FeO	MgO	CaO	Na2O	K2O	Total	Comment	Comment2
191	43%	55%	2%	55.8038	0.0444	27.7347	0.1963	0.0173	9.1866	5.9887	0.2769	99.2488	Line 1 111-2s2-3line1	Large residual plag
192	46%	53%	1%	55.1581	0.0233	28.0364	0.22	0.0055	9.7936	5.8125	0.2576	99.3071	Line 2 111-2s2-3line1	Large residual plag
193	40%	58%	2%	57.0299	0.0243	27.1625	0.2223	0	8.6515	6.3495	0.3626	99.8027	Line 3 111-2s2-3line1	Large residual plag
194	35%	56%	8%	56.7452	0.0198	26.0636	1.0243	0.1751	7.4964	6.1624	1.5063	99.1932	Line 4 111-2s2-3line1	Large residual plag
196	39%	59%	3%	57.2562	0.0032	26.8582	0.1961	0.0326	8.3184	6.3457	0.4716	99.4821	Line 6 111-2s2-3line1	Large residual plag
197	39%	58%	3%	57.1492	0.0006	26.9119	0.2332	0.0245	8.508	6.4217	0.4743	99.7235	Line 7 111-2s2-3line1	Large residual plag
198	39%	58%	3%	57.2345	0.0006	26.6928	0.2129	0.0101	8.1643	6.1463	0.5293	98.9909	Line 8 111-2s2-3line1	Large residual plag
199	39%	59%	2%	57.4832	0.0147	26.5654	0.213	0.0021	8.2677	6.4546	0.3827	99.3835	Line 9 111-2s2-3line1	Large residual plag
200	39%	58%	3%	57.3747	0	26.7903	0.1856	0.0226	8.3577	6.2144	0.5652	99.5106	Line 10 111-2s2-3line1	Large residual plag
201	40%	58%	2%	57.3097	0.023	26.7649	0.2215	0.0133	8.4035	6.2446	0.3939	99.3745	Line 11 111-2s2-3line1	Large residual plag
204	39%	58%	3%	56.6154	0.0051	26.5703	0.2561	0.0448	8.1621	6.2399	0.54	98.4337	Line 14 111-2s2-3line1	Large residual plag
205	41%	54%	6%	56.7589	0.0019	26.661	0.2411	0.0397	8.1607	5.5728	0.969	98.4052	Line 15 111-2s2-3line1	Large residual plag
206	39%	59%	2%	56.783	0.0415	26.9096	0.3412	0.0193	8.4434	6.4495	0.2969	99.2844	Line 16 111-2s2-3line1	Large residual plag
207	40%	57%	3%	56.8143	0	26.7415	0.2957	0.0142	8.3312	6.0164	0.4752	98.6886	Line 17 111-2s2-3line1	Large residual plag
208	40%	58%	2%	56.2672	0.014	26.5309	0.2562	0.0284	8.2901	6.3618	0.3108	98.0595	Line 18 111-2s2-3line1	Large residual plag
209	40%	58%	2%	57.1	0.0288	26.706	0.2294	0.005	8.3078	6.1846	0.2714	98.8331	Line 19 111-2s2-3line1	Large residual plag
210	39%	59%	2%	57.1434	0	26.8529	0.2758	0.0239	8.2878	6.4202	0.3987	99.4027	Line 20 111-2s2-3line1	Large residual plag
211	39%	58%	4%	57.1847	0	26.726	0.2946	0.0134	8.2683	6.2548	0.6463	99.3882	Line 21 111-2s2-3line1	Large residual plag
212	37%	62%	1%	57.4934	0	26.5822	0.2535	0.019	7.9266	6.783	0.2563	99.3141	Line 22 111-2s2-3line1	Large residual plag
213	38%	59%	3%	57.2557	0.0208	26.7987	0.2973	0.0138	8.1824	6.4019	0.4799	99.4505	Line 23 111-2s2-3line1	Large residual plag
214	40%	58%	2%	57.0425	0.0137	26.61	0.347	0.0127	8.4169	6.3075	0.3131	99.0635	Line 24 111-2s2-3line1	Large residual plag
215	38%	59%	2%	56.8602	0	26.6299	0.347	0.0213	8.0411	6.4218	0.4049	98.7262	Line 25 111-2s2-3line1	Large residual plag
216	39%	58%	2%	57.1281	0	26.742	0.3604	0.025	8.4868	6.4201	0.4437	99.6062	Line 26 111-2s2-3line1	Large residual plag
217	38%	59%	4%	57.2129	0.0288	26.1931	0.2578	0.0269	8.0093	6.4169	0.6285	98.7743	Line 27 111-2s2-3line1	Large residual plag
218	39%	58%	3%	57.248	0.0029	26.5652	0.3538	0.0057	8.3265	6.241	0.4969	99.2401	Line 28 111-2s2-3line1	Large residual plag
219	39%	58%	2%	57.5318	0.0144	26.4712	0.3002	0.0283	8.1722	6.1973	0.4367	99.1521	Line 29 111-2s2-3line1	Large residual plag
220	39%	58%	3%	57.1408	0.0358	26.3893	0.281	0.0152	8.2483	6.3325	0.5179	98.9608	Line 30 111-2s2-3line1	Large residual plag
221	39%	59%	2%	56.8715	0.0201	26.8812	0.5915	0.0132	8.451	6.3916	0.3956	99.6158	Line 31 111-2s2-3line1	Large residual plag
222	39%	59%	3%	57.4022	0.0029	26.7167	0.2768	0.0022	8.3955	6.4173	0.4617	99.6754	Line 32 111-2s2-3line1	Large residual plag
223	39%	58%	3%	56.6085	0.0256	26.6716	0.2614	0.0149	8.2445	6.3344	0.6087	98.7697	Line 33 111-2s2-3line1	Large residual plag
224	40%	58%	2%	56.8192	0.0288	26.9496	0.2834	0.0137	8.4965	6.2818	0.3899	99.263	Line 34 111-2s2-3line1	Large residual plag
225	40%	58%	1%	56.7867	0.0355	27.0785	0.2087	0.013	8.5541	6.2644	0.2501	99.1911	Line 35 111-2s2-3line1	Large residual plag
Average	39%	58%	3%											
Stdev	2%	2%	1%											

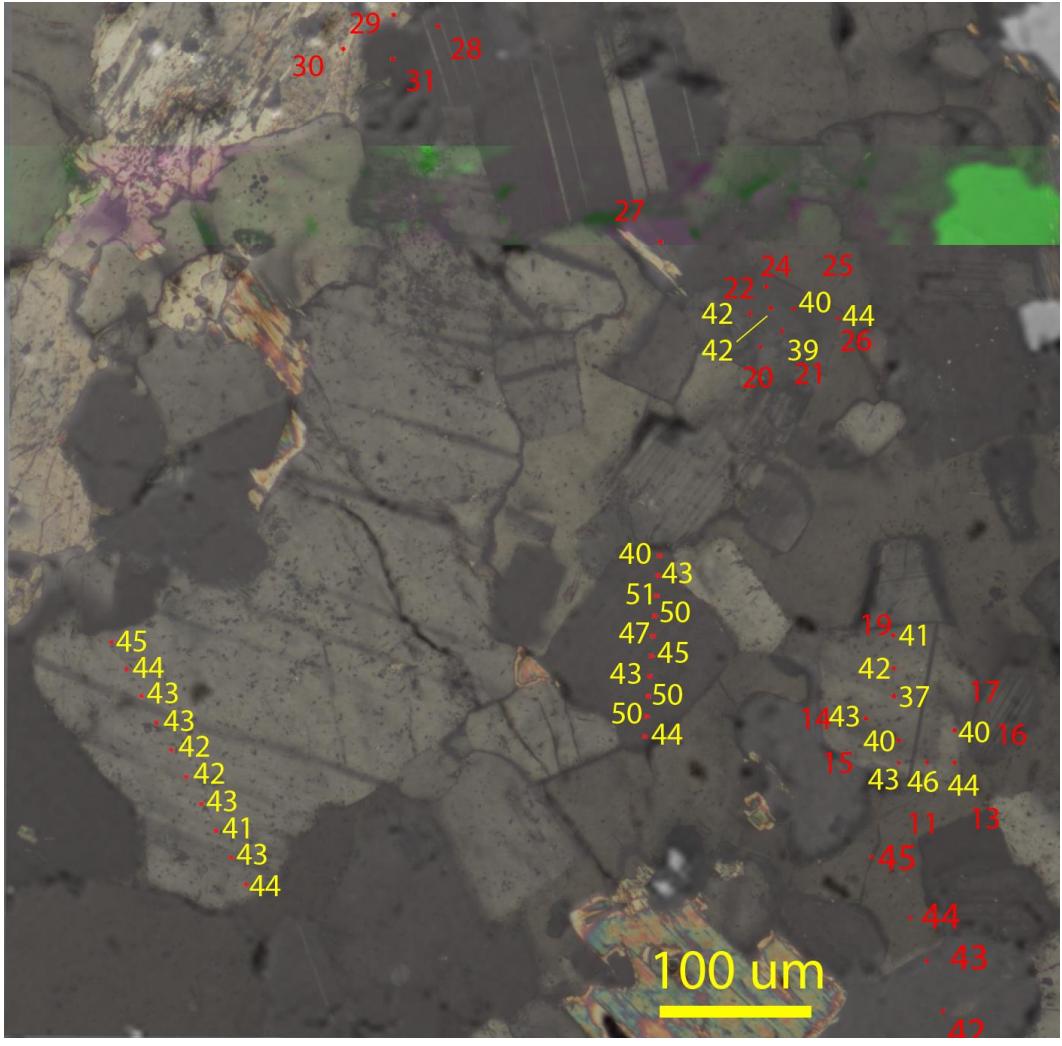


Figure A4 Sample 111-2. SEM-BSE image with photomicrograph underlay of LPP. Rod dots indicate EPMA targets. Red numbers indicate sample run numbers. Yellow numbers indicate An % content of plagioclase. Red dots with no values are not plagioclase. Refer to tables A29-32 for corresponding EPMA analysis.

Table A29 EPMA results of the middle LPP plagioclase. Refer to Figure A4 for targets.

Sample 111-2 LPP Plagioclase (middle)														
No.	An%	Ab%	Or%	SiO2	TiO2	Al2O3	FeO	MgO	CaO	Na2O	K2O	Total	Comment	Comment2
1	40%	58%	1%	58.75	0.01	26.57	0.16	0.01	8.10	5.81	0.20	99.62	Line 1 111-2-lpp1	Euhedral Plag 1
2	43%	55%	1%	57.43	0.03	27.08	0.15	0.02	8.86	5.67	0.26	99.50	Line 2 111-2-lpp1	Euhedral Plag 1
3	51%	48%	1%	55.76	0.00	28.33	0.22	0.01	10.35	4.96	0.23	99.86	Line 3 111-2-lpp1	Euhedral Plag 1
4	50%	49%	1%	56.24	0.00	28.13	0.20	0.00	10.21	5.05	0.23	100.05	Line 4 111-2-lpp1	Euhedral Plag 1
5	47%	51%	2%	56.74	0.00	27.18	0.18	0.01	9.51	5.22	0.25	99.08	Line 5 111-2-lpp1	Euhedral Plag 1
6	45%	53%	1%	58.35	0.01	27.16	0.15	0.00	9.02	5.28	0.24	100.22	Line 6 111-2-lpp1	Euhedral Plag 1
7	43%	56%	2%	59.06	0.02	26.95	0.16	0.00	8.64	5.47	0.26	100.57	Line 7 111-2-lpp1	Euhedral Plag 1
8	50%	49%	1%	56.17	0.00	28.13	0.21	0.00	10.36	5.17	0.16	100.20	Line 8 111-2-lpp1	Euhedral Plag 1
9	50%	49%	1%	57.31	0.01	27.47	0.19	0.01	9.56	4.69	0.23	99.47	Line 9 111-2-lpp1	Euhedral Plag 1
10	44%	54%	2%	57.83	0.01	26.96	0.20	0.01	8.89	5.47	0.27	99.64	Line 10 111-2-lpp1	Euhedral Plag 1
Average	46%	52%	1%											
Stdev	4%	4%	0%											

Table A30 EPMA results of the top LPP plagioclase. Refer to Figure A4 for targets.

Large Pseudomelt Pocket Plagioclase (top)														
No.	An%	Ab%	Or%	SiO2	TiO2	Al2O3	FeO	MgO	CaO	Na2O	K2O	Total	Comment	Comment2
21	41%	58%	1%	60.10	0.02	26.48	0.21	0.01	8.24	5.62	0.22	100.89	111-2-lpp3pl	Euhedral Plag 3 optically zoned
22	46%	52%	2%	58.64	0.02	26.52	0.24	0.01	8.55	4.85	0.29	99.12	111-2-lpp3pl	Euhedral Plag 3 optically zoned
23	46%	52%	2%	58.40	0.03	26.84	0.21	0.00	8.99	4.98	0.29	99.74	111-2-lpp3pl	Euhedral Plag 3 optically zoned
24	49%	50%	1%	56.96	0.03	28.00	0.15	0.00	9.86	5.06	0.22	100.28	111-2-lpp3pl	Euhedral Plag 3 optically zoned
25	51%	47%	1%	56.59	0.00	28.20	0.22	0.00	10.42	4.80	0.24	100.47	111-2-lpp3pl	Euhedral Plag 3 optically zoned
26	46%	53%	1%	58.78	0.03	26.99	0.18	0.00	9.07	5.14	0.25	100.45	111-2-lpp3pl	Euhedral Plag 3 optically zoned
Average	46%	52%	2%											
Stdev	3%	3%	0%											

Table A31 EPMA results of the right LPP plagioclase. Refer to Figure A4 for targets.

Large Pseudomelt Pocket Plagioclase 2 (right)														
No.	An%	Ab%	Or%	SiO2	TiO2	Al2O3	FeO	MgO	CaO	Na2O	K2O	Total	Comment	Comment2
11	49%	50%	1%	56.21	0.00	28.14	0.17	0.01	9.85	5.00	0.20	99.56	Line 10 111-2-lpp2-1	Euhedral Plag 2 optically zoned
12	49%	50%	1%	56.46	0.03	27.73	0.19	0.00	10.05	5.25	0.19	99.90	Line 10 111-2-lpp2-2	Euhedral Plag 2 optically zoned
13	47%	52%	1%	56.95	0.03	27.58	0.17	0.01	9.58	5.31	0.22	99.85	Line 10 111-2-lpp2-3	Euhedral Plag 2 optically zoned
14	52%	46%	1%	55.38	0.00	28.26	0.25	0.01	10.63	4.81	0.24	99.57	Line 10 111-2-lpp2-4	Euhedral Plag 2 optically zoned
15	48%	50%	1%	57.11	0.03	27.79	0.25	0.02	9.69	5.00	0.24	100.12	Line 10 111-2-lpp2-5	Euhedral Plag 2 optically zoned
16	51%	48%	1%	56.18	0.03	28.40	0.23	0.00	10.54	4.93	0.22	100.52	Line 10 111-2-lpp2-6	Euhedral Plag 2 optically zoned
17	48%	50%	1%	56.39	0.05	28.05	0.23	0.02	10.16	5.31	0.26	100.46	Line 10 111-2-lpp2-7	Euhedral Plag 2 optically zoned
18	48%	51%	2%	57.36	0.00	27.78	0.21	0.00	9.77	5.14	0.30	100.55	Line 10 111-2-lpp2-8	Euhedral Plag 2 optically zoned
19	42%	56%	2%	58.85	0.03	27.23	0.19	0.01	8.85	5.79	0.31	101.25	Line 10 111-2-lpp2-9	Euhedral Plag 2 optically zoned
Average	48%	50%	1%											
Stdev	3%	3%	0%											

Table A32 EPMA results of the left residual plagioclase. Refer to Figure A4 for targets.

Large Pseudomelt Pocket Residual Plagioclase (left)														
No.	%An	%Ab	%Or	SiO2	TiO2	Al2O3	FeO	MgO	CaO	Na2O	K2O	Total	Comment	Comment2
32	44%	54%	1%	58.93	0.02	27.01	0.15	0.00	8.65	5.22	0.23	100.22	Line 1 111-2-lpp5pl	Residual Plag
33	43%	56%	2%	59.23	0.00	26.77	0.18	0.00	8.28	5.32	0.28	100.07	Line 2 111-2-lpp5pl	Residual Plag
34	41%	57%	2%	58.81	0.00	26.91	0.19	0.00	8.30	5.70	0.27	100.19	Line 3 111-2-lpp5pl	Residual Plag
35	43%	56%	1%	60.25	0.01	26.49	0.15	0.00	8.19	5.11	0.14	100.34	Line 4 111-2-lpp5pl	Residual Plag
36	42%	57%	2%	58.90	0.00	26.49	0.20	0.01	8.27	5.56	0.29	99.71	Line 5 111-2-lpp5pl	Residual Plag
37	42%	55%	2%	59.57	0.01	26.55	0.21	0.01	8.13	5.23	0.39	100.09	Line 6 111-2-lpp5pl	Residual Plag
38	43%	56%	1%	59.19	0.00	26.66	0.18	0.00	8.48	5.39	0.19	100.10	Line 7 111-2-lpp5pl	Residual Plag
39	43%	55%	2%	59.81	0.03	26.63	0.17	0.02	8.47	5.25	0.31	100.69	Line 8 111-2-lpp5pl	Residual Plag
40	44%	55%	2%	59.32	0.01	26.72	0.15	0.00	8.51	5.24	0.29	100.25	Line 9 111-2-lpp5pl	Residual Plag
41	45%	54%	1%	59.05	0.01	26.63	0.16	0.00	8.58	5.01	0.17	99.62	Line 10 111-2-lpp5pl	Residual Plag
Average	43%	55%	2%											
Stdev	1%	1%	0%											

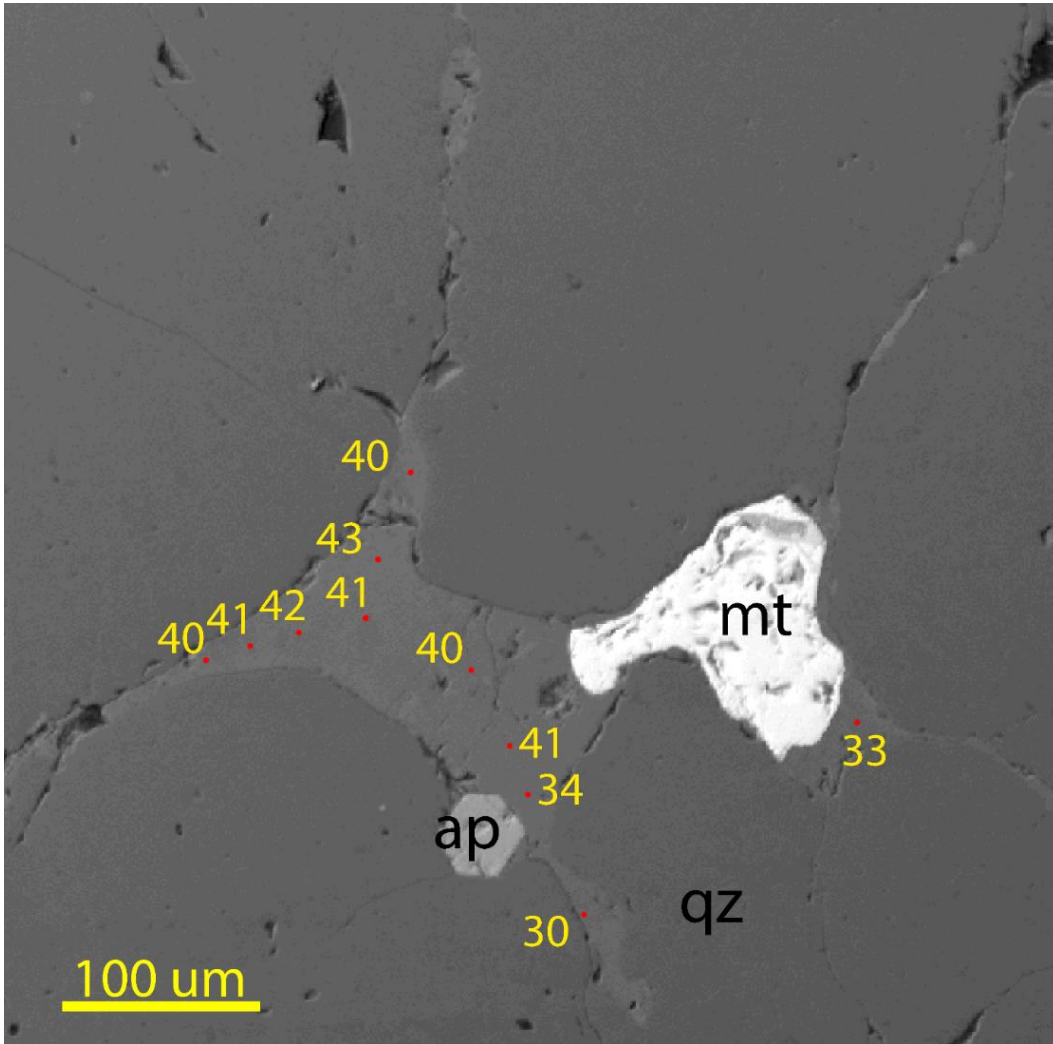


Figure A5 Sample 111-4a. SEM-BSE image of a melt film. Rod dots indicate EPMA targets. Yellow numbers indicate An % content of plagioclase. Refer to table A33 for corresponding EPMA analysis.

Table A33 EPMA results of melt film plagioclase. Refer to Figure A5 for targets.

Sample 111-4a Melt Film Plagioclase														
No.	An%	Ab%	Or%	SiO2	TiO2	Al2O3	FeO	MgO	CaO	Na2O	K2O	Total	Comment	Comment2
10	40%	59%	1%	57.641	0	26.9382	0.1767	0.033	8.579	6.4073	0.2489	100.024	111-4a-mf-1	Melt Film
11	43%	56%	2%	57.1516	0	27.3259	0.2073	0	9.0738	5.9744	0.2776	100.0106	111-4a-mf-2	Melt Film
12	41%	58%	2%	57.6705	0	27.1213	0.2338	0.0208	8.8491	6.2378	0.3221	100.4553	111-4a-mf-3	Melt Film
13	42%	56%	2%	57.2192	0.0301	26.7542	0.2068	0	8.7182	5.9445	0.3432	99.2163	111-4a-mf-4	Melt Film
14	41%	57%	2%	57.2775	0	27.1747	0.2155	0.0177	8.8294	6.144	0.2712	99.9301	111-4a-mf-5	Melt Film
15	41%	58%	1%	56.6354	0	26.8435	0.1388	0.0086	8.6724	6.2515	0.2368	98.787	111-4a-mf-6	Melt Film
16	40%	53%	8%	57.2568	0.0206	26.4413	0.2221	0.0157	8.1515	5.587	1.3113	99.0064	111-4a-mf-7	Melt Film
17	41%	58%	1%	57.1924	0.0127	26.8585	0.3009	0.0129	8.7073	6.2367	0.2565	99.578	111-4a-mf-8	Melt Film
18	34%	65%	1%	59.1225	0.0006	25.9685	0.2352	0.0019	7.4472	7.0582	0.2495	100.0835	111-4a-mf-9	Melt Film
19	30%	68%	2%	60.4549	0.0278	24.7379	0.1869	0	6.2695	7.0994	0.3248	99.1012	111-4a-mf-10	Melt Film
20	33%	66%	1%	59.3239	0	25.2041	0.4712	0.0032	7.0691	7.0682	0.2462	99.386	111-4a-mf-11	Melt Film
Average	39%	59%	2%											
Stdev	4%	5%	2%											

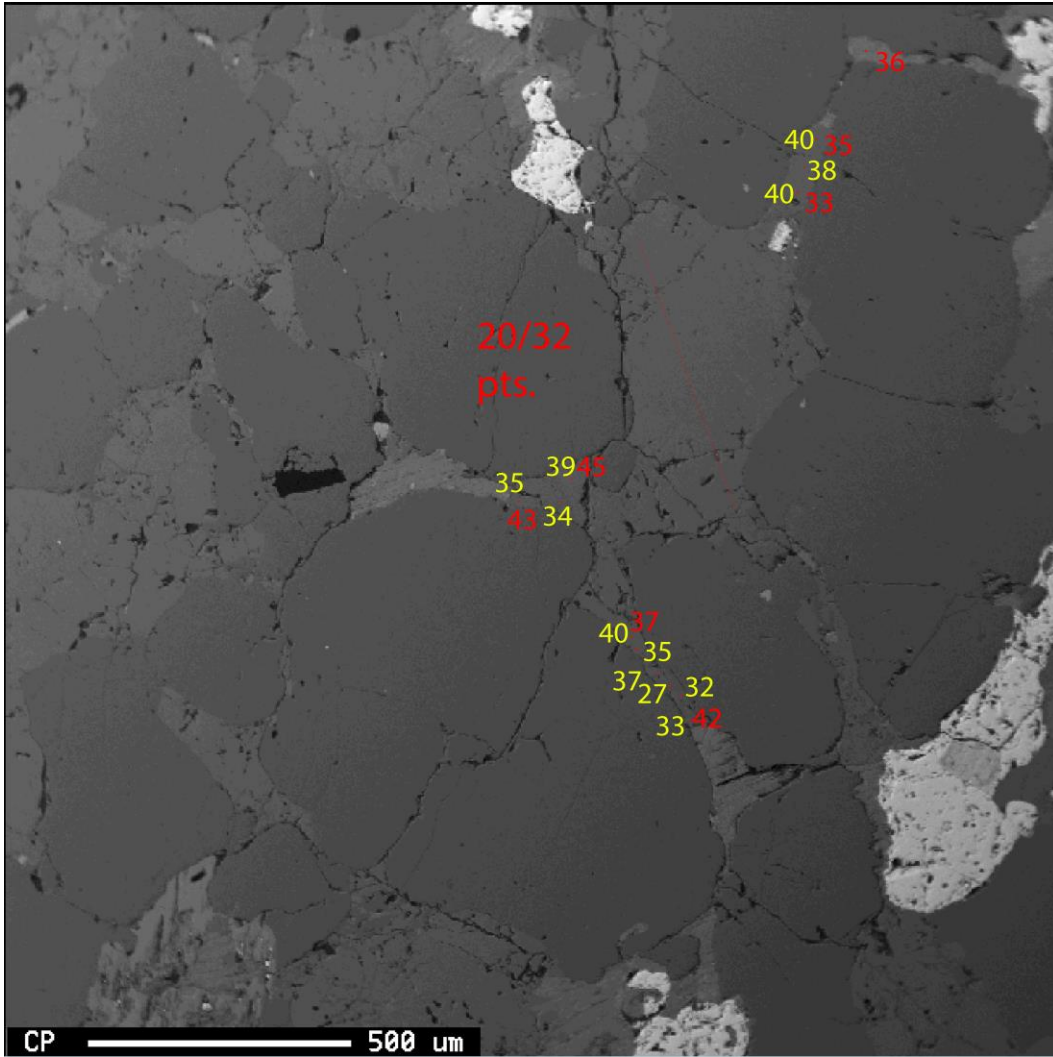


Figure A6 Sample 111-4a. SEM-BSE image of a melt films and overgrowths. Rod dots indicate EPMA targets. Red numbers indicate target number. Yellow numbers indicate An % content of plagioclase. Refer to tables A34-36 for corresponding EPMA analysis. 20/32 refers to the line information, i.e. 20 μm interval between analysis, 32 points.

Table A34 EPMA results of melt film plagioclase. Refer to Figure A6 for targets.

Sample 111-4a Melt Film Plagioclase														
No.	An%	Ab%	Or%	SiO2	TiO2	Al2O3	FeO	MgO	CaO	Na2O	K2O	Total	Comment	Comment2
53	40%	59%	2%	57.6379	0.0073	26.6343	0.205	0.0123	8.2088	6.1583	0.288	99.152	111-4a-mf2-33	Melt Film
54	38%	60%	2%	58.1582	0.0013	26.7766	0.1765	0.0096	8.1856	6.4187	0.2713	99.9979	111-4a-mf2-34	Melt Film
55	40%	58%	1%	57.8569	0.0187	26.8411	0.2283	0.0164	8.5142	6.1378	0.2458	99.8593	111-4a-mf2-35	Melt Film
57	40%	59%	2%	57.9965	0	26.7954	0.3012	0.0298	8.4421	6.2645	0.2978	100.1272	111-4a-mf2-37	Melt Film
58	35%	63%	2%	58.737	0	26.2257	0.2486	0.0071	7.512	6.6901	0.3017	99.7223	111-4a-mf2-38	Melt Film
60	27%	72%	1%	60.5462	0	24.4842	0.1423	0.0188	5.7308	7.7737	0.2307	98.9268	111-4a-mf2-40	Melt Film
61	32%	67%	2%	59.7598	0.0133	25.3781	0.2092	0.015	6.7263	7.0464	0.3054	99.4535	111-4a-mf2-41	Melt Film
62	33%	65%	2%	59.6246	0.0294	25.6751	0.2818	0.0224	7.2182	7.0457	0.2957	100.1929	111-4a-mf2-42	Melt Film
63	35%	63%	2%	58.5729	0.0057	25.8406	0.2803	0.0123	7.4633	6.7758	0.353	99.3039	111-4a-mf2=43	Melt Film
64	34%	64%	2%	58.973	0	25.8855	0.269	0.0164	7.3111	6.8596	0.4114	99.7261	111-4a-mf2=44	Melt Film
65	39%	59%	1%	57.8024	0.012	26.8123	0.2489	0.0107	8.4758	6.4043	0.258	100.0244	111-4a-mf2=45	Melt Film
Average	36%	63%	2%											
Stdev	4%	4%	0%											

Table A35 EPMA results of overgrowth plagioclase. Refer to Figure A6 for targets.

Overgrowth Plagioclase														
No.	An	Ab	Or	SiO2	TiO2	Al2O3	FeO	MgO	CaO	Na2O	K2O	Total	Comment	Comment2
42	50%	49%	1%	55.1547	0.0006	28.4196	0.2712	0.0153	10.4437	5.2044	0.2259	99.7355	Line 22 111-4mf2	Large Pl
43	51%	48%	1%	55.0145	0	28.2388	0.266	0.0075	10.8065	5.136	0.1987	99.6681	Line 23 111-4mf2	Large Pl
44	47%	52%	1%	55.9347	0.0272	28.2735	0.2427	0.0056	9.6056	5.4222	0.2326	99.7441	Line 24 111-4mf2	Large Pl
45	46%	52%	2%	56.2104	0.0092	27.6728	0.2101	0.0005	9.5877	5.444	0.2768	99.4116	Line 25 111-4mf2	Large Pl
46	43%	55%	2%	56.6373	0	27.2827	0.2357	0	9.2348	5.9912	0.277	99.6588	Line 26 111-4mf2	Large Pl
47	42%	56%	2%	57.3581	0	27.2288	0.2184	0.0082	8.9906	6.0612	0.3115	100.1767	Line 27 111-4mf2	Large Pl
48	41%	58%	2%	57.1515	0	26.0274	0.2166	0.0237	8.6882	6.3085	0.2779	98.6939	Line 28 111-4mf2	Large Pl
49	43%	56%	1%	56.755	0.0244	27.3496	0.2353	0.0028	9.1859	5.9527	0.2303	99.7361	Line 29 111-4mf2	Large Pl
50	35%	64%	2%	59.1909	0.0047	26.1987	0.1653	0.0114	7.4544	6.7937	0.3154	100.1344	Line 30 111-4mf2	Large Pl
51	34%	65%	2%	59.045	0.0281	25.3934	0.2126	0.0082	7.1906	6.9853	0.3046	99.1679	Line 31 111-4mf2	Large Pl
Average	43%	55%	1%											
Stdev	6%	6%	0%											

Table A36 EPMA results of residual plagioclase. Refer to Figure A6 for targets.

Sample 111-4a Residual Plagioclase														
No.	An%	Ab%	Or%	SiO2	TiO2	Al2O3	FeO	MgO	CaO	Na2O	K2O	Total	Comment	Comment2
21	44%	55%	1%	57.1381	0.0095	27.5177	0.2347	0.0164	8.9801	5.6587	0.21	99.7653	Line 1 111-4mf2	Large Pl
22	40%	59%	2%	57.2935	0.0092	26.7692	0.1916	0	8.4667	6.3171	0.272	99.3194	Line 2 111-4mf2	Large Pl
23	43%	55%	2%	57.8431	0.0279	26.7687	0.1945	0.0083	8.6224	5.5368	0.2619	99.2637	Line 3 111-4mf2	Large Pl
24	40%	59%	1%	57.7549	0.0215	27.1268	0.1846	0.005	8.5435	6.1915	0.2159	100.0436	Line 4 111-4mf2	Large Pl
25	41%	59%	1%	57.6344	0.0351	26.8247	0.1975	0.0016	8.6613	6.2843	0.142	99.781	Line 5 111-4mf2	Large Pl
26	40%	59%	1%	57.3759	0.0108	27.0647	0.1961	0	8.6811	6.319	0.1536	99.8013	Line 6 111-4mf2	Large Pl
27	41%	59%	1%	57.6378	0.0199	27.2044	0.1217	0.0039	8.7831	6.3156	0.1444	100.2307	Line 7 111-4mf2	Large Pl
28	43%	56%	1%	56.8604	0.037	27.7148	0.1936	0	8.861	5.8045	0.1505	99.6218	Line 8 111-4mf2	Large Pl
29	41%	58%	1%	57.3533	0.0275	27.1911	0.179	0.0046	8.7766	6.186	0.1964	99.9146	Line 9 111-4mf2	Large Pl
30	40%	58%	2%	57.8259	0.0013	26.8982	0.2464	0	8.5492	6.2294	0.2807	100.031	Line 10 111-4mf2	Large Pl
31	39%	58%	2%	57.6164	0.0136	26.7404	0.2662	0.0269	8.4906	6.3247	0.4386	99.9175	Line 11 111-4mf2	Large Pl
32	39%	59%	2%	58.1373	0.025	26.7426	0.2045	0.0086	8.1878	6.2601	0.3303	99.8963	Line 12 111-4mf2	Large Pl
33	38%	58%	4%	57.8665	0	26.7137	0.2033	0.0008	8.2145	6.2679	0.744	100.0107	Line 13 111-4mf2	Large Pl
34	40%	58%	2%	57.7981	0	26.7777	0.2545	0.0118	8.544	6.2689	0.3339	99.989	Line 14 111-4mf2	Large Pl
36	40%	58%	2%	57.7496	0.0054	26.6609	0.2405	0.0177	8.6754	6.25	0.3368	99.9363	Line 16 111-4mf2	Large Pl
37	39%	59%	2%	58.1179	0	26.7987	0.2509	0.0037	8.4707	6.2936	0.3521	100.2875	Line 17 111-4mf2	Large Pl
38	40%	58%	2%	57.8929	0.0003	26.8972	0.2439	0.0044	8.5058	6.1231	0.3319	99.9995	Line 18 111-4mf2	Large Pl
39	40%	59%	2%	57.8568	0	26.8286	0.2734	0.0049	8.571	6.2852	0.3027	100.1225	Line 19 111-4mf2	Large Pl
40	38%	58%	4%	58.2096	0.0184	26.3769	0.2454	0	7.9734	6.2333	0.7162	99.7733	Line 20 111-4mf2	Large Pl
41	41%	58%	1%	57.8151	0.007	26.7143	0.2615	0.0209	8.6211	6.1971	0.2013	99.8384	Line 21 111-4mf2	Large Pl
Average	40%	58%	2%											
Stdev	2%	1%	1%											

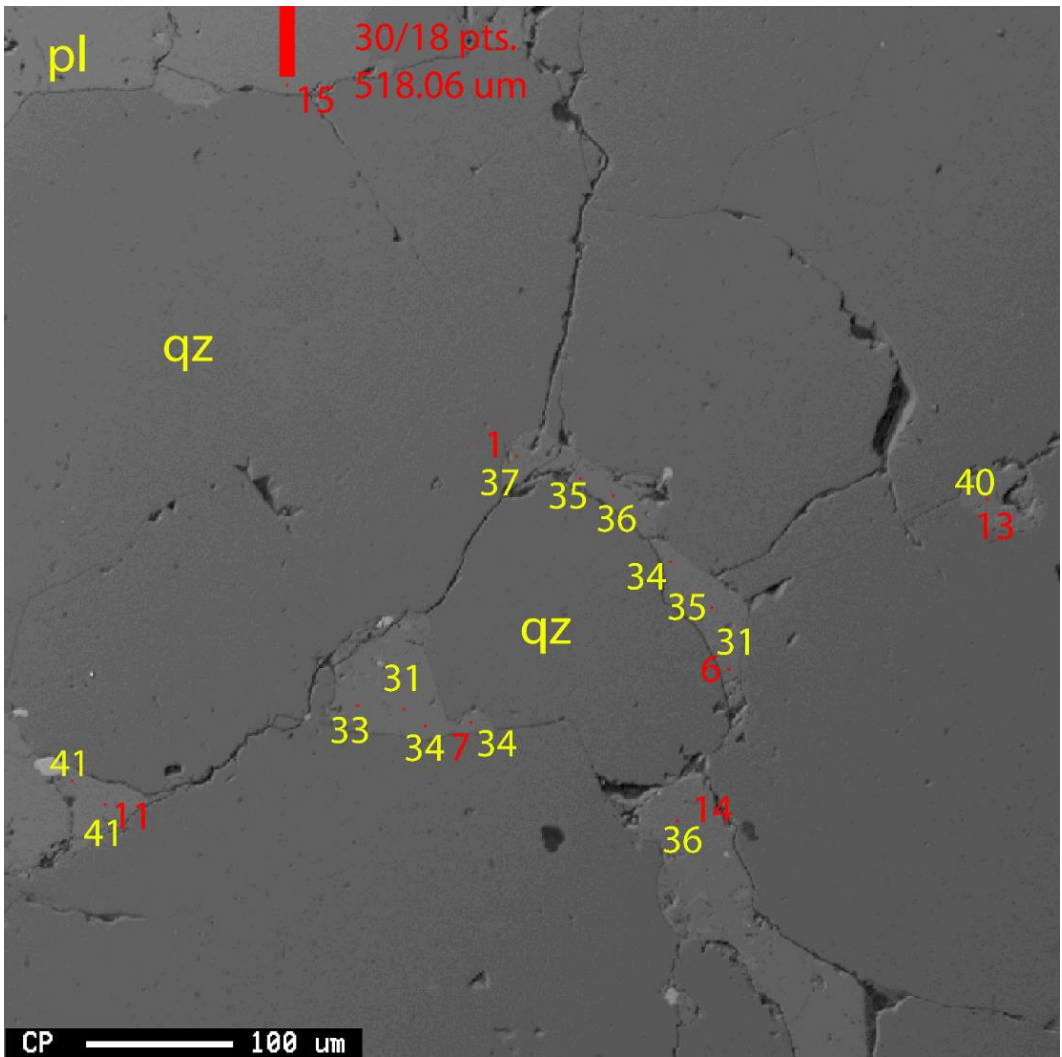


Figure A7 Sample 111-4a. SEM-BSE image of a melt films and residual. Rod dots indicate EPMA targets. Red numbers indicate target number. Yellow numbers indicate An % content of plagioclase. Red number 15 refers to the starting point of a line analysis (off picture). Refer to tables A37-38 for corresponding EPMA analysis. Qz = quartz, pl = plagioclase.

Table A37 EPMA results of melt film plagioclase. Refer to Figure A7 for targets.

Sample 111-4a Melt Film Plagioclase														
No.	An%	Ab%	Or%	SiO2	TiO2	Al2O3	FeO	MgO	CaO	Na2O	K2O	Total	Comment	Comment2
66	37%	61%	2%	57.7005	0	25.9982	0.1871	0.0228	7.6835	6.6037	0.3242	98.5201	111-4a-mf3-1	Melt Film
67	35%	64%	2%	59.1751	0.0209	26.048	0.18	0.0045	7.5465	6.898	0.2757	100.1486	111-4a-mf3-2	Melt Film
68	36%	62%	2%	58.6615	0.0066	26.1057	0.2082	0	7.8161	6.628	0.3067	99.7328	111-4a-mf3-3	Melt Film
69	34%	64%	2%	59.1492	0.0051	25.962	0.2178	0.0054	7.3516	6.8319	0.3467	99.8698	111-4a-mf3-4	Melt Film
70	35%	63%	2%	58.7012	0	26.073	0.1933	0.0094	7.512	6.8231	0.3821	99.6942	111-4a-mf3-5	Melt Film
71	31%	67%	2%	59.8428	0.0019	25.3487	0.2018	0.0068	6.7956	7.233	0.3003	99.731	111-4a-mf3-6	Melt Film
72	34%	64%	2%	59.3101	0.0108	25.8906	0.1589	0.0121	7.337	6.9114	0.3225	99.9535	111-4a-mf3-7	Melt Film
73	34%	64%	2%	59.0936	0.0152	25.7062	0.1822	0.0021	7.0949	6.647	0.3427	99.0839	111-4a-mf3-8	Melt Film
74	31%	67%	2%	59.7389	0	25.2366	0.2217	0.0103	6.6863	7.1768	0.4398	99.5105	111-4a-mf3-9	Melt Film
75	33%	65%	2%	59.3256	0	25.703	0.1985	0	7.0297	7.0068	0.334	99.5976	111-4a-mf3-10	Melt Film
76	41%	57%	2%	57.5272	0.0317	27.084	0.2303	0.0106	8.3871	5.8807	0.3262	99.4779	111-4a-mf3-11	Melt Film
77	41%	57%	2%	57.5601	0.019	27.1664	0.2331	0.0102	8.9089	6.1753	0.2789	100.3518	111-4a-mf3-12	Melt Film
78	40%	58%	2%	57.2129	0.0085	26.845	0.187	0.0106	8.3693	6.1124	0.359	99.1048	111-4a-mf3-13	Melt Film
79	36%	62%	2%	58.6521	0	26.041	0.2258	0.0138	7.5871	6.4873	0.3385	99.3456	111-4a-mf3-14	Melt Film
Average	36%	63%	2%											
Stdev	3%	3%	0%											

Table A38 EPMA results of residual plagioclase. Refer to Figure A7 for targets.

Sample 111-4a Residual Plagioclase														
No.	An%	Ab%	Or%	SiO2	TiO2	Al2O3	FeO	MgO	CaO	Na2O	K2O	Total	Comment	Comment2
80	43%	56%	1%	56.9211	0.0237	27.5675	0.2395	0	9.1226	5.8987	0.2536	100.0266	Line 1 111-4amf3pl	residual Plag
81	45%	53%	2%	56.4161	0.0127	27.7069	0.2501	0.0194	9.6504	5.7319	0.2705	100.058	Line 2 111-4amf3pl	residual Plag
82	48%	50%	1%	55.7074	0.0193	28.1415	0.2868	0.0131	10.2808	5.379	0.2592	100.0871	Line 3 111-4amf3pl	residual Plag
83	39%	59%	2%	57.4273	0	26.3453	0.576	0.1093	7.9165	6.1108	0.4265	98.9118	Line 4 111-4amf3pl	residual Plag
84	41%	57%	3%	57.6065	0.0127	26.3469	0.2443	0.0088	8.433	6.01	0.4474	99.1097	Line 5 111-4amf3pl	residual Plag
85	38%	58%	4%	58.0445	0	26.6029	0.2516	0.0154	8.2073	6.179	0.7103	100.0109	Line 6 111-4amf3pl	residual Plag
87	37%	57%	6%	58.208	0	26.3996	0.2296	0.0139	7.7571	6.0659	0.9848	99.659	Line 8 111-4amf3pl	residual Plag
88	39%	56%	5%	57.9482	0.0123	26.3168	0.2628	0.0008	8.103	5.9074	0.8079	99.3592	Line 9 111-4amf3pl	residual Plag
90	40%	58%	2%	57.8779	0.0224	26.4298	0.3056	0.0156	8.3432	6.0706	0.3204	99.3856	Line 11 111-4amf3pl	residual Plag
91	39%	59%	2%	58.0349	0	26.7791	0.2557	0	8.3971	6.2987	0.3933	100.1588	Line 12 111-4amf3pl	residual Plag
92	40%	58%	1%	57.4529	0	26.7583	0.2598	0.0031	8.5781	6.2548	0.2191	99.5262	Line 13 111-4amf3pl	residual Plag
94	40%	59%	1%	57.8354	0	26.9075	0.1857	0.0158	8.4803	6.3442	0.201	99.97	Line 15 111-4amf3pl	residual Plag
96	42%	56%	2%	58.0015	0	26.5936	0.2303	0.0121	8.4316	5.6334	0.3212	99.2237	Line 17 111-4amf3pl	residual Plag
97	38%	57%	5%	57.6996	0.0317	26.1367	0.2645	0.0115	7.9565	6.1961	0.9143	99.211	Line 18 111-4amf3pl	residual Plag
Average	41%	57%	3%											
Stdev	3%	2%	2%											

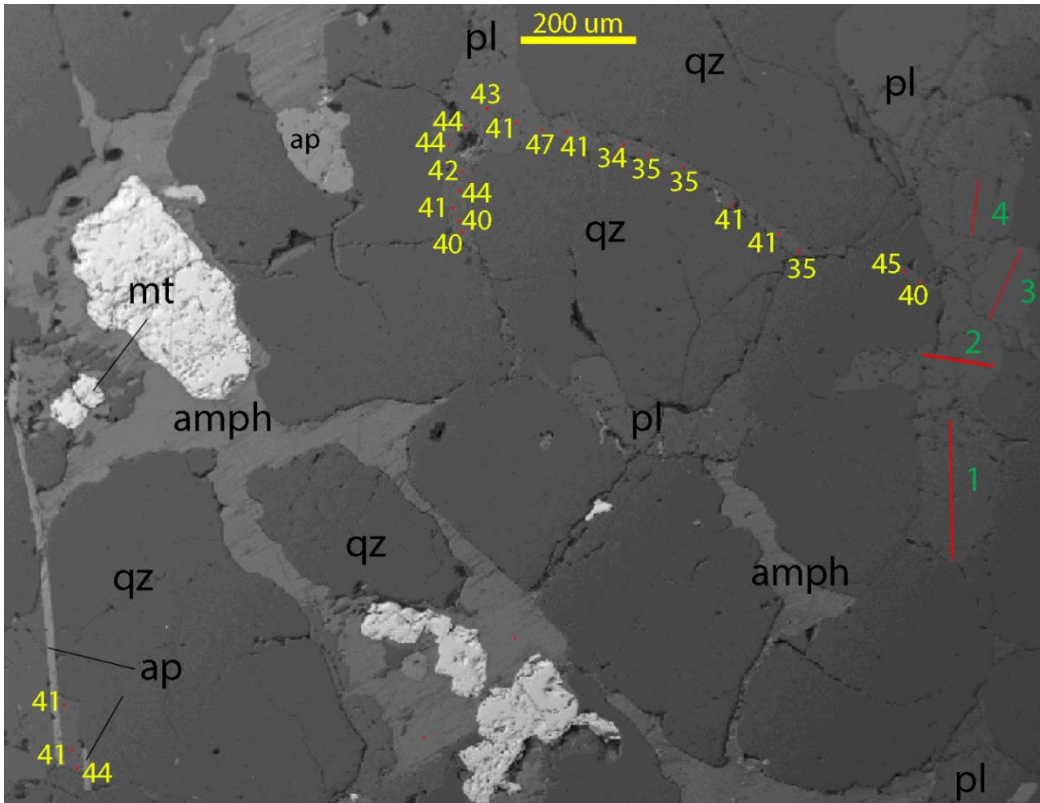


Figure A8 Sample 111-4a. SEM-BSE image of a melt films and string of beads plagioclase. Rod dots indicate EPMA targets. Yellow numbers indicate An % content of plagioclase. Refer to tables A39-40 for corresponding EPMA analysis. Red lines with corresponding green numbers indicate line scans on Table A40. Qz = quartz, pl = plagioclase, amph = amphibole, mt = magnetite, ap = apatite.

Table A39 EPMA results of melt film plagioclase. Refer to Figure A8 for targets.

Sample 111-4a Melt Film Plagioclase														
No.	An%	Ab%	Or%	SiO2	TiO2	Al2O3	FeO	MgO	CaO	Na2O	K2O	Total	Comment	Comment2
100	41%	58%	1%	57.4027	0.0522	27.0978	0.1938	0.0114	8.7626	6.1812	0.2417	99.9435	111-4amf5-1	Melt Film
102	41%	57%	1%	57.5367	0.0266	27.2746	0.1935	0	8.8652	6.1427	0.2693	100.3085	111-4amf5-3	Melt Film
103	44%	55%	1%	56.9644	0	27.7138	0.1702	0.0144	9.3157	5.8513	0.2297	100.2594	111-4amf5-4	Melt Film
106	40%	58%	2%	57.8015	0.0013	26.8276	0.2028	0.0142	8.4406	6.1662	0.318	99.7722	111-4amf5-7	Melt Film
107	40%	58%	2%	57.8564	0.018	27.0827	0.1822	0.0207	8.6491	6.24	0.303	100.3521	111-4amf5-8	Melt Film
108	41%	58%	1%	57.2436	0.0009	27.2345	0.1956	0.0042	8.6581	6.2243	0.2662	99.8274	111-4amf5-9	Melt Film
109	44%	55%	1%	57.2785	0.0291	27.2027	0.2024	0.0121	8.8228	5.6241	0.2491	99.4208	111-4amf5-10	Melt Film
110	42%	57%	2%	56.4995	0.0149	27.274	0.2117	0.0005	8.6844	5.9843	0.2716	98.941	111-4amf5-11	Melt Film
111	44%	51%	5%	56.3601	0.0317	27.6285	0.1935	0.0199	9.1723	5.358	0.9322	99.6963	111-4amf5-12	Melt Film
112	44%	55%	2%	56.1777	0.0424	27.4251	0.2295	0.0347	9.1151	5.8018	0.2871	99.1135	111-4amf5-13	Melt Film
113	43%	55%	2%	57.2063	0.0117	27.2992	0.2116	0.009	8.934	5.7749	0.3072	99.754	111-4amf5-14	Melt Film
114	41%	57%	2%	57.1064	0.0218	26.9662	0.1873	0.0113	8.5713	6.0078	0.2992	99.1714	111-4amf5-15	Melt Film
115	47%	52%	1%	55.9263	0.0307	27.8707	0.2099	0.0058	9.8509	5.5409	0.2556	99.6908	111-4amf5-16	Melt Film
116	41%	58%	1%	57.3738	0.0003	26.868	0.2183	0.0116	8.6778	6.1293	0.2193	99.4985	111-4amf5-17	Melt Film
117	34%	64%	2%	58.8141	0.0085	26.016	0.1843	0.0068	7.3567	6.8792	0.3173	99.5829	111-4amf5-18	Melt Film
118	35%	62%	2%	58.5763	0.0164	25.7213	0.2004	0.0039	7.4591	6.6592	0.3862	99.0229	111-4amf5-19	Melt Film
119	35%	63%	2%	59.0418	0	25.7509	0.2297	0.0016	7.3957	6.733	0.3789	99.5317	111-4amf5-20	Melt Film
120	41%	57%	2%	57.1223	0.0364	27.2668	0.2258	0.0149	8.6527	6.0781	0.3011	99.6982	111-4amf5-21	Melt Film
121	41%	58%	1%	57.5798	0.0089	27.0219	0.221	0.0088	8.8523	6.1863	0.2545	100.1334	111-4amf5-22	Melt Film
122	35%	63%	2%	59.1917	0.0127	25.8663	0.2533	0.0299	7.4798	6.6698	0.3585	99.8621	111-4amf5-23	Melt Film
123	40%	58%	2%	57.1385	0.0193	27.08	0.1907	0.0146	8.4353	6.1761	0.2844	99.339	111-4amf5-24	Melt Film
124	45%	54%	2%	55.4203	0.0393	27.1971	0.2353	0.0251	9.1411	5.7293	0.3014	98.089	111-4amf5-25	Melt Film
Average	41%	57%	2%											
Stdev	3%	3%	1%											

Table A40 EPMA results of string of beads plagioclase. Refer to Figure A8 for targets. Line number refers to the green number in Figure A8.

111-4a String of Beads Plagioclase														
No.	An%	Ab%	Or%	SiO2	TiO2	Al2O3	FeO	MgO	CaO	Na2O	K2O	Total	Comment	Comment2
Line 1														
125	43%	56%	1%	56.8046	0.0282	27.5705	0.2394	0.0107	8.957	5.9397	0.2277	99.7779	Line 1 111-4a-mf5-ln1	string of beads
126	40%	57%	3%	57.5123	0.0082	26.8024	0.2211	0.0192	8.4156	6.003	0.5474	99.5293	Line 2 111-4a-mf5-ln1	string of beads
127	41%	57%	2%	57.3055	0.0133	26.981	0.2379	0.0288	8.6372	6.0621	0.3589	99.6248	Line 3 111-4a-mf5-ln1	string of beads
128	41%	57%	3%	57.7749	0.012	26.3949	0.2123	0.0065	8.6763	6.093	0.4906	99.6606	Line 4 111-4a-mf5-ln1	string of beads
131	40%	58%	2%	57.5747	0	26.6726	0.2222	0	8.2078	6.0588	0.4023	99.1385	Line 7 111-4a-mf5-ln1	string of beads
132	40%	58%	2%	57.4427	0	26.7376	0.2416	0.0069	8.5682	6.2347	0.4175	99.6493	Line 8 111-4a-mf5-ln1	string of beads
133	41%	58%	1%	57.3632	0.0184	27.0542	0.2233	0.0108	8.6788	6.1597	0.2525	99.761	Line 9 111-4a-mf5-ln1	string of beads
134	40%	58%	1%	57.676	0.0032	27.0857	0.2079	0.0241	8.4379	6.0924	0.2444	99.7717	Line 10 111-4a-mf5-ln1	string of beads
Line 2														
136	42%	57%	2%	57.3511	0	27.0691	0.2372	0.0124	8.6917	5.975	0.2747	99.6113	Line 2 111-4a-mf5-ln2	string of beads
137	41%	57%	2%	57.5454	0	27.1739	0.2635	0.0158	8.9774	6.1586	0.3028	100.4374	Line 3 111-4a-mf5-ln2	string of beads
138	41%	57%	2%	57.5083	0.0174	26.999	0.2498	0.0098	8.6451	6.0665	0.3337	99.8297	Line 4 111-4a-mf5-ln2	string of beads
139	37%	61%	2%	58.3165	0.0152	26.7903	0.2255	0.0045	7.7866	6.326	0.4032	99.8679	Line 5 111-4a-mf5-ln2	string of beads
142	42%	57%	2%	57.1364	0.0304	26.7166	0.223	0.0019	8.6206	5.966	0.3062	99.0012	Line 8 111-4a-mf5-ln2	string of beads
143	39%	54%	6%	57.698	0.0269	26.5265	0.2184	0	8.2611	5.7264	1.1214	99.5788	Line 9 111-4a-mf5-ln2	string of beads
144	46%	53%	1%	55.7863	0	27.9113	0.251	0	9.5767	5.6196	0.2012	99.3462	Line 10 111-4a-mf5-ln2	string of beads
Line 3														
145	37%	61%	2%	58.4494	0.006	26.3178	0.2257	0.0202	8.0792	6.5265	0.3357	99.9606	Line 1 111-4a-mf5-ln3	string of beads
146	43%	56%	2%	56.8694	0.0009	27.1203	0.248	0.0173	8.9654	5.8991	0.2867	99.4072	Line 2 111-4a-mf5-ln3	string of beads
147	49%	49%	2%	55.0948	0.0364	28.2484	0.2386	0.0037	10.2155	5.2705	0.2703	99.3783	Line 3 111-4a-mf5-ln3	string of beads
149	40%	58%	2%	57.4372	0.0243	26.7875	0.2396	0.005	8.4065	6.0548	0.3356	99.2906	Line 5 111-4a-mf5-ln3	string of beads
150	41%	57%	2%	57.6028	0.0035	27.022	0.2597	0.0037	8.7513	6.1597	0.3705	100.1731	Line 6 111-4a-mf5-ln3	string of beads
151	41%	57%	2%	57.3635	0.0139	27.0543	0.2337	0.0084	8.8152	6.1159	0.3244	99.9294	Line 7 111-4a-mf5-ln3	string of beads
152	41%	56%	3%	58.4127	0	26.1404	0.2638	0.0152	8.4535	5.7493	0.4971	99.5321	Line 8 111-4a-mf5-ln3	string of beads
154	42%	57%	1%	57.1533	0	27.1766	0.2083	0.0053	8.7706	5.9676	0.263	99.5448	Line 10 111-4a-mf5-ln3	string of beads
Line 4														
155	43%	55%	2%	56.7934	0	26.8988	0.1982	0.0149	9.1623	5.9727	0.2769	99.3173	Line 1 111-4a-mf5-ln4	string of beads
156	48%	51%	2%	55.7146	0.0158	28.0575	0.252	0.023	10.0204	5.3748	0.2738	99.732	Line 2 111-4a-mf5-ln4	string of beads
157	50%	49%	2%	55.076	0.0282	28.1937	0.2759	0.0099	10.5461	5.2344	0.2712	99.6355	Line 3 111-4a-mf5-ln4	string of beads
158	51%	48%	2%	55.0631	0.013	28.4784	0.2565	0.008	10.579	5.0263	0.2699	99.6943	Line 4 111-4a-mf5-ln4	string of beads
159	44%	54%	2%	56.5456	0.0085	27.326	0.2364	0.0208	9.3897	5.8472	0.3315	99.7058	Line 5 111-4a-mf5-ln4	string of beads
160	42%	54%	5%	57.0307	0.0199	26.3055	0.2915	0.0192	8.8033	5.8154	0.8505	99.1361	Line 6 111-4a-mf5-ln4	string of beads
161	43%	56%	2%	57.3347	0.0044	26.9634	0.2654	0.0075	8.6697	5.726	0.3332	99.3044	Line 7 111-4a-mf5-ln4	string of beads
162	43%	55%	2%	57.1421	0.018	26.366	0.225	0.0116	8.814	5.7922	0.293	98.6619	Line 8 111-4a-mf5-ln4	string of beads
163	39%	59%	2%	57.761	0.012	26.4415	0.2522	0.0088	8.0263	6.1091	0.3344	98.9454	Line 9 111-4a-mf5-ln4	string of beads
164	41%	58%	1%	57.6008	0.0066	26.8144	0.223	0.0166	8.5611	6.0468	0.2582	99.5276	Line 10 111-4a-mf5-ln4	string of beads
Average	42%	56%	2%											
Stdev	3%	3%	1%											

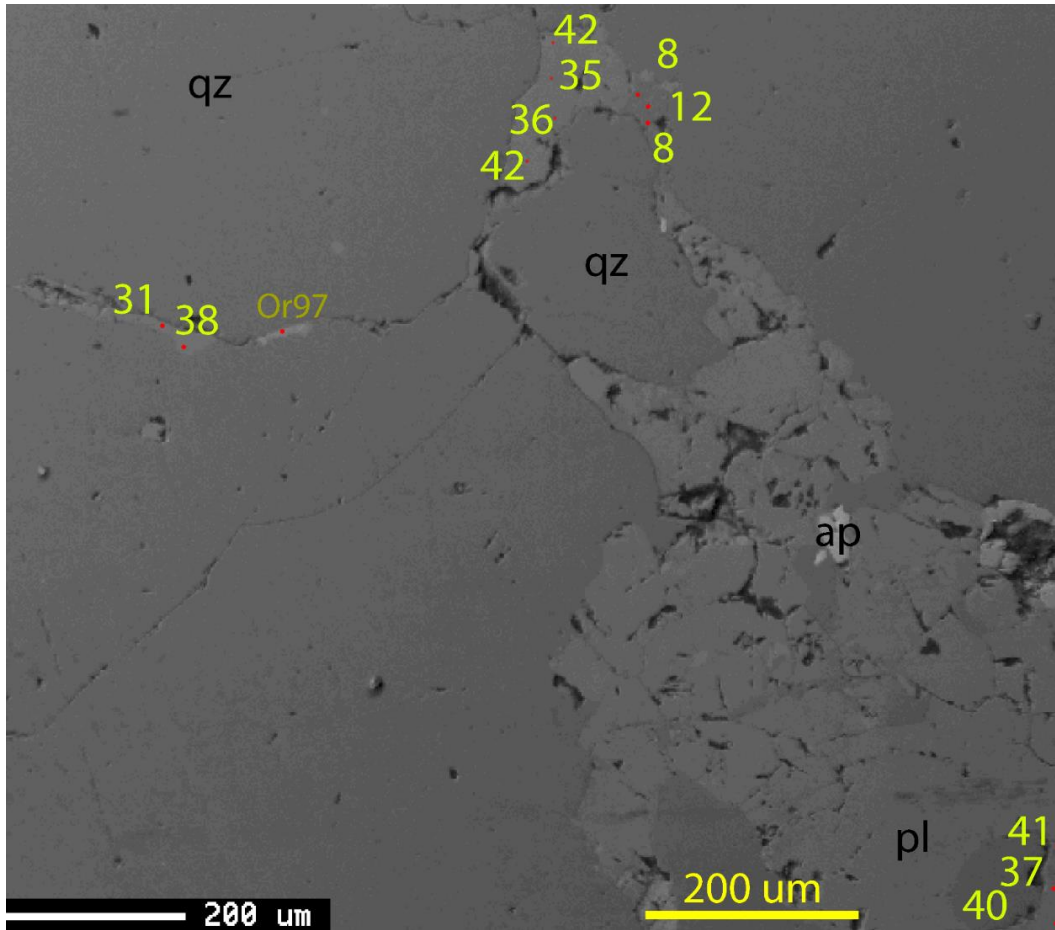


Figure A9 Sample 111-4a. SEM-BSE image of a melt films plagioclase. Rod dots indicate EPMA targets. Yellow numbers indicate An % content of plagioclase. Refer to table A41 for corresponding EPMA analysis. Qz = quartz, pl = plagioclase, ap = apatite, Or97 = K-feldspar with Or97 composition.

Table A41 EPMA results of melt film plagioclase. Refer to Figure A9 for targets.

Sample 111-4a Melt Film Plagioclase														
No.	An%	Ab%	Or%	SiO2	TiO2	Al2O3	FeO	MgO	CaO	Na2O	K2O	Total	Comment	Comment2
165	42%	56%	2%	56.731	0	27.1641	0.1867	0.0166	8.8168	5.9177	0.2878	99.1208	111-4a-mf6-1	Melt Film
166	35%	63%	2%	58.5317	0.0148	25.6951	0.2304	0.0018	7.4369	6.7447	0.3518	99.0073	111-4a-mf6-2	Melt Film
167	36%	62%	2%	57.6253	0.019	25.8921	0.2268	0.0062	7.6977	6.7465	0.3618	98.5754	111-4a-mf6-3	Melt Film
168	42%	57%	1%	56.8268	0.0247	27.0935	0.2002	0	8.8421	6.124	0.2489	99.3603	111-4a-mf6-4	Melt Film
169	38%	61%	2%	58.0621	0.0019	26.1461	0.1979	0	7.8358	6.4045	0.2721	98.9204	111-4a-mf6-5	Melt Film
170	31%	67%	2%	59.6695	0.0152	24.6508	0.1625	0.0078	6.5798	7.1461	0.3056	98.5374	111-4a-mf6-6	Melt Film
171	8%	91%	1%	65.3053	0.0022	21.161	0	0.0131	1.8786	9.942	0.1693	98.4715	111-4a-mf6-7	Melt Film
172	12%	88%	1%	64.4162	0.0085	21.8335	0.0112	0	2.5859	9.615	0.1598	98.6301	111-4a-mf6-8	Melt Film
173	8%	91%	1%	65.8296	0.0343	21.3104	0.0059	0.0058	1.8421	10.1558	0.1285	99.3125	111-4a-mf6-9	Melt Film
174	41%	58%	2%	57.3791	0	27.1969	0.2524	0.0144	8.7213	6.1608	0.3004	100.0252	111-4a-mf6-10	Melt Film
175	37%	54%	9%	57.9468	0.0446	26.2478	0.2421	0.0072	7.796	5.7261	1.5195	99.5302	111-4a-mf6-11	Melt Film
176	40%	58%	1%	57.6083	0.0136	26.9921	0.2266	0.0123	8.5887	6.1871	0.2398	99.8686	111-4a-mf6-12	Melt Film
Average	31%	67%	2%											
Stdev	13%	14%	2%											

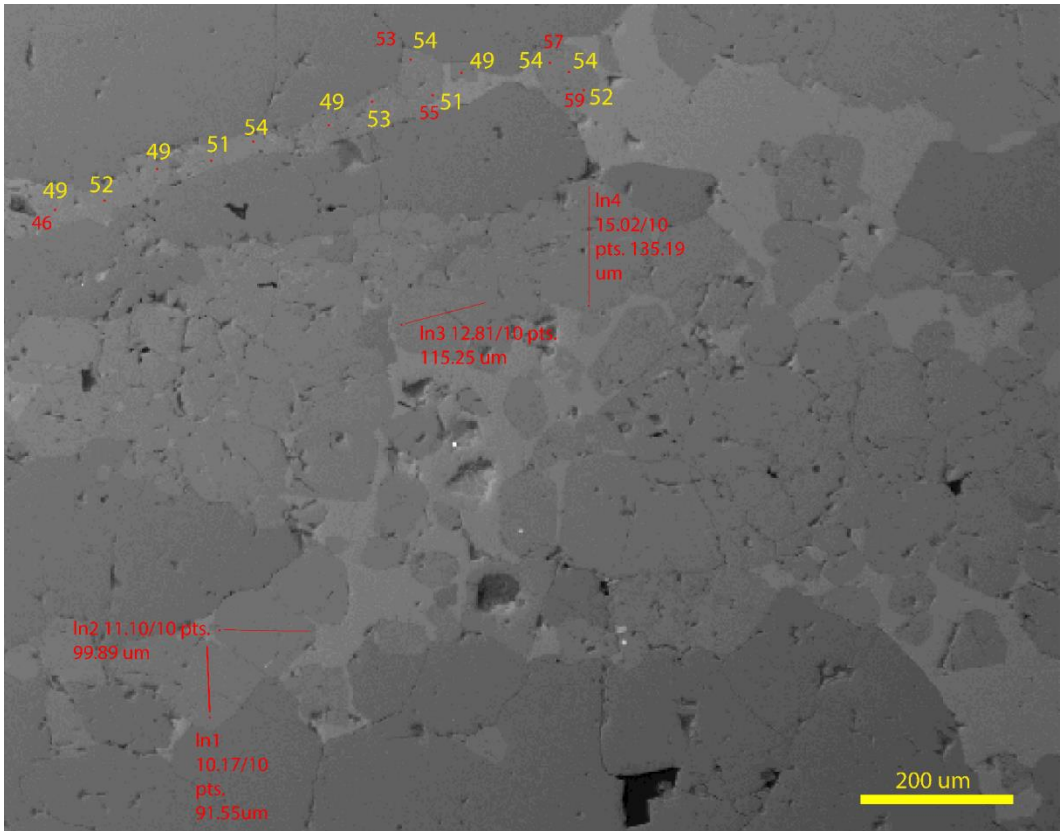


Figure A10 Sample 925-1. SEM-BSE image of string of beads and residual plagioclase. Rod dots indicate EPMA targets. Yellow numbers indicate An % content of plagioclase. Refer to tables A42-46 for corresponding EPMA analysis. Red lines indicate EPMA line analysis. Each line analysis can be associated with the corresponding Table under the comment column. The numbers refer to the spacing interval between each target followed by the amount of points analyzed on each line. Lastly, the total line length is listed.

Table A42 EPMA results of residual plagioclase line 1. Refer to Figure A10 for targets.

Sample 925-1 Residual Plagioclase													
No.	An%	Ab%	Or%	SiO2	TiO2	Al2O3	FeO	MgO	CaO	Na2O	K2O	Total	Comment
177	38%	61%	1%	5808%	0.03	26.6729	0.1618	0.0086	8.0196	6.5495	0.2163	99.7374	Line 1 925-1lpp2ln1
178	38%	61%	1%	5835%	0.00	26.5813	0.1727	0.0081	8.0324	6.4704	0.2618	99.8729	Line 2 925-1lpp2ln1
179	39%	61%	1%	5801%	0.00	26.5228	0.1334	0.0074	8.1852	6.4632	0.1742	99.5008	Line 3 925-1lpp2ln1
181	39%	59%	2%	5834%	0.01	26.703	0.184	0.0038	8.2288	6.257	0.2833	100.0129	Line 5 925-1lpp2ln1
182	39%	60%	2%	5824%	0.00	26.5588	0.1655	0	8.0837	6.2326	0.3062	99.5876	Line 6 925-1lpp2ln1
183	38%	61%	2%	5822%	0.00	26.6062	0.2012	0.002	8.0662	6.4457	0.2717	99.8113	Line 7 925-1lpp2ln1
184	36%	62%	2%	5821%	0.00	26.4612	0.174	0	7.5537	6.4604	0.3119	99.1798	Line 8 925-1lpp2ln1
185	37%	62%	2%	5852%	0.00	26.2745	0.2008	0.0013	7.6992	6.509	0.2926	99.4954	Line 9 925-1lpp2ln1
186	30%	68%	1%	5693%	0.01	24.7985	3.7075	0.0036	6.3236	7.4288	0.2569	99.4626	Line 10 925-1lpp2ln1
Average	37%	62%	1%										
Stdev	3%	3%	0%										

Table A43 EPMA results of residual plagioclase line 2 Refer to Figure A10 for targets.

Sample 925-1 Residual Plagioclase													
No.	An%	Ab%	Or%	SiO2	TiO2	Al2O3	FeO	MgO	CaO	Na2O	K2O	Total	Comment
187	33%	65%	2%	59.2409	0	25.6453	0.1861	0	7.0844	7.0027	0.2905	99.45	Line 1 925-1pp2-ln2
188	34%	64%	2%	59.2459	0	25.6467	0.1657	0	7.2082	6.8663	0.3274	99.4603	Line 2 925-1pp2-ln2
189	38%	60%	2%	58.1823	0.0025	26.4747	0.1925	0	7.9839	6.3079	0.2766	99.4205	Line 3 925-1pp2-ln2
190	38%	60%	2%	57.9712	0.0016	26.1822	0.225	0.0114	7.9281	6.3427	0.294	98.9563	Line 4 925-1pp2-ln2
191	37%	61%	2%	58.4782	0.018	26.6593	0.174	0.0186	7.959	6.4311	0.3064	100.0445	Line 5 925-1pp2-ln2
192	38%	61%	2%	57.9147	0.0073	26.6108	0.1854	0.0083	7.952	6.4495	0.3135	99.4416	Line 6 925-1pp2-ln2
193	38%	60%	2%	57.6925	0	26.3947	0.1852	0.029	8.0119	6.3878	0.2978	98.999	Line 7 925-1pp2-ln2
194	37%	62%	2%	58.5996	0.0044	26.4938	0.1838	0.0121	7.8499	6.6075	0.2875	100.0385	Line 8 925-1pp2-ln2
195	38%	60%	2%	58.2913	0.0319	26.5632	0.2048	0.0092	8.025	6.4066	0.3022	99.8343	Line 9 925-1pp2-ln2
196	33%	65%	2%	59.5547	0.0512	25.3964	0.1765	0.0053	6.9368	6.9574	0.3536	99.432	Line 10 925-1pp2-ln2
Average	36%	62%	2%										
Stdev	2%	2%	0%										

Table A44 EPMA results of residual plagioclase line 3. Refer to Figure A10 for targets.

925-1 Residual Plagioclase													
No.	An%	Ab%	Or%	SiO2	TiO2	Al2O3	FeO	MgO	CaO	Na2O	K2O	Total	Comment
197	33%	65%	2%	59.117	0	25.6226	0.1804	0.0009	7.0961	6.9	0.3129	99.23	Line 1 925-1lpp2-ln3
198	38%	60%	2%	58.2877	0.0123	26.3764	0.1831	0.0116	7.8629	6.2782	0.2645	99.2768	Line 2 925-1lpp2-ln3
199	37%	61%	2%	58.3004	0.0104	26.6424	0.1879	0.0104	8.0653	6.5763	0.2975	100.0905	Line 3 925-1lpp2-ln3
200	38%	60%	2%	58.2862	0.0013	26.4826	0.2003	0	8.0472	6.3536	0.3378	99.709	Line 4 925-1lpp2-ln3
201	38%	60%	2%	58.1804	0.0047	26.9336	0.2046	0.0112	8.2383	6.4902	0.324	100.3869	Line 5 925-1lpp2-ln3
203	38%	60%	2%	58.3117	0.0006	26.5244	0.198	0.0023	8.0307	6.3941	0.3399	99.8018	Line 7 925-1lpp2-ln3
204	38%	61%	2%	58.166	0.0044	26.5418	0.2046	0.0118	8.0943	6.5106	0.3256	99.8592	Line 8 925-1lpp2-ln3
205	36%	62%	2%	58.5983	0.0215	26.2073	0.2157	0.0054	7.6283	6.6349	0.29	99.6015	Line 9 925-1lpp2-ln3
206	35%	63%	2%	58.6936	0	25.607	0.1687	0.0024	7.1915	6.6135	0.302	98.5788	Line 10 925-1lpp2-ln3
Average	37%	61%	2%										
Stdev	2%	2%	0%										

Table A45 EPMA results of residual plagioclase line 4. Refer to Figure A10 for targets.

925-1 Residual Plagioclase													
No.	An%	Ab%	Or%	SiO2	TiO2	Al2O3	FeO	MgO	CaO	Na2O	K2O	Total	Comment
207	32%	66%	2%	59.8218	0	25.4267	0.1863	0.0134	7.0267	7.1092	0.3213	99.9054	Line 1 925-1-lpp2-ln4
208	35%	63%	2%	58.8503	0.0465	26.2093	0.153	0.0107	7.5667	6.7972	0.3302	99.964	Line 2 925-1-lpp2-ln4
209	38%	60%	1%	57.9883	0.0247	26.4396	0.1679	0.006	8.0254	6.3924	0.2627	99.3071	Line 3 925-1-lpp2-ln4
210	37%	61%	2%	58.288	0.0076	26.5412	0.2071	0	7.9128	6.46	0.3533	99.7701	Line 4 925-1-lpp2-ln4
211	39%	59%	2%	58.2897	0.0149	25.8806	0.2011	0.0045	7.9545	6.2223	0.3566	98.9243	Line 5 925-1-lpp2-ln4
213	37%	62%	2%	58.6093	0	26.4869	0.1524	0	7.6982	6.4874	0.3032	99.7374	Line 7 925-1-lpp2-ln4
215	36%	62%	1%	58.543	0.012	26.5143	0.1265	0.012	7.8729	6.7018	0.2112	99.9938	Line 9 925-1-lpp2-ln4
216	36%	63%	1%	58.3489	0.0016	26.4497	0.139	0.015	7.4944	6.6305	0.2509	99.3301	Line 10 925-1-lpp2-ln4
Average	36%	62%	2%										
Stdev	2%	2%	0%										

Table A46 EPMA results of string of beads plagioclase. Refer to Figure A10 for targets.

Sample 925-1 String of Beads Plagioclase													
No.	An%	Ab%	Or%	SiO2	TiO2	Al2O3	FeO	MgO	CaO	Na2O	K2O	Total	Comment
222	33%	66%	2%	59.1181	0	25.1759	0.1751	0.005	6.9636	7.0731	0.278	98.7889	925-1-lpp2-46
223	35%	64%	1%	58.8713	0	26.3575	0.1758	0	7.533	6.8096	0.2447	99.992	925-1-lpp2-47
224	33%	66%	2%	59.6406	0	25.738	0.1471	0.0008	6.8581	6.84	0.2976	99.5222	925-1-lpp2-48
225	34%	65%	1%	59.2108	0	26.0438	0.1555	0.0119	7.0297	6.6461	0.216	99.3139	925-1-lpp2-49
226	38%	61%	1%	57.9796	0	26.6023	0.189	0.0012	7.9451	6.4228	0.2586	99.3987	925-1-lpp2-50
227	33%	66%	1%	59.4723	0	25.8018	0.1878	0	7.1024	7.1021	0.2721	99.9386	925-1-lpp2-51
228	37%	62%	1%	58.2358	0	26.2396	0.1541	0.0027	7.7492	6.6357	0.2552	99.2724	925-1-lpp2-52
229	37%	61%	2%	58.2644	0	26.6069	0.2104	0.0092	8.0016	6.5771	0.2831	99.9528	925-1-lpp2-53
231	34%	64%	2%	58.724	0	26.2039	0.1744	0.0046	7.2472	6.7511	0.2662	99.3715	925-1-lpp2-55
232	33%	65%	2%	59.6668	0	25.7893	0.1349	0.0004	7.0901	7.0074	0.3133	100.0021	925-1-lpp2-56
233	37%	61%	2%	57.964	0	26.3458	0.1895	0	7.9245	6.5502	0.2849	99.259	925-1-lpp2-57
234	37%	61%	2%	58.1343	0	26.2111	0.1964	0.0061	7.941	6.5433	0.3137	99.3459	925-1-lpp2-58
235	36%	62%	2%	58.5428	0.0215	26.0493	0.1626	0	7.4739	6.5669	0.3042	99.1213	925-1-lpp2-59
Average	35%	63%	2%										
Stdev	2%	2%	0%										

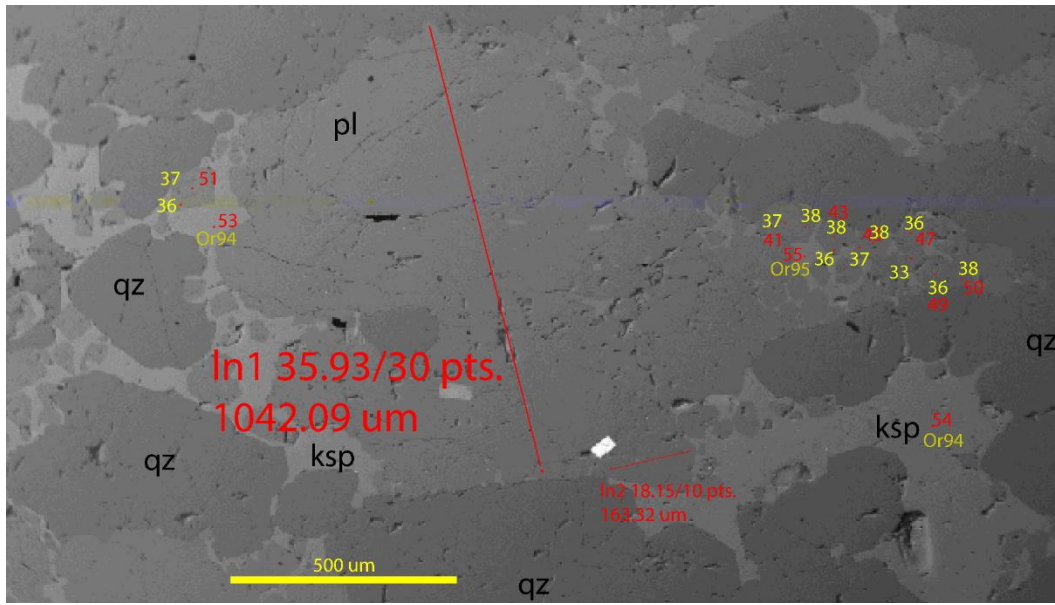


Figure A11 Sample 925-1. SEM-BSE image of LPP and residual plagioclase. Rod dots indicate EPMA targets. Yellow numbers indicate An % content of plagioclase. Faded yellow numbers refer to K-spar analysis on Table A50. Refer to tables A47-50 for corresponding EPMA analysis. Red line indicates EPMA line analysis. Ln1 refers to Table A49, and Ln2 refers to Table A48. The numbers refer to the spacing interval between each target followed by the amount of points analyzed on each line. Lastly, the total line length is listed.

Table A47 EPMA results of LPP plagioclase. Refer to Figure A11 for targets.

925-1 Large Pseudomelt Pocket Rounded Plagioclase													
No.	An%	Ab%	Or%	SiO2	TiO2	Al2O3	FeO	MgO	CaO	Na2O	K2O	Total	Comment
276	37%	61%	2%	58.394	0	26.5189	0.1918	0.0119	7.9551	6.5676	0.3412	99.9806	925-1-lpp3-41
277	38%	60%	2%	57.9406	0.0108	26.4805	0.2101	0	7.8388	6.2365	0.2619	98.9793	925-1-lpp3-42
278	38%	61%	2%	58.1571	0	26.6526	0.2109	0	8.0391	6.4863	0.2724	99.8185	925-1-lpp3-43
279	36%	62%	2%	58.8875	0.0117	26.2206	0.1925	0.0067	7.5423	6.5119	0.304	99.6773	925-1-lpp3-44
280	38%	61%	2%	57.9378	0.0139	26.5737	0.1887	0.0078	8.0667	6.5269	0.2817	99.5973	925-1-lpp3-45
281	37%	62%	2%	58.641	0.0127	25.9439	0.1719	0	7.8564	6.6296	0.3063	99.5619	925-1-lpp3-46
282	36%	63%	2%	58.7189	0	26.2127	0.1555	0.0071	7.6428	6.6736	0.2866	99.6973	925-1-lpp3-47
283	33%	65%	2%	59.4389	0	25.5647	0.1645	0.0196	7.1903	7.0404	0.3059	99.7243	925-1-lpp3-48
284	36%	62%	2%	57.9122	0	26.7113	0.2159	0	7.5028	6.5203	0.3041	99.1666	925-1-lpp3-49
285	38%	60%	1%	57.6655	0.0089	26.5278	0.2183	0	8.1047	6.4704	0.2658	99.2615	925-1-lpp3-50
286	32%	66%	2%	59.8879	0	25.4728	0.1875	0.0003	6.8264	6.9737	0.421	99.7697	925-1-lpp3-51
287	36%	63%	1%	58.3508	0	26.3472	0.165	0.0019	7.6682	6.7396	0.1897	99.4624	925-1-lpp3-52
Average	36%	62%	2%										
Stdev	2%	2%	0%										

Table A48 EPMA results of residual line 2 plagioclase. Refer to Figure A11 for targets.

Sample 925-1 Residual Plagioclase													
No.	An%	Ab%	Or%	SiO2	TiO2	Al2O3	FeO	MgO	CaO	Na2O	K2O	Total	Comment
266	32%	66%	1%	59.5918	0	25.5721	0.2763	0.0093	6.9515	7.1337	0.2672	99.8019	Line 1 925-1-lpp3-ln2
267	38%	61%	2%	58.1043	0.025	26.6999	0.2473	0.012	7.9468	6.3901	0.2861	99.7116	Line 2 925-1-lpp3-ln2
268	38%	61%	2%	58.2895	0	26.4393	0.1907	0.0007	7.9614	6.4465	0.2828	99.611	Line 3 925-1-lpp3-ln2
269	38%	60%	2%	57.8354	0.0089	25.8115	0.2054	0.0081	7.7776	6.3684	0.3037	98.3191	Line 4 925-1-lpp3-ln2
270	38%	60%	2%	58.3026	0.0142	26.5672	0.2126	0	8.0182	6.3809	0.3684	99.8642	Line 5 925-1-lpp3-ln2
271	38%	60%	2%	58.0748	0	26.6972	0.1955	0	8.0162	6.388	0.347	99.7188	Line 6 925-1-lpp3-ln2
272	37%	60%	2%	57.9646	0	26.4491	0.2151	0.0024	8.0208	6.5216	0.3678	99.5415	Line 7 925-1-lpp3-ln2
273	37%	61%	2%	58.2822	0.0079	26.7567	0.1954	0	8.0056	6.5014	0.3297	100.0788	Line 8 925-1-lpp3-ln2
274	38%	61%	2%	58.2173	0.0288	26.6701	0.2011	0	7.9605	6.4136	0.3325	99.8239	Line 9 925-1-lpp3-ln2
275	33%	65%	2%	59.2377	0.0142	26.057	0.183	0.015	7.2558	6.9575	0.3328	100.0529	Line 10 925-1-lpp3-ln2
Average	37%	62%	2%										
Stdev	2%	2%	0%										

Table A49 EPMA results of residual line 1 plagioclase. Refer to Figure A11 for targets.

Sample 925-1 Residual Plagioclase													
No.	An%	Ab%	Or%	SiO2	TiO2	Al2O3	FeO	MgO	CaO	Na2O	K2O	Total	Comment
236	37%	62%	1%	58.4008	0.0193	26.1063	0.1776	0.007	7.8542	6.7187	0.2272	99.5112	Line 1 925-1-lpp3-ln1
237	36%	63%	2%	58.9478	0.0133	26.2486	0.1709	0.0075	7.7629	6.7617	0.339	100.2516	Line 2 925-1-lpp3-ln1
238	35%	62%	3%	58.8302	0.007	25.2633	0.2014	0.0162	7.4898	6.6084	0.5072	98.9236	Line 3 925-1-lpp3-ln1
239	37%	61%	2%	57.5747	0.0288	25.8207	0.217	0	7.6093	6.5694	0.3012	98.1212	Line 4 925-1-lpp3-ln1
240	36%	62%	2%	58.7458	0.0139	26.3458	0.1667	0.0072	7.792	6.6318	0.3261	100.0293	Line 5 925-1-lpp3-ln1
241	36%	63%	1%	58.5708	0.0054	26.1336	0.186	0.0109	7.6785	6.7065	0.2615	99.5533	Line 6 925-1-lpp3-ln1
242	36%	63%	1%	58.5759	0.0003	26.3909	0.148	0.0185	7.6782	6.7604	0.1497	99.7219	Line 7 925-1-lpp3-ln1
243	36%	62%	2%	58.4991	0	26.1076	0.1845	0	7.6964	6.6764	0.2927	99.4567	Line 8 925-1-lpp3-ln1
244	34%	64%	2%	59.3741	0	26.1662	0.1609	0.0171	7.3976	6.7459	0.3257	100.1874	Line 9 925-1-lpp3-ln1
245	35%	63%	2%	59.0219	0	26.1063	0.185	0.0077	7.5179	6.7774	0.2962	99.9125	Line 10 925-1-lpp3-ln1
246	35%	63%	2%	58.6912	0.0152	25.9643	0.1439	0.017	7.6349	6.7874	0.337	99.591	Line 11 925-1-lpp3-ln1
248	36%	62%	2%	58.7129	0	26.146	0.1456	0.01	7.582	6.6624	0.3762	99.6352	Line 13 925-1-lpp3-ln1
249	36%	62%	2%	58.7535	0	25.7965	0.1253	0.0206	7.4033	6.5027	0.3388	98.9408	Line 14 925-1-lpp3-ln1
250	35%	62%	3%	57.8882	0.0108	25.4753	0.118	0.0205	7.3246	6.6793	0.4877	98.0045	Line 15 925-1-lpp3-ln1
251	34%	63%	3%	59.1566	0	25.8723	0.1034	0.0122	7.3297	6.8241	0.4718	99.7702	Line 16 925-1-lpp3-ln1
252	35%	62%	2%	58.967	0	25.9192	0.1553	0.0036	7.4164	6.5934	0.4348	99.4898	Line 17 925-1-lpp3-ln1
253	35%	63%	3%	59.013	0.0186	25.6094	0.1491	0.0141	7.3422	6.7304	0.4466	99.3235	Line 18 925-1-lpp3-ln1
254	33%	65%	2%	59.3101	0.0158	25.8231	0.123	0.0186	7.1417	6.8607	0.3556	99.6487	Line 19 925-1-lpp3-ln1
256	35%	62%	3%	58.2537	0	25.537	0.1463	0.0163	7.4909	6.7375	0.4812	98.663	Line 21 925-1-lpp3-ln1
257	36%	62%	2%	59.016	0.0411	26.0078	0.1396	0.0114	7.4837	6.5225	0.4319	99.6541	Line 22 925-1-lpp3-ln1
258	36%	62%	3%	58.4814	0	25.9765	0.1486	0.0175	7.5663	6.584	0.4788	99.2532	Line 23 925-1-lpp3-ln1
259	36%	61%	3%	58.8245	0.0127	25.6836	0.1451	0.004	7.5972	6.5205	0.506	99.2937	Line 24 925-1-lpp3-ln1
260	36%	61%	3%	58.6046	0.0167	26.23	0.1702	0.0164	7.6435	6.5155	0.4908	99.6878	Line 25 925-1-lpp3-ln1
263	36%	63%	2%	58.7005	0.024	26.1179	0.1878	0.004	7.48	6.6332	0.3017	99.4492	Line 28 925-1-lpp3-ln1
264	35%	64%	1%	58.8137	0.0095	26.1068	0.1595	0.0175	7.4845	6.855	0.2014	99.648	Line 29 925-1-lpp3-ln1
265	35%	65%	1%	59.0377	0.0006	25.6583	0.1362	0	7.4052	6.9462	0.1692	99.3535	Line 30 925-1-lpp3-ln1
Average	35%	63%	2%										
Stdev	1%	1%	1%										

Table A50 EPMA results K-feldspar analysis. Refer to Figure A11 for targets.

Sample 925-1 K-feldspar													
No.	An%	Ab%	Or%	SiO2	TiO2	Al2O3	FeO	MgO	CaO	Na2O	K2O	Total	Comment
288	0%	9%	91%	63.5161	0.0162	18.7036	0.1052	0	0	1.0124	15.116	98.4696	925-1-lpp3-53
289	0%	9%	91%	63.1838	0	18.8781	0.0946	0	0	0.9216	15.0744	98.1525	925-1-lpp3-54
290	0%	7%	93%	63.4997	0.013	18.4615	0.1176	0.0062	0	0.7659	15.5957	98.4597	925-1-lpp3-55
Average	0%	8%	92%										
Stdev	0%	1%	1%										

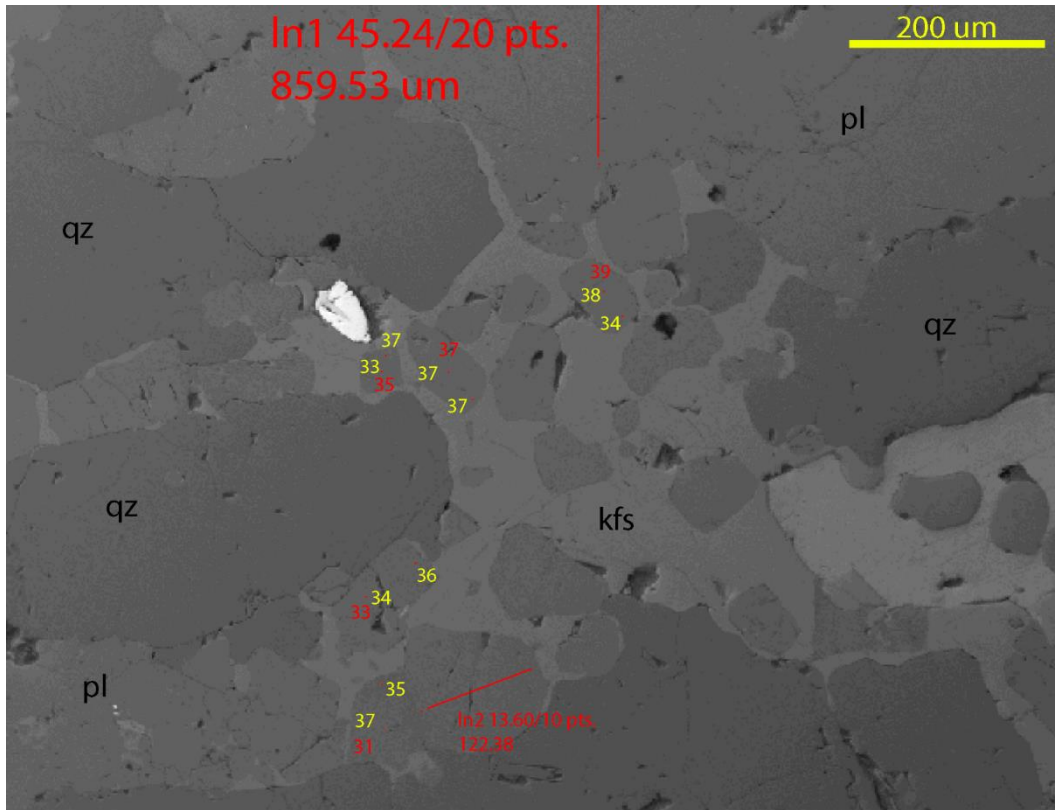


Figure A12 Sample 925-1. SEM-BSE image of LPP and residual plagioclase. Rod dots indicate EPMA targets. Yellow numbers indicate An % content of plagioclase. Refer to tables A51-53 for corresponding EPMA analysis. Red line indicates EPMA line analysis. Ln1 refers to Table A52, and ln2 refers to Table A53. The numbers refer to the spacing interval between each target followed by the amount of points analyzed on each line. Lastly, the total line length is listed. Qz = quartz, kfs = K-feldspar, pl = plagioclase

Table A51 EPMA results LPP plagioclase analysis. Refer to Figure A12 for targets.

Sample 925-1 Large Pseudomelt Pocket Rounded Plagioclase													
No.	An%	Ab%	Or%	SiO2	TiO2	Al2O3	FeO	MgO	CaO	Na2O	K2O	Total	Comment
321	54%	45%	1%	58.3754	0.0148	26.439	0.0925	0	7.9409	6.6405	0.1606	99.6637	925-1-lpp4-31
322	52%	47%	1%	58.4975	0.0013	26.2724	0.1075	0.0023	7.494	6.8671	0.1655	99.4076	925-1-lpp4-32
323	50%	48%	2%	59.0449	0	25.1483	0.1913	0	7.2224	6.97	0.3002	98.8772	925-1-lpp4-33
324	52%	46%	2%	58.5548	0.0215	25.6905	0.184	0.0101	7.6466	6.7829	0.2709	99.1613	925-1-lpp4-34
325	49%	48%	2%	58.8729	0.0259	25.7552	0.205	0	7.1897	7.0646	0.3137	99.4271	925-1-lpp4-35
326	54%	45%	2%	58.1772	0	26.455	0.2455	0.0081	7.7168	6.4457	0.2592	99.3076	925-1-lpp4-36
327	54%	45%	2%	58.3714	0.0174	26.4631	0.1671	0.0053	7.9676	6.5858	0.2311	99.8089	925-1-lpp4-37
328	53%	45%	1%	58.2577	0	26.425	0.1497	0.0118	7.8816	6.6555	0.2201	99.6014	925-1-lpp4-38
329	54%	44%	1%	58.2828	0	26.5137	0.1774	0	7.9914	6.4935	0.2189	99.6778	925-1-lpp4-39
330	51%	48%	2%	59.5085	0.0107	25.8311	0.181	0	7.2252	6.8159	0.2469	99.8194	925-1-lpp4-40
Average	52%	46%	2%										
Stdev	2%	2%	0%										

Table A52 EPMA results residual line 1 plagioclase analysis. Refer to Figure A12 for targets.

Sample 925-1 Residual Plagioclase													
No.	An%	Ab%	Or%	SiO2	TiO2	Al2O3	FeO	MgO	CaO	Na2O	K2O	Total	Comment
291	49%	49%	1%	59.2101	0	24.9752	0.1594	0	7.047	7.0191	0.1983	98.6092	Line 1 925-1-lpp4-ln1
293	53%	45%	2%	58.2903	0.0025	26.2468	0.1798	0	7.8269	6.6095	0.3117	99.4676	Line 3 925-1-lpp4-ln1
294	53%	45%	2%	58.711	0.0136	26.1209	0.1766	0.0064	7.8331	6.5572	0.2884	99.7073	Line 4 925-1-lpp4-ln1
295	53%	45%	2%	58.6611	0.0073	26.045	0.1582	0.0098	7.7796	6.6551	0.2416	99.5577	Line 5 925-1-lpp4-ln1
296	53%	46%	2%	57.8033	0.025	26.3619	0.155	0.0058	7.7031	6.6677	0.2736	98.9955	Line 6 925-1-lpp4-ln1
297	52%	47%	1%	58.2983	0.0123	26.0454	0.1417	0.0034	7.4989	6.8496	0.1778	99.0275	Line 7 925-1-lpp4-ln1
302	53%	45%	2%	58.4147	0.012	26.0448	0.1987	0.0096	7.6247	6.4696	0.332	99.1062	Line 12 925-1-lpp4-ln1
304	52%	45%	3%	58.7282	0	26.2652	0.2202	0.0082	7.7023	6.6877	0.3962	100.0079	Line 14 925-1-lpp4-ln1
305	52%	45%	3%	58.7588	0.0098	26.1728	0.2035	0	7.5434	6.5568	0.4476	99.6928	Line 15 925-1-lpp4-ln1
307	52%	45%	3%	58.6821	0	26.1654	0.2078	0.0023	7.46	6.4782	0.3857	99.3815	Line 17 925-1-lpp4-ln1
308	52%	45%	4%	57.7602	0	25.2787	1.6398	0.1576	7.0446	6.1149	0.5148	98.5107	Line 18 925-1-lpp4-ln1
309	53%	45%	2%	58.3841	0	26.0216	0.2307	0.0173	7.8446	6.6059	0.3475	99.4518	Line 19 925-1-lpp4-ln1
310	55%	44%	2%	58.037	0.0253	26.2723	0.1815	0	7.8323	6.2475	0.222	98.818	Line 20 925-1-lpp4-ln1
Average	52%	45%	2%										
Stdev	1%	1%	1%										

Table A53 EPMA results residual line 2 plagioclase analysis. Refer to Figure A12 for targets.

Sample 925-1 Rounded Plagioclase													
No.	An%	Ab%	Or%	SiO2	TiO2	Al2O3	FeO	MgO	CaO	Na2O	K2O	Total	Comment
311	55%	43%	2%	58.2359	0.0215	26.5128	0.1743	0.008	8.0543	6.3167	0.2261	99.5497	Line 1 925-1-lpp4-ln2
312	50%	48%	2%	58.9211	0.0234	25.8327	0.2003	0.0116	7.2093	6.9576	0.3215	99.4776	Line 2 925-1-lpp4-ln2
313	53%	45%	2%	58.6759	0	26.4012	0.1783	0.0073	7.8595	6.6532	0.3331	100.1084	Line 3 925-1-lpp4-ln2
314	56%	42%	2%	58.0966	0	26.6672	0.1768	0.0155	8.0841	6.1386	0.3292	99.508	Line 4 925-1-lpp4-ln2
315	55%	43%	2%	58.2839	0.0057	26.6019	0.1917	0.0085	8.1168	6.4191	0.2997	99.9274	Line 5 925-1-lpp4-ln2
316	55%	43%	2%	58.2909	0.0063	26.3455	0.1828	0	8.0604	6.2027	0.2772	99.3659	Line 6 925-1-lpp4-ln2
317	55%	43%	2%	58.4727	0.0082	26.4969	0.1827	0	8.0852	6.3361	0.2345	99.8164	Line 7 925-1-lpp4-ln2
318	51%	44%	5%	58.6684	0.0066	26.339	0.1364	0.0087	7.49	6.5093	0.8047	99.9632	Line 8 925-1-lpp4-ln2
319	51%	48%	1%	58.8541	0.0092	25.9149	0.1961	0.01	7.4792	6.958	0.2031	99.6247	Line 9 925-1-lpp4-ln2
320	49%	49%	1%	59.5244	0.0107	25.8496	0.1554	0.0053	7.1345	7.1471	0.2043	100.0312	Line 10 925-1-lpp4-ln2
Average	53%	45%	2%										
Stdev	3%	3%	1%										

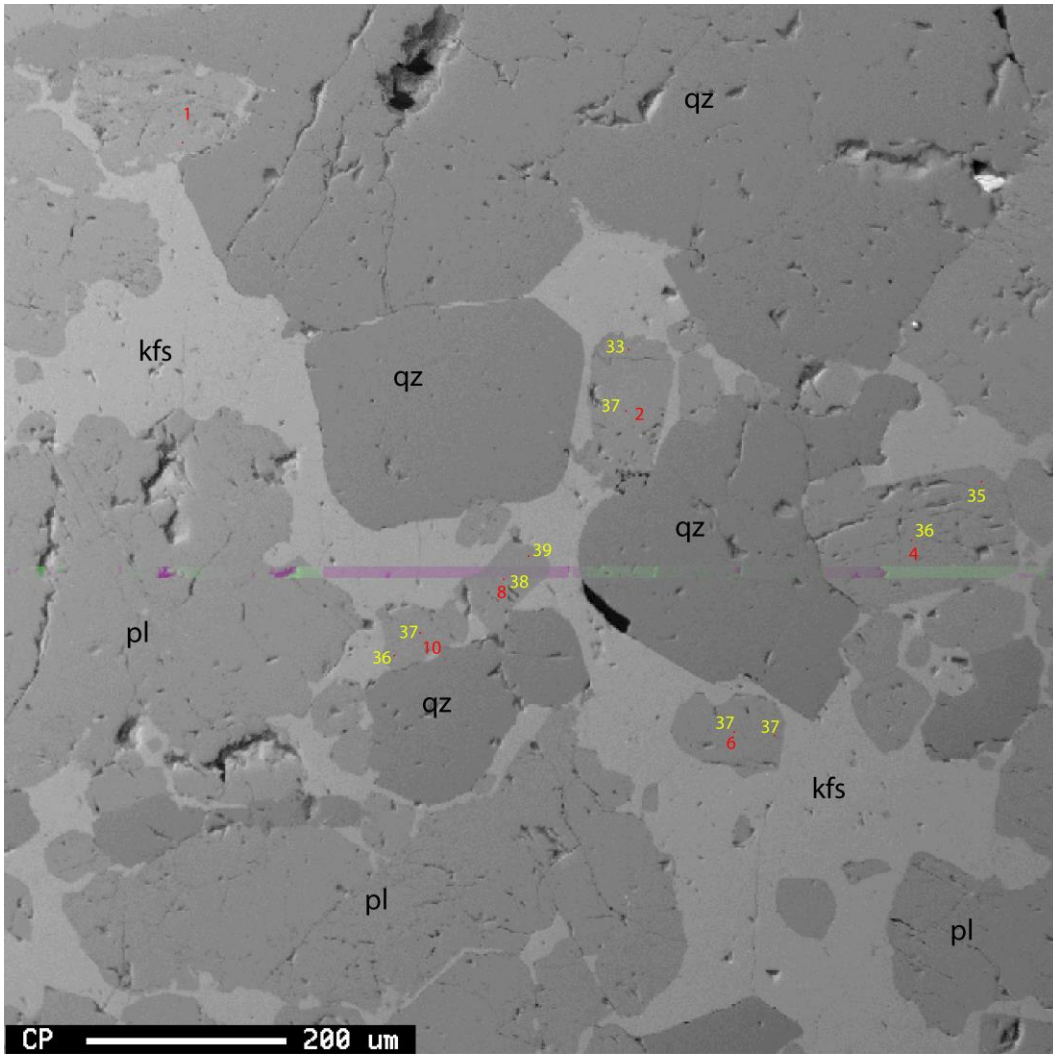


Figure A13 Sample 925-1. SEM-BSE image of LPP plagioclase. Red numbers indicate run numbers in comments column (Table A54). Rod dots indicate EPMA targets. Yellow numbers indicate An % content of plagioclase. Refer to table A54 for corresponding EPMA analysis. Qz = quartz, kfs = K-feldspar, pl = plagioclase

Table A54 EPMA results residual LPP plagioclase analysis. Refer to Figure A13 for targets.

Sample 925-1 Large Pseudomelt Pocket Rounded Plagioclase													
No.	An%	Ab%	Or%	SiO2	TiO2	Al2O3	FeO	MgO	CaO	Na2O	K2O	Total	Comment
331	36%	63%	1%	58.67	0	26.2648	0.1481	0.001	7.7017	6.7447	0.1491	99.6834	925-1-mf3-1
332	37%	61%	1%	58.28	0	26.6963	0.1825	0.0134	8.0135	6.5247	0.2695	99.9786	925-1-mf3-2
333	33%	65%	1%	59.42	0.0227	25.3921	0.1961	0.0108	7.0961	6.9995	0.2695	99.4088	925-1-mf3-3
334	36%	62%	1%	58.34	0.012	26.3273	0.2288	0.0011	7.5808	6.5632	0.2315	99.2816	925-1-mf3-4
335	35%	63%	1%	58.55	0	26.1854	0.1973	0.0103	7.5118	6.8202	0.2622	99.5342	925-1-mf3-5
336	37%	62%	2%	57.84	0.0183	26.5087	0.1882	0	7.6306	6.5211	0.3016	99.0109	925-1-mf3-6
337	37%	61%	1%	58.32	0.0129	26.4536	0.2138	0.0045	7.9862	6.5198	0.249	99.7648	925-1-mf3-7
338	38%	61%	1%	58.34	0.024	26.0667	0.1537	0.0082	7.9784	6.4746	0.1373	99.1842	925-1-mf3-8
339	37%	62%	1%	58.56	0.0035	26.24	0.1402	0.0126	7.8143	6.6347	0.1506	99.5536	925-1-mf3-9
340	37%	62%	1%	58.22	0	26.7318	0.1242	0.0044	7.8461	6.5426	0.1884	99.6601	925-1-mf3-10
341	36%	63%	1%	58.40	0.0041	26.3737	0.1415	0.0107	7.7264	6.783	0.1656	99.6088	925-1-mf3-11
Average	36%	62%	1%										
Stdev	1%	1%	0%										

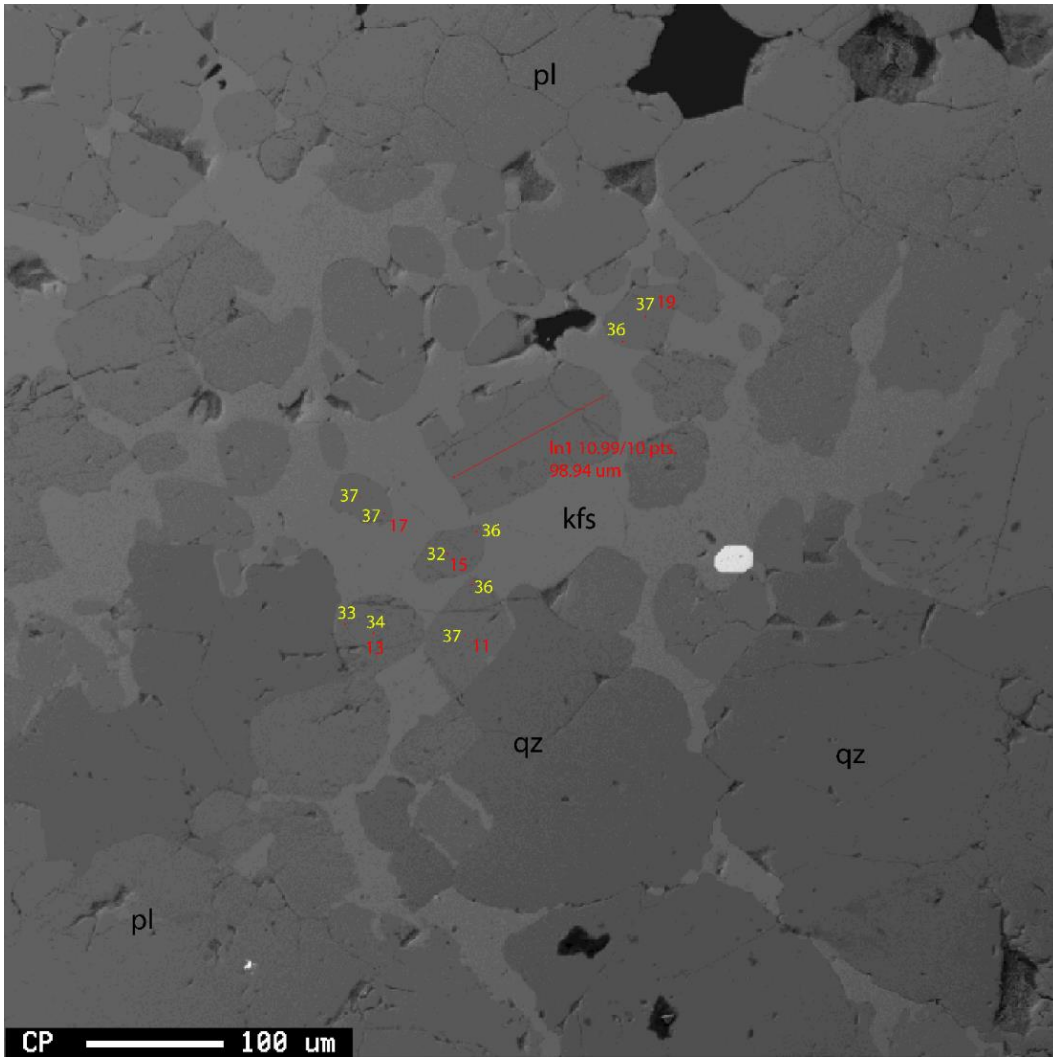


Figure A14 Sample 925-1. SEM-BSE image of LPP plagioclase. Rod dots indicate EPMA targets. Red numbers indicate run numbers. Yellow numbers indicate An % content of plagioclase. Refer to tables A55-56 for corresponding EPMA analysis. Red line indicates EPMA line analysis. Ln1 refers to Table A55. The numbers refer to the spacing interval between each target followed by the amount of points analyzed on each line. Lastly, the total line length is listed. Qz = quartz, kfs = K-feldspar, pl = plagioclase.

Table A55 EPMA results residual LPP line 1 plagioclase analysis. Refer to Figure A14 for targets.

Sample 925-1 Large Pseudomelt Pocket Euhedral Plagioclase													
No.	An%	Ab%	Or%	SiO2	TiO2	Al2O3	FeO	MgO	CaO	Na2O	K2O	Total	Comment
342	36%	63%	1%	57.8974	0.00	26.3089	0.172	0.0088	7.6751	6.699	0.199	98.9603	Line 1 925-1-mf4-ln1
343	34%	65%	1%	58.9718	0.00	25.9853	0.1671	0.013	7.3171	6.9154	0.2026	99.5723	Line 2 925-1-mf4-ln1
344	39%	60%	1%	57.2	0.01	26.6248	0.2018	0.0011	8.182	6.3911	0.2448	98.8539	Line 3 925-1-mf4-ln1
345	39%	59%	2%	57.4004	0.01	26.3567	0.1824	0	8.017	6.2611	0.3121	98.5415	Line 4 925-1-mf4-ln1
346	37%	61%	2%	58.2566	0.00	26.0881	0.2011	0.0017	7.9717	6.5347	0.3128	99.3668	Line 5 925-1-mf4-ln1
347	38%	61%	2%	57.7951	0.00	26.4316	0.2088	0.0162	7.9691	6.489	0.2988	99.2087	Line 6 925-1-mf4-ln1
348	38%	61%	1%	58.1175	0.02	25.4549	0.1523	0	7.8374	6.4027	0.218	98.2047	Line 7 925-1-mf4-ln1
349	35%	64%	1%	58.4959	0.00	25.9201	0.1389	0	7.3752	6.9211	0.2006	99.0518	Line 8 925-1-mf4-ln1
350	34%	64%	2%	59.4053	0.03	25.8267	0.2042	0.0142	7.224	6.827	0.3006	99.8343	Line 9 925-1-mf4-ln1
351	34%	65%	2%	59.3279	0.02	25.7145	0.2182	0.0065	7.1283	6.8556	0.3435	99.6097	Line 10 925-1-mf4-ln1
Average	36%	62%	1%										
Stdev	2%	2%	0%										

Table A56 EPMA results residual LPP plagioclase analysis. Refer to Figure A14 for targets.

Sample 925-1 Large Pseudomelt Pocket Rounded Plagioclase													
No.	An%	Ab%	Or%	SiO2	TiO2	Al2O3	FeO	MgO	CaO	Na2O	K2O	Total	Comment
352	37%	62%	1%	58.1787	0	26.2111	0.1463	0	7.9857	6.6633	0.1703	99.3555	925-1-mf4-11
353	36%	62%	2%	58.451	0.0174	26.4972	0.21	0.0102	7.8533	6.6969	0.3106	100.0465	925-1-mf4-12
354	34%	65%	1%	58.7493	0	26.3135	0.1677	0	7.3893	6.9898	0.1812	99.7908	925-1-mf4-13
355	33%	65%	1%	59.2423	0.0076	25.5503	0.1562	0.0108	7.1134	6.9778	0.2593	99.3177	925-1-mf4-14
356	32%	66%	2%	59.1235	0.0016	25.5528	0.2018	0	6.8534	7.0611	0.306	99.1003	925-1-mf4-15
357	36%	63%	1%	58.6389	0.0028	26.2439	0.1707	0.0263	7.5766	6.7565	0.2006	99.6164	925-1-mf4-16
358	37%	62%	1%	58.1689	0	26.3661	0.1332	0	7.7643	6.4597	0.1727	99.0649	925-1-mf4-17
359	37%	62%	1%	58.5363	0	26.23	0.17	0.0128	7.9306	6.5962	0.2185	99.6945	925-1-mf4-18
360	37%	62%	1%	58.359	0	26.4746	0.1383	0.0069	7.8664	6.5631	0.1551	99.5635	925-1-mf4-19
361	36%	63%	1%	58.8845	0.0092	26.3981	0.156	0.0217	7.8372	6.6954	0.2077	100.2098	925-1-mf4-20
Average	36%	63%	1%										
Stdev	2%	2%	0%										

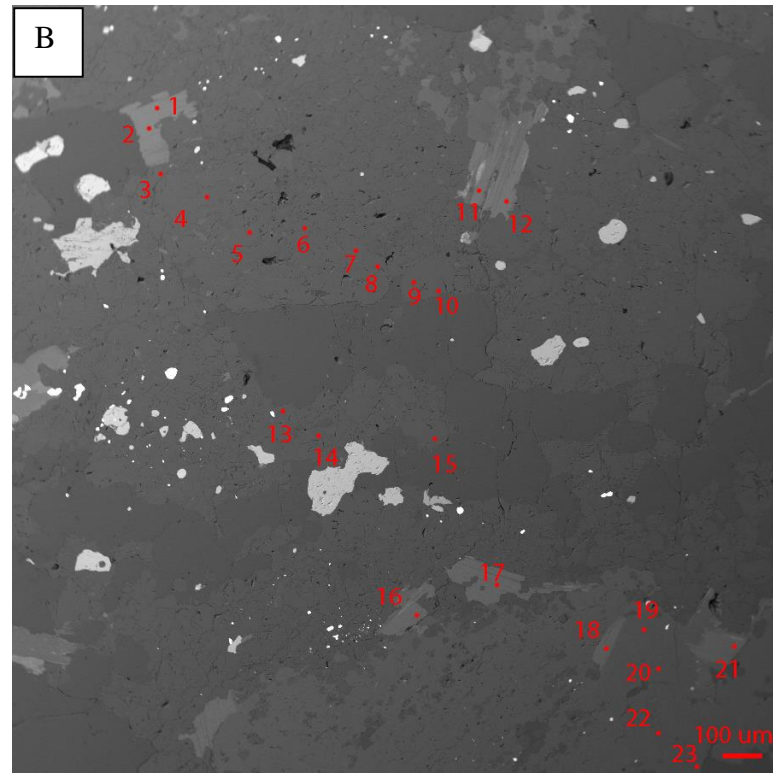
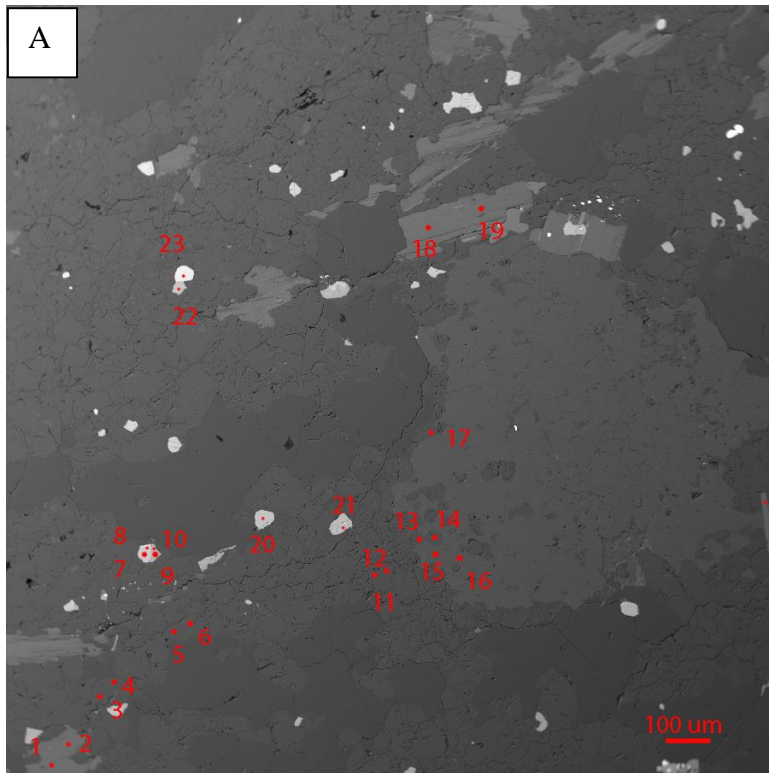


Figure A15 Sample 136-1A. EPMA analysis of various minerals from two areas (A and B). Red dots indicate EPMA targets. Red numbers indicate run number on Table A57.

Table A57 EPMA results of various minerals. Refer to Figure A15 for targets.

Sample 136-A1 EPMA Analysis																			
No.	Location	SiO2	TiO2	Al2O3	Cr2O3	FeO	MnO	MgO	CaO	Na2O	K2O	P2O5	F	Cl	Total	Comment2	An%	Ab%	Or%
19	A-19	65.433	0.051	19.671	0	0.044	0	0	0.143	1.807	13.872	0.059	0.022	0.011	101.102	K-feldspar	1%	16%	83%
20	A-20	64.502	0	19.025	0.006	0.018	0.001	0.012	0.055	1.541	13.998	0	0.044	0.007	99.188	K-feldspar	0%	14%	85%
22	A-22	64.432	0.016	19.511	0	0.022	0	0	0.077	1.441	14.215	0.004	0	0.005	99.722	K-feldspar	0%	13%	86%
23	A-23	64.133	0.023	19.535	0	0.076	0.003	0.005	0.062	1.236	14.345	0.03	0	0.092	99.519	K-feldspar	0%	12%	88%
38	B-15	63.588	0.026	18.563	0	0.068	0.008	0	0.124	1.249	14.15	0.059	0.099	0.015	97.904	K-feldspar	1%	12%	88%
39	B-16	63.49	0.009	19.28	0	0	0.007	0	0.033	1.071	14.562	0.016	0.098	0.001	98.526	K-feldspar	0%	10%	90%
3	A-3	60.23	0.018	26.458	0.017	0.207	0	0.008	7.209	7.726	0.214	0.035	0	0	102.122	Plagioclase	34%	65%	1%
4	A-4	59.775	0.017	26.455	0	0.017	0	0	7.053	7.75	0.132	0.028	0	0.016	101.239	Plagioclase	33%	66%	1%
8	A-8	59.507	0	26.926	0	0.053	0.005	0	7.645	7.56	0.104	0.048	0	0.007	101.853	Plagioclase	36%	64%	1%
17	B-4	59.363	0.034	26.577	0	0.045	0.03	0.006	7.24	7.495	0.179	0.023	0	0.003	100.994	Plagioclase	34%	65%	1%
13	A-13	59.315	0.018	27.082	0	0.018	0	0	7.714	7.106	0.118	0	0	0	101.371	Plagioclase	37%	62%	1%
15	A-15	59.249	0.035	27.088	0	0.147	0	0	7.689	7.289	0.27	0.056	0	0	101.823	Plagioclase	36%	62%	2%
14	A-14	59.162	0.052	26.701	0	0.152	0	0	7.447	7.451	0.234	0.027	0.084	0.011	101.284	Plagioclase	35%	64%	1%
28	B-5	59.139	0.034	26.728	0	0.039	0	0.002	7.623	7.115	0.109	0.029	0	0	100.818	Plagioclase	37%	62%	1%
36	B-13	59.13	0.004	26.914	0.038	0.027	0.012	0	7.909	6.93	0.175	0.009	0.021	0.007	101.165	Plagioclase	38%	61%	1%
9	A-9	59.079	0.028	26.598	0	0.11	0	0	7.447	7.256	0.303	0.039	0.074	0	100.903	Plagioclase	36%	63%	2%
7	A-7	59.023	0.061	26.849	0.016	0.082	0.009	0	7.742	7.207	0.16	0	0.053	0	101.18	Plagioclase	37%	62%	1%
6	A-6	58.791	0.001	26.9	0	0.06	0.005	0.002	7.514	7.558	0.082	0.03	0.126	0.001	101.017	Plagioclase	35%	64%	0%
40	B-17	58.69	0.011	27.327	0	0.074	0	0	7.925	6.769	0.137	0.028	0	0	100.961	Plagioclase	39%	60%	1%
5	A-5	58.493	0.013	26.599	0	0.062	0.018	0.009	7.861	7.101	0.166	0.01	0.021	0	100.344	Plagioclase	38%	61%	1%
10	A-10	58.476	0.022	27.409	0	0.075	0.001	0	7.905	7.146	0.199	0.028	0.053	0.008	101.298	Plagioclase	38%	61%	1%
35	B-12	58.34	0.018	27.338	0.017	0.059	0.032	0	7.825	7.186	0.171	0.011	0	0	100.997	Plagioclase	37%	62%	1%
34	B-11	58.282	0	27.244	0.013	0.105	0	0.013	8.053	6.995	0.175	0.024	0	0	100.904	Plagioclase	38%	61%	1%
37	B-14	58.157	0.013	27.432	0.012	0.1	0	0.005	8.198	6.869	0.145	0.011	0.095	0	100.997	Plagioclase	39%	60%	1%
26	B-3	57.969	0.046	26.973	0.014	0.067	0.019	0.007	8.569	6.847	0.128	0	0	0	100.639	Plagioclase	41%	59%	1%
29	B-6	57.663	0.015	27.685	0.033	0.083	0	0	8.557	6.721	0.146	0	0	0	100.903	Plagioclase	41%	58%	1%
42	B-19	36.847	3.648	16.217	0	18.062	0.188	11.664	0.105	0.2	9.15	0	0.749	0.364	96.797	Biotite			
1	A-1	36.845	4.416	16.292	0.014	17.928	0.231	11.15	0	0.119	9.488	0	0.932	0.319	97.27	Biotite			
17	A-17	36.777	3.605	16.357	0	18.75	0.215	11.179	0	0.145	9.502	0.008	0.848	0.356	97.305	Biotite			
18	A-18	36.574	4.083	16.323	0.003	18.442	0.268	11.019	0.028	0.081	9.363	0	0.899	0.364	96.986	Biotite	An%	0%	0%
12	A-12	36.568	4.301	16.804	0	18.701	0.21	10.93	0.025	0.1	9.391	0	0.75	0.365	97.747	Biotite	Ab%	13%	2%
2	A-2	36.491	4.169	16.359	0	18.571	0.203	11.472	0	0.097	9.645	0	0.769	0.339	97.714	Biotite	Or%	87%	2%
41	B-18	36.49	3.71	16.468	0.029	18.486	0.222	11.112	0.051	0.178	9.412	0.01	0.924	0.365	96.986	Biotite			
11	A-11	36.346	3.678	16.281	0	18.415	0.235	11.293	0.069	0.131	9.42	0	0.757	0.312	96.548	Biotite			
25	B-2	36.318	3.718	16.34	0.026	18.207	0.279	11.592	0.047	0.103	9.428	0.025	0.889	0.357	96.874	Biotite			
24	B-1	36.281	3.753	16.097	0.028	17.443	0.228	11.756	0.036	0.105	9.34	0	0.697	0.312	95.713	Biotite	An%	37%	2%
16	A-16	36.22	3.271	16.249	0.015	18.962	0.266	11.526	0.01	0.148	9.567	0	0.881	0.365	97.027	Biotite	Ab%	62%	2%
21	A-21	35.868	3.674	16.249	0	18.213	0.289	11.224	0	0.15	9.525	0	1.21	0.33	96.149	Biotite	Or%	1%	0%
31	B-8	0.103	0.318	0.227	0.026	95.046	0.032	0.015	0	0	0	0	0	0	95.767	Magnetite			
30	B-7	0.089	0.361	0.265	0.03	94.63	0.034	0.036	0	0.082	0	0	0	0	95.527	Magnetite			
43	B-20	0.073	0.01	0.059	0.074	94.889	0.01	0	0	0	0	0	0	0	95.115	Magnetite			
44	B-21	0.07	0.024	0.108	0.002	94.82	0	0.018	0	0.038	0	0	0	0.005	95.084	Magnetite			
45	B-22	0.07	43.037	0.05	0.027	52.98	2.552	0.021	0.039	0	0	0	0.019	0.006	98.792	Ilmenite			
33	B-10	0.065	44.695	0.026	0.007	50.878	3.205	0.046	0.042	0.008	0.011	0	0	0.007	98.988	Ilmenite			
32	B-9	0.052	45.418	0.028	0	49.8	3.187	0.012	0.023	0.016	0.02	0	0	0	98.556	Ilmenite			

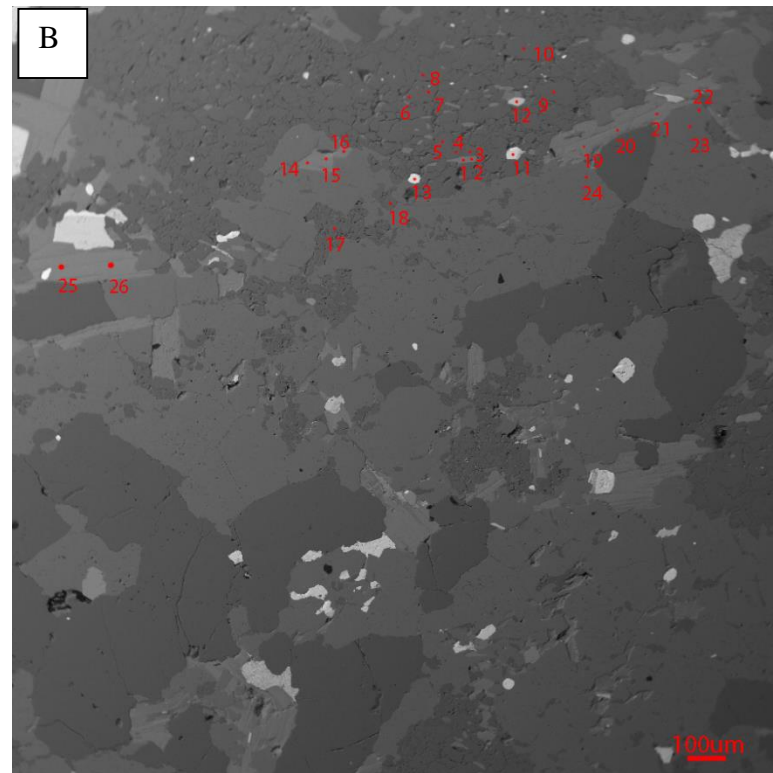
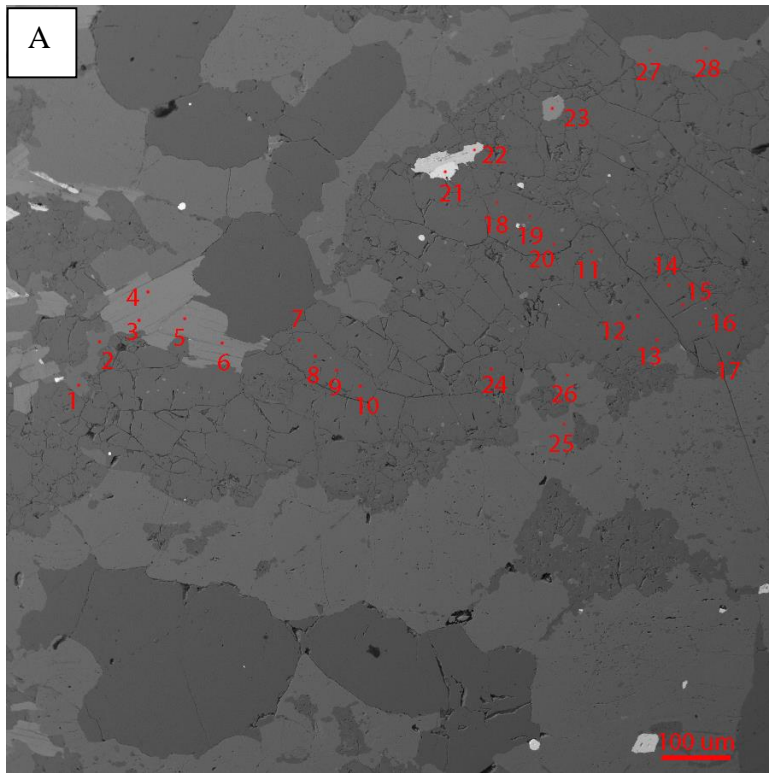


Figure A16 Sample 136-6A. EPMA analysis of various minerals from two areas (A and B). Red dots indicate EPMA targets. Red numbers indicate run number on Table A58.

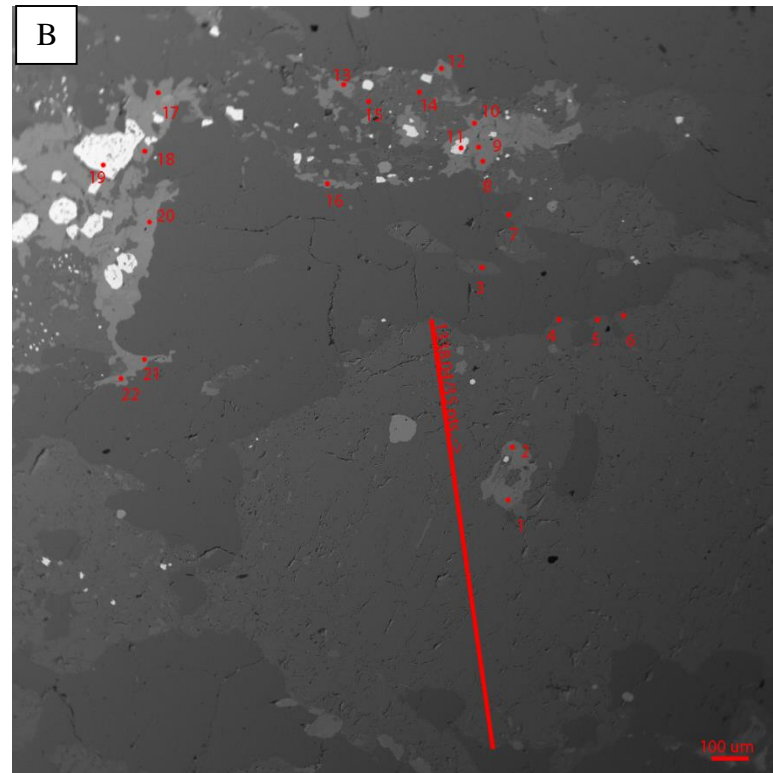
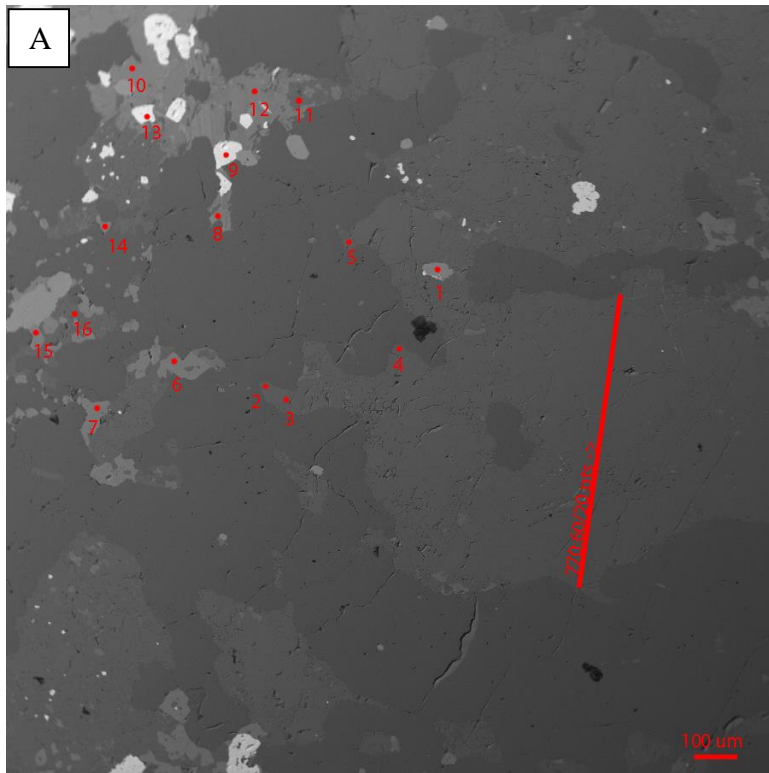


Figure A17 Sample 136-11A. EPMA analysis of various minerals from two areas (A and B). Red dots indicate EPMA targets. Red numbers indicate run number on Tables A59-61. Red line in A and B are EPMA line analysis with the total length of the line followed by the number of points, and the arrow indicates the direction of line analysis. Refer to Table A60 for the line in A, and Table 61 for the line in B.

Table A59 EPMA results of various minerals. Refer to Figure A17 for targets.

Sample 136-11A EPMA Analysis																					
No.	Comment	SiO2	TiO2	Al2O3	Cr2O3	FeO	MnO	MgO	CaO	Na2O	K2O	P2O5	F	Cl	Total	Comment2	An%	Ab%	Or%		
186	B-15	58.333	0.047	27.741	0	0.245	0	0.001	8.501	6.722	0.153	0	0.032	0	101.762	plagioclase	41%	58%	1%		
185	B-14	58.137	0.028	27.723	0.003	0.277	0.005	0	8.504	6.862	0.157	0	0.127	0	101.77	plagioclase	40%	59%	1%		
131	A-11	57.831	0.004	28.213	0.014	0.405	0	0.007	9.011	6.53	0.17	0	0	0.022	102.202	plagioclase	43%	56%	1%		
178	B-7	57.621	0.002	27.015	0.026	0.156	0	0.007	8.153	6.864	0.12	0	0	0.023	99.982	plagioclase	39%	60%	1%		
123	A-3	57.392	0	26.227	0.008	0.172	0.014	0	8.544	6.573	0.194	0.002	0.021	0.003	99.14	plagioclase	41%	58%	1%		
122	A-2	57.285	0	27.966	0.007	0.15	0	0	8.871	6.65	0.198	0	0.021	0	101.139	plagioclase	42%	57%	1%		
136	A-16	56.982	0.007	28.132	0	0.224	0	0.027	9.336	6.361	0.181	0	0	0	101.25	plagioclase	44%	55%	1%		
124	A-4	56.966	0	30.086	0	0.154	0.018	0.005	10.626	6.063	0.147	0	0.055	0	104.097	plagioclase	49%	50%	1%		
176	B-5	56.468	0.002	28.687	0.011	0.155	0.006	0.006	9.952	5.992	0.135	0	0.011	0.001	101.421	plagioclase	47%	52%	1%		
174	B-3	56.166	0	28.813	0.004	0.184	0	0.01	9.993	5.76	0.222	0	0	0.002	101.154	plagioclase	48%	50%	1%		
175	B-4	56.116	0	28.864	0.003	0.139	0.008	0	10.256	5.669	0.153	0	0	0	101.208	plagioclase	50%	50%	1%		
125	A-5	55.92	0	29.153	0	0.171	0	0.002	10.521	5.718	0.151	0	0.032	0.017	101.668	plagioclase	50%	49%	1%		
177	B-6	55.769	0	28.611	0	0.155	0	0	9.594	6.094	0.112	0	0.022	0	100.348	plagioclase	46%	53%	1%		
135	A-15	48.818	0.301	5.956	0	15.28	0.772	12.928	11.839	0.698	0.449	0.031	0.228	0.097	97.279	amphibole					
130	A-10	48.793	0.561	6.458	0	15.29	0.704	13.312	11.903	0.739	0.498	0.021	0.06	0.097	98.389	amphibole					
126	A-6	48.76	0.189	6.403	0.017	15.346	0.778	13.452	11.873	0.778	0.448	0	0.198	0.06	98.205	amphibole	Plagioclase (total)				
127	A-7	48.384	0.321	6.751	0.001	15.605	0.793	12.959	11.876	0.794	0.471	0	0	0.087	98.022	amphibole	0%	Average	Stdev		
183	B-12	48.177	0.592	6.098	0	15.759	0.785	12.874	11.946	0.875	0.518	0	0.06	0.137	97.765	amphibole	An%	45%	3%		
192	B-21	47.749	0.539	7.156	0	16.142	0.831	12.495	11.828	0.921	0.498	0	0	0.101	98.237	amphibole	Ab%	53%	3%		
187	B-16	47.36	0.531	7.625	0.016	15.73	0.711	12.231	12.206	0.808	0.594	0.015	0.159	0.125	98.016	amphibole	Or%	2%	3%		
134	A-14	47.271	0.492	7.731	0.03	16.395	0.682	12.103	12.103	0.922	0.614	0	0.099	0.132	98.502	amphibole					
172	B-1	47.055	0.823	7.297	0	16.236	0.772	12.124	12.083	0.792	0.651	0	0.218	0.126	98.057	amphibole					
193	B-22	47.055	0.643	7.585	0.011	16.226	0.704	11.994	12.207	0.766	0.601	0	0	0.131	97.893	amphibole					
180	B-9	46.687	0.712	7.745	0	16.847	0.759	11.92	11.821	0.978	0.685	0	0	0.137	98.26	amphibole					
179	B-8	46.431	0.635	8.231	0.018	16.76	0.713	11.493	12.193	0.853	0.673	0	0.04	0.155	98.143	amphibole					
184	B-13	45.164	0.678	8.902	0.015	16.873	0.697	11.57	11.797	1.192	0.681	0	0.108	0.136	97.737	amphibole					
173	B-2	43.035	1.117	10.315	0	17.949	0.718	10.429	12.252	1	1.081	0	0.265	0.228	98.226	amphibole					
128	A-8	36.428	2.857	15.134	0.002	19.622	0.313	11.494	0	0.102	9.051	0.001	0.399	0.284	95.455	biotite					
189	B-18	36.411	4.905	14.854	0	18.897	0.32	10.835	1.24	0.062	8.723	0	0.153	0.264	96.54	biotite					
191	B-20	36.305	3.15	15.266	0.034	19.386	0.281	11.673	0	0.138	9.164	0	0.159	0.309	95.728	biotite					
188	B-17	36.259	4.182	15.298	0	20.364	0.329	10.774	0	0.06	9.066	0	0.122	0.286	96.624	biotite					
181	B-10	36.015	3.594	14.974	0	19.26	0.241	10.828	0.016	0.074	9.051	0.008	0.16	0.268	94.362	biotite					
121	A-1	0.089	0	0.015	0	0.109	0.123	0.027	56.903	0	0	41.155	4.05	0.556	101.197	apatite					
182	B-11	0.064	0.133	0.128	0.025	95.351	0.061	0.009	0	0.01	0	0	0	0	95.781	magnetite					
190	B-19	0.064	0.043	0.258	0.023	95.239	0.046	0.016	0	0	0.014	0	0	0.008	95.709	magnetite					
129	A-9	0.06	0.171	0.076	0	94.514	0.02	0	0	0.01	0.011	0	0	0.01	94.87	magnetite					

Table A60 EPMA results of plagioclase line A. Refer to Figure A17 for targets.

Sample 136-11A EPMA Plagioclase Analysis Line A																				
No.	Comment	SiO2	TiO2	Al2O3	Cr2O3	FeO	MnO	MgO	CaO	Na2O	K2O	P2O5	F	Cl	Total	Comment2	An%	Ab%	Or%	
101	Line 1 A	54.773	0	28.923	0	0.124	0	0	9.984	6.027	0.115	0	0	0.013	99.956	plagioclase	47%	52%	1%	
102	Line 2 A	56.762	0.015	28.67	0.017	0.183	0.01	0	9.657	5.815	0.154	0	0.011	0.047	101.325	plagioclase	47%	52%	1%	
103	Line 3 A	56.144	0	28.522	0	0.19	0.009	0	10.142	5.794	0.173	0	0.096	0	101.03	plagioclase	49%	50%	1%	
104	Line 4 A	56.363	0.001	28.546	0	0.151	0	0.015	9.896	5.755	0.236	0.001	0	0.002	100.966	plagioclase	48%	51%	1%	
105	Line 5 A	56.593	0.004	28.528	0	0.177	0.005	0.024	9.66	5.927	0.294	0	0	0.007	101.217	plagioclase	47%	52%	2%	
107	Line 7 A	56.933	0	28.29	0	0.145	0	0	9.485	5.891	0.336	0	0	0	101.08	plagioclase	46%	52%	2%	
108	Line 8 A	58.196	0.013	26.62	0	0.12	0	0.63	5.821	5.182	0.78	0	0	0.005	97.366	plagioclase	36%	58%	6%	
109	Line 9 A	56.843	0.04	28.621	0	0.164	0	0.003	9.462	6.188	0.261	0	0.011	0	101.588	plagioclase	45%	53%	1%	
110	Line 10 A	56.96	0.06	28.148	0	0.139	0.011	0.004	9.49	6.176	0.284	0	0	0.005	101.276	plagioclase	45%	53%	2%	
111	Line 11 A	57.102	0	28.38	0.026	0.153	0.035	0	9.421	6.36	0.184	0.02	0.011	0.016	101.699	plagioclase	45%	54%	1%	
112	Line 12 A	57.022	0	28.266	0	0.117	0.017	0	9.361	6.126	0.237	0	0.032	0.027	101.186	plagioclase	45%	53%	1%	
113	Line 13 A	56.936	0.063	28.111	0	0.186	0.005	0	9.17	6.284	0.184	0	0	0.012	100.948	plagioclase	44%	55%	1%	
114	Line 14 A	56.491	0.015	28.209	0	0.096	0	0.011	9.59	6.042	0.312	0.003	0	0.071	100.824	plagioclase	46%	52%	2%	
115	Line 15 A	56.887	0	28.435	0.005	0.125	0.008	0.029	9.598	5.868	0.342	0	0	0	101.297	plagioclase	47%	51%	2%	
116	Line 16 A	56.241	0.028	27.945	0	0.118	0.014	0.012	9.266	5.887	0.323	0	0	0.007	99.839	plagioclase	46%	52%	2%	
117	Line 17 A	57.072	0.02	28.237	0.01	0.144	0	0.004	9.423	6.004	0.307	0	0	0	101.221	plagioclase	46%	53%	2%	
118	Line 18 A	57	0	28.477	0	0.143	0	0	9.217	6.194	0.28	0	0	0.01	101.319	plagioclase	44%	54%	2%	
119	Line 19 A	57.243	0.006	28.098	0	0.145	0.026	0.016	9.645	6.153	0.291	0.007	0.054	0.006	101.666	plagioclase	46%	53%	2%	
120	Line 20 A	55.556	0	27.836	0	0.128	0.029	0.018	9.986	5.735	0.194	0.011	0	0.002	99.495	plagioclase	48%	50%	1%	
																	Average	46%	53%	2%
																	Stdev	3%	2%	1%

Table A61 EPMA results of plagioclase line B. Refer to Figure A17 for targets.

Sample 136-11A EPMA Plagioclase Analysis Line B																			
No.	Comment	SiO2	TiO2	Al2O3	Cr2O3	FeO	MnO	MgO	CaO	Na2O	K2O	P2O5	F	Cl	Total	Comment2	An%	Ab%	Or%
137	Line 1 B	56.569	0	28.154	0.016	0.121	0.029	0.011	9.915	5.899	0.225	0	0	0	100.939	plagioclase	48%	51%	1%
138	Line 2 B	56.309	0.021	27.953	0	0.172	0.002	0.03	9.619	5.908	0.279	0	0.011	0.005	100.303	plagioclase	47%	52%	2%
139	Line 3 B	56.053	0.027	27.415	0.007	0.262	0.032	0.401	8.661	5.077	0.379	0.002	0.022	0	98.329	plagioclase	47%	50%	2%
140	Line 4 B	57.11	0.014	28.682	0.01	0.228	0.02	0.001	9.532	6.113	0.282	0	0.021	0.008	102.01	plagioclase	46%	53%	2%
141	Line 5 B	55.792	0	27.107	0.019	0.133	0	0.009	8.592	6.287	0.325	0	0	0.014	98.275	plagioclase	42%	56%	2%
142	Line 6 B	57.285	0	27.902	0.004	0.116	0.024	0	8.709	6.762	0.123	0.003	0	0.007	100.933	plagioclase	41%	58%	1%
143	Line 7 B	56.862	0	27.05	0.012	0.159	0	0.005	8.164	5.896	1.707	0	0.021	0.005	99.871	plagioclase	39%	51%	10%
144	Line 8 B	56.893	0.02	27.709	0	0.148	0.022	0.015	9.037	6.497	0.141	0.017	0	0.024	100.518	plagioclase	43%	56%	1%
145	Line 9 B	56.806	0.022	27.626	0	0.162	0.01	0.01	9.253	6.439	0.187	0	0.139	0.021	100.611	plagioclase	44%	55%	1%
146	Line 10 B	56.204	0	27.672	0	0.164	0	0.048	9.036	5.851	0.258	0	0	0.025	99.252	plagioclase	45%	53%	2%
147	Line 11 B	57.088	0.008	28.161	0.028	0.183	0.003	0.012	9.352	6.461	0.301	0.001	0.075	0.011	101.65	plagioclase	44%	55%	2%
148	Line 12 B	56.935	0	28.083	0	0.139	0	0.001	9.505	5.99	0.255	0	0	0	100.908	plagioclase	46%	52%	1%
149	Line 13 B	56.492	0.048	28.356	0	0.15	0.011	0	9.605	5.903	0.271	0	0	0.001	100.837	plagioclase	47%	52%	2%
150	Line 14 B	57.137	0.019	28.257	0	0.174	0.032	0.099	9.228	6.207	0.272	0.035	0	0.004	101.463	plagioclase	44%	54%	2%
151	Line 15 B	56.855	0.013	28.5	0	0.175	0.046	0.027	9.491	6.302	0.313	0	0	0	101.722	plagioclase	45%	54%	2%
152	Line 16 B	57.25	0	28.201	0	0.138	0.017	0.001	9.173	5.915	0.242	0	0.032	0.002	100.958	plagioclase	45%	53%	1%
153	Line 17 B	56.807	0	27.881	0.011	0.169	0	0.006	9.432	5.999	0.274	0	0	0.003	100.581	plagioclase	46%	53%	2%
154	Line 18 B	56.648	0.004	28.273	0.002	0.145	0.035	0.017	9.362	6.122	0.243	0	0.096	0	100.907	plagioclase	45%	53%	1%
155	Line 19 B	56.986	0	28.338	0.009	0.207	0.006	0.015	9.383	6.327	0.234	0	0.054	0.008	101.542	plagioclase	44%	54%	1%
156	Line 20 B	56.969	0	28.283	0	0.149	0	0.007	9.326	6.159	0.212	0	0.107	0	101.167	plagioclase	45%	54%	1%
157	Line 21 B	56.837	0.03	28.097	0	0.127	0	0.021	9.034	6.159	0.298	0	0	0.022	100.62	plagioclase	44%	54%	2%
158	Line 22 B	56.821	0.008	28.418	0	0.135	0.011	0.009	9.423	5.867	0.281	0.009	0	0	100.982	plagioclase	46%	52%	2%
159	Line 23 B	57.649	0	28.695	0.023	0.159	0	0	9.54	6.287	0.275	0	0.022	0	102.641	plagioclase	45%	54%	2%
160	Line 24 B	57.083	0	28.01	0.024	0.128	0.005	0	9.165	6.03	0.262	0	0	0.005	100.711	plagioclase	45%	54%	2%
161	Line 25 B	57.688	0	27.621	0.011	0.116	0.023	0	8.845	6.586	0.188	0	0.011	0.014	101.095	plagioclase	42%	57%	1%
162	Line 26 B	56.568	0.002	28.313	0	0.108	0.014	0	9.447	6.173	0.292	0	0.064	0.001	100.955	plagioclase	45%	53%	2%
163	Line 27 B	56.773	0.024	28.027	0	0.145	0	0.003	9.469	6.021	0.27	0.01	0.064	0	100.779	plagioclase	46%	53%	2%
164	Line 28 B	57.204	0	26.717	0.011	0.154	0.017	0.008	8.018	3.713	4.631	0	0.087	0.008	100.529	plagioclase	40%	33%	27%
165	Line 29 B	56.464	0	28.408	0.001	0.192	0.014	0.012	9.569	6.008	0.216	0	0	0	100.884	plagioclase	46%	53%	1%
166	Line 30 B	54.984	0	27.952	0.018	0.155	0	0	9.572	5.883	0.201	0	0	0.009	98.772	plagioclase	47%	52%	1%
167	Line 31 B	56.828	0.01	28.587	0	0.133	0.046	0	9.657	5.952	0.201	0	0	0	101.414	plagioclase	47%	52%	1%
168	Line 32 B	55.766	0	28.469	0	0.098	0	0.012	9.969	6.06	0.165	0	0.043	0.003	100.566	plagioclase	47%	52%	1%
169	Line 33 B	56.906	0.001	28.371	0	0.091	0	0	9.262	6.403	0.183	0	0	0.002	101.219	plagioclase	44%	55%	1%
170	Line 34 B	57.638	0.022	27.238	0	0.096	0.005	0	8.65	6.705	0.137	0	0.043	0.007	100.521	plagioclase	41%	58%	1%
171	Line 35 B	55.935	0	29.139	0	0.167	0	0.001	10.297	5.692	0.127	0	0.086	0.001	101.409	plagioclase	50%	50%	1%
																Average	45%	53%	2%
																Stdev	2%	4%	5%

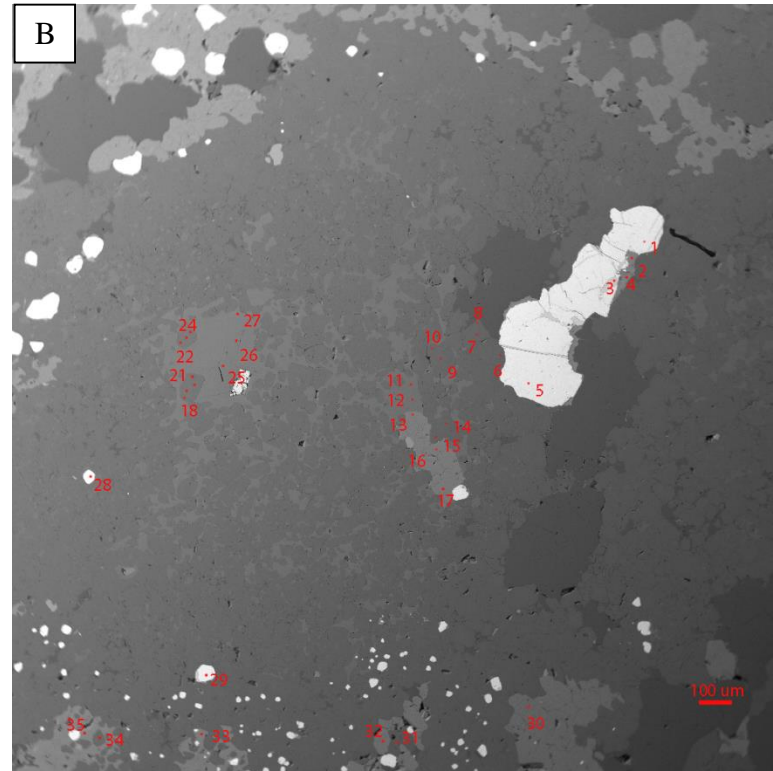
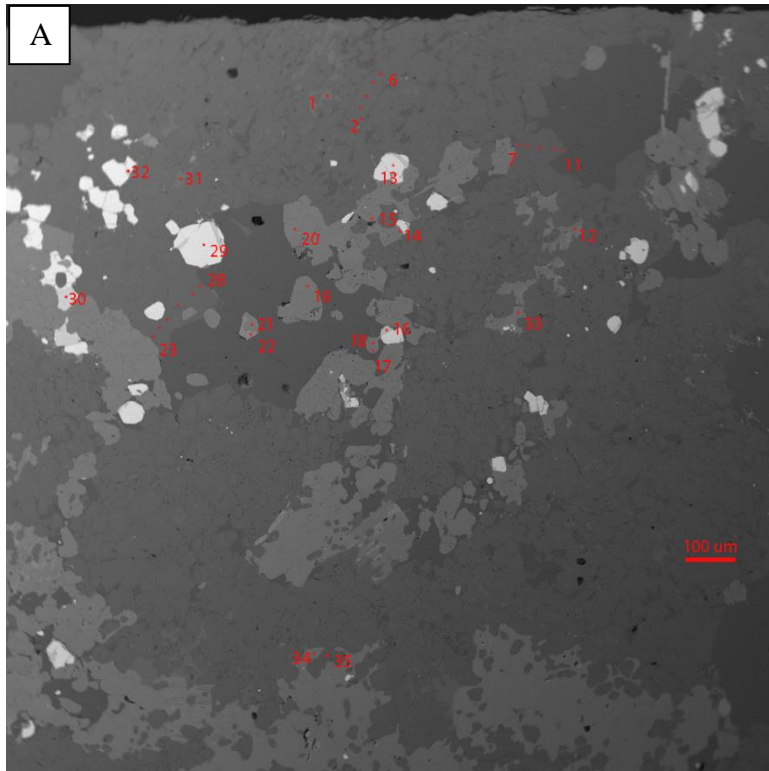


Figure A18 Sample 136-2B. EPMA analysis of various minerals from two areas (A and B). Red dots indicate EPMA targets. Red numbers indicate run number on Table A62.

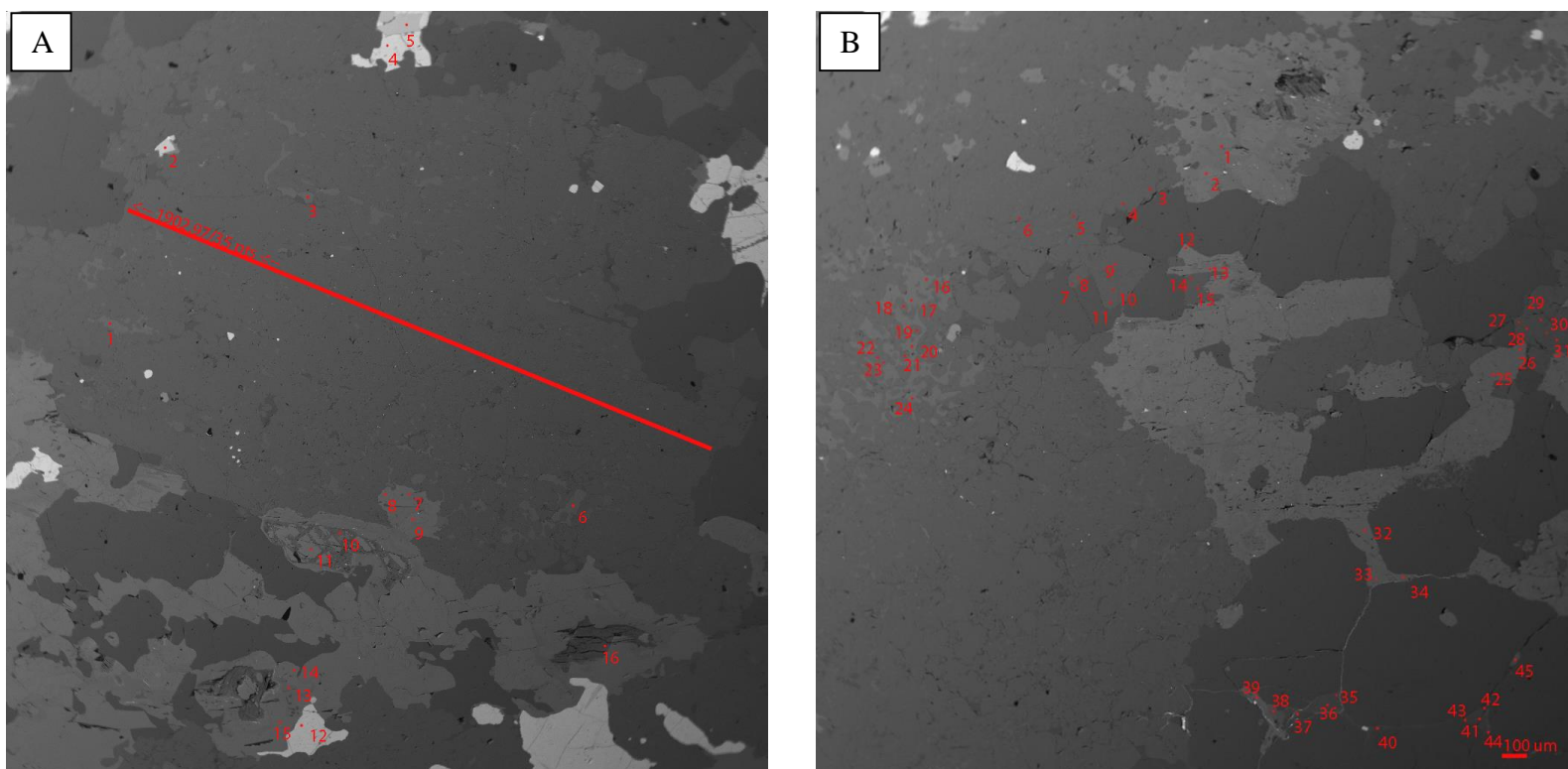


Figure A19 Sample 136-8B. EPMA analysis of various minerals from two areas (A and B). Red dots indicate EPMA targets. Red numbers indicate run number on Tables A63-64 Red line in A are EPMA line analysis with the total length of the line followed by the number of points, and the arrow indicates the direction of line analysis. Refer to Table A64 for the line in A.

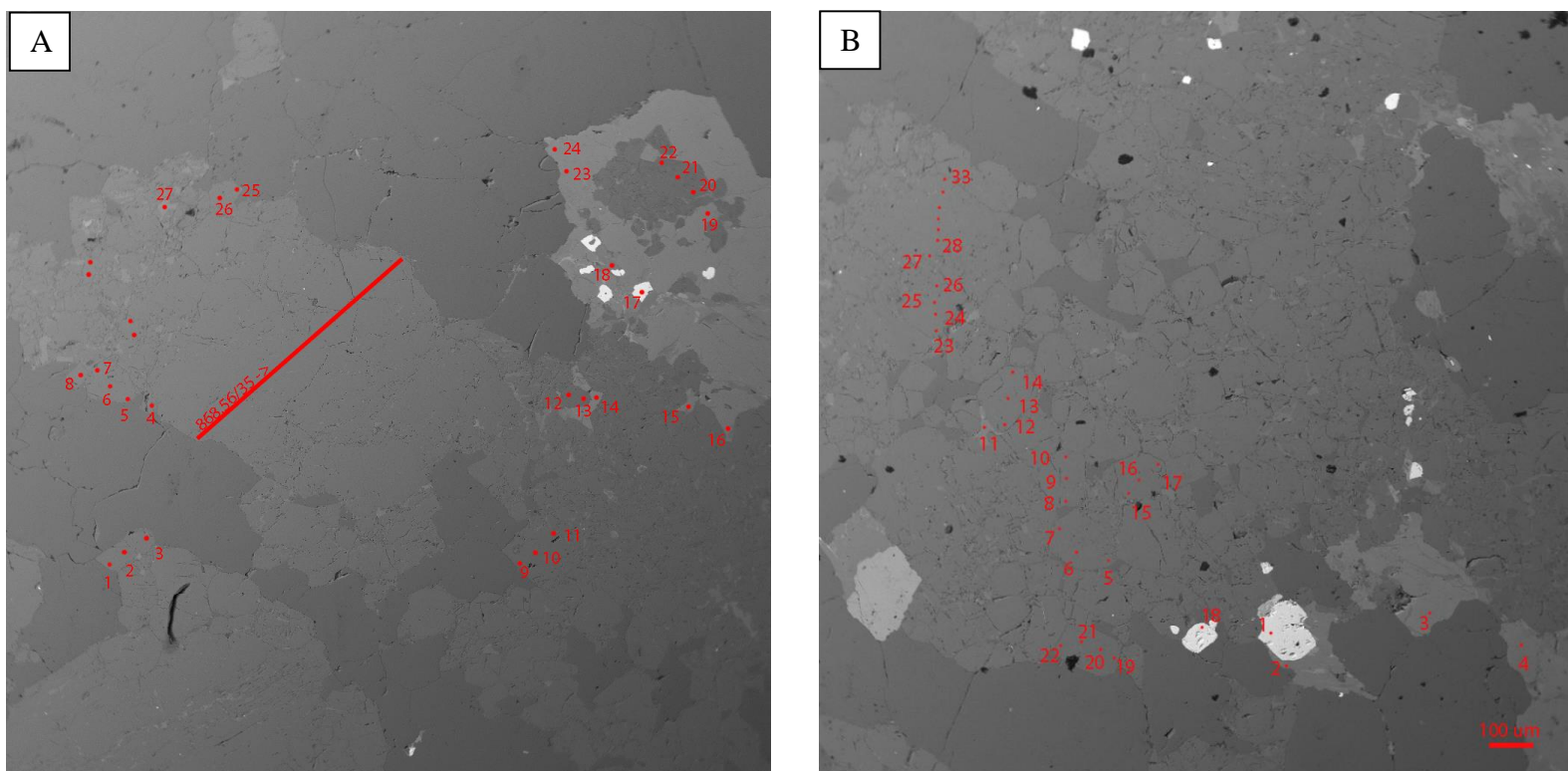


Figure A20 Sample 136-14B. EPMA analysis of various minerals from two areas (A and B). Red dots indicate EPMA targets. Red numbers indicate run number on Tables A65-66 Red line in A are EPMA line analysis with the total length of the line followed by the number of points, and the arrow indicates the direction of line analysis. Refer to Table A66 for the line in A.

Table A66 EPMA results of plagioclase Line A. Refer to Figure A20 for targets.

Sample 136-14B Plagioclase EPMA Analysis Line A																			
No.	Comment	SiO2	TiO2	Al2O3	Cr2O3	FeO	MnO	MgO	CaO	Na2O	K2O	P2O5	F	Cl	Total	Comment2	An%	Ab%	Or%
1	Line 1 A	57.906	0.02	27.502	0.045	0.222	0.031	0.018	8.508	6.796	0.361	0.006	0.157	0	101.506	plagioclase	40%	58%	2%
2	Line 2 A	58.975	0.003	26.833	0.002	0.23	0.007	0.004	7.716	6.249	1.344	0	0.032	0	101.382	plagioclase	37%	55%	8%
3	Line 3 A	57.913	0	27.328	0	0.298	0.02	0.004	8.677	6.719	0.29	0	0.01	0	101.255	plagioclase	41%	57%	2%
4	Line 4 A	56.519	0.014	26.437	0.003	0.302	0	0	8.914	6.384	0.622	0	0	0.007	99.2	plagioclase	42%	54%	3%
5	Line 5 A	58.141	0.009	27.402	0.011	0.288	0	0.003	8.64	6.624	0.312	0	0	0	101.43	plagioclase	41%	57%	2%
6	Line 6 A	58.215	0	27.157	0	0.305	0	0.021	8.527	6.734	0.266	0	0.042	0.009	101.256	plagioclase	41%	58%	2%
7	Line 7 A	58.058	0	27.377	0	0.29	0	0	8.354	6.709	0.408	0	0	0.001	101.197	plagioclase	40%	58%	2%
8	Line 8 A	57.637	0.034	27.05	0.023	0.302	0	0.024	8.311	6.518	0.398	0	0.116	0	100.364	plagioclase	40%	57%	2%
9	Line 9 A	58.837	0.033	28.149	0	0.17	0	0	8.66	6.831	0.493	0	0	0.018	103.187	plagioclase	40%	57%	3%
10	Line 10 A	56.736	0	26.335	0	0.278	0.03	0.037	7.896	6.23	0.799	0	0.105	0.033	98.428	plagioclase	39%	56%	5%
11	Line 11 A	58.218	0.025	27.324	0.019	0.304	0	0.001	8.365	6.708	0.396	0	0	0.011	101.369	plagioclase	40%	58%	2%
12	Line 12 A	59.212	0	27.723	0	0.274	0	0.013	8.626	6.788	0.421	0	0.139	0	103.137	plagioclase	40%	57%	2%
13	Line 13 A	59.096	0	27.644	0	0.27	0	0.014	8.961	6.512	0.261	0	0.011	0	102.764	plagioclase	43%	56%	1%
14	Line 14 A	58.108	0	26.984	0.008	0.296	0.013	0.008	8.397	6.404	0.406	0	0.031	0.008	100.648	plagioclase	41%	57%	2%
15	Line 15 A	58.076	0	26.97	0.006	0.298	0.026	0.004	8.322	6.477	0.455	0	0	0.005	100.638	plagioclase	40%	57%	3%
16	Line 16 A	58.11	0	26.681	0	0.296	0	0.02	8.289	6.467	0.486	0	0.147	0	100.434	plagioclase	40%	57%	3%
17	Line 17 A	58.044	0.039	27.058	0.02	0.284	0.031	0.002	8.352	6.443	0.514	0	0.116	0.009	100.861	plagioclase	40%	57%	3%
18	Line 18 A	58.299	0.012	26.571	0.011	0.27	0	0.018	8.255	6.586	0.494	0	0	0	100.516	plagioclase	40%	57%	3%
19	Line 19 A	58.222	0	27.135	0.005	0.285	0	0.004	8.304	6.476	0.453	0	0	0	100.884	plagioclase	40%	57%	3%
20	Line 20 A	58.396	0	26.811	0	0.307	0.021	0.017	8.379	6.682	0.498	0	0.063	0	101.147	plagioclase	40%	57%	3%
21	Line 21 A	58.246	0	26.702	0	0.304	0	0.024	8.425	6.457	0.489	0	0	0	100.647	plagioclase	41%	56%	3%
22	Line 22 A	58.12	0	27.085	0	0.26	0.009	0.008	8.391	6.624	0.477	0	0	0.001	100.975	plagioclase	40%	57%	3%
23	Line 23 A	58.062	0	26.385	0.01	0.301	0.024	0.024	8.371	6.488	0.491	0	0.01	0	100.162	plagioclase	40%	57%	3%
24	Line 24 A	58.417	0	26.555	0	0.275	0.004	0.348	8.062	6.077	0.495	0	0.095	0	100.288	plagioclase	41%	56%	3%
25	Line 25 A	58.046	0.005	27.336	0.003	0.303	0.037	0.07	8.423	6.449	0.432	0	0	0	101.104	plagioclase	41%	57%	2%
26	Line 26 A	58.375	0.003	27.06	0.007	0.271	0	0	8.44	6.622	0.362	0	0	0.018	101.154	plagioclase	40%	57%	2%
27	Line 27 A	57.818	0	26.802	0	0.332	0	0.011	8.451	6.495	0.46	0	0.042	0	100.393	plagioclase	41%	57%	3%
28	Line 28 A	56.931	0	26.688	0.003	0.326	0	0.22	8.002	6.141	0.382	0	0.084	0.006	98.747	plagioclase	41%	57%	2%
29	Line 29 A	57.894	0	27.248	0	0.301	0.001	0	8.523	6.623	0.377	0	0	0.005	100.971	plagioclase	41%	57%	2%
30	Line 30 A	58.184	0	27.128	0.007	0.304	0	0.028	8.459	6.56	0.387	0	0	0	101.057	plagioclase	41%	57%	2%
31	Line 31 A	58.078	0.049	27.08	0	0.307	0.003	0.018	8.541	6.506	0.33	0.011	0	0.014	100.934	plagioclase	41%	57%	2%
32	Line 32 A	57.81	0.006	27.439	0.017	0.283	0	0.029	8.582	6.62	0.372	0	0.074	0	101.201	plagioclase	41%	57%	2%
33	Line 33 A	57.872	0.03	27.204	0	0.281	0	0.01	8.676	6.575	0.361	0	0.074	0.009	101.059	plagioclase	41%	57%	2%
34	Line 34 A	57.379	0.018	27.172	0	0.268	0.012	0.028	8.672	6.429	0.278	0	0	0.005	100.26	plagioclase	42%	56%	2%
35	Line 35 A	57.966	0.013	27.623	0.002	0.289	0	0.013	8.917	6.536	0.279	0	0.074	0.001	101.682	plagioclase	42%	56%	2%
																Average	41%	57%	3%
																Stdev	1%	1%	1%

Appendix C

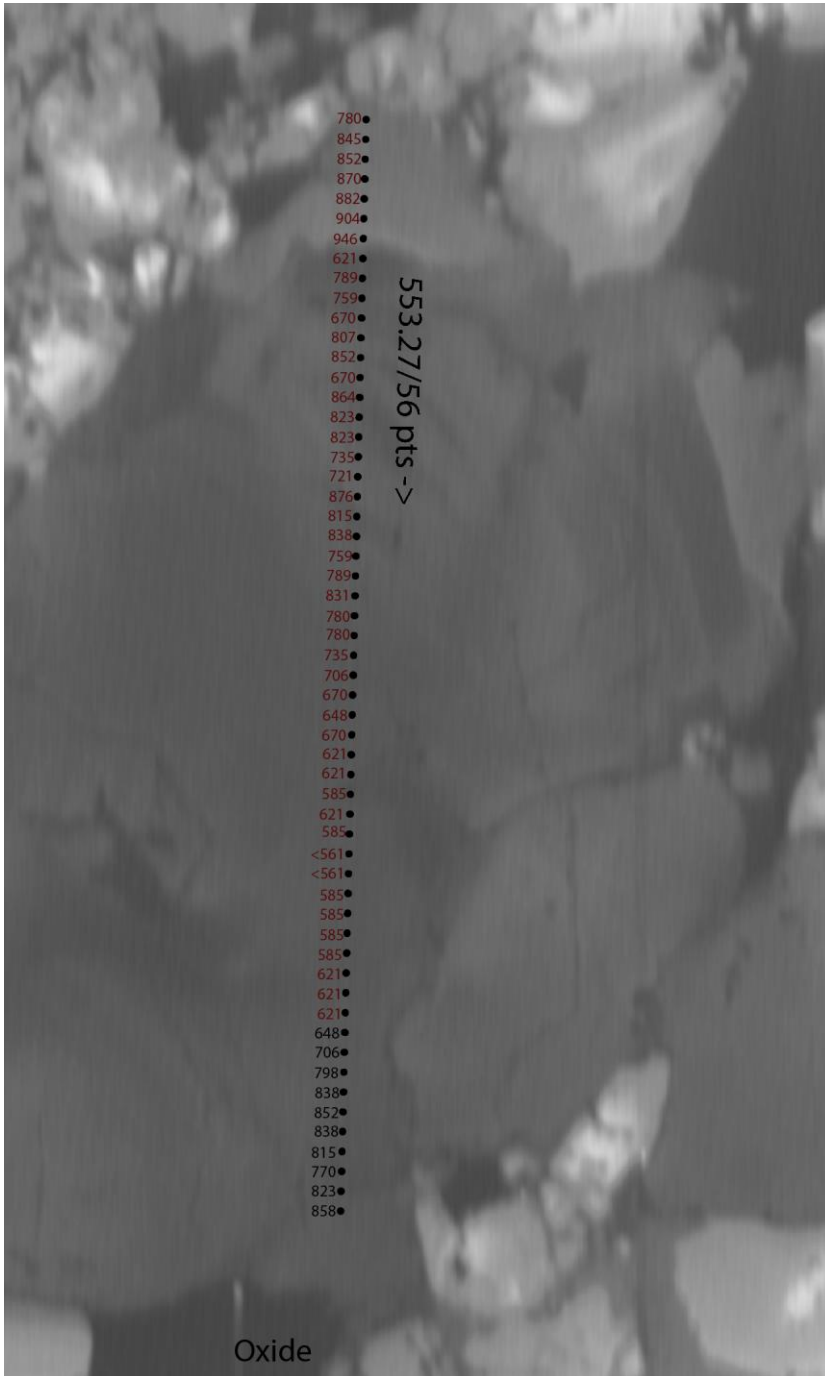


Figure A21 EPMA capture of site 1A on Sample 136-1A. Each black dot is a point analyzed for Ti concentration followed by the TitaniQ result at $a\text{TiO}_2 = 0.6$. Red numbers represent good data, while black numbers represent targets that are too close to an oxide for accurate analysis. The length of the traverse is $553.27\mu\text{m}$ and has 56 points. The arrow indicates the direction of the traverse. Table A67 has the corresponding EPMA and TitaniQ data.

Table A67 EPMA and TitaniQ results for Figure A21. No. 45 corresponds with the uppermost point on Figure A21. Oxide! refers to a point too close to an oxide for accurate analysis. BDL = Below Detection Limit.

Sample 136-1A TitaniQ Temperatuers Site 1A									
No.	TiO2 (wt. %)	TiO2(ppm)	Ti (ppm)	SiO2 (wt. %)	Total	Comment	Comment2	Comment3	T (°C)
45	0.013	130	78	100	100.013	1 Site 1A	rim		780
46	0.021	210	126	100	100.021	2 Site 1A	rim		845
47	0.022	220	132	100	100.022	3 Site 1A	rim		852
48	0.025	250	150	100	100.025	4 Site 1A	rim		870
49	0.027	270	162	100	100.027	5 Site 1A	rim		882
50	0.031	310	186	100	100.031	6 Site 1A	rim		904
51	0.04	400	240	100	100.04	7 Site 1A	rim		946
52	0.003	30	18	100	100.003	8 Site 1A	core		621
53	0.014	140	84	100	100.014	9 Site 1A	core		789
54	0.011	110	66	100	100.011	10 Site 1A	core		759
55	0.005	50	30	100	100.005	11 Site 1A	core		670
56	0.016	160	96	100	100.016	12 Site 1A	core		807
57	0.022	220	132	100	100.022	13 Site 1A	core		852
58	0.005	50	30	100	100.005	14 Site 1A	core		670
59	0.024	240	144	100	100.024	15 Site 1A	core		864
60	0.018	180	108	100	100.018	16 Site 1A	core		823
61	0.018	180	108	100	100.018	17 Site 1A	core		823
62	0.009	90	54	100	100.009	18 Site 1A	core		735
63	0.008	80	48	100	100.008	19 Site 1A	core		721
64	0.026	260	156	100	100.026	20 Site 1A	core		876
65	0.017	170	102	100	100.017	21 Site 1A	core		815
66	0.02	200	120	100	100.02	22 Site 1A	core		838
67	0.011	110	66	100	100.011	23 Site 1A	core		759
68	0.014	140	84	100	100.014	24 Site 1A	core		789
69	0.019	190	114	100	100.019	25 Site 1A	core		831
70	0.013	130	78	100	100.013	26 Site 1A	core		780
71	0.013	130	78	100	100.013	27 Site 1A	core		780
72	0.009	90	54	100	100.009	28 Site 1A	core		735
73	0.007	70	42	100	100.007	29 Site 1A	core		706
74	0.005	50	30	100	100.005	30 Site 1A	core		670
75	0.004	40	24	100	100.004	31 Site 1A	core		648
76	0.005	50	30	100	100.005	32 Site 1A	core		670
77	0.003	30	18	100	100.003	33 Site 1A	core		621
78	0.003	30	18	100	100.003	34 Site 1A	core		621
79	0.002	20	12	100	100.002	35 Site 1A	core		585
80	0.003	30	18	100	100.003	36 Site 1A	core		621
81	0.002	20	12	100	100.002	37 Site 1A	core		585
82	0.001	10	6	100	100.001	38 Site 1A	core	BDL	<561
83	0.001	10	6	100	100.001	39 Site 1A	core	BDL	<561
84	0.002	20	12	100	100.002	40 Site 1A	core		585
85	0.002	20	12	100	100.002	41 Site 1A	core		585
86	0.002	20	12	100	100.002	42 Site 1A	core		585
87	0.002	20	12	100	100.002	43 Site 1A	core		585
88	0.003	30	18	100	100.003	44 Site 1A	core		621
89	0.003	30	18	100	100.003	45 Site 1A	core		621
90	0.003	30	18	100	100.003	46 Site 1A	core		621
91	0.004	40	24	100	100.004	47 Site 1A	Oxide!		648
92	0.007	70	42	100	100.007	48 Site 1A	Oxide!		706
93	0.015	150	90	100	100.015	49 Site 1A	Oxide!		798
94	0.02	200	120	100	100.02	50 Site 1A	Oxide!		838
95	0.022	220	132	100	100.022	51 Site 1A	Oxide!		852
96	0.02	200	120	100	100.02	52 Site 1A	Oxide!		838
97	0.017	170	102	100	100.017	53 Site 1A	Oxide!		815
98	0.012	120	72	100	100.012	54 Site 1A	Oxide!		770
99	0.018	180	108	100	100.018	55 Site 1A	Oxide!		823
100	0.023	230	138	100	100.023	56 Site 1A	Oxide!		858



Figure A22 EPMA capture of site 5A on Sample 136-1A. Each black dot is a point analyzed for Ti concentration followed by the TitaniQ result at $a\text{TiO}_2 = 0.6$. Red numbers represent good data, while black numbers represent targets that are too close to an oxide for accurate analysis. The length of the traverse is $266.01\mu\text{m}$ and has 27 points. The arrow indicates the direction of the traverse. Table A68 has the corresponding EPMA and TitaniQ data.

Table A68 EPMA and TitaniQ results for Figure A22. No. 101 corresponds with the lowermost point on Figure A22. Oxide! refers to a point too close to an oxide for accurate analysis.

Sample 136-1A TitaniQ Temperatures Site 5A									
No.	TiO2 (wt. %)	TiO2(ppm)	Ti(ppm)	SiO2 (wt. %)	Total	Comment	Comment2	Comment3	T (°C)
101	0.893	8930	5352	100	100.893	Line 1 136A-5	Oxide!		1891
102	0.171	1710	1025	100	100.171	Line 2 136A-5	Oxide!		1259
103	0.103	1030	617	100	100.103	Line 3 136A-5	Oxide!		1133
104	0.075	750	450	100	100.075	Line 4 136A-5	Oxide!		1064
105	0.07	700	420	100	100.07	Line 5 136A-5	Oxide!		1050
106	0.045	450	270	100	100.045	Line 6 136A-5	Oxide!		967
107	0.02	200	120	100	100.02	Line 7 136A-5	core		838
108	0.008	80	48	100	100.008	Line 8 136A-5	core		721
109	0.007	70	42	100	100.007	Line 9 136A-5	core		706
110	0.009	90	54	100	100.009	Line 10 136A-5	mix		735
111	0.034	340	204	100	100.034	Line 11 136A-5	rim		919
112	0.035	350	210	100	100.035	Line 12 136A-5	rim		924
113	0.027	270	162	100	100.027	Line 13 136A-5	rim		882
114	0.021	210	126	100	100.021	Line 14 136A-5	rim		845
115	0.022	220	132	100	100.022	Line 15 136A-5	rim		852
116	0.024	240	144	100	100.024	Line 16 136A-5	rim		864
117	0.03	300	180	100	100.03	Line 17 136A-5	rim		899
118	0.021	210	126	100	100.021	Line 18 136A-5	rim		845
119	0.019	190	114	100	100.019	Line 19 136A-5	rim		831
120	0.018	180	108	100	100.018	Line 20 136A-5	rim		823
121	0.015	150	90	100	100.015	Line 21 136A-5	rim		798
122	0.014	140	84	100	100.014	Line 22 136A-5	rim		789
123	0.016	160	96	100	100.016	Line 23 136A-5	rim		807
124	0.009	90	54	100	100.009	Line 24 136A-5	rim		735
125	0.008	80	48	100	100.008	Line 25 136A-5	rim		721
126	0.014	140	84	100	100.014	Line 26 136A-5	rim		789
127	0.006	60	36	100	100.006	Line 27 136A-5	rim		689

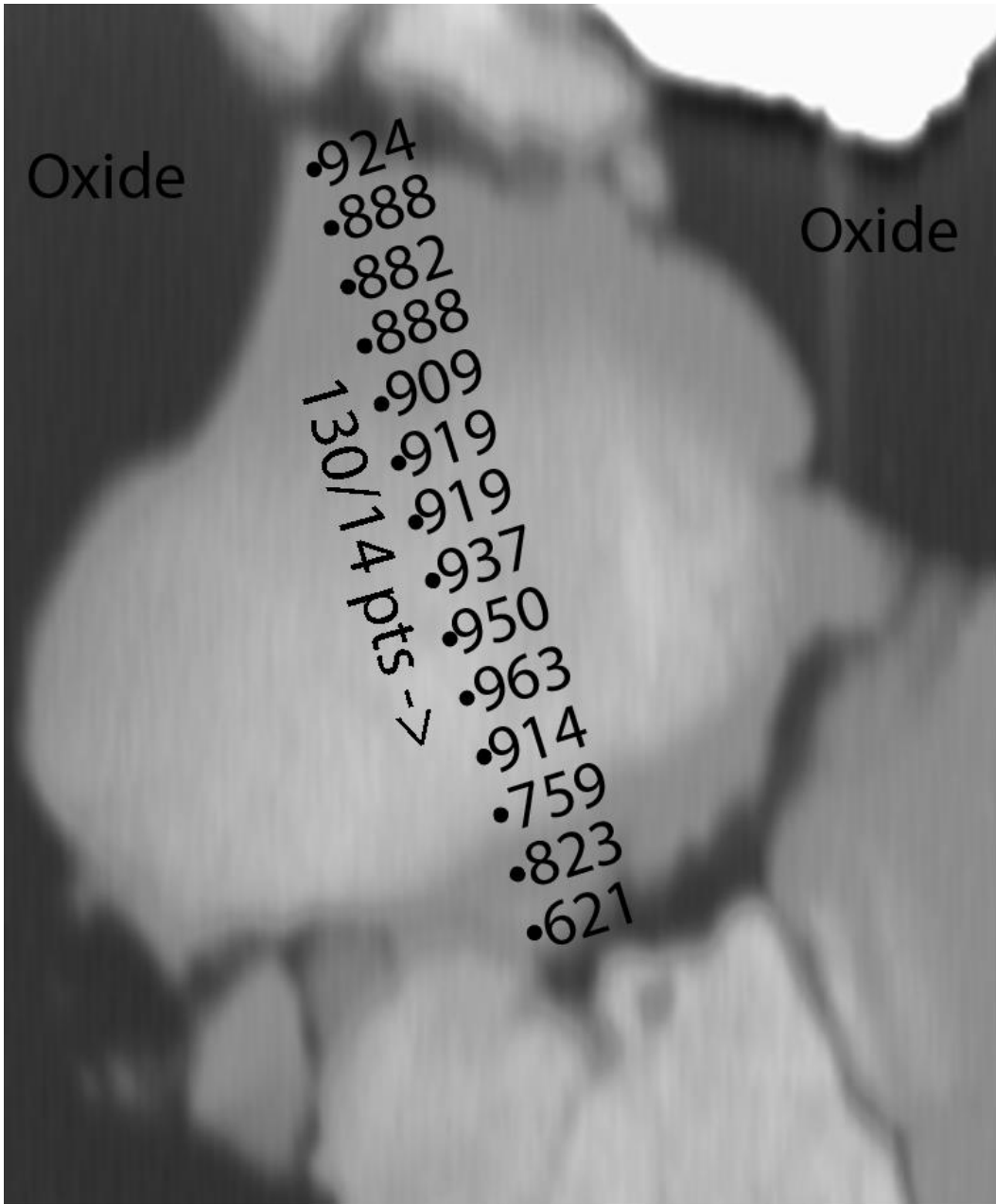


Figure A23 EPMA capture of site 10A on Sample 136-1A. Each black dot is a point analyzed for Ti concentration followed by the TitaniQ result at $a\text{TiO}_2 = 0.6$. Red numbers represent good data, while black numbers represent targets that are too close to an oxide for accurate analysis. The length of the traverse is 130.00 μm and has 14 points. The arrow indicates the direction of the traverse. Table A69 has the corresponding EPMA and TitaniQ data.

Table A69 EPMA and TitaniQ results for Figure A23. No. 1 corresponds with the uppermost point on Figure A23. Oxide! refers to a point too close to an oxide for accurate analysis.

Sample 136-1A TitaniQ Temperatures Site 10A									
No.	TiO2 (Wt. %)	TiO2(ppm)	Ti(ppm)	SiO2 (wt. %)	Total	Comment	Comment2	Comment3	Temp (°C)
1	0.035	350	210	100	100.035	Line 1 136A-10	Oxide!		924
2	0.028	280	168	100	100.028	Line 2 136A-10	Oxide!		888
3	0.027	270	162	100	100.027	Line 3 136A-10	Oxide!		882
4	0.028	280	168	100	100.028	Line 4 136A-10	Oxide!		888
5	0.032	320	192	100	100.032	Line 5 136A-10	Oxide!		909
6	0.034	340	204	100	100.034	Line 6 136A-10	Oxide!		919
7	0.034	340	204	100	100.034	Line 7 136A-10	Oxide!		919
8	0.038	380	228	100	100.038	Line 8 136A-10	Oxide!		937
9	0.041	410	246	100	100.041	Line 9 136A-10	Oxide!		950
10	0.044	440	264	100	100.044	Line 10 136A-10	Oxide!		963
11	0.033	330	198	100	100.033	Line 11 136A-10	Oxide!		914
12	0.011	110	66	100	100.011	Line 12 136A-10	Oxide!		759
13	0.018	180	108	100	100.018	Line 13 136A-10	Oxide!		823
14	0.003	30	18	100	100.003	Line 14 136A-10	Oxide!		621

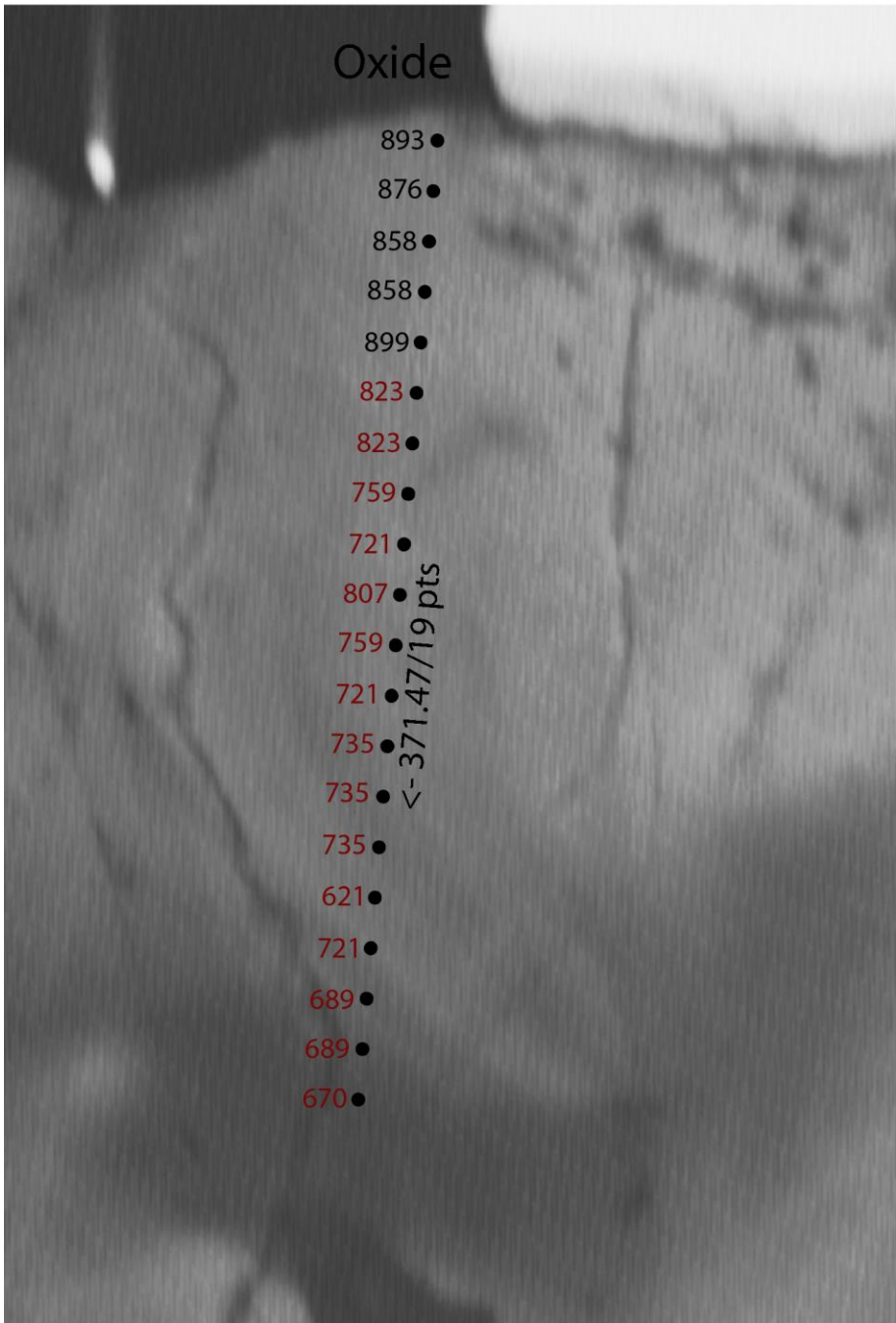


Figure A24 EPMA capture of site 1B on Sample 136-1A. Each black dot is a point analyzed for Ti concentration followed by the TitaniQ result at $a\text{TiO}_2 = 0.6$. Red numbers represent good data, while black numbers represent targets that are too close to an oxide for accurate analysis. The length of the traverse is 371.47 μm and has 19 points. The arrow indicates the direction of the traverse. Table A70 has the corresponding EPMA and TitaniQ data.

Table A70 EPMA and TitaniQ results for Figure A24. No. 27 corresponds with the uppermost point on Figure A24. Oxide! refers to a point too close to an oxide for accurate analysis.

Sample 136-1A TitaniQ Temperatures Site 1B									
No.	TiO2 (Wt. %)	TiO2(ppm)	Ti (ppm)	SiO2 (wt. %)	Total	Comment	Comment2	Comment3	Temp (°C)
27	0.029	290	174	100	100.029	Line 1 136-1A-A1-L1	Oxide!		893
28	0.026	260	156	100	100.026	Line 2 136-1A-A1-L1	Oxide!		876
29	0.023	230	138	100	100.023	Line 3 136-1A-A1-L1	Oxide!		858
30	0.023	230	138	100	100.023	Line 4 136-1A-A1-L1	Oxide!		858
31	0.03	300	180	100	100.03	Line 5 136-1A-A1-L1	Oxide!		899
32	0.018	180	108	100	100.018	Line 6 136-1A-A1-L1	rim		823
33	0.018	180	108	100	100.018	Line 7 136-1A-A1-L1	rim		823
34	0.011	110	66	100	100.011	Line 8 136-1A-A1-L1	rim		759
35	0.008	80	48	100	100.008	Line 9 136-1A-A1-L1	rim		721
36	0.016	160	96	100	100.016	Line 10 136-1A-A1-L1	rim		807
37	0.011	110	66	100	100.011	Line 11 136-1A-A1-L1	rim		759
38	0.008	80	48	100	100.008	Line 12 136-1A-A1-L1	rim		721
39	0.009	90	54	100	100.009	Line 13 136-1A-A1-L1	rim		735
40	0.009	90	54	100	100.009	Line 14 136-1A-A1-L1	rim		735
41	0.009	90	54	100	100.009	Line 15 136-1A-A1-L1	core		735
42	0.003	30	18	100	100.003	Line 16 136-1A-A1-L1	core		621
43	0.008	80	48	100	100.008	Line 17 136-1A-A1-L1	core		721
44	0.006	60	36	100	100.006	Line 18 136-1A-A1-L1	core		689
45	0.006	60	36	100	100.006	Line 19 136-1A-A1-L1	core		689
46	0.005	50	30	100	100.005	Line 20 136-1A-A1-L1	core		670

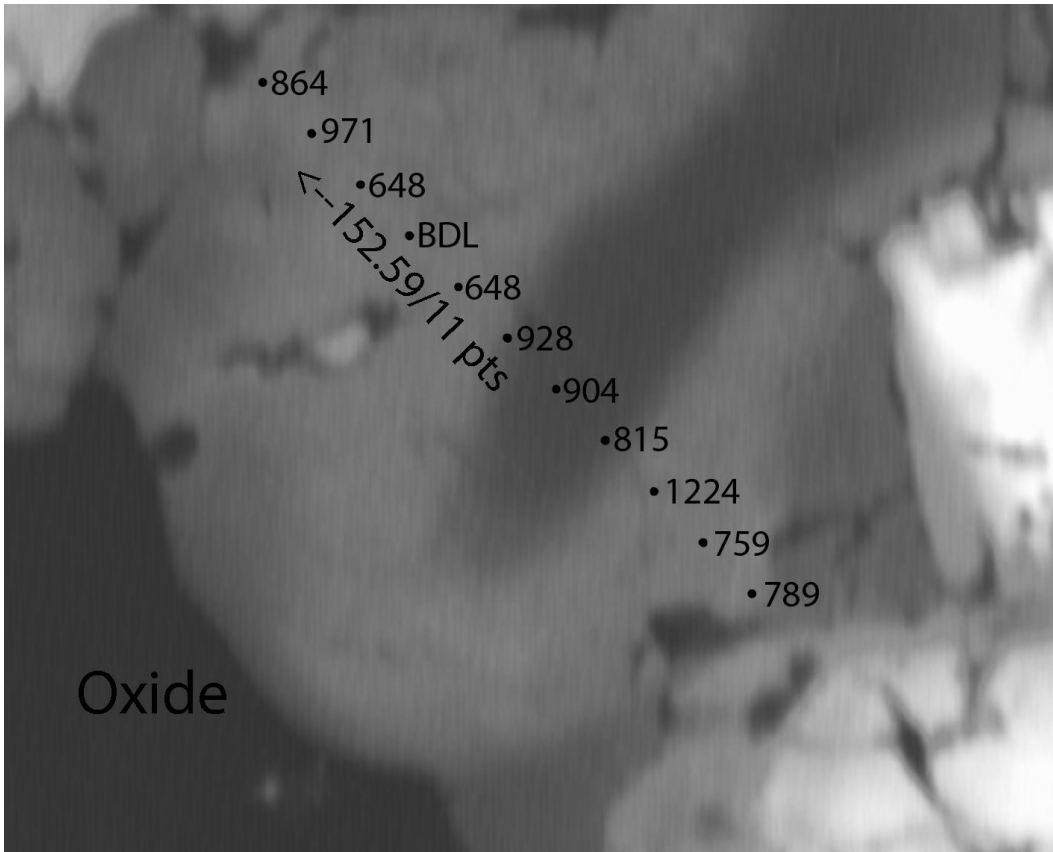


Figure A25 EPMA capture of site 8B on Sample 136-1A. Each black dot is a point analyzed for Ti concentration followed by the TitaniQ result at $a\text{TiO}_2 = 0.6$. Red numbers represent good data, while black numbers represent targets that are too close to an oxide for accurate analysis. The length of the traverse is 152.59 μm and has 11 points. The arrow indicates the direction of the traverse. Table A71 has the corresponding EPMA and TitaniQ data.

Table A71 EPMA and TitaniQ results for Figure A25. No. 47 corresponds with the lowermost point on Figure A25. Oxide! refers to a point too close to an oxide for accurate analysis.

Sample 136-1A TitaniQ Temperatures Site 8B									
No.	TiO2 (Wt. %)	TiO2(ppm)	Ti (ppm)	SiO2 (wt. %)	Total	Comment	Comment2	Comment3	Temp (°C)
47	0.014	140	84	100	100.014	136-1A-A8 1	Oxide!		789
48	0.011	110	66	100	100.011	136-1A-A8 2	Oxide!		759
49	0.15	1500	899	100	100.15	136-1A-A8 3	Oxide!		1224
50	0.017	170	102	100	100.017	136-1A-A8 4	Oxide!		815
51	0.031	310	186	100	100.031	136-1A-A8 5	Oxide!		904
52	0.036	360	216	100	100.036	136-1A-A8 6	Oxide!		928
53	0.004	40	24	100	100.004	136-1A-A8 7	Oxide!		648
54	0.002	20	12	100	100.002	136-1A-A8 8	Oxide!		585
55	0.004	40	24	100	100.004	136-1A-A8 9	Oxide!		648
56	0.046	460	276	100	100.046	136-1A-A8 10	Oxide!		971
57	0.024	240	144	100	100.024	136-1A-A8 11	Oxide!		864

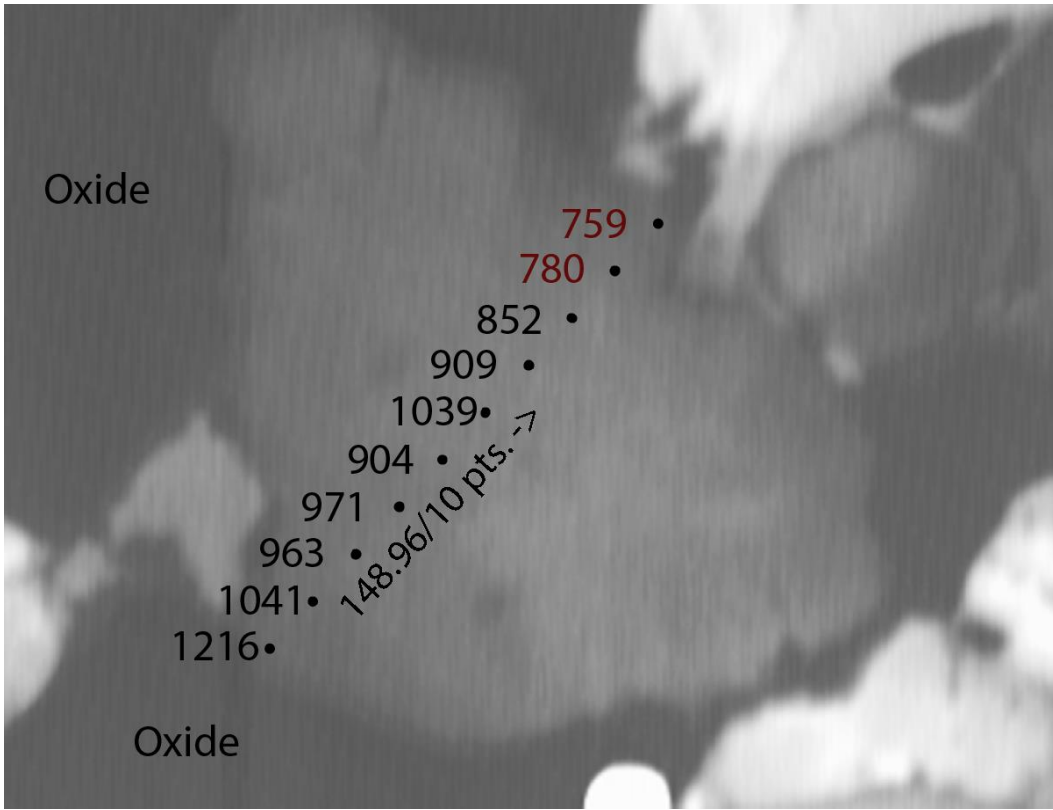


Figure A26 EPMA capture of site 9B on Sample 136-1A. Each black dot is a point analyzed for Ti concentration followed by the TitaniQ result at $a\text{TiO}_2 = 0.6$. Red numbers represent good data, while black numbers represent targets that are too close to an oxide for accurate analysis. The length of the traverse is $148.96\ \mu\text{m}$ and has 10 points. The arrow indicates the direction of the traverse. Table A71 has the corresponding EPMA and TitaniQ data.

Table A72 EPMA and TitaniQ results for Figure A26. No. 58 corresponds with the lowermost point on Figure A26. Oxide! refers to a point too close to an oxide for accurate analysis.

Sample 136-1A TitaniQ Temperatures Site 9B									
No.	TiO2 (Wt. %)	TiO2(ppm)	Ti(ppm)	SiO2 (wt. %)	Total	Comment	Comment2	Comment3	Temp (°C)
58	0.145	1450	869	100	100.145	Line 1 136-1A-A9-L1	Oxide!		1216
59	0.067	670	402	100	100.067	Line 2 136-1A-A9-L1	Oxide!		1041
60	0.044	440	264	100	100.044	Line 3 136-1A-A9-L1	Oxide!		963
61	0.046	460	276	100	100.046	Line 4 136-1A-A9-L1	Oxide!		971
62	0.031	310	186	100	100.031	Line 5 136-1A-A9-L1	Oxide!		904
63	0.038	380	228	100	100.038	Line 6 136-1A-A9-L1	Oxide!		937
64	0.032	320	192	100	100.032	Line 7 136-1A-A9-L1	Oxide!		909
65	0.022	220	132	100	100.022	Line 8 136-1A-A9-L1	Oxide!		852
66	0.013	130	78	100	100.013	Line 9 136-1A-A9-L1	Core		780
67	0.011	110	66	100	100.011	Line 10 136-1A-A9-L1	Core		759

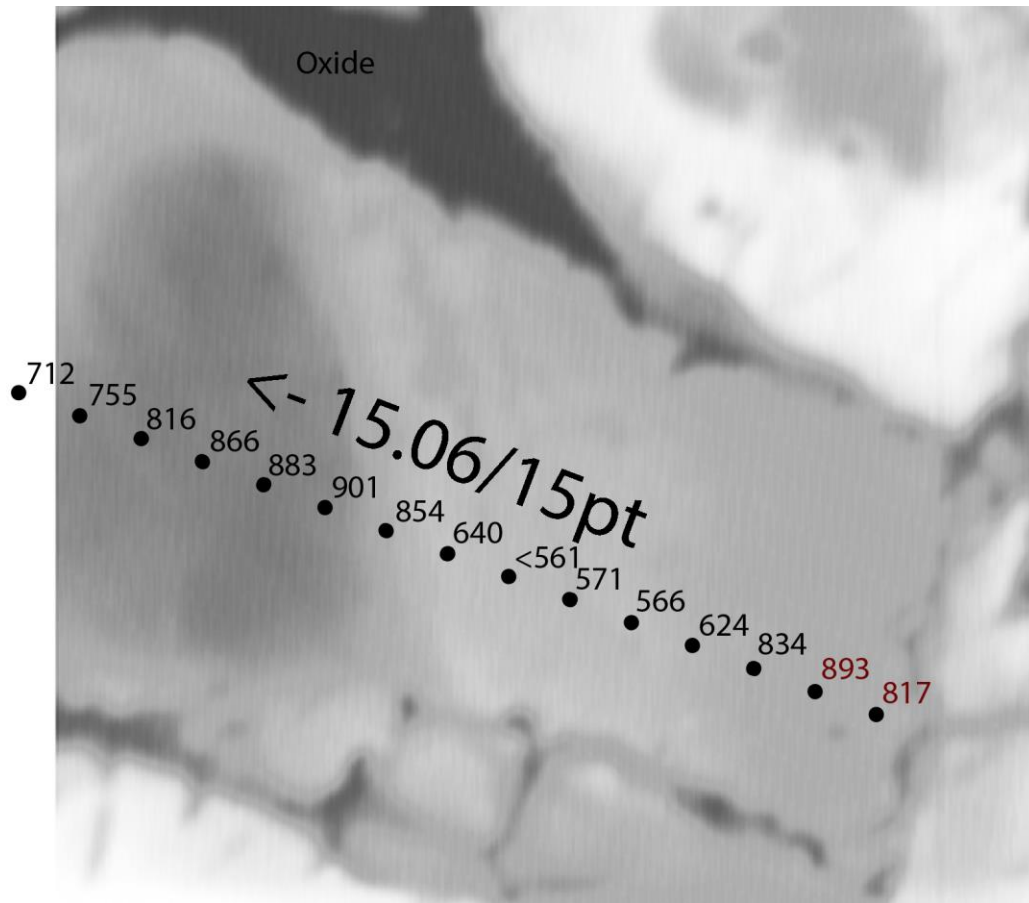


Figure A27 EPMA capture of site 3 on Sample 136-6A. Each black dot is a point analyzed for Ti concentration followed by the TitaniQ result at $a\text{TiO}_2 = 0.6$. Red numbers represent good data, while black numbers represent targets that are too close to an oxide for accurate analysis. The length of the traverse is 15.06 μm and has 15 points. The arrow indicates the direction of the traverse. Table A72 has the corresponding EPMA and TitaniQ data.

Table A73 EPMA and TitaniQ results for Figure A27. No. 1 corresponds with the lowermost point on Figure A27. Oxide! refers to a point too close to an oxide for accurate analysis. BDL = Below Detection Limit.

Sample 136-6A TitaniQ Temps Site 3									
No.	TiO2 (wt. %)	TiO2 (ppm)	Ti(ppm)	SiO2 (wt. %)	Total	Comment	Comment2	Comment3	Temp (°C)
1	0.0172	172	103	100	100.0171	Line 1 136-6A-a3	Rim		868
2	0.0289	289	173	100	100.0288	Line 2 136-6A-a3	Rim		952
3	0.0195	195	117	100	100.0194	Line 3 136-6A-a3	Oxide!		887
4	0.0031	31	19	100	100.003	Line 4 136-6A-a3	Oxide!		658
5	0.0016	16	10	100	100.0015	Line 5 136-6A-a3	Oxide!		596
6	0.0017	17	10	100	100.0016	Line 6 136-6A-a3	Oxide!		602
7	0.0008	8	5	100	100.0007	Line 7 136-6A-a3	Oxide!	BDL	<561
8	0.0037	37	22	100	100.0036	Line 8 136-6A-a3	Oxide!		676
9	0.0224	224	134	100	100.0223	Line 9 136-6A-a3	Oxide!		909
10	0.0305	305	183	100	100.0304	Line 10 136-6A-a3	Oxide!		961
11	0.0272	272	163	100	100.0271	Line 11 136-6A-a3	Oxide!		941
12	0.0243	243	146	100	100.0242	Line 12 136-6A-a3	Oxide!		922
13	0.0171	171	102	100	100.017	Line 13 136-6A-a3	Oxide!		867
14	0.0107	107	64	100	100.0106	Line 14 136-6A-a3	Oxide!		801
15	0.0074	74	44	100	100.0073	Line 15 136-6A-a3	Oxide!		754

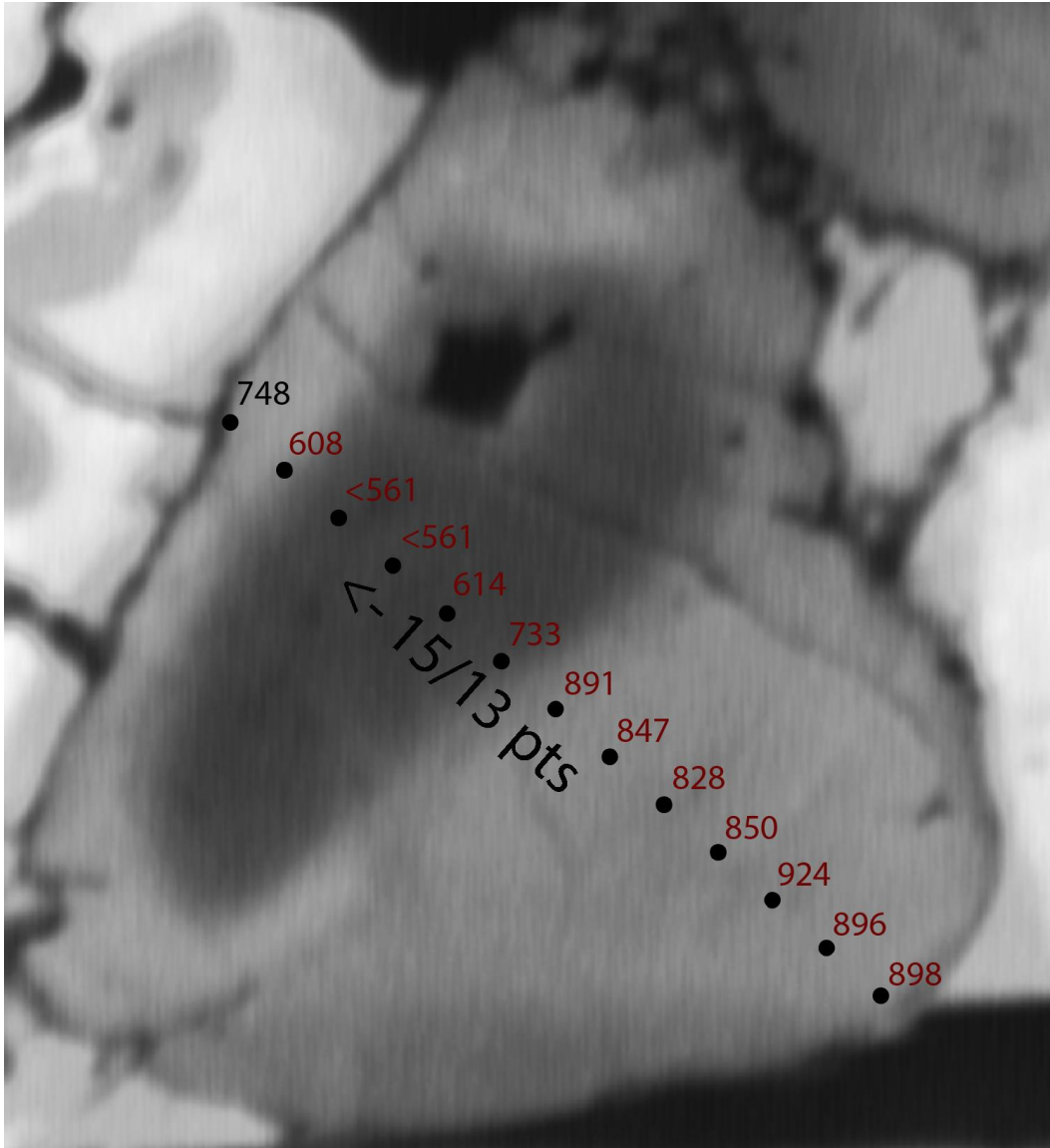


Figure A28 EPMA capture of site 4 on Sample 136-6A. Each black dot is a point analyzed for Ti concentration followed by the TitaniQ result at $a\text{TiO}_2 = 0.6$. Red numbers represent good data, while black numbers represent targets that are too close to an oxide for accurate analysis. The length of the traverse is 15.00 μm and has 13 points. The arrow indicates the direction of the traverse. Table A73 has the corresponding EPMA and TitaniQ data.

Table A74 EPMA and TitaniQ results for Figure A28. No. 52 corresponds with the lowermost point on Figure A28. Oxide! refers to a point too close to an oxide for accurate analysis. BDL = Below Detection Limit.

Sample 136-6A TitaniQ Temperatures Site 04									
No.	TiO2 (wt. %)	TiO2 (ppm)	Ti(ppm)	SiO2 (wt. %)	Total	Comment	Comment2	Comment3	Temp (°C)
52	0.0299	299	179	100	100.0298	Line 1 136-A6-a4	Rim		898
53	0.0295	295	177	100	100.0294	Line 2 136-A6-a4	Rim		896
54	0.035	350	210	100	100.035	Line 3 136-A6-a4	Rim		924
55	0.0218	218	131	100	100.0217	Line 4 136-A6-a4	Rim		850
56	0.0186	186	111	100	100.0185	Line 5 136-A6-a4	Rim		828
57	0.0213	213	128	100	100.0212	Line 6 136-A6-a4	Rim		847
58	0.0286	286	171	100	100.0285	Line 7 136-A6-a4	Rim		891
59	0.0089	89	53	100	100.0089	Line 8 136-A6-a4	Core		733
60	0.0028	28	17	100	100.0027	Line 9 136-A6-a4	Core		614
61	0.0012	12	7	100	100.0011	Line 10 136-A6-a4	Core	BDL	<561
62	0.0015	15	9	100	100.0014	Line 11 136-A6-a4	Core	BDL	<561
63	0.0026	26	16	100	100.0025	Line 12 136-A6-a4	Core		608
64	0.0101	101	61	100	100.01	Line 13 136-A6-a4	?		748

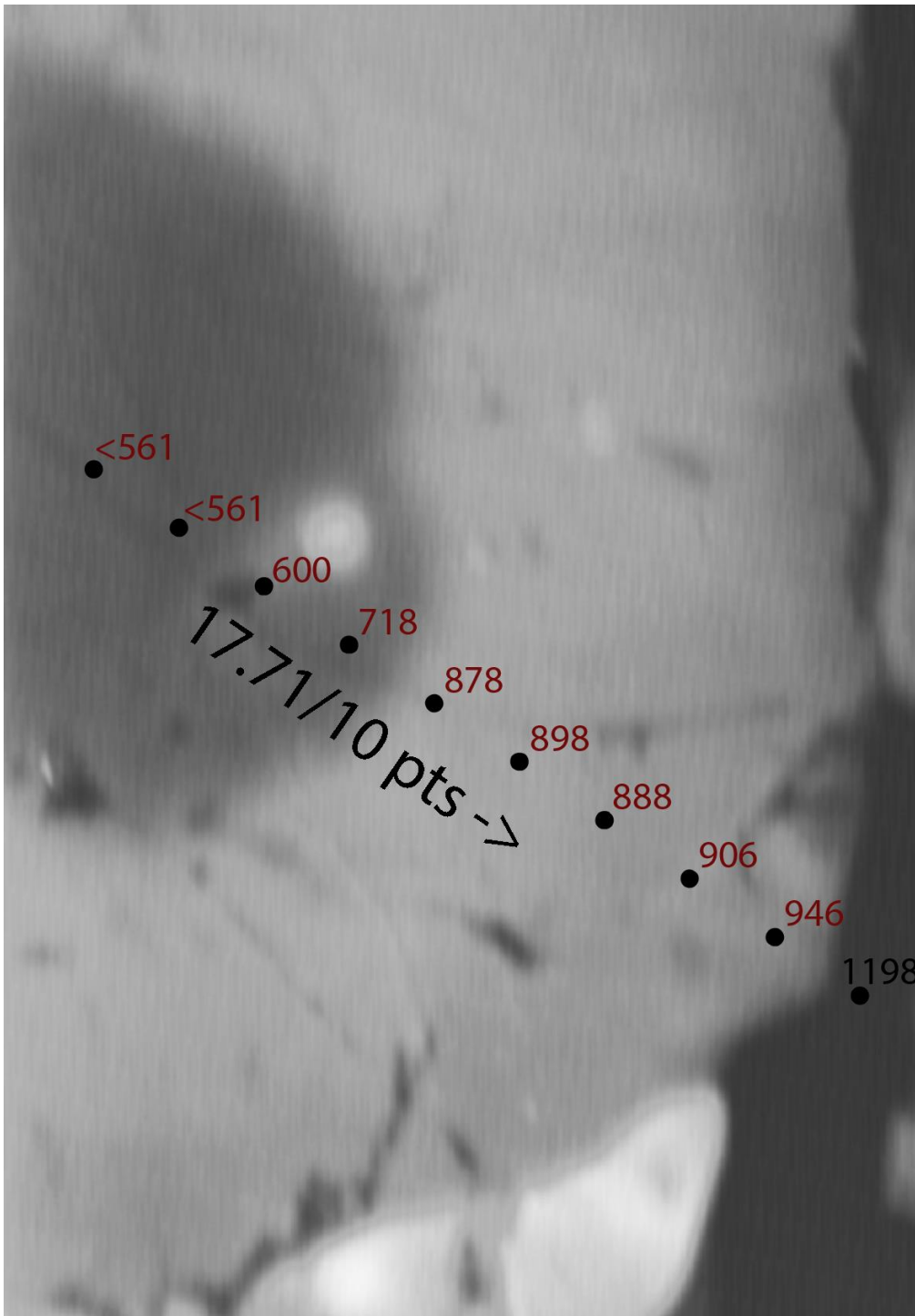


Figure A29 EPMA capture of site 8 on Sample 136-6A. Each black dot is a point analyzed for Ti concentration followed by the TitaniQ result at $a\text{TiO}_2 = 0.6$. Red numbers represent good data, while black numbers represent targets that are too close to an oxide for accurate analysis. The length of the traverse is 17.71 μm and has 10 points. The arrow indicates the direction of the traverse. Table A74 has the corresponding EPMA and TitaniQ data.

Table A75 EPMA and TitaniQ results for Figure A29. No. 16 corresponds with the uppermost point on Figure A29. Oxide! refers to a point too close to an oxide for accurate analysis. BDL = Below Detection Limit.

Sample 136-6A TitaniQ Temperatures Site 08									
No.	TiO2 (wt. %)	TiO2 (ppm)	Ti(ppm)	SiO2 (wt. %)	Total	Comment	Comment2	Comment3	Temp (°C)
16	0.0014	14	8	100	100.0014	Line 1 136-A6-a8	Core	BDL	<561
17	0.0007	7	4	100	100.0006	Line 2 136-A6-a8	Core	BDL	<561
18	0.0024	24	14	100	100.0023	Line 3 136-A6-a8	Core		600
19	0.0078	78	47	100	100.0077	Line 4 136-A6-a8	Core		718
20	0.0262	262	157	100	100.0261	Line 5 136-A6-a8	Rim		878
21	0.0299	299	179	100	100.0298	Line 6 136-A6-a8	Rim		898
22	0.0281	281	168	100	100.028	Line 7 136-A6-a8	Rim		888
23	0.0315	315	189	100	100.0314	Line 8 136-A6-a8	Rim		906
24	0.0401	401	240	100	100.04	Line 9 136-A6-a8	Rim		946
25	0.1354	1354	812	100	100.1353	Line 10 136-A6-a8	?		1198

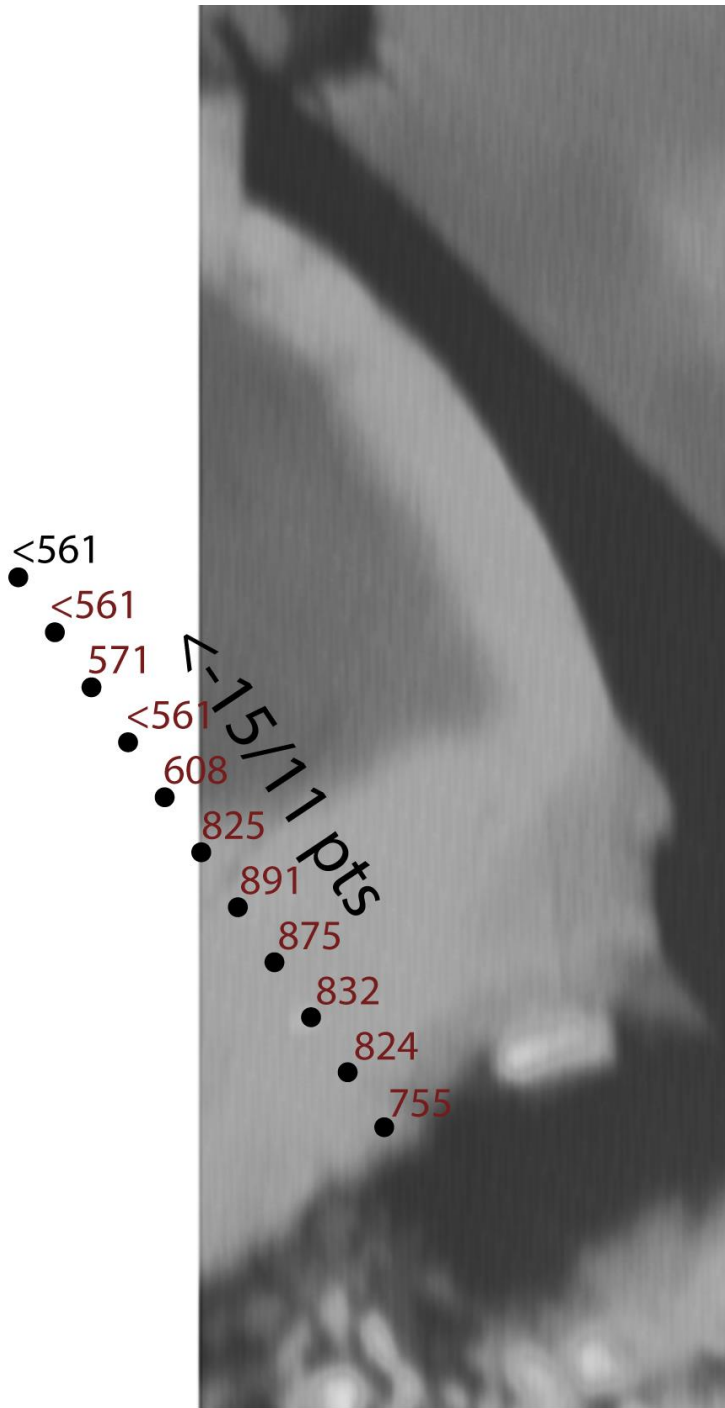


Figure A30 EPMA capture of site 9 on Sample 136-6A. Each black dot is a point analyzed for Ti concentration followed by the TitaniQ result at $a\text{TiO}_2 = 0.6$. Red numbers represent good data, while black numbers represent targets that are too close to an oxide for accurate analysis. The length of the traverse is 15.00 μm and has 11 points. The arrow indicates the direction of the traverse. Table A75 has the corresponding EPMA and TitaniQ data.

Table A76 EPMA and TitaniQ results for Figure A30. No. 41 corresponds with the lowermost point on Figure A30. Oxide! refers to a point too close to an oxide for accurate analysis. BDL = Below Detection Limit.

Sample 136-6A TitaniQ Temperatures Site 09									
No.	TiO2 (wt. %)	TiO2 (ppm)	Ti(ppm)	SiO2 (wt. %)	Total	Comment	Comment2	Comment3	Temp (°C)
41	0.0107	107	64	100	100.0106	Line 1 136-A6-a9	Rim		755
42	0.0181	181	108	100	100.018	Line 2 136-A6-a9	Rim		824
43	0.0192	192	115	100	100.0191	Line 3 136-A6-a9	Rim		832
44	0.0257	257	154	100	100.0257	Line 4 136-A6-a9	Rim		875
45	0.0285	285	171	100	100.0285	Line 5 136-A6-a9	Rim		891
46	0.0182	182	109	100	100.0182	Line 6 136-A6-a9	Rim		825
47	0.0026	26	16	100	100.0025	Line 7 136-A6-a9	Core		608
48	0.0012	12	7	100	100.0011	Line 8 136-A6-a9	Core	BDL	<561
49	0.0017	17	10	100	100.0016	Line 9 136-A6-a9	Core		571
50	0.0004	4	2	100	100.0003	Line 10 136-A6-a9	Core	BDL	<561
51	0	0	0	100	100	Line 11 136-A6-a9	?	BDL	<561

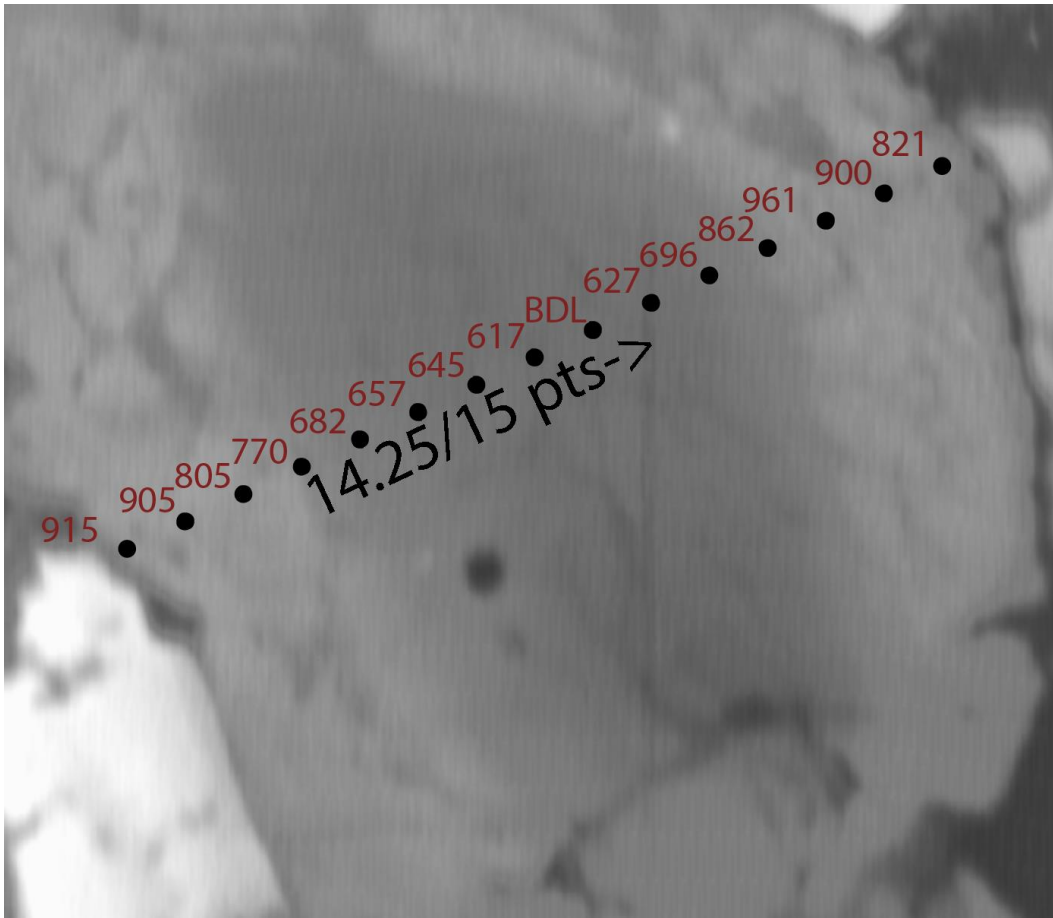


Figure A31 EPMA capture of site 10 on Sample 136-6A. Each black dot is a point analyzed for Ti concentration followed by the TitaniQ result at $a\text{TiO}_2 = 0.6$. Red numbers represent good data, while black numbers represent targets that are too close to an oxide for accurate analysis. The length of the traverse is $14.25\ \mu\text{m}$ and has 15 points. The arrow indicates the direction of the traverse. Table A76 has the corresponding EPMA and TitaniQ data.

Table A77 EPMA and TitaniQ results for Figure A31. No. 26 corresponds with the lowermost point on Figure A31. Oxide! refers to a point too close to an oxide for accurate analysis.

Sample 136-6A TitaniQ Temperatures Site 10									
No.	TiO2 (wt. %)	TiO2 (ppm)	Ti(ppm)	SiO2 (wt. %)	Total	Comment	Comment2	Comment3	Temp (°C)
26	0.0333	333	200	100	100.0332	Line 1 136-A6-a10	Rim		915
27	0.0313	313	188	100	100.0312	Line 2 136-A6-a10	Rim		905
28	0.0158	158	95	100	100.0157	Line 3 136-A6-a10	Rim		805
29	0.012	120	72	100	100.0119	Line 4 136-A6-a10	Rim		770
30	0.0056	56	34	100	100.0055	Line 5 136-A6-a10	Core		682
31	0.0044	44	26	100	100.0043	Line 6 136-A6-a10	Core		657
32	0.0039	39	23	100	100.0038	Line 7 136-A6-a10	Core		645
33	0.0029	29	17	100	100.0028	Line 8 136-A6-a10	Core		617
34	0.0023	23	14	100	100.0022	Line 9 136-A6-a10	Core		597
35	0.0032	32	19	100	100.0031	Line 10 136-A6-a10	Core		627
36	0.0064	64	38	100	100.0063	Line 11 136-A6-a10	Core		696
37	0.0236	236	141	100	100.0235	Line 12 136-A6-a10	Rim		862
38	0.0437	437	262	100	100.0436	Line 13 136-A6-a10	Rim		961
39	0.0302	302	181	100	100.0301	Line 14 136-A6-a10	Rim		900
40	0.0177	177	106	100	100.0176	Line 15 136-A6-a10	Rim		821

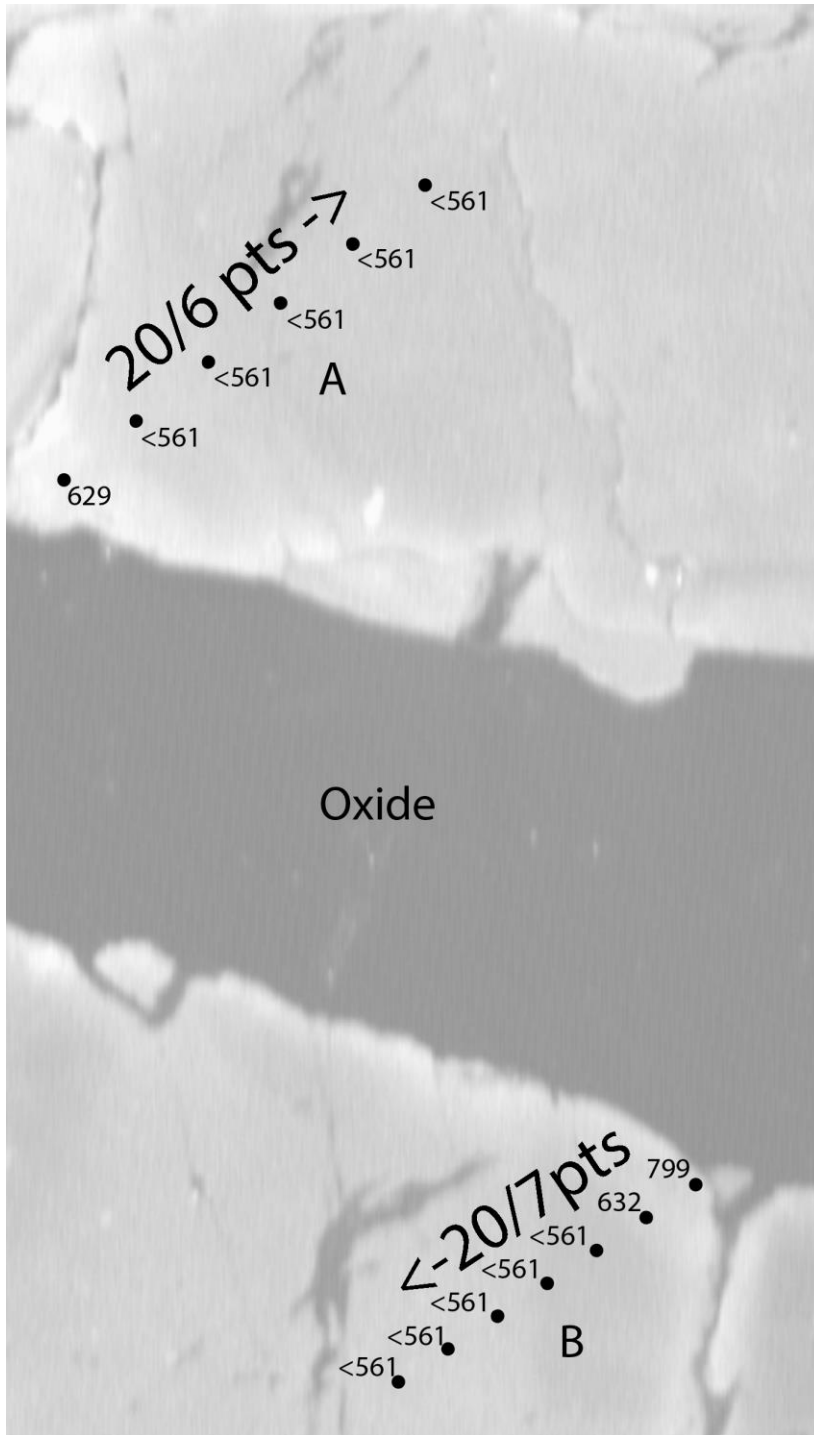


Figure A32 EPMA capture of site 5 on Sample 136-11A. Each black dot is a point analyzed for Ti concentration followed by the TitaniQ result at $a\text{TiO}_2 = 0.6$. Red numbers represent good data, while black numbers represent targets that are too close to an oxide for accurate analysis. The length of each traverse is 20.00 μm and the uppermost traverse has 6 points, while the lowermost traverse has 7 points. The arrow indicates the direction of the traverse. Table A77 has the corresponding EPMA and TitaniQ data.

Table A78 EPMA and TitaniQ results for Figure A32. No. 93 corresponds with the lowermost point on the A traverse and No. 99 corresponds with the uppermost point on the B traverse in Figure A32. Oxide! refers to a point too close to an oxide for accurate analysis. BDL = Below Detection Limit.

Sample 136-11A TitaniQ Temperatures Site 5									
No.	TiO2 (wt. %)	TiO2(ppm)	Ti(ppm)	SiO2 (wt. %)	Total	Comment	Comment2	Comment3	Temp (°C)
93	0.0033	33	20	100	100.0033	Line 1 136-A11-a5	Oxide!		629
94	0.0011	11	7	100	100.001	Line 2 136-A11-a5	Oxide!	BDL	<561
95	0.0005	5	3	100	100.0005	Line 3 136-A11-a5	Oxide!	BDL	<561
96	0.0007	7	4	100	100.0006	Line 4 136-A11-a5	Oxide!	BDL	<561
97	0.0004	4	2	100	100.0003	Line 5 136-A11-a5	Oxide!	BDL	<561
98	0.0014	14	8	100	100.0014	Line 6 136-A11-a5	Oxide!	BDL	<561
99	0.0151	151	91	100	100.015	Line 1 136-A11-a5b	Oxide!		799
100	0.0034	34	20	100	100.0033	Line 2 136-A11-a5b	Oxide!		632
101	0.001	10	6	100	100.0009	Line 3 136-A11-a5b	Oxide!	BDL	<561
102	0.0013	13	8	100	100.0012	Line 4 136-A11-a5b	Oxide!	BDL	<561
103	0.0011	11	7	100	100.001	Line 5 136-A11-a5b	Oxide!	BDL	<561
104	0.0003	3	2	100	100.0002	Line 6 136-A11-a5b	Oxide!	BDL	<561
105	0.0012	12	7	100	100.0011	Line 7 136-A11-a5b	Oxide!	BDL	<561

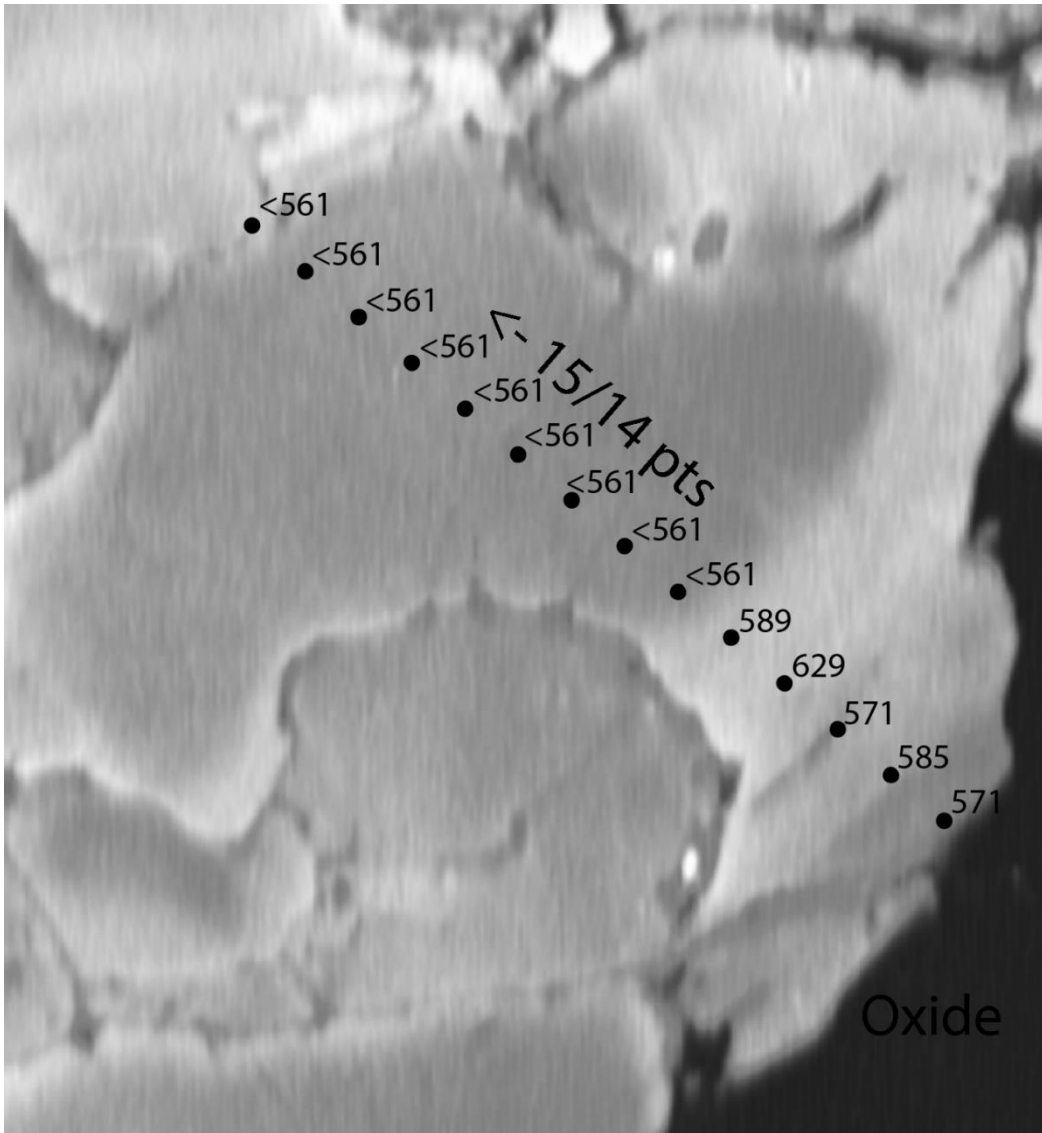


Figure A33 EPMA capture of site 7 on Sample 136-11A. Each black dot is a point analyzed for Ti concentration followed by the TitaniQ result at $a\text{TiO}_2 = 0.6$. Red numbers represent good data, while black numbers represent targets that are too close to an oxide for accurate analysis. The length of the traverse is 15.00 μm and has 14 points. The arrow indicates the direction of the traverse. Table A78 has the corresponding EPMA and TitaniQ data.

Table A79 EPMA and TitaniQ results for Figure A33. No. 65 corresponds with the lowermost point on Figure A33. Oxide! refers to a point too close to an oxide for accurate analysis. BDL = Below Detection Limit.

Sample 136-11A TitaniQ Temperatures Site 7									
No.	TiO2 (wt. %)	TiO2(ppm)	Ti(ppm)	SiO2 (wt. %)	Total	Comment	Comment2	Comment3	Temp (°C)
65	0.0017	17	10	100	100.0016	Line 1 136-A11-a7	Oxide!		571
66	0.002	20	12	100	100.0019	Line 2 136-A11-a7	Oxide!		585
67	0.0017	17	10	100	100.0016	Line 3 136-A11-a7	Oxide!		571
68	0.0033	33	20	100	100.0033	Line 4 136-A11-a7	Oxide!		629
69	0.0021	21	13	100	100.002	Line 5 136-A11-a7	Oxide!		589
70	0.0013	13	8	100	100.0012	Line 6 136-A11-a7	Oxide!	BDL	<561
71	0.0002	2	1	100	100.0001	Line 7 136-A11-a7	Oxide!	BDL	<561
72	0.001	10	6	100	100.0009	Line 8 136-A11-a7	Core	BDL	<561
73	0.0004	4	2	100	100.0003	Line 9 136-A11-a7	Core	BDL	<561
74	0.0011	11	7	100	100.001	Line 10 136-A11-a7	Core	BDL	<561
75	0.0007	7	4	100	100.0006	Line 11 136-A11-a7	Core	BDL	<561
76	0.0004	4	2	100	100.0003	Line 12 136-A11-a7	Core	BDL	<561
77	0.0007	7	4	100	100.0006	Line 13 136-A11-a7	Rim	BDL	<561
78	0.0007	7	4	100	100.0006	Line 14 136-A11-a7	Rim	BDL	<561

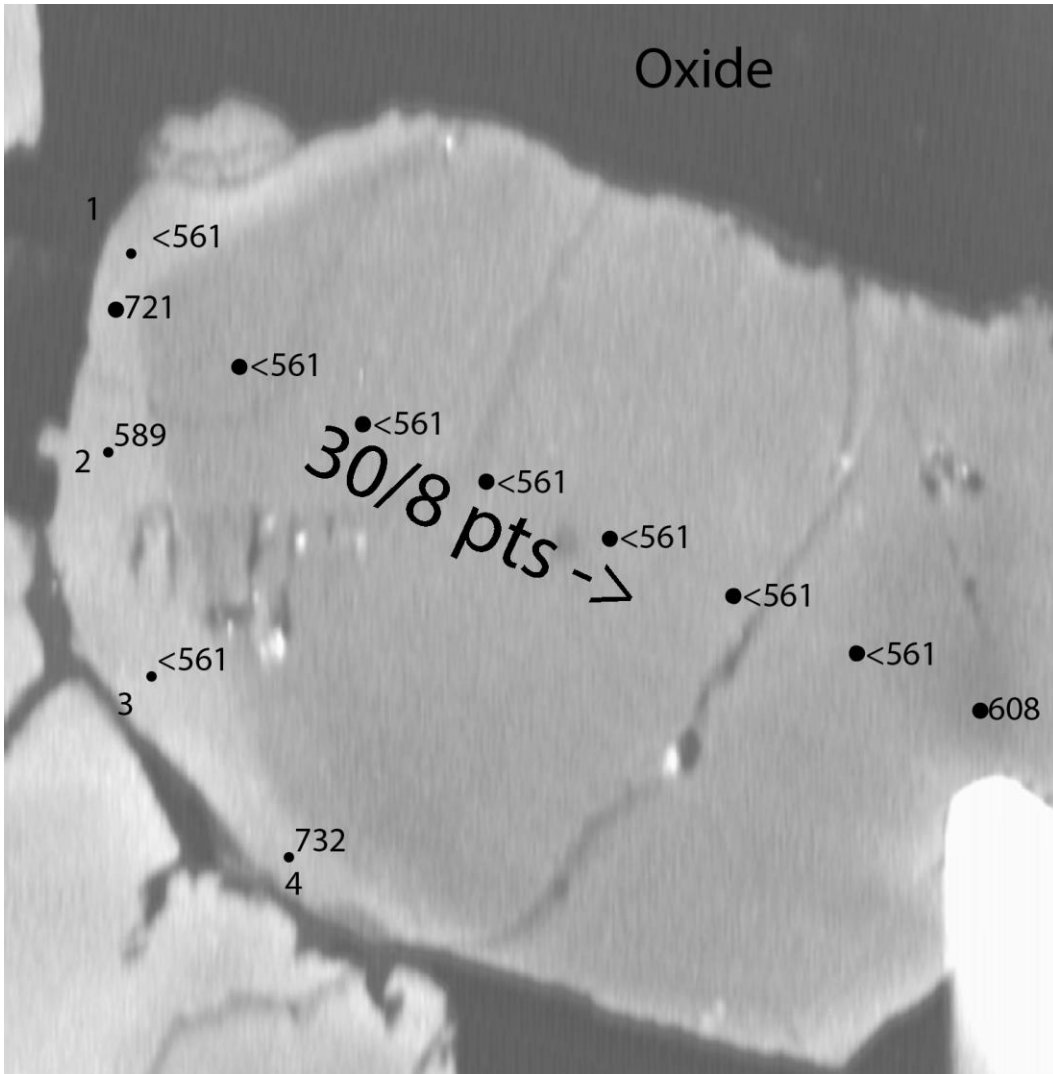


Figure A34 EPMA capture of site 9 on Sample 136-11A. Each black dot is a point analyzed for Ti concentration followed by the TitaniQ result at $a\text{TiO}_2 = 0.6$. Red numbers represent good data, while black numbers represent targets that are too close to an oxide for accurate analysis. The length of the traverse is 30.00 μm and has 8 points. The arrow indicates the direction of the traverse. Table A79 has the corresponding EPMA and TitaniQ data.

Table A80 EPMA and TitaniQ results for Figure A34. No. 81 corresponds with the point number 1, and number 85 corresponds to the uppermost point on the traverse (recorded as 783) on Figure A34. Oxide! refers to a point too close to an oxide for accurate analysis. BDL = Below Detection Limit.

Sample 136-11A TitaniQ Temperatures Site 9									
No.	TiO2	TiO2 (ppm)	Ti(ppm)	SiO2	Total	Comment	Comment2	Comment3	Temp (°C)
81	0.001	10	6	100	100.0009	136-A11-a9 1	Oxide!	BDL	<561
82	0.0021	21	13	100	100.002	136-A11-a9 2	Oxide!		589
83	0.0008	8	5	100	100.0007	136-A11-a9 3	Oxide!	BDL	<561
84	0.0088	88	53	100	100.0087	136-A11-a9 4	Oxide!		732
85	0.008	80	48	100	100.0079	Line 1 136-A11-a9	Oxide!		721
86	0.0007	7	4	100	100.0006	Line 2 136-A11-a9	Oxide!	BDL	<561
87	0.0001	1	1	100	100	Line 3 136-A11-a9	Oxide!	BDL	<561
88	0	0	0	100	100	Line 4 136-A11-a9	Oxide!	BDL	<561
89	0.0003	3	2	100	100.0002	Line 5 136-A11-a9	Oxide!	BDL	<561
90	0.0008	8	5	100	100.0007	Line 6 136-A11-a9	Oxide!	BDL	<561
91	0.0005	5	3	100	100.0005	Line 7 136-A11-a9	Oxide!	BDL	<561
92	0.0026	26	16	100	100.0025	Line 8 136-A11-a9	Oxide!		608

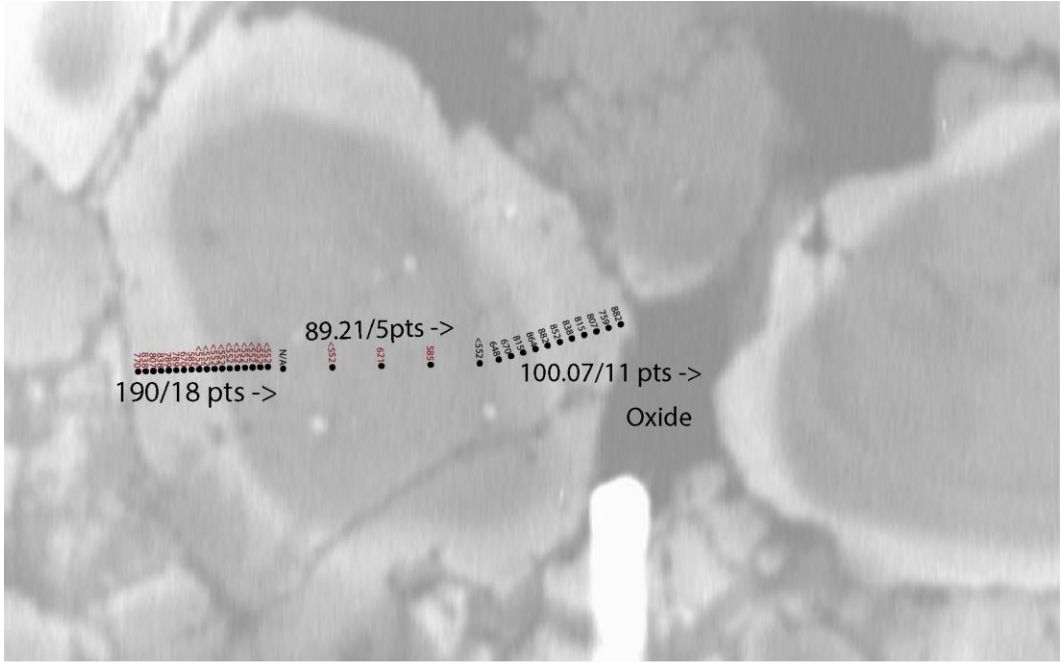


Figure A35 EPMA capture of site 1 on Sample 136-2B. Each black dot is a point analyzed for Ti concentration followed by the TitaniQ result at $a\text{TiO}_2 = 0.6$. Red numbers represent good data, while black numbers represent targets that are too close to an oxide for accurate analysis. The length of the left, middle, and right traverses are 190.00, 89.21, and 100.07 μm and has 18, 5, and 11 points, respectively. The arrow indicates the direction of the traverse. Table A80 has the corresponding EPMA and TitaniQ data.

Table A81 EPMA and TitaniQ results for Figure A35. No. 44 corresponds with the leftmost point on Figure A35. Oxide! refers to a point too close to an oxide for accurate analysis. BDL = Below Detection Limit.

Sample 136-2B TitaniQ Temperatures Site 1									
No.	TiO2 (wt. %)	TiO2(ppm)	Ti(ppm)	SiO2 (wt. %)	Total	Comment	Comment2	Comment3	Temp (°C)
44	0.012	120	72	100	100.012	Line 1 136-B2-A1-L1a	rim		770
45	0.02	200	120	100	100.02	Line 2 136-B2-A1-L1a	rim		838
46	0.016	160	96	100	100.016	Line 3 136-B2-A1-L1a	rim		807
47	0.02	200	120	100	100.02	Line 4 136-B2-A1-L1a	rim		838
48	0.014	140	84	100	100.014	Line 5 136-B2-A1-L1a	rim		789
49	0.014	140	84	100	100.014	Line 6 136-B2-A1-L1a	rim		789
50	0.005	50	30	100	100.005	Line 7 136-B2-A1-L1a	rim		670
51	0.002	20	12	100	100.002	Line 8 136-B2-A1-L1a	rim		585
52	0.003	30	18	100	100.003	Line 9 136-B2-A1-L1a	rim		621
53	0.002	20	12	100	100.002	Line 10 136-B2-A1-L1a	?		585
54	0	0	0	100	100	Line 11 136-B2-A1-L1a	core	BDL	<552
55	0	0	0	100	100	Line 12 136-B2-A1-L1a	core	BDL	<552
56	0.001	10	6	100	100.001	Line 13 136-B2-A1-L1a	core	BDL	<552
57	0.001	10	6	100	100.001	Line 14 136-B2-A1-L1a	core	BDL	<552
58	0	0	0	100	100	Line 15 136-B2-A1-L1a	core	BDL	<552
59	0	0	0	100	100	Line 16 136-B2-A1-L1a	core	BDL	<552
60	0.001	10	6	100	100.001	Line 17 136-B2-A1-L1a	core	BDL	<552
61	0.001	10	6	100	100.001	Line 18 136-B2-A1-L1a	core	BDL	<552
62	0.02	200	120	100	100.02	Line 1 136-B2-L1b	?		838
63	0.001	10	6	100	100.001	Line 2 136-B2-L1b	core	BDL	<552
64	0.003	30	18	100	100.003	Line 3 136-B2-L1b	core		621
65	0.002	20	12	100	100.002	Line 4 136-B2-L1b	core		585
66	0	0	0	100	100	Line 5 136-B2-L1b	core	BDL	<552
67	0.004	40	24	100	100.004	Line 1 136-B2-L1c	core		648
68	0.005	50	30	100	100.005	Line 2 136-B2-L1c	core		670
69	0.017	170	102	100	100.017	Line 3 136-B2-L1c	Oxide!		815
70	0.024	240	144	100	100.024	Line 4 136-B2-L1c	Oxide!		864
71	0.027	270	162	100	100.027	Line 5 136-B2-L1c	Oxide!		882
72	0.022	220	132	100	100.022	Line 6 136-B2-L1c	Oxide!		852
73	0.02	200	120	100	100.02	Line 7 136-B2-L1c	Oxide!		838
74	0.017	170	102	100	100.017	Line 8 136-B2-L1c	Oxide!		815
75	0.016	160	96	100	100.016	Line 9 136-B2-L1c	Oxide!		807
76	0.011	110	66	100	100.011	Line 10 136-B2-L1c	Oxide!		759
77	0.027	270	162	100	100.027	Line 11 136-B2-L1c	Oxide!		882

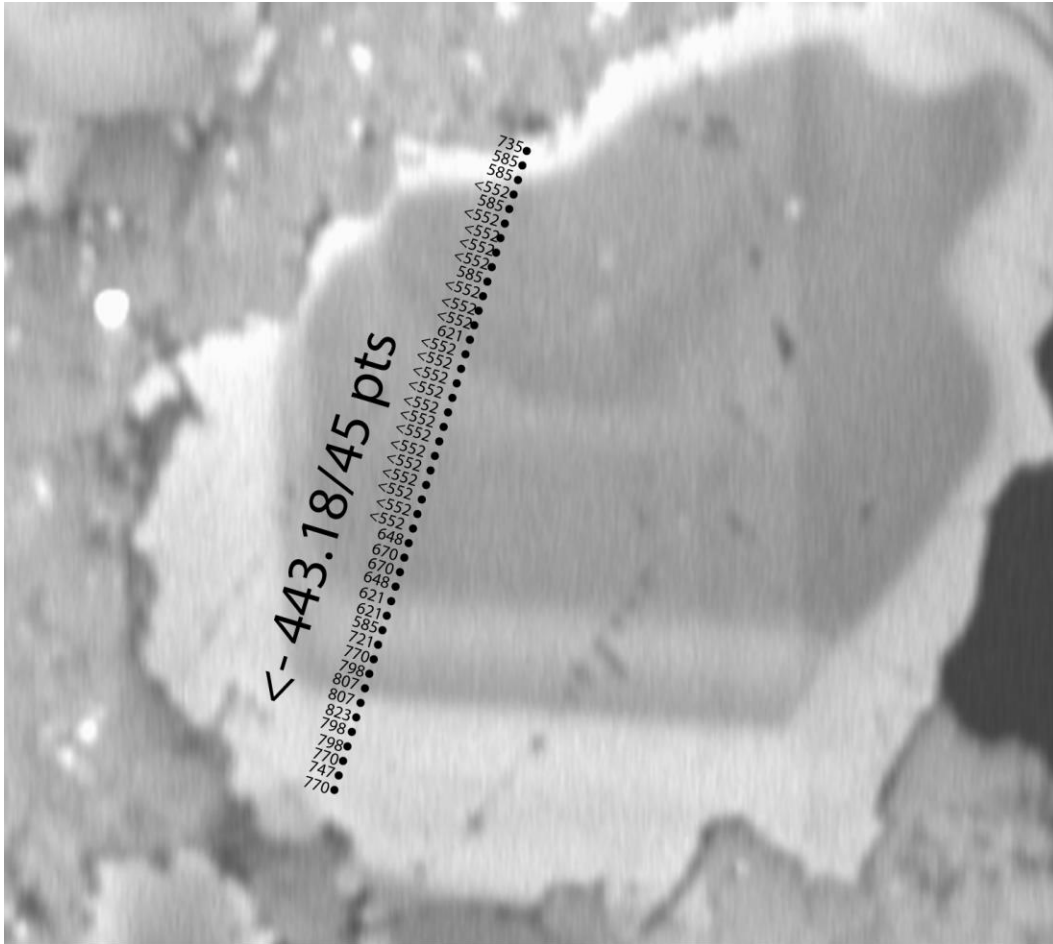


Figure A36 EPMA capture of site 5 on Sample 136-2B. Each black dot is a point analyzed for Ti concentration followed by the TitaniQ result at $a\text{TiO}_2 = 0.6$. The length of the traverse is 443.18 μm and has 45 points. The arrow indicates the direction of the traverse. Table A81 has the corresponding EPMA and TitaniQ data.

Table A82 EPMA and TitaniQ results for Figure A36. No. 78 corresponds with the uppermost point on Figure A36. Oxide! refers to a point too close to an oxide for accurate analysis. BDL = Below Detection Limit.

Sample 136-2B TitaniQ Temps Site 5									
No.	TiO2 (wt. %)	TiO2 (ppm)	Ti(ppm)	SiO2 (wt. %)	Total	Comment	Comment2	Comment3	Temp (°C)
78	0.009	90	54	100	100.009	Line 1 136-B2-A5-L1	rim		735
79	0.002	20	12	100	100.002	Line 2 136-B2-A5-L1	rim		585
80	0.002	20	12	100	100.002	Line 3 136-B2-A5-L1	mix		585
81	0.001	10	6	100	100.001	Line 4 136-B2-A5-L1	core	BDL	<552
82	0.002	20	12	100	100.002	Line 5 136-B2-A5-L1	core		585
83	0.001	10	6	100	100.001	Line 6 136-B2-A5-L1	core	BDL	<552
84	0.002	20	12	100	100.002	Line 7 136-B2-A5-L1	core		585
85	0	0	0	100	100	Line 8 136-B2-A5-L1	core	BDL	<552
86	0	0	0	100	100	Line 9 136-B2-A5-L1	core	BDL	<552
87	0.001	10	6	100	100.001	Line 10 136-B2-A5-L1	core	BDL	<552
88	0.002	20	12	100	100.002	Line 11 136-B2-A5-L1	core		585
89	0.001	10	6	100	100.001	Line 12 136-B2-A5-L1	core	BDL	<552
90	0	0	0	100	100	Line 13 136-B2-A5-L1	core	BDL	<552
91	0	0	0	100	100	Line 14 136-B2-A5-L1	core	BDL	<552
92	0.003	30	18	100	100.003	Line 15 136-B2-A5-L1	core		621
93	0.001	10	6	100	100.001	Line 16 136-B2-A5-L1	core	BDL	<552
94	0.001	10	6	100	100.001	Line 17 136-B2-A5-L1	core	BDL	<552
95	0	0	0	100	100	Line 18 136-B2-A5-L1	core	BDL	<552
96	0.001	10	6	100	100.001	Line 19 136-B2-A5-L1	core	BDL	<552
97	0	0	0	100	100	Line 20 136-B2-A5-L1	core	BDL	<552
98	0	0	0	100	100	Line 21 136-B2-A5-L1	core	BDL	<552
99	0	0	0	100	100	Line 22 136-B2-A5-L1	core	BDL	<552
100	0.001	10	6	100	100.001	Line 23 136-B2-A5-L1	core	BDL	<552
101	0	0	0	100	100	Line 24 136-B2-A5-L1	core	BDL	<552
102	0	0	0	100	100	Line 25 136-B2-A5-L1	core	BDL	<552
103	0.001	10	6	100	100.001	Line 26 136-B2-A5-L1	core	BDL	<552
104	0.001	10	6	100	100.001	Line 27 136-B2-A5-L1	core	BDL	<552
105	0.001	10	6	100	100.001	Line 28 136-B2-A5-L1	core	BDL	<552
106	0.004	40	24	100	100.004	Line 29 136-B2-A5-L1	core		648
107	0.005	50	30	100	100.005	Line 30 136-B2-A5-L1	core		670
108	0.005	50	30	100	100.005	Line 31 136-B2-A5-L1	core		670
109	0.004	40	24	100	100.004	Line 32 136-B2-A5-L1	mix		648
110	0.003	30	18	100	100.003	Line 33 136-B2-A5-L1	rim		621
111	0.003	30	18	100	100.003	Line 34 136-B2-A5-L1	rim		621
112	0.002	20	12	100	100.002	Line 35 136-B2-A5-L1	rim		585
113	0.008	80	48	100	100.008	Line 36 136-B2-A5-L1	mix		721
114	0.012	120	72	100	100.012	Line 37 136-B2-A5-L1	core		770
115	0.015	150	90	100	100.015	Line 38 136-B2-A5-L1	core		798
116	0.016	160	96	100	100.016	Line 39 136-B2-A5-L1	mix		807
117	0.016	160	96	100	100.016	Line 40 136-B2-A5-L1	rim		807
118	0.018	180	108	100	100.018	Line 41 136-B2-A5-L1	rim		823
119	0.015	150	90	100	100.015	Line 42 136-B2-A5-L1	rim		798
120	0.012	120	72	100	100.012	Line 43 136-B2-A5-L1	rim		770
121	0.01	100	60	100	100.01	Line 44 136-B2-A5-L1	rim		747
122	0.012	120	72	100	100.012	Line 45 136-B2-A5-L1	rim		770



Figure A37 EPMA capture of site 9 on Sample 136-2B. Each black dot is a point analyzed for Ti concentration followed by the TitaniQ result at $a\text{TiO}_2 = 0.6$. The length of the traverse is 548.25 μm and has 57 points. The arrow indicates the opposite direction of the traverse. Table A82 has the corresponding EPMA and TitaniQ data.

Table A83 EPMA and TitaniQ results for Figure A37. No. 123 corresponds with the lowermost point on Figure A37. Oxide! refers to a point too close to an oxide for accurate analysis. BDL = Below Detection Limit.

Sample 136-2B TitaniQ Temperatures Site 9									
No.	TiO2 (wt. %)	TiO2 (ppm)	Ti(ppm)	SiO2 (wt. %)	Total	Comment	Comment2	Comment3	Temp (°C)
123	0.013	130	78	100	100.013	Line 1 136-B2-A9-L1	rim		780
124	0.021	210	126	100	100.021	Line 2 136-B2-A9-L1	rim		845
125	0.022	220	132	100	100.022	Line 3 136-B2-A9-L1	rim		852
126	0.023	230	138	100	100.023	Line 4 136-B2-A9-L1	rim		858
127	0.018	180	108	100	100.018	Line 5 136-B2-A9-L1	rim		823
128	0.013	130	78	100	100.013	Line 6 136-B2-A9-L1	rim		780
129	0.013	130	78	100	100.013	Line 7 136-B2-A9-L1	rim		780
130	0.016	160	96	100	100.016	Line 8 136-B2-A9-L1	rim		807
131	0.013	130	78	100	100.013	Line 9 136-B2-A9-L1	rim		780
132	0.015	150	90	100	100.015	Line 10 136-B2-A9-L1	mix		798
133	0.013	130	78	100	100.013	Line 11 136-B2-A9-L1	rim		780
134	0.007	70	42	100	100.007	Line 12 136-B2-A9-L1	rim		706
135	0.004	40	24	100	100.004	Line 13 136-B2-A9-L1	rim		648
136	0.006	60	36	100	100.006	Line 14 136-B2-A9-L1	rim		689
137	0.004	40	24	100	100.004	Line 15 136-B2-A9-L1	core		648
138	0.001	10	6	100	100.001	Line 16 136-B2-A9-L1	core	BDL	<552
139	0.002	20	12	100	100.002	Line 17 136-B2-A9-L1	core		585
140	0	0	0	100	100	Line 18 136-B2-A9-L1	core	BDL	<552
141	0.001	10	6	100	100.001	Line 19 136-B2-A9-L1	rim	BDL	<552
142	0	0	0	100	100	Line 20 136-B2-A9-L1	core	BDL	<552
143	0.001	10	6	100	100.001	Line 21 136-B2-A9-L1	core	BDL	<552
144	0	0	0	100	100	Line 22 136-B2-A9-L1	core	BDL	<552
145	0.002	20	12	100	100.002	Line 23 136-B2-A9-L1	core		585
146	0.002	20	12	100	100.002	Line 24 136-B2-A9-L1	core		585
147	0	0	0	100	100	Line 25 136-B2-A9-L1	core	BDL	<552
148	0	0	0	100	100	Line 26 136-B2-A9-L1	core	BDL	<552
149	0	0	0	100	100	Line 27 136-B2-A9-L1	core	BDL	<552
150	0	0	0	100	100	Line 28 136-B2-A9-L1	core	BDL	<552
151	0	0	0	100	100	Line 29 136-B2-A9-L1	core	BDL	<552
152	0	0	0	100	100	Line 30 136-B2-A9-L1	core	BDL	<552
153	0	0	0	100	100	Line 31 136-B2-A9-L1	core	BDL	<552
154	0	0	0	100	100	Line 32 136-B2-A9-L1	core	BDL	<552
155	0	0	0	100	100	Line 33 136-B2-A9-L1	core	BDL	<552
156	0	0	0	100	100	Line 34 136-B2-A9-L1	core	BDL	<552
157	0	0	0	100	100	Line 35 136-B2-A9-L1	core	BDL	<552
158	0	0	0	100	100	Line 36 136-B2-A9-L1	core	BDL	<552
159	0	0	0	100	100	Line 37 136-B2-A9-L1	core	BDL	<552
160	0	0	0	100	100	Line 38 136-B2-A9-L1	core	BDL	<552
161	0	0	0	100	100	Line 39 136-B2-A9-L1	core	BDL	<552
162	0.001	10	6	100	100.001	Line 40 136-B2-A9-L1	core	BDL	<552
163	0	0	0	100	100	Line 41 136-B2-A9-L1	core	BDL	<552
164	0.001	10	6	100	100.001	Line 42 136-B2-A9-L1	core	BDL	<552
165	0	0	0	100	100	Line 43 136-B2-A9-L1	core	BDL	<552
166	0	0	0	100	100	Line 44 136-B2-A9-L1	core	BDL	<552

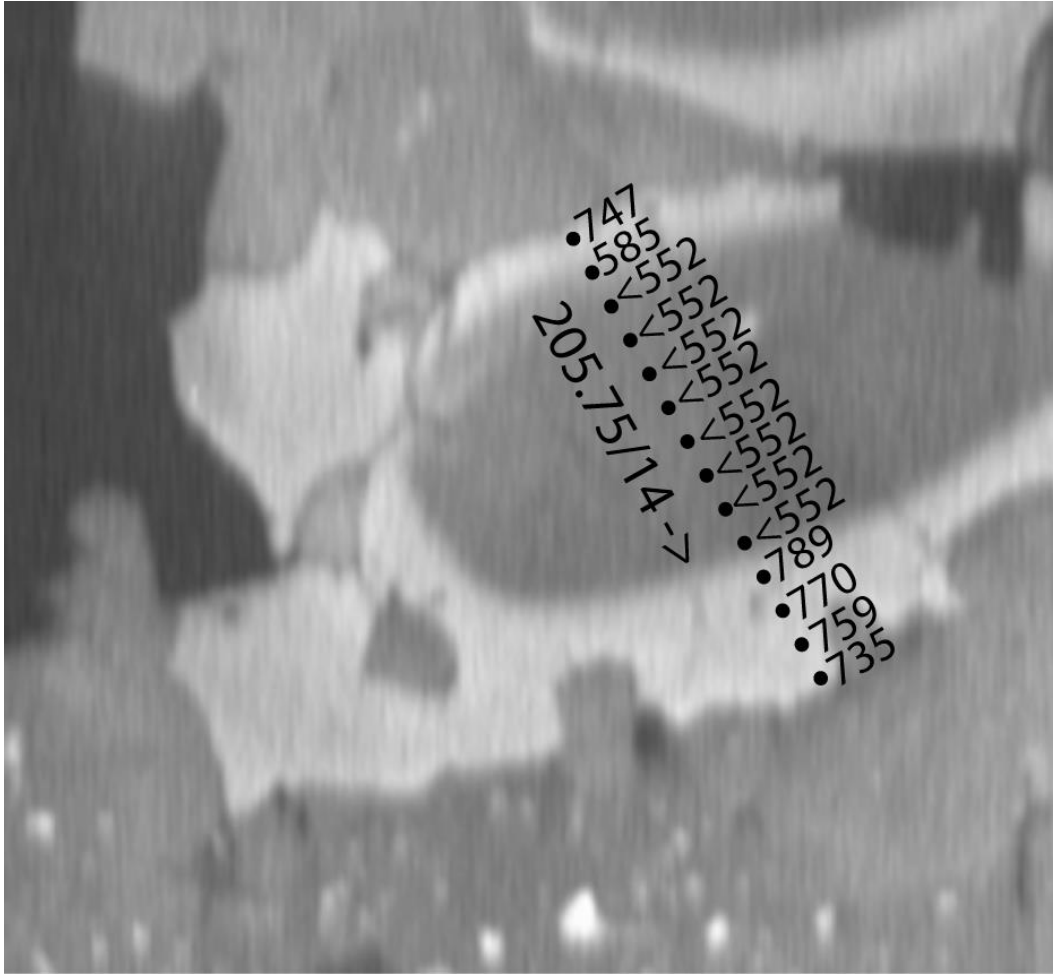


Figure A38 EPMA capture of site 2 on Sample 136-8B. Each black dot is a point analyzed for Ti concentration followed by the TitaniQ result at $a\text{TiO}_2 = 0.6$. The length of the traverse is 205.75 μm and has 14 points. The arrow indicates the direction of the traverse. Table A83 has the corresponding EPMA and TitaniQ data.

Table A84 EPMA and TitaniQ results for Figure A38. No. 74 corresponds with the uppermost point on Figure A38. Oxide! refers to a point too close to an oxide for accurate analysis. BDL = Below Detection Limit.

Sample 136-8B TitaniQ Temperature Site 2									
No.	TiO2 (wt. %)	TiO2 (ppm)	Ti(ppm)	SiO2 (wt. %)	Total	Comment	Comment2	Comment3	Temp (°C)
74	0.01	100	60	100	100.01	Line 1 136-8B-A2-L1	rim		747
75	0.002	20	12	100	100.002	Line 2 136-8B-A2-L1	mix		585
76	0	0	0	100	100	Line 3 136-8B-A2-L1	core	BDL	<552
77	0	0	0	100	100	Line 4 136-8B-A2-L1	core	BDL	<552
78	0	0	0	100	100	Line 5 136-8B-A2-L1	core	BDL	<552
79	0	0	0	100	100	Line 6 136-8B-A2-L1	core	BDL	<552
80	0	0	0	100	100	Line 7 136-8B-A2-L1	core	BDL	<552
81	0	0	0	100	100	Line 8 136-8B-A2-L1	core	BDL	<552
82	0	0	0	100	100	Line 9 136-8B-A2-L1	core	BDL	<552
83	0	0	0	100	100	Line 10 136-8B-A2-L1	core	BDL	<552
84	0.014	140	84	100	100.014	Line 11 136-8B-A2-L1	rim		789
85	0.012	120	72	100	100.012	Line 12 136-8B-A2-L1	rim		770
86	0.011	110	66	100	100.011	Line 13 136-8B-A2-L1	rim		759
87	0.009	90	54	100	100.009	Line 14 136-8B-A2-L1	rim		735

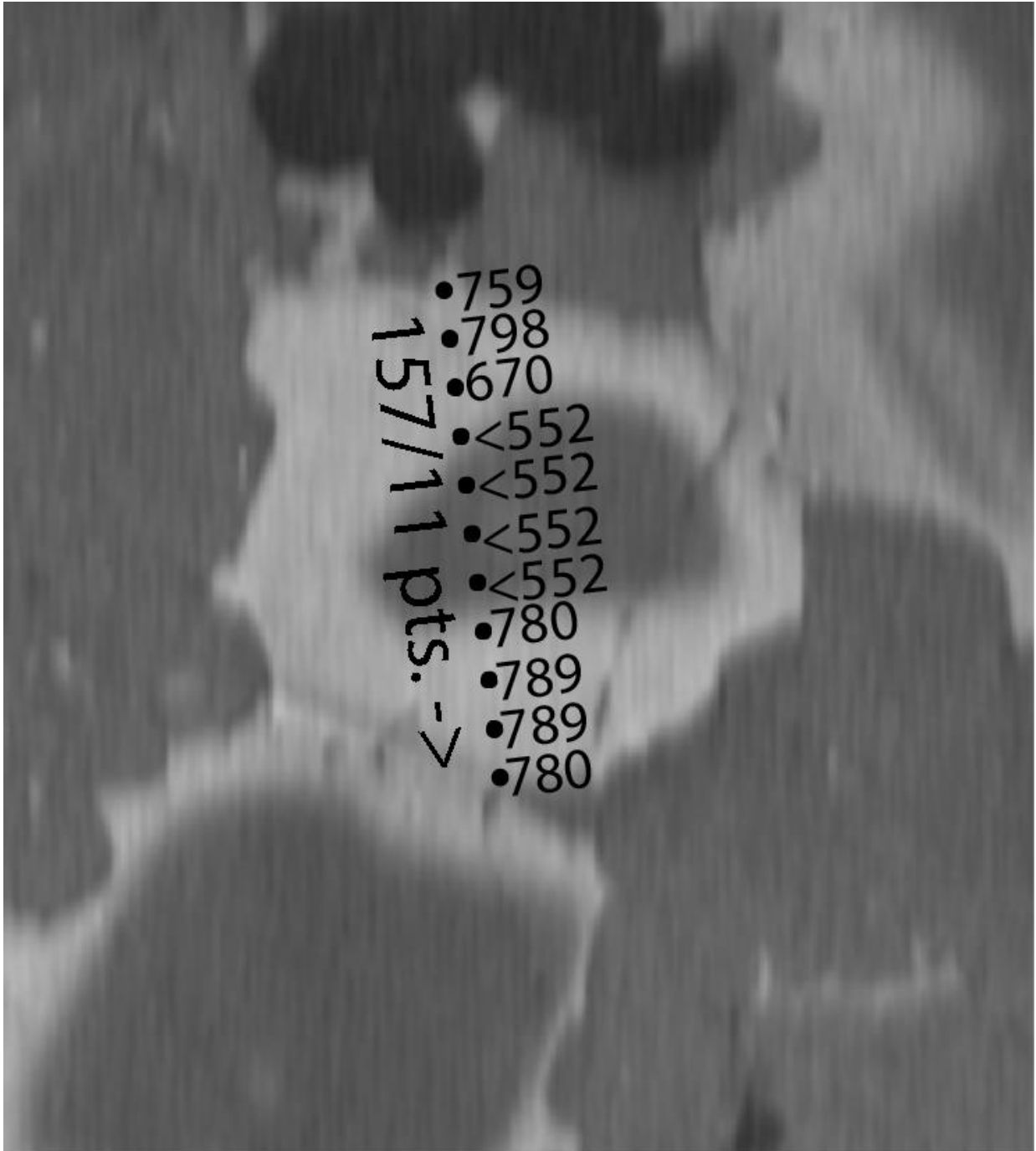


Figure A39 EPMA capture of site 6 on Sample 136-8B. Each black dot is a point analyzed for Ti concentration followed by the TitaniQ result at $a\text{TiO}_2 = 0.6$. The length of the traverse is 157.00 μm and has 11 points. The arrow indicates the direction of the traverse. Table A84 has the corresponding EPMA and TitaniQ data.

Table A85 EPMA and TitaniQ results for Figure A39. No. 88 corresponds with the uppermost point on Figure A39. Oxide! refers to a point too close to an oxide for accurate analysis. BDL = Below Detection Limit.

Sample 136-8B TitaniQ Temperatures Site 6									
No.	TiO2 (wt. %)	TiO2 (ppm)	Ti(ppm)	SiO2 (wt. %)	Total	Comment	Comment2	Comment3	Temp (°C)
88	0.011	110	66	100	100.011	Line 1 136-8b-A6-l1	rim		759
89	0.015	150	90	100	100.015	Line 2 136-8b-A6-l1	rim		798
90	0.005	50	30	100	100.005	Line 3 136-8b-A6-l1	rim		670
91	0	0	0	100	100	Line 4 136-8b-A6-l1	mix	BDL	<552
92	0	0	0	100	100	Line 5 136-8b-A6-l1	core	BDL	<552
93	0.001	10	6	100	100.001	Line 6 136-8b-A6-l1	core	BDL	<552
94	0	0	0	100	100	Line 7 136-8b-A6-l1	core	BDL	<552
95	0.013	130	78	100	100.013	Line 8 136-8b-A6-l1	rim		780
96	0.014	140	84	100	100.014	Line 9 136-8b-A6-l1	rim		789
97	0.014	140	84	100	100.014	Line 10 136-8b-A6-l1	rim		789
98	0.013	130	78	100	100.013	Line 11 136-8b-A6-l1	rim		780

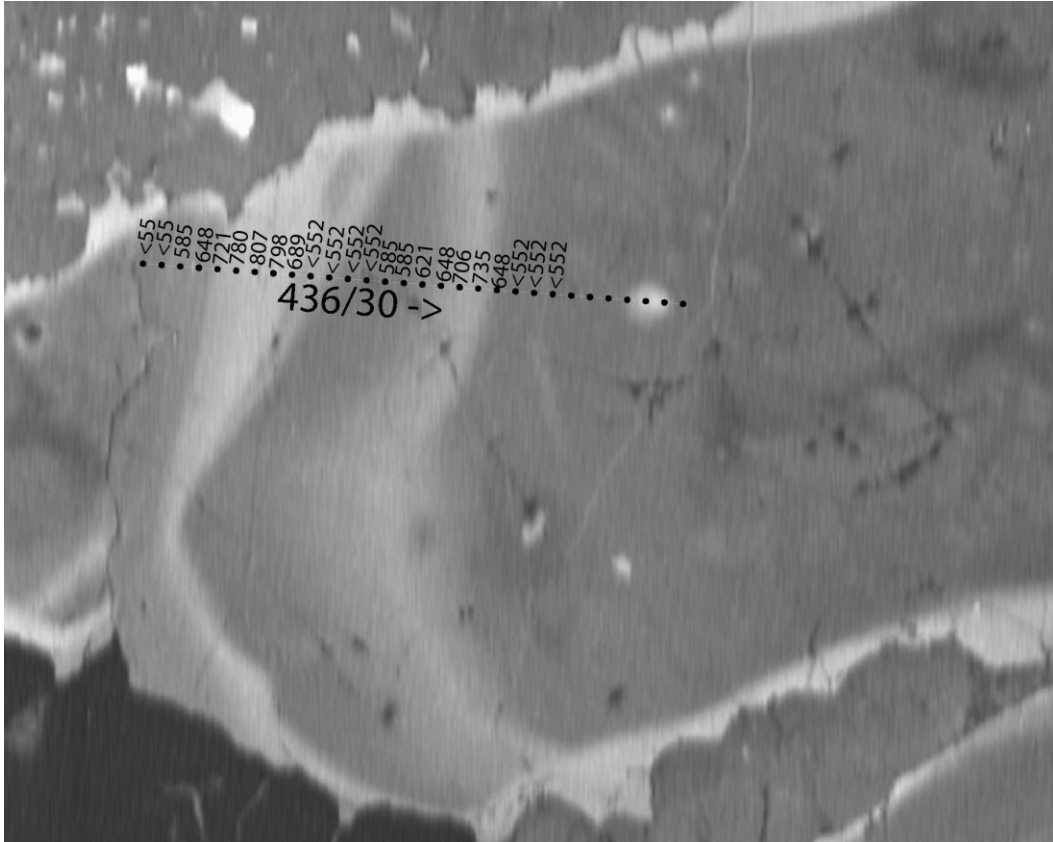


Figure A40 EPMA capture of site 7 on Sample 136-8B. Each black dot is a point analyzed for Ti concentration followed by the TitaniQ result at $a\text{TiO}_2 = 0.6$. Dots with no numbers represent points with no data. The length of the traverse is 436.00 μm and has 30 points. The arrow indicates the direction of the traverse. Table A85 has the corresponding EPMA and TitaniQ data.

Table A86 EPMA and TitaniQ results for Figure A40. No. 138 corresponds with the uppermost point on Figure A40. Oxide! refers to a point too close to an oxide for accurate analysis. BDL = Below Detection Limit.

Sample 136-8B TitaniQ Temperatures Site 7									
No.	TiO2 (wt. %)	TiO2 (ppm)	Ti(ppm)	SiO2 (wt. %)	Total	Comment	Comment2	Comment3	Temp (°C)
138	0	0	0	100	100	Line 1 136-8B-A7-L1	core	BDL	<552
139	0.001	10	6	100	100.001	Line 2 136-8B-A7-L1	core	BDL	<552
140	0.002	20	12	100	100.002	Line 3 136-8B-A7-L1	core		585
141	0.004	40	24	100	100.004	Line 4 136-8B-A7-L1	core		648
142	0.008	80	48	100	100.008	Line 5 136-8B-A7-L1	rim		721
143	0.013	130	78	100	100.013	Line 6 136-8B-A7-L1	rim		780
144	0.016	160	96	100	100.016	Line 7 136-8B-A7-L1	rim		807
145	0.015	150	90	100	100.015	Line 8 136-8B-A7-L1	rim		798
146	0.006	60	36	100	100.006	Line 9 136-8B-A7-L1	rim		689
147	0.001	10	6	100	100.001	Line 10 136-8B-A7-L1	rim	BDL	<552
148	0.001	10	6	100	100.001	Line 11 136-8B-A7-L1	mix	BDL	<552
149	0.001	10	6	100	100.001	Line 12 136-8B-A7-L1	core	BDL	<552
150	0.001	10	6	100	100.001	Line 13 136-8B-A7-L1	core	BDL	<552
151	0.002	20	12	100	100.002	Line 14 136-8B-A7-L1	core		585
152	0.002	20	12	100	100.002	Line 15 136-8B-A7-L1	core		585
153	0.003	30	18	100	100.003	Line 16 136-8B-A7-L1	mix		621
154	0.004	40	24	100	100.004	Line 17 136-8B-A7-L1	rim		648
155	0.007	70	42	100	100.007	Line 18 136-8B-A7-L1	rim		706
156	0.009	90	54	100	100.009	Line 19 136-8B-A7-L1	rim		735
157	0.004	40	24	100	100.004	Line 20 136-8B-A7-L1	core		648
158	0.001	10	6	100	100.001	Line 21 136-8B-A7-L1	core	BDL	<552
159	0.001	10	6	100	100.001	Line 22 136-8B-A7-L1	core	BDL	<552
160	0.001	10	6	100	100.001	Line 23 136-8B-A7-L1	core	BDL	<552

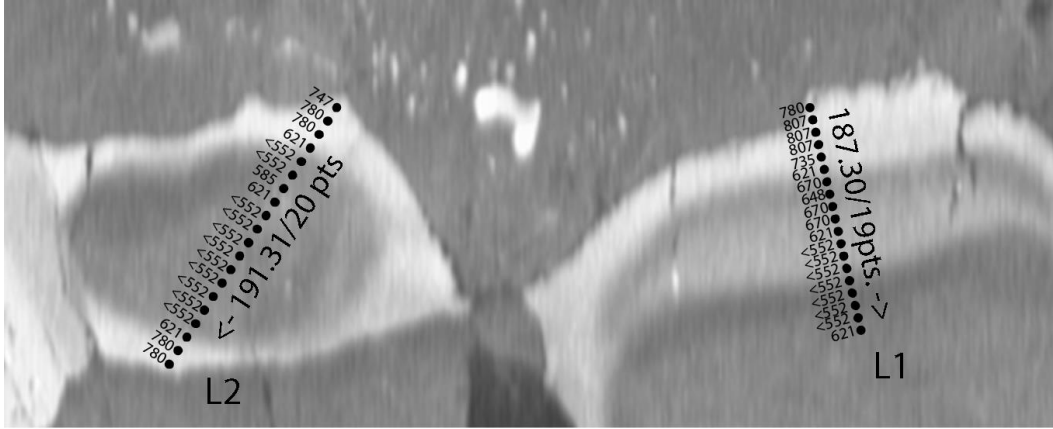


Figure A41 EPMA capture of site 9 on Sample 136-8B. Each black dot is a point analyzed for Ti concentration followed by the TitaniQ result at $a\text{TiO}_2 = 0.6$. The L2 and L1 traverse length is 191.31 μm with 20 points and 187.30 μm . with 19 points, respectively. The arrow indicates the direction of the traverse. Table A86 has the corresponding EPMA and TitaniQ data.

Table A87 EPMA and TitaniQ results for Figure A41. No. 99 corresponds with the uppermost point on traverse L1, and No. 118 corresponds with the uppermost point on traverse L2 on Figure A41. Oxide! refers to a point too close to an oxide for accurate analysis. BDL = Below Detection Limit.

Sample 136-8B TitaniQ Temperatures Site 9									
No.	TiO2 (wt. %)	TiO2 (ppm)	Ti(ppm)	SiO2 (wt. %)	Total	Comment	Comment2	Comment3	Temp (°C)
99	0.013	130	78	100	100.013	Line 1 136-8B-A9-L1	rim		780
100	0.016	160	96	100	100.016	Line 2 136-8B-A9-L1	rim		807
101	0.016	160	96	100	100.016	Line 3 136-8B-A9-L1	rim		807
102	0.016	160	96	100	100.016	Line 4 136-8B-A9-L1	rim		807
103	0.009	90	54	100	100.009	Line 5 136-8B-A9-L1	rim		735
104	0.003	30	18	100	100.003	Line 6 136-8B-A9-L1	mix		621
105	0.005	50	30	100	100.005	Line 7 136-8B-A9-L1	core		670
106	0.004	40	24	100	100.004	Line 8 136-8B-A9-L1	core		648
107	0.005	50	30	100	100.005	Line 9 136-8B-A9-L1	mix		670
108	0.005	50	30	100	100.005	Line 10 136-8B-A9-L1	rim		670
109	0.003	30	18	100	100.003	Line 11 136-8B-A9-L1	rim		621
110	0	0	0	100	100	Line 12 136-8B-A9-L1	rim	BDL	<552
111	0	0	0	100	100	Line 13 136-8B-A9-L1	rim	BDL	<552
112	0	0	0	100	100	Line 14 136-8B-A9-L1	rim	BDL	<552
113	0	0	0	100	100	Line 15 136-8B-A9-L1	mix	BDL	<552
114	0.001	10	6	100	100.001	Line 16 136-8B-A9-L1	core	BDL	<552
115	0.001	10	6	100	100.001	Line 17 136-8B-A9-L1	core	BDL	<552
116	0.001	10	6	100	100.001	Line 18 136-8B-A9-L1	core	BDL	<552
117	0.003	30	18	100	100.003	Line 19 136-8B-A9-L1	core		621
118	0.01	100	60	100	100.01	Line 1 136-8B-A9-L2	rim		747
119	0.013	130	78	100	100.013	Line 2 136-8B-A9-L2	rim		780
120	0.013	130	78	100	100.013	Line 3 136-8B-A9-L2	rim		780
121	0.003	30	18	100	100.003	Line 4 136-8B-A9-L2	mix		621
122	0	0	0	100	100	Line 5 136-8B-A9-L2	core	BDL	<552
123	0	0	0	100	100	Line 6 136-8B-A9-L2	core	BDL	<552
124	0.002	20	12	100	100.002	Line 7 136-8B-A9-L2	core		585
125	0.003	30	18	100	100.003	Line 8 136-8B-A9-L2	core		621
126	0.001	10	6	100	100.001	Line 9 136-8B-A9-L2	core	BDL	<552
127	0.001	10	6	100	100.001	Line 10 136-8B-A9-L2	core	BDL	<552
128	0	0	0	100	100	Line 11 136-8B-A9-L2	core	BDL	<552
129	0	0	0	100	100	Line 12 136-8B-A9-L2	core	BDL	<552
130	0.001	10	6	100	100.001	Line 13 136-8B-A9-L2	core	BDL	<552
131	0.001	10	6	100	100.001	Line 14 136-8B-A9-L2	core	BDL	<552
132	0	0	0	100	100	Line 15 136-8B-A9-L2	core	BDL	<552
133	0.001	10	6	100	100.001	Line 16 136-8B-A9-L2	core	BDL	<552
134	0.001	10	6	100	100.001	Line 17 136-8B-A9-L2	core	BDL	<552
135	0.003	30	18	100	100.003	Line 18 136-8B-A9-L2	mix		621
136	0.013	130	78	100	100.013	Line 19 136-8B-A9-L2	rim		780
137	0.013	130	78	100	100.013	Line 20 136-8B-A9-L2	rim		780

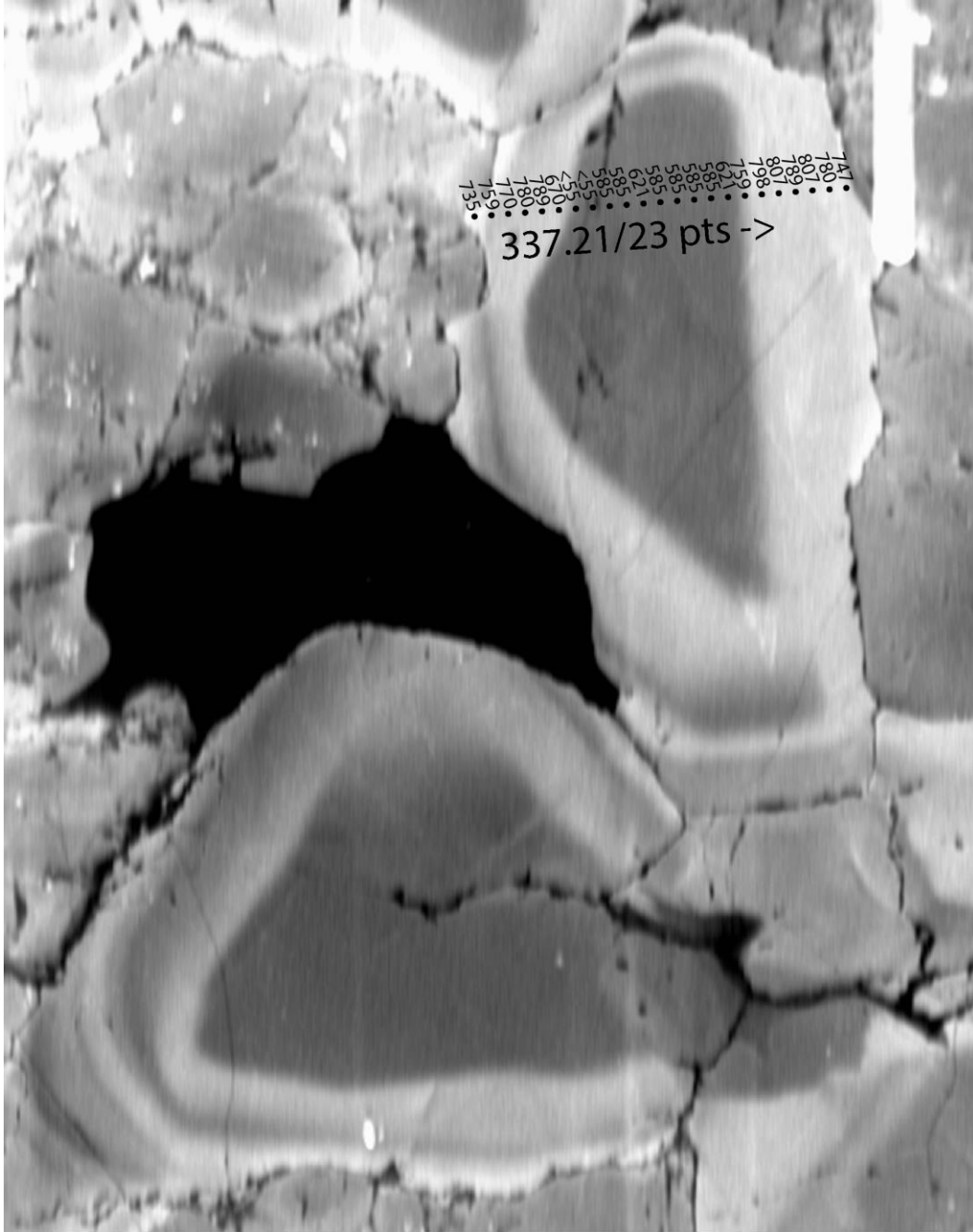


Figure A42 EPMA capture of site 1 on Sample 136-14B. Each black dot is a point analyzed for Ti concentration followed by the TitaniQ result at $a\text{TiO}_2 = 0.6$. The traverse length is 337.21 μm with 23 points. The arrow indicates the direction of the traverse. Table A87 has the corresponding EPMA and TitaniQ data.

Table A88 EPMA and TitaniQ results for Figure A42. No. 1 corresponds with the leftmost point on Figure A42. Oxide! refers to a point too close to an oxide for accurate analysis. BDL = Below Detection Limit.

Sample 136-14B TitaniQ Temperatures Site 1									
No.	TiO2 (wt. %)	TiO2 (ppm)	Ti(ppm)	SiO2 (wt. %)	Total	Comment	Comment2	Comment3	Temp (°C)
1	0.009	90	54	100	100.009	Line 1 136-14B-a1-L1	rim		735
2	0.011	110	66	100	100.011	Line 2 136-14B-a1-L1	rim		759
3	0.012	120	72	100	100.012	Line 3 136-14B-a1-L1	rim		770
4	0.013	130	78	100	100.013	Line 4 136-14B-a1-L1	rim		780
5	0.014	140	84	100	100.014	Line 5 136-14B-a1-L1	rim		789
6	0.005	50	30	100	100.005	Line 6 136-14B-a1-L1	rim		670
7	0.001	10	6	100	100.001	Line 7 136-14B-a1-L1	core	BDL	<552
8	0.001	10	6	100	100.001	Line 8 136-14B-a1-L1	core	BDL	<552
9	0.002	20	12	100	100.002	Line 9 136-14B-a1-L1	core		585
10	0.002	20	12	100	100.002	Line 10 136-14B-a1-L1	core		585
11	0.003	30	18	100	100.003	Line 11 136-14B-a1-L1	core		621
12	0.002	20	12	100	100.002	Line 12 136-14B-a1-L1	core		585
13	0.002	20	12	100	100.002	Line 13 136-14B-a1-L1	core		585
14	0.002	20	12	100	100.002	Line 14 136-14B-a1-L1	core		585
15	0.002	20	12	100	100.002	Line 15 136-14B-a1-L1	core		585
16	0.003	30	18	100	100.003	Line 16 136-14B-a1-L1	mix		621
17	0.011	110	66	100	100.011	Line 17 136-14B-a1-L1	rim		759
18	0.015	150	90	100	100.015	Line 18 136-14B-a1-L1	rim		798
19	0.016	160	96	100	100.016	Line 19 136-14B-a1-L1	rim		807
20	0.014	140	84	100	100.014	Line 20 136-14B-a1-L1	rim		789
21	0.016	160	96	100	100.016	Line 21 136-14B-a1-L1	rim		807
22	0.013	130	78	100	100.013	Line 22 136-14B-a1-L1	rim		780
23	0.01	100	60	100	100.01	Line 23 136-14B-a1-L1	rim		747

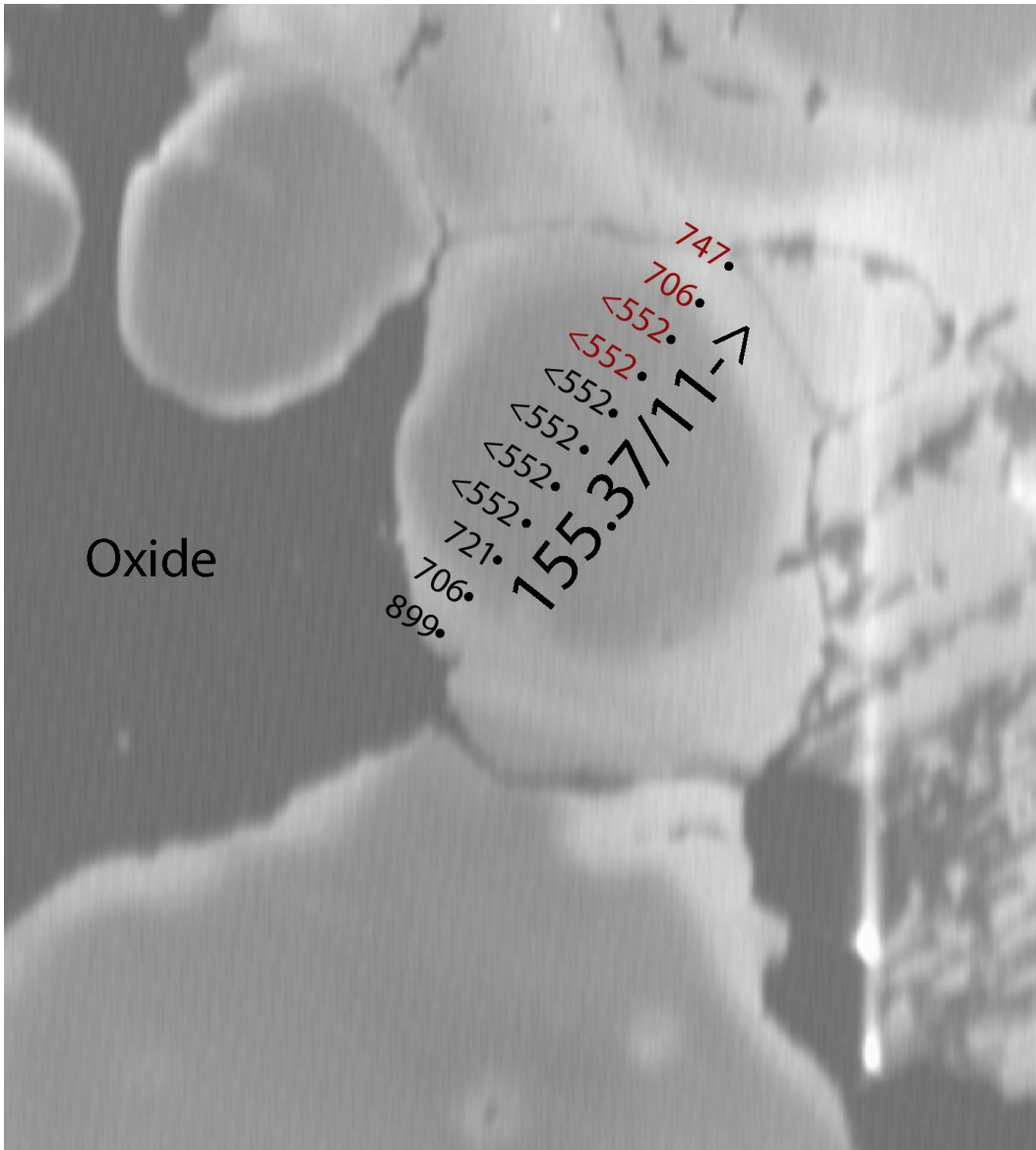


Figure A43 EPMA capture of site 4 on Sample 136-14B. Each black dot is a point analyzed for Ti concentration followed by the TitaniQ result at $a\text{TiO}_2 = 0.6$. Red numbers indicate good results, while black numbers represent values that are too close to an oxide for accurate analysis. The traverse length is $155.37 \mu\text{m}$ with 11 points. The arrow indicates the direction of the traverse. Table A88 has the corresponding EPMA and TitaniQ data.

Table A89 EPMA and TitaniQ results for Figure A43. No. 24 corresponds with the lowermost point on Figure A43. Oxide! refers to a point too close to an oxide for accurate analysis. BDL = Below Detection Limit.

Sample 136-14B TitaniQ Temperatures Site 4									
No.	TiO2 (wt. %)	TiO2 (ppm)	Ti(ppm)	SiO2 (wt. %)	Total	Comment	Comment2	Comment3	Temp (°C)
24	0.03	300	180	100	100.03	Line 1 136-14B-A6-L1	Oxide!		899
25	0.007	70	42	100	100.007	Line 2 136-14B-A6-L1	Oxide!		706
26	0.008	80	48	100	100.008	Line 3 136-14B-A6-L1	Oxide!		721
27	0	0	0	100	100	Line 4 136-14B-A6-L1	Oxide!	BDL	<552
28	0.001	10	6	100	100.001	Line 5 136-14B-A6-L1	Oxide!	BDL	<552
29	0	0	0	100	100	Line 6 136-14B-A6-L1	Oxide!	BDL	<552
30	0	0	0	100	100	Line 7 136-14B-A6-L1	Oxide!	BDL	<552
31	0	0	0	100	100	Line 8 136-14B-A6-L1	core	BDL	<552
32	0.001	10	6	100	100.001	Line 9 136-14B-A6-L1	core	BDL	<552
33	0.007	70	42	100	100.007	Line 10 136-14B-A6-L1	mix		706
34	0.01	100	60	100	100.01	Line 11 136-14B-A6-L1	rim		747

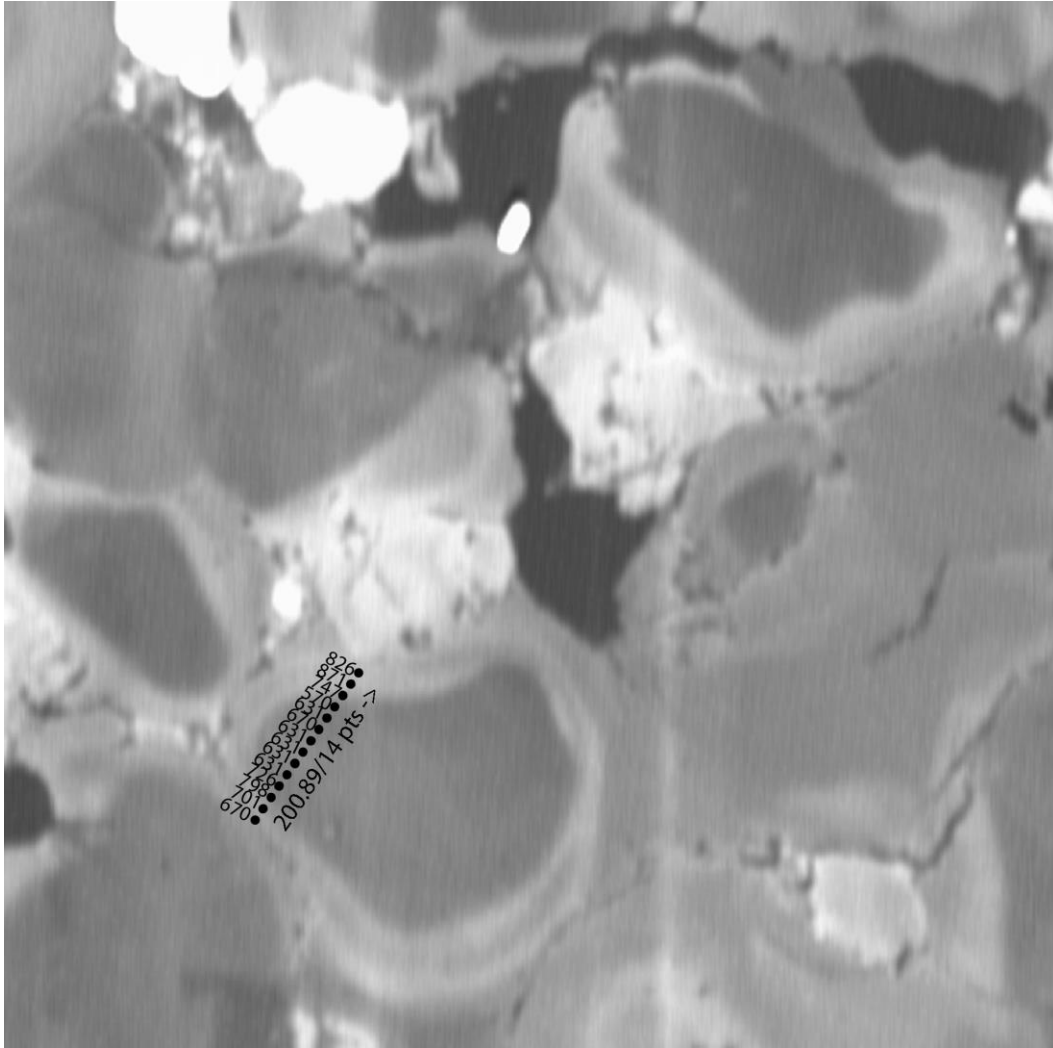


Figure A44 EPMA capture of site 6 on Sample 136-14B. Each black dot is a point analyzed for Ti concentration followed by the TitaniQ result at $a\text{TiO}_2 = 0.6$. The traverse length is 200.89 μm with 14 points. The arrow indicates the direction of the traverse. Table A89 has the corresponding EPMA and TitaniQ data.

Table A90 EPMA and TitaniQ results for Figure A44. No. 35 corresponds with the lowermost point on Figure A44. Oxide! refers to a point too close to an oxide for accurate analysis. BDL = Below Detection Limit.

Sample 136-14B TitaniQ Temperatures Site 6									
No.	TiO2 (wt. %)	TiO2 (ppm)	Ti(ppm)	SiO2 (wt. %)	Total	Comment	Comment2	Comment3	Temp (°C)
35	0.003	30	18	100	100.003	Line 1 136-14B-A6-L1	rim		621
36	0.004	40	24	100	100.004	Line 2 136-14B-A6-L1	rim		648
37	0.009	90	54	100	100.009	Line 3 136-14B-A6-L1	rim		735
38	0.005	50	30	100	100.005	Line 4 136-14B-A6-L1	core		670
39	0.002	20	12	100	100.002	Line 5 136-14B-A6-L1	core		585
40	0.002	20	12	100	100.002	Line 6 136-14B-A6-L1	core		585
41	0.002	20	12	100	100.002	Line 7 136-14B-A6-L1	core		585
42	0.002	20	12	100	100.002	Line 8 136-14B-A6-L1	core		585
43	0.003	30	18	100	100.003	Line 9 136-14B-A6-L1	core		621
44	0.002	20	12	100	100.002	Line 10 136-14B-A6-L1	core		585
45	0.001	10	6	100	100.001	Line 11 136-14B-A6-L1	core	BDL	<552
46	0.006	60	36	100	100.006	Line 12 136-14B-A6-L1	rim		689
47	0.015	150	90	100	100.015	Line 13 136-14B-A6-L1	rim		798
48	0.011	110	66	100	100.011	Line 14 136-14B-A6-L1	rim		759

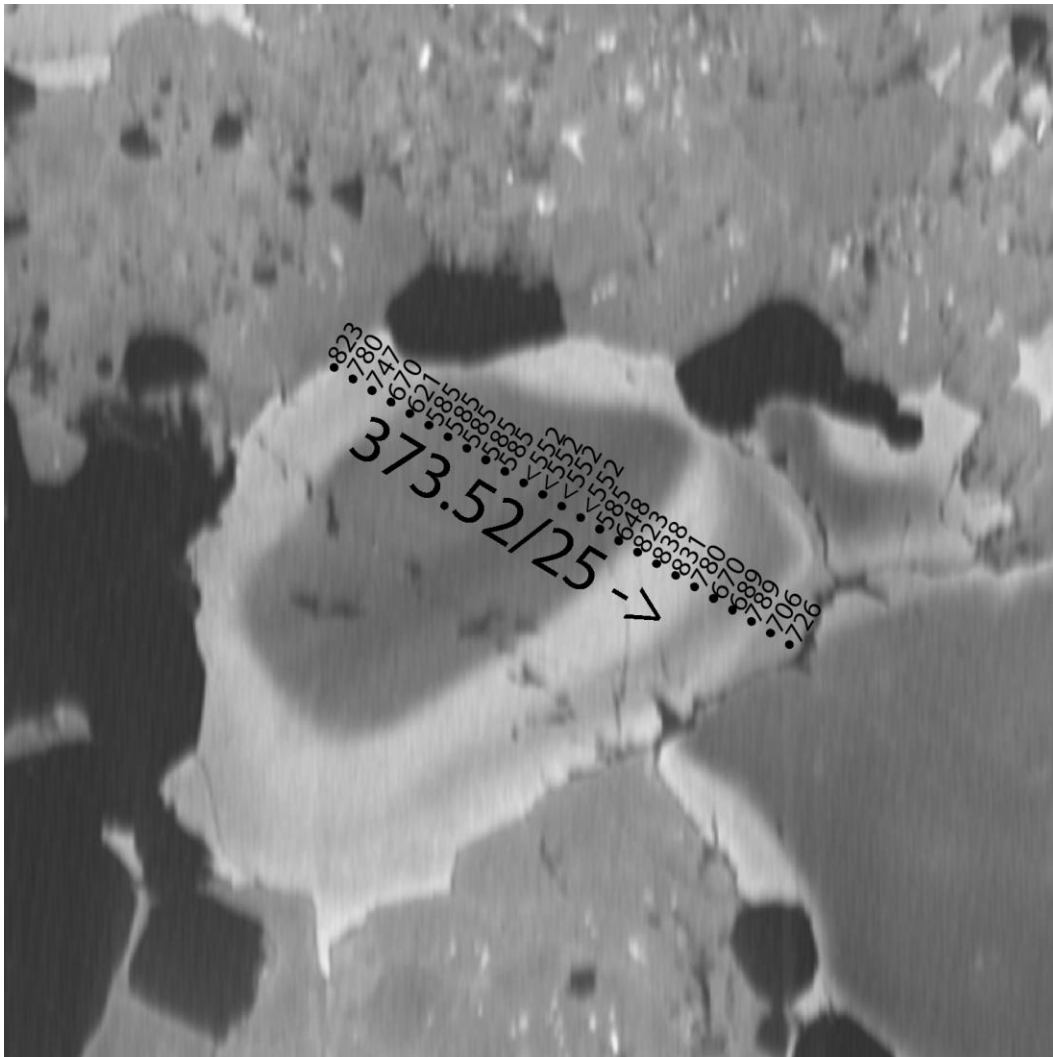


Figure A45 EPMA capture of site 8 on Sample 136-14B. Each black dot is a point analyzed for Ti concentration followed by the TitaniQ result at $a\text{TiO}_2 = 0.6$. The traverse length is 373.52 μm with 25 points. The arrow indicates the direction of the traverse. Table A90 has the corresponding EPMA and TitaniQ data.

Table A91 EPMA and TitaniQ results for Figure A45. No. 49 corresponds with the uppermost point on Figure A45. Oxide! refers to a point too close to an oxide for accurate analysis. BDL = Below Detection Limit.

Sample 136-14B TitaniQ Temperatures Site 8									
No.	TiO2 (wt. %)	TiO2 (ppm)	Ti(ppm)	SiO2 (wt. %)	Total	Comment	Comment2	Comment3	Temp (°C)
49	0.018	180	108	100	100.018	Line 1 136-14A-A8-L1	rim		823
50	0.013	130	78	100	100.013	Line 2 136-14A-A8-L1	rim		780
51	0.01	100	60	100	100.01	Line 3 136-14A-A8-L1	rim		747
52	0.005	50	30	100	100.005	Line 4 136-14A-A8-L1	mix		670
53	0.003	30	18	100	100.003	Line 5 136-14A-A8-L1	core		621
54	0.002	20	12	100	100.002	Line 6 136-14A-A8-L1	core		585
55	0.002	20	12	100	100.002	Line 7 136-14A-A8-L1	core		585
56	0.002	20	12	100	100.002	Line 8 136-14A-A8-L1	core		585
57	0.002	20	12	100	100.002	Line 9 136-14A-A8-L1	core		585
58	0.002	20	12	100	100.002	Line 10 136-14A-A8-L1	core		585
59	0.001	10	6	100	100.001	Line 11 136-14A-A8-L1	core	BDL	<552
60	0.001	10	6	100	100.001	Line 12 136-14A-A8-L1	core	BDL	<552
61	0	0	0	100	100	Line 13 136-14A-A8-L1	core	BDL	<552
62	0.001	10	6	100	100.001	Line 14 136-14A-A8-L1	core	BDL	<552
63	0.002	20	12	100	100.002	Line 15 136-14A-A8-L1	core		585
64	0.004	40	24	100	100.004	Line 16 136-14A-A8-L1	core		648
65	0.018	180	108	100	100.018	Line 17 136-14A-A8-L1	rim		823
66	0.02	200	120	100	100.02	Line 18 136-14A-A8-L1	rim		838
67	0.019	190	114	100	100.019	Line 19 136-14A-A8-L1	rim		831
68	0.013	130	78	100	100.013	Line 20 136-14A-A8-L1	rim		780
69	0.005	50	30	100	100.005	Line 21 136-14A-A8-L1	core		670
70	0.006	60	36	100	100.006	Line 22 136-14A-A8-L1	core		689
71	0.014	140	84	100	100.014	Line 23 136-14A-A8-L1	rim		789
72	0.007	70	42	100	100.007	Line 24 136-14A-A8-L1	core		706
73	0.005	50	30	100	100.005	Line 25 136-14A-A8-L1	core		670

Table A92 Summary of TitaniQ temperatures divided on core and rim analysis. Averages are calculated from data from each sample, and are not to be confused with the estimated error associated with the TitaniQ geothermometer (Wark and Watson, 2006).

TitaniQ Averages				
Sample	Average Core (°C)	<i>n</i>	Average Rim (°C)	<i>n</i>
A-traverse				
136-1A	721 ± 82	47	823 ± 70	45
136-6A	644 ± 50	13	868 ± 50	28
136-11A	<561	0	<561	0
B-traverse				
136-2B	639 ± 65	17	748 ± 85	33
136-8B	619 ± 33	10	754 ± 50	32
136-14B	610 ± 40	26	764 ± 53	28

References

- Acosta-Vigil, A., London, D., and Morgan, G. B., 2006, Experiments on the kinetics of partial melting of a leucogranite at 200 MPa H₂O and 690–800C: compositional variability of melts during the onset of H₂O-saturated crustal anatexis: *Contributions to Mineral Petrology*, v. 151, p. 539-557.
- Ashworth, J. R., 1985, Introduction, *in* Ashworth, J. R., eds., *Migmatites*: Chapman and Hall, New York, p. 1-35.
- Brown, M., Korhonen, F. J., and Siddoway, C. S., 2011, Organizing melt flow through the crust: *Elements*, v. 7, p. 261-266.
- Bowen, N. L., 1913, The melting phenomena of the plagioclase feldspars: *American Journal of Science*, v. 35, n. 210 p. 577-599.
- Büsch, W., Schneider, G., and Mehnert, K. R., 1974, Part II: Melting in rocks of granodioritic, quartzdioritic and tonalitic composition: Stuttgart, Germany, *Jahrbuch. Mineralogie Monatshefte*, p. 345-370.
- Cmiral, M., Fitz Gerald, J. D., Faul, U. H., and Green, D. H., 1998, A close look at dihedral angles and melt geometry in olivine-basalt aggregates: a TEM study: *Contributions to Mineral Petrology*, v. 130, p. 336-345.
- Davidson, J. P., Morgan, D. J., Charlier, B. L. A., Harlou, R., and Hora, J. M., 2007, Microsampling and Isotopic Analysis of Igneous Rocks: Implications for the Study of Magmatic Systems: *Annual Review of Earth and Planetary Sciences*, v. 35, p. 273-311.
- Duebendorfer, E. M., Chamberlain, K. R., and Fry, B., 2006, Mojave – Yavapai boundary zone, southwestern United States: A rifting model for the formation of an isotopically mixed crustal boundary zone: *Geology*, v. 34, no. 8, p. 681-684.
- Faulds, J. E., 1995, The Mt. Perkins block, northwestern Arizona; an exposed cross-section of a tilted synextensional volcano in a highly extended terrane: *Geological Society of America Abstracts with Programs*, v. 25, p. 36.
- Ghent, E. D., and Stout, M. Z., 1984, TiO₂ activity in metamorphosed pelitic and basic rocks: principles and applications to metamorphism in southeastern Canadian Cordillera: *Contributions to Mineralogy and Petrology*, v. 86, p. 248-255.
- Götze, J., Plötze, M., and Habermann, D., 2001, Origin, spectral characteristics and practical application of the cathodoluminescence (CL) of quartz – a review: *Mineralogy and Petrology*, v. 71, p. 225-250.
- Grapes, R., 2006, *Pyrometamorphism*: New York, Springer, 275 p.

- Gupta L. N., and Johannes, W., 1982, Petrogenesis of a stromatic migmatite (Nelaug, Southern Norway): *Journal of Petrology*, v. 23, part 4, p. 548-567.
- Holland, T. and Blundy, J., 1994, Non-ideal interactions in calcic amphiboles and their bearing on amphibole-plagioclase thermometry: *Contributions to Mineralogy and Petrology*, v. 116, p. 433-447.
- Holness, M. B., 2008, Decoding migmatite microstructures, *in* Sawyer, E. W., eds., *Working with migmatites: Mineral Association of Canada Short Course 38*, p. 57-76.
- Holness, M. B., Cesare, B. and Sawyer, E. W., 2011, Melted rocks under the microscope: microstructures and their interpretation: *Elements*, v. 7, p. 245–250.
- Holness, M. B., and Clemons, J. D., 1999, Partial melting of the Appin Quartzite driven by fracture-controlled H₂O infiltration in the aureole of the Ballachulish Igneous Complex, Scottish Highlands: *Contributions to Mineral Petrology*, v. 136, p. 154-168.
- Holness, M. B., Dane, K., Sides, R., Richardson C., and Caddick, M., 2005, Melting and melt segregation in the aureole of the Glenmore plug, Ardnamurchan: *Journal of Metamorphic Geology*, v. 23, n. 1, p. 29-43.
- Holness, M. B., and Isherwood, 2003, The aureole of the Rum Tertiary Igneous Complex, Scotland: *Journal of the Geological Society, London*, v. 160, p. 15-27.
- Holness, M. B. and Sawyer, E. W., 2008, On the pseudomorphing of melt-filled pores during the crystallization of migmatites: *Journal of Petrology*, v. 49, p. 1343–1363.
- Holness M. B., Watt G. R., 2002, The aureole of the Traigh Bhan na Sgurra sill, Isle of Mull: reaction-driven micro-cracking during pyrometamorphism: *Journal of Petrology*, v.43, n. 3, p. 511-534.
- Johannes, W., 1978, Melting of plagioclase in the system Ab – An – H₂O and Qz – Ab – An – H₂O at P_{H₂O} = 5 kbars, an equilibrium problem: *Contributions to Mineralogy and Petrology*, v. 66, p. 295-303.
- Johannes, W., 1983, Metastable melting in granite and related systems, *in*, Athertone, M. P., and Gribble, C. D., eds., *Migmatites, melting and metamorphism*: Cheshire, U.K., Shiva Publishing Limited, p. 27-36.
- Johannes, W., 1984, Beginning of melting in the granite system Qz-Or-Ab-An-H₂O: *Contributions to Mineralogy and Petrology*, v. 86, p. 114-123.
- Johannes, W., 1985, The significance of experimental studies for the formation of migmatites, *in* Ashworth, J. R., eds., *Migmatites*: Chapman and Hall, New York, p. 36-85.
- Johannes, W., 1989, Melting of plagioclase-quartz assemblages at 2 kbar water pressure: *Contributions to Mineral Petrology*, v. 103, p. 270-276.

- Johannes, W., and Gupta, L. N., 1982, Origin and evolution of a migmatite: Contributions to Mineralogy and Petrology, v. 79, p. 114-123.
- Johannes, W., and Holtz, F., 1992, Melting of plagioclase in granite and related systems: composition of coexisting phases and kinetic observations: Transactions of the Royal Society of Edinburgh: Earth Sciences, v. 83, p. 417-422.
- Manning, D. A. C., and Pichavant, M., 1983, The role of fluorine and boron in the generation of granitic melts, *in*, Atherton, M. P., and Gribble, C. D., eds., Migmatites, melting and metamorphism: Cheshire, U.K., Shiva Publishing Limited, p. 94-109.
- Mehnert, K. R., Büsch, W., and Schneider, G., 1973, Initial melting at grain boundaries of quartz and feldspar in gneisses and granulites: Stuttgart, Germany, Jahrbuch f. Mineralogie Monatshefte, p. 165-183.
- Metcalf, R. V., Smith, E. I., Walker, J. D., Reed, R. C., and Gonzales, D. A., 1995, Isotopic disequilibrium among commingled hybrid magmas: evidence for a two-stage magma mixing – commingling process in the Mt. Perkins Pluton, Arizona: The Journal of Geology, v. 103, p. 509-527.
- Metcalf, R. V., 2004, Volcanic-plutonic links, plutons as magma chambers and crust-mantle interaction: a lithospheric scale view of magma systems: Transactions of the Royal Society of Edinburgh: Earth Sciences, v. 95, p. 357-374.
- Metcalf, R. V., 2013, Timescale of petrogenetic processes recorded in the mount perkins magma system, northern Colorado extensional corridor, Arizona: Geological Society of America Abstracts with Programs, v. 45, No. 7, p. 229.
- Metcalf, R. V., and Smith, E. I., 1991, Hornblende geobarometry from two Miocene plutons: Implications regarding uplift and block rotation during Basin and Range extension: Geological Society of America Programs with Abstracts, v. 23, n. 5, p. A245.
- Metcalf, R. V., and Kopietz, C., 2011, Grain-scale melt pseudomorph microstructures from the pyrometamorphic aureole of the Miocene Mount Perkins pluton: A potential link to open system processes during pluton crystallization: Geological Society of America Abstracts with Programs, v. 43, n. 4, p. 63.
- Pattison, D. R. M. and Harte, B., 1988, Evolution of structurally contrasting anatectic migmatites in the 3-kbar Ballachulish aureole, Scotland: Journal of Metamorphic Petrology, v. 6, p. 475-494.
- Piwinskii, A. J., and Wyllie, P. J., 1968, Experimental studies of igneous rock series: A zoned pluton in the Wallowa batholith, Oregon: Journal of Geology, v. 76, p. 205-234.
- Powell, R., and Powell, M., 1977, Geothermometry and oxygen barometry using coexisting iron-titanium oxides: a reappraisal: Mineralogical Magazine, v. 41, p. 257-263.

- Rosenberg, C. L. and Riller, U., 2000, Partial-melt topology in statically and dynamically recrystallized granite: *Geology*, v. 28, n. 1, p. 7-10.
- Sawyer, E. W., 2001, Melt segregation in the continental crust: distribution and movement of melt in anatectic rocks: *Journal of Metamorphic Petrology*, v. 19, p. 291-309.
- Sawyer, E. W., 1999, Criteria for the recognition of partial melting: *Physics and Chemistry of the Earth*, v. 24, n. 3, p. 269-279.
- Shcherbakov, V. D., Plechov, P. Y., Izbekov, P. E., and Shipman, J. S., 2011, Plagioclase zoning as an indicator of magma processes at Bezymianny Volcano, Kamchatka: *Contributions to Mineral Petrology*, v. 162, p. 83-99.
- Stewart, D. B., Walker, G. W., Wright, T. L., and Fahey, J. J., 1966, Physical properties of calcic labradorite from Lake County, Oregon: *American Mineralogist*, v. 51, p. 177-197.
- Tuttle, O. F., and Bowen, N. L., 1958, Origin of granite in the light of experimental studies in the system $\text{NaAlSi}_3\text{O}_8\text{-KAlSi}_3\text{O}_8\text{-SiO}_2\text{-H}_2\text{O}$: *Geological Society of America Memoir* 74, 153 p.
- Wohletz, K., Civetta, L., and Orsi, G., 1999, Thermal evolution of the Phlegraean Magmatic System: *Journal of Volcanology and Geothermal Energy*, v. 91, p. 381-414.
- Wyllie, P. J., 1977, Crustal anatexis: an experimental review, *in* Green, D. H., eds., *Experimental petrology related to extreme metamorphism: Tectonophysics*, v. 43, p. 41-71.

Curriculum Vitae

Mathew Beshears

5245 New Bedford Circle
Las Vegas, NV 89122
317-289-1209
beshears@unlv.nevada.edu

Education

Graduate

May 2016

University of Nevada – Las Vegas
Master of Science in geology in progress
Thesis: The earliest stages of partial melting: A study of the pyrometamorphic contact aureole of Miocene Mt. Perkins pluton, NW Arizona.

Undergraduate

2006-2011

Indiana University – Purdue University Indianapolis
Bachelor of Science in geology with a minor in mathematics
Independent Research
Nutrient cycles through the evolution of plant rootedness
Determining subglacial Antarctic geology using glaciology concepts

Professional Experience

Staff Geologist, Active Environmental

Spring 2012 – Summer 2012

- Assisted with Phase II investigations on underground storage tanks
- Collected groundwater and soil samples
- Edited state reports

Geochemistry and Sedimentology Lab Assistant, IUPUI

Fall 2010 – Winter 2011

- Assisted with operation of an ICP-OES and Shimadzu UV-2401PC Spectrophotometer
- Used ICP-OES to analyze major element chemistry in Devonian rocks in effort to identify global nutrient cycle changes through the evolution of plant rootedness
- Created thin sections and used optical microscopy to identify and categorized 100s of clasts taken from Antarctica
- Used topographic maps and aerial photos to infer the origin of clasts transported to the surface by glacial movement
- Worked with graduate students to identify various Antarctic rocks
- Managed supplies
- Revised lab instructions for cutting thin sections

Teaching Experience

Physical Geology Teaching Assistant, UNLV

Fall 2012 and Spring 2013

- Instructed geology 101 lab sections with a total of approximately 85 students over 4 sections
- Topics include: Identifying rocks, understanding groundwater flow, topographic maps, geologic structure, and simple mapping techniques
- Lead field trips for multiple sections
- Managed lab supplies

Field Methods and Advanced Field Methods Teaching Assistant, UNLV

2013-2014

- Create maps of field exercises
- Grade students' notes, maps, reports, and cross-sections
- Assist students on various field geology problems on day and weekend trips
- Ensure safety of all participants

Volunteer Experience

Astronomy night at Coronado High School, Las Vegas Nevada

Spring 2013

- Used telescopes to track planets and stars
- Answered any questions parents or students of all ages may have
- Helped with the setup and removal of equipment

Geosymposium, Chair of the field trip committee, UNLV

Spring 2013

- Organized a field trip for professionals and students to Nellis Dunes and Mormon Mesa to discuss medical geology and petrocalcic soil
- Secured vehicles and gathered drivers for the field trip
- Managed lunch and breakfast for participants
- Edited field trip literature

Geosymposium, Chair of food and beverage committee, UNLV

Spring 2014

- Organized and coordinated catering and beverage services
- Recruited and managed volunteers

Skills

Instruments: Petrothin, Petrographic microscope and imagery, ICP-OES, Shimadzu UV-2401PC Spectrophotometer, SEM with emphasis on BSE and CL imaging

Software: Heat3D, Iqpet, ArcGIS, AutoCADD, SigmaPlot, Microsoft Office Suite, Adobe Photoshop and Illustrator

Honors and Awards

Graduate

Bernada French Scholarship, Edwards and Olswang Geology Scholarship

Undergraduate

Deans Honor's List, STAR Mentor Scholarship, Federal SMART Grant, Central Indiana Technical and Environmental Societies Scholarship, Indiana Geology and Gem Society Scholarship, Top 100 Students at IUPUI Nominee

Elected Positions

2011 IUPUI Geology Club President

Professional Memberships

Geological Society of America
Geological Society of Nevada
Society of Economic Geologists

Personal Interests

Hiking and backpacking, fishing, travelling, rock collecting, cooking, general outdoor activities